Contribution of 1D local hydraulic modeling to improve simulations of river stages and stream-aquifer interactions at regional scale

Firas Saleh

THESE DE DOCTORAT DE
L'UNIVERSITE PIERRE ET MARIE CURIE

Spécialité

Hydrologie et Hydrogéologie Quantitative

Ecole Doctorale Géosciences et Ressources Naturelles 398 Paris

Présentée par

M. Firas S. M. SALEH

Pour obtenir le grade de

DOCTEUR de l'UNIVERSITÉ PIERRE ET MARIE CURIE

Sujet de la thèse :

Apport de la modélisation hydraulique pour une meilleure simulation des tirants d'eau et des échanges nappe-rivière à l'échelle régionale

soutenue le 15 décembre 2010

devant le jury composé de :

M. Jean-Marie MOUCHEL : Président

Mme. Isabelle BRAUD : Rapporteur

M. Julio GONCALVES : Rapporteur

M. Philippe BELLEUDY : Examinateur

M. Emmanuel LEDOUX : Directeur de thèse

Mme. Agnès DUCHARNE : Co-directeur de thèse

M. Nicolas FLIPO : Co-directeur de thèse

Université Pierre & Marie Curie - Paris 6
Bureau d'accueil, inscription des doctorants
Esc G, 2ème étage
15 rue de l'école de médecine
75270-PARIS CEDEX 06

Tél. Secrétariat : 01 44 27 28 10
Fax : 01 44 27 23 95
Tél. pour les étudiants de A à EL : 01 44 27 28 07
Tél. pour les étudiants de EM à MON : 01 44 27 28 05
Tél. pour les étudiants de MOO à Z : 01 44 27 28 02
E-mail : scolarite.doctorat@upmc.fr

Contribution of 1D local hydraulic modeling to improve simulations of river stages and stream-aquifer interactions at regional scale

Abstract

This thesis contributes to the development of the integrated model EauDyssée of regional scale river systems, in the pilot case study of the Seine River basin. The main objective is to provide a realistic simulation of river stage and discharge at the regional scale, in order to improve the simulation of stream-aquifer interactions and better assess piezometric heads.

The first part of the thesis aims at establishing whether a reliable hydrodynamic routing model can be developed based on limited river bed morphological data. A wide variety of "what if" river geometry scenarios are explored to determine the most appropriate river representation geometry in areas where cross sections surveys are not always accessible. This study is carried out in the Serein River (tributary of the Yonne River), between the gauging stations of Dissangis et Beaumont, in a well surveyed reach (20 cross sections over 89 km). River discharge and stage are simulated by the hydraulic model HEC-RAS (1D Saint-Venant equations), while lateral inflows are simulated by the regional hydrogeological model EauDyssée. The results of this study show that a 1D Saint-Venant model is not suitable for simulating water levels in areas where river geomorphologic date is not available. Based on these conclusions, we developed an original upscaling strategy, which allows for benefiting from high resolution hydraulic modeling outputs to describe fluctuating river stage and improve the regional scale simulation of stream-aquifer interactions in the integrated model EauDyssée.

The validity of this approach has been illustrated in a 4500 km^2 sub-basin of the Oise River, for the period 1990-1995. We used the HEC-RAS to achieve a hydrodynamic simulation of a 188-km reach, where 420 surveyed cross sections are available. This model is used to interpolate rating curves (river stage vs. discharge) with a mean resolution of 200 m. The

latter are then projected onto the river grid cells of the regional model EauDyssée (1-km resolution), where they allow for fluctuating river stage, as a function of the discharge routed at the regional scale by EauDyssée. The altitude of the river surface defining its hydraulic head, these fluctuations influence the exchanges between the river and aquifer cells, which depend on the related vertical hydraulic gradient (Darcy's law).

This work outlines the efficiency of the approach to better simulate river stages and stream-aquifer interactions at regional scale with low computing cost. Furthermore, this framework coupling strategy have several perspectives: for example simulating the hydrodynamic behavior of alluvial wetlands, modeling more accurately the impact of climate change on hydrosystems, especially concerning pollutants removal or release by biogeochemical processes, or better assessing the risk of inundations at the regional scale.

Keywords: Stream-aquifer interactions, Hydrology, Hydrogeology, Upscaling, Regional scale, Local scale, EauDyssée platform, river morphology

Résumé court en français

Cette thèse s'inscrit dans le développement de la plateforme EauDyssée de modélisation intégrée des hydrosystèmes régionaux, au sein du bassin pilote de la Seine. L'objectif principal est de contribuer à une meilleure simulation des tirants d'eau à l'échelle régionale afin d'améliorer la simulation des interactions nappe-rivière et de mieux quantifier les niveaux piézométriques dans les aquifères.

La première partie de la thèse vise à évaluer la sensibilité d'un modèle hydraulique à la précision de la description géomorphologique des lits pour identifier le meilleur compromis entre parcimonie et réalisme et identifier les facteurs morphologiques les plus importants pour obtenir une simulation satisfaisante des tirants d'eau à l'échelle régionale. Cette étude est menée sur le Serein (affluent de l'Yonne), entre les stations limnimétriques de Dissangis et

Beaumont, dans un bief bien renseigné (20 sections transversales sur 89 kms). Débits et tirants d'eau sont simulés par le modèle hydraulique HEC-RAS (équations de Saint-Venant 1D), en fonction des apports latéraux simulés par le modèle régional EauDyssée.

Les résultats de cette étude montrent qu'un modèle 1D type Saint-Venant n'est pas adapté à la simulation des écoulements à l'échelle régionale. Nous avons donc développé une méthode de changement d'échelle originale, dans laquelle la modélisation fine des processus hydrauliques à haute résolution permet d'améliorer la représentation des profils d'eau en rivière et les interactions nappe-rivière simulées à l'échelle régionale par le modèle intégré EauDyssée.

Cette méthodologie de changement d'échelle a été validée dans un sous bassin versant de l'Oise d'une superficie de 4500 km^2, pour la période 1990-1995. Nous avons utilisé HEC-RAS pour la modélisation hydraulique d'un tronçon de l'Oise de 188 km, où 420 sections transversales sont disponibles. Le modèle permet d'interpoler des courbes de tarage simulées tous les 200m en moyenne. Ces courbes de tarage sont ensuite projetées sur les mailles rivière du modèle régional EauDyssée (résolution de 1 km), où elles permettent de simuler la fluctuation du niveau d'eau en fonction du débit à l'échelle régionale par EauDyssée. La cote de la surface libre de la rivière définissant sa charge hydraulique, ces fluctuations influencent alors les échanges entre les mailles rivière et les nappes, qui dépendent des gradients de charge verticaux entre rivière et nappe (loi de Darcy).

Ce travail montre l'intérêt de l'approche pour mieux évaluer les interactions nappes-rivières à l'échelle régionale avec un faible coût de calcul. Il offre des perspectives intéressantes pour simuler des processus jusque là négligés par le modèle EauDyssée : élimination de nitrate dans les zones humides qui sont souvent situées à la zone de contact entre les nappes souterraines et la rivière, ou l'impact du changement climatique sur le fonctionnement des hydrosystèmes et plus particulièrement sur l'élimination ou le relarguage de polluants par des

processus biogéochimiques, ainsi que de mieux estimer les risques d'inondation à l'échelle régionale.

Un résumé long en français de la thèse se trouve dans l'appendice B.

Mots clés: Interactions nappe-rivière, hydrologie, hydrogéologie, Changement d'échelle, Plateforme EauDyssée, morphologie des rivières

DEDICATION

This thesis is dedicated to the memory of my mother,

Layla S. Khalil (1952-2009)

ACKNOWLEDGMENTS

This thesis owes its existence to the help, support, and inspiration of many people. It is a pleasure to convey my deep appreciation and gratitude to them all in my humble acknowledgment.

First, I am proud to record that I had the opportunity to work with exceptionally experienced scientists in France.

I would like to express my sincere appreciation and gratitude to my supervisor Dr. Emmanuel Ledoux for his advice and guidance as well as giving me extraordinary experiences through out the work. Above all and the most needed, he provided me unflinching encouragement and support in various ways.

I gratefully acknowledge Dr. Nicolas Flipo for his advice, supervision, and crucial contribution to this work. He always granted me his time even for answering some of my unintelligent questions in the science of hydrology. Nicolas, I am grateful in every possible way and hope to keep up our collaboration in the future.

I am grateful to Dr. Agnès Ducharne for her supervision, patience, enthusiasm as well as her help whenever I was in need during more than three years. I am indebted to her more than she knows.

Many thanks go in particular to Dr. Ludovic Oudin. I am much indebted to Ludovic for his valuable advice in science discussion, supervision and furthermore, using his precious time to read my scientific reports and gave his critical comments about them.

I would like to express my sincere appreciation and gratitude to Dr. Isabelle Braud and Dr. Julio Goncalves for accepting to review my thesis and participate in my thesis jury, I am confident that their review and constructive feedback will enrich this study.

I am indebted to Dr. Jean-Marie Mouchel and Dr. Philippe Belleudy for accepting to be examiners in my thesis jury.

I am indebted to Dr. Florence Habets and Pascal Viennot, who have been a source of support and encouragement over many years. Thank you Florence for supporting me through the modelization phase and helping me better understand the EauDyssée platform.

I am grateful for the data provided by Yan Lacaze and the Direction Régionale de l'Environnement Ile de France (DIREN).

I am also grateful to the members of the UMR Sisyphe and the members of the SHR team of the Center of Geosciences of MINES ParisTech for their support and their comradeship, especially Céline Monteil for her motivating discussions and ideas.

I am thankful for the financial support provided by the PIREN-Seine research program on the Seine basin and the Centre National des Oeuvres Universitaires et Scolaires (CNOUS).

Finally, I would like to express my deepest gratitude for the constant support, understanding and love that I received from my wife and my family during the past years.

TABLE OF CONTENTS

LIST OF TABLES

Page

LIST OF FIGURES

Number *Page*

CHAPTER 1. INTRODUCTION

Accurate simulation of river stage is important for numerous water resources applications such as floodplain management, flood control operations, overtopping frequency, wave time of transfer, average river velocity, water quality and stream-aquifer interactions. In this thesis, we will focus on the importance of accurately simulating river stage for simulating stream-aquifer interactions.

Streams and aquifer units are connected components of the hydrosystem (Winter, 1998), they interact in a variety of physiographic and climatic landscapes. Thus, contamination of one of them commonly affects the other one. Therefore, an understanding of the basic principles of interactions between streams and aquifer units is important for effective management of water resources.

In low flow periods, river flow is usually controlled by stream-aquifer exchange. The magnitude of exchange is governed by the hydraulic properties of aquifer and bed level material as well as the water stage in the river. The accurate determination of water depth during low river flow has an important impact on ecology and biochemical processes.

Interactions between groundwater and streams have been studied since the 1960s (Cooper and Rorabaugh, 1963; Meyboom, 1961; Pinder and Jones, 1969). The increasing concerns in the past few decades over in-stream flows, riparian conditions, Total Maximum Daily Load (TMDL) limits and nitrate contamination have motivated researches to expand the stream aquifer interactions scope to include studies of headwater streams, wetlands, nutrient discharge, climate change, lakes and estuaries (Anderson, 2003; Henderson et al., 2009; Hunt et al., 2008; Smith and Townley, 2002; Smith and Turner, 2001; Walker et al., 2008; Winter, 1995).

The interaction between streams and aquifers is a complex process and depends on many physical factors that are directly related to topography, geology, and climate (Sophocleous, 2002; Winter, 2002). Due to the level of complexity, many modelers have considered limited or no interactions between stream and aquifer units. Therefore, even though specific models provide good results for simulating the water flows, deviations occur when the interactions between these domains become important (Gunduz and Aral, 2005). Furthermore, fluctuations of in-stream water levels are acknowledged to influence the aquifer system to which it is connected and the hydraulic gradients in areas surrounding the stream (Ataie-Ashtianti et al., 1999; Cooper, 1959; Glover, 1959; Reilly and Goodman, 1985; Winter, 1998).

The recognition of those interactions motivated researchers to focus on coupled models (Abbott et al., 1986b; Cunningham and Sinclair, 1979; Freeze, 1971; Graham and Refsgaard, 2001; Gunduz and Aral, 2005; Harbaugh and McDonald, 1996; Ledoux et al., 1984; Markstrom et al., 2008; Morita and Yen, 2002; Pinder and Sauer, 1971; Swain and Wexler, 1996; VanderKwaak, 1999). The aforementioned coupled models simulate stream-aquifer interactions with different levels of complexity. The levels of complexity are based on the type of equations and the spatial dimension (1-D, 2-D or 3-D) used to describe surface water and groundwater flows and on the coupling method of the stream and the aquifer units. Nevertheless, these fully stream-aquifer coupling approaches, endemic to distributed physics-based models, face a number of challenges, such as spatial and temporal scale issues (Kollet and Maxwell, 2006; Loague and Corwin, 2007; Loague and VanderKwaak, 2004; Sudicky et al., 2005; Werner et al., 2006), initial conditions (Noto et al., 2008), absence or inadequacy of measured data to calibrate/control model outputs (Beven and Binley, 1992; Lefebvre et al., 2010; Uhlenbrook et al., 1999), equifinality (Beven, 2006; Beven and Freer, 2001a; Ebel and

Loague, 2006), insufficient computational power and conceptual and numerical difficulties (Jolly and Rassam, 2009).

The main objective of this thesis is to provide a realistic simulation of river stage and discharge in regional scale river networks in order to improve stream-aquifer interactions and potentially better assess piezometric heads as well as exchanged fluxes at this scale. To achieve the aforementioned objectives, the present research focuses on improving coupling methods for stream-aquifer interactions at regional scale basins.

The objectives of this thesis are attained through addressing the following sets of research questions:

- Can a hydrodynamic model provide reliable in-stream discharge and water level simulations with limited morphological data at regional scale?

- Which framework strategy should be implemented to improve stream-aquifer interactions at regional scale?

- What is the local and regional impact of river stage fluctuations on stream-aquifer interactions, the distribution of simulated piezometric heads and the stream-aquifer exchanged flux?

The present work is motivated by the need to perform reliable simulations of river stage and discharge in the Seine regional scale hydro(geo)logical[1] model (Gomez, 2002; Gomez et al.,

[1] Hydro(geo)logical modeling: It is a hydrosystem modeling tool that explicitly simulates the hydrogeological behavior of the aquifer system. The simulation of the aquifer system is physically based. We thus exclude from the hydro(geo)logical model models that simulate aquifer system with a conceptual model such as SWAT (Arnold et al., 1993).

2003; Ledoux et al., 2007) in order to improve stream-aquifer interactions and better assess piezometric head distributions over time as well as exchanged fluxes between the river network and the aquifer units. In the initial version of the Seine model, in-stream water levels, that are obtained from a Digital Elevation Model (DEM), are imposed as constant boundary conditions along the Seine River network. In consequence, these in-stream water levels do not fluctuate as function of the hydrological event or the discharge routed by the river network. But as exchanged fluxes are controlled by in-stream water levels, these in-stream water levels are of primary importance for simulating stream-aquifer interactions. Additionally, in-stream water levels are of importance on river average velocity, inundations, low flows and water quality. In this study we focus on stream-aquifer interactions, with the objective to improve the Seine model for better taking into account stream-aquifer interactions.

This thesis consists of six chapters in addition to this introductory chapter. In chapter two, a synopsis of surface routing and stream-aquifer modeling techniques at multiple scales is presented. In particular, this chapter provides an overview of available hydrologic and hydraulic routing techniques at multi scales as well as an overview of selected hydrologic problems investigated using models that fully couple stream-aquifer interactions. Furthermore, the mechanisms of stream-aquifer interactions as they affect infiltration and exfiltration processes are presented.

Chapter three is devoted to presenting the different models composing the initial version of the hydrological modeling platform EauDyssée

Chapter four of this thesis aims at establishing whether a reliable hydraulic routing model can be developed based on limited morphological data at regional scale. A wide variety of "what if" river geometry scenarios are explored to determine the most appropriate river representation geometry in areas where cross sections surveys are not available.

Chapter five is devoted to present the strategy we developed to improve modeling of stream-aquifer interactions in the regional hydrological model EauDyssée. The developed strategy is validated in the Oise River basin, sub basin of the Seine River. The impacts of resulting river stage fluctuations on stream-aquifer interactions, exfiltration-infiltration rates and piezometric head distribution are demonstrated.

Finally, chapter six represents the summary of the work and some suggestions for further research.

Introduction en Français

La simulation de niveau d'eau en rivière est importante pour les applications des ressources en eau, telles que la gestion des plaines inondables, la prévention contre les inondations, les fréquences de débordements, la vitesse moyenne de la rivière, la qualité de l'eau et les interactions nappe-rivière. Dans cette thèse, nous nous focalisons sur l'importance de la précision de niveau d'eau en rivière pour simuler les interactions nappe-rivière.

Les nappes et les rivières sont des composantes connectées de l'hydrosystème. Elles interagissent de manière variée selon les conditions hydrologiques et climatiques (Winter, 1998). En conséquence, la contamination de l'une des deux a un impact important sur le système hydro(géo)logique. Pour cela, une meilleure compréhension des principes des interactions nappe-rivière est nécessaire pour une gestion efficace des ressources en eau.

Les interactions nappe-rivière ont été étudiées depuis les années 1960 (Cooper et Rorabaugh, 1963; Meyboom, 1961; Pinder et Jones, 1969).

L'importance croissante de caractériser ou quantifier la qualité des eaux et l'impact de la contamination de surface ou souterraine par des polluants comme les nitrates a conduit les chercheurs à développer des modèles couplés (Anderson, 2003; Henderson et al., 2009; Hunt

et al., 2008; Smith et Townley, 2002; Smith et Turner, 2001; Walker et al., 2008; d'hiver, 1995).

Les interactions nappe-rivière sont un processus complexe et elles dépendent de nombreux facteurs physiques qui sont directement liés à la topographie, à la géologie et au climat (Sophocleous, 2002; Winter, 2002). En raison du niveau de complexité, de nombreux modèles considèrent peu ou pas d'interactions entre les écoulements surface et souterrains. Par conséquent, même si certains modèles donnent de bons résultats pour la simulation de l'écoulement de l'eau, des écarts se produisent lorsque les interactions entre les domaines de surface et souterrain deviennent importantes (Gunduz et Aral, 2005).

La reconnaissance de ces interactions a motivé les chercheurs à se focaliser sur les modèles couplés (Abbott et al., 1986; Cunningham et Sinclair, 1979; Freeze, 1971; Graham et Refsgaard, 2001; Gunduz et Aral, 2005; Harbaugh et McDonald, 1996; Ledoux et al., 1984; Markstrom et al., 2008; Morita et Yen, 2002; Pinder et Sauer, 1971; Swain et Wexler, 1996; VanderKwaak, 1999). Ces modèles couplés simulent les interactions nappe-rivière avec différents niveaux de complexité. En général, les niveaux de complexité sont basés sur le type d'équations et la discrétisation spatiale (1-D, 2-D ou 3-D) utilisée pour décrire les écoulements ainsi que la méthode de couplage.

Toutefois, les modélisation nappe-rivière font face à un certain nombre de défis : l'échelle (Kollet and Maxwell, 2006; Loague and Corwin, 2007; Loague and VanderKwaak, 2004; Sudicky et al., 2005; Werner et al., 2006), les conditions initiales (Noto et al., 2008), l'absence ou l'insuffisance des données de mesure pour valider le modèle (Beven and Binley, 1992; Lefebvre et al., 2010; Uhlenbrook et al., 1999), l'équifinalité (Beven, 2006; Beven and Freer, 2001a; Ebel and Loague, 2006) et les problèmes conceptuels ou numériques (Jolly and Rassam, 2009).

Le présent travail a pour but d'effectuer des simulations précises et fiables de tirants d'eau et de débit à l'échelle régionale du réseau hydrographique de la Seine (Gomez, 2002; Gomez et al., 2003; Ledoux et al., 2007) afin d'améliorer la simulation des interactions nappe-rivière et de mieux quantifier les niveaux piézométriques dans les aquifères.

Cette étude est motivée par la version initiale du modèle Seine dans laquelle les échanges nappe-rivière sont simulés avec une cote d'eau imposée en rivière obtenue à partir d'un Modèle Numérique de Terrain (MNT). En conséquence ces cotes d'eau ne fluctuent pas en fonction de l'événement hydrologique ou du débit en rivière. En revanche, les dynamiques des fluctuations des cotes en rivière ont des impacts important sur les écoulements en rivière, la vitesse moyenne d'écoulement, les fréquences de débordements et la simulation des interactions nappe-rivière.

Pour attendre les objectifs de cette thèse, nous cherchons à répondre aux questions scientifiques suivantes :

- Quelle est la capacité d'un modèle hydraulique à géométrie simplifiée pour simuler les niveaux d'eau et les débits à l'échelle régionale ?
- Comment faire le lien entre un modèle hydraulique local et un modèle hydrologique régional ?
- Quel est l'impact local et régional de la fluctuation des niveaux d'eau en rivière sur les niveaux piézométriques et les échanges nappe-rivière ?

Le présent mémoire est structuré en six chapitres:

Le Chapitre 1 présente les objectifs généraux dans lesquels s'inscrit cette étude ainsi que la problématique qui motive cette étude.

Le Chapitre 2 est consacré à la révision des différents modèles de routage de surface hydraulique et hydrologique, ainsi qu'un nombre de problèmes hydro(géo)logiques qui ont

été abordés en utilisant des modèles nappe-rivière couplés. Les mécanismes des interactions nappe-rivière, que ce soit les processus d'infiltration ou d'alimentation de la rivière par la nappe, sont également décrits.

Le chapitre 3 décrit les différents composants qui composent la version initiale de la plateforme de modélisation intégrée des hydrosystèmes EauDyssée.

Le Chapitre 4 vise à évaluer la sensibilité d'un modèle hydraulique type Saint-Venant à la précision de la description géomorphologique des lits et à la géométrie réduite afin d'identifier le meilleur compromis entre parcimonie et réalisme et d'identifier les facteurs morphologiques les plus importants pour obtenir une simulation satisfaisante des hauteurs d'eau. Les tests de sensibilités ont été réalisés sur les biefs du Serein (affluent de l'Yonne) entre Dissangis et Beaumont.

Dans chapitre 5 nous avons développé une méthode de changement d'échelle dans laquelle la modélisation fine des processus hydrauliques à haute résolution permet d'améliorer la représentation des profils d'eau en rivière et les interactions nappe-rivière simulées à l'échelle régionale. Cette méthode a été validée dans le bassin versant de l'Oise. L'impact de la fluctuation des niveaux en rivière sur les isopièzes a été analysé par rapport à un état de référence pour lequel les niveaux en rivière sont fixes.

Le dernier chapitre présente les conclusions et les recommandations qui ont été tirées des cette étude.

CHAPTER 2. INTEGRATED MODELING OF HYDROSYSTEMS: A FOCUS ON STREAM-AQUIFER INTERACTIONS

Résumé en Français

Dans ce chapitre, nous avons réalisé une revue des différentes techniques de modélisation hydrologiques, hydrauliques et hydro(geo)logique à des échelles multiples, ainsi qu'un nombre de problèmes hydro(géo)logiques qui ont été abordés en utilisant des modèles nappe-rivière couplés. Les mécanismes des interactions nappe-rivière, que ce soit les processus d'infiltration ou d'alimentation de la rivière par la nappe, sont également décrits.

L'objectif principal de cette revue est d'identifier les avantages et les limites de chaque modèle ainsi que les principaux défis à relever dans la discipline de la modélisation nappe-rivière afin d'avoir une vision claire sur les besoins et de compléter la gamme d'applicabilité des modèles nappe-rivière à l'échelle locale et régionale.

Les différentes techniques qui ont été revues montrent que le choix final d'un modèle est un compromis entre un certain nombre de facteurs tels que la précision requise, le type et la disponibilité des données, le coût de calcul, l'importance de simuler les niveaux d'eau dans la rivière, l'échelle spatiale et temporelle. Nous pouvons conclure qu'il n'y a pas de modèle supérieur et que le choix d'une méthodologie dépend du problème hydrologique en question.

L'étude illustre également l'importance de modèles hydrologiques capables de simuler les échanges nappe-rivière pour mener des études interdisciplinaires en sciences hydrologiques. Le choix d'une technique de modélisation nappe-rivière est fonction de l'objectif de l'application et de la capacité du modèle pour simuler certains aspects du problème scientifique.

Abstract

This chapter provides first an overview and background information of available hydrodynamic and hydrological surface routing techniques, followed by the review of different hydr(geo)logical models that integrate stream and aquifer models at multi scale with their advantages and limitations. This chapter also provides an overview of selected hydrologic problems investigated using models that fully couple stream-aquifer flow. Furthermore, the mechanisms of interactions between streams and aquifer units as they affect infiltration and exfiltration processes are outlined.

The main objective of this review is to identify the capabilities and limitations of each modeling methodolgy as well as the main challenges faced in the discipline of stream-aquifer modeling in order to come up with a clear vision on major necessities required to complement stream-aquifer model's range of applicability at local and regional scale. This clear vision will eventually lead to identifying an optimal framework strategy to improve stream-aquifer and basin hydrological behavior at different scales as well as expanding the domains of application.

The modeling techniques reviewed herein demonstrate that the final choice of a routing model is a trade off between a number of factors such as required accuracy, type and availability of data, available computational facilities, extent of required information on water levels, temporal and spatial scale. Having reached this conclusion, there is no universal routing model, as choosing the appropriate routing approach depends to a great extent on the questioned hydrological problem. The review also illustrates the importance of hydrologic models capable of simulating coupled stream-aquifer water flow for conducting interdisciplinary investigations in hydrologic sciences. The rational for selecting a particular stream-aquifer modeling technique is function of the application's objective and of the model's suitability for modeling key aspects of the problem at hand.

Tab. 2.1 Chapter 2 table of symbols

Symbol	Description	Dimension
A	cross sectional area	$[L^2]$
B	bottom width	[L]
C	flood wave celerity	$[L.T^{-1}]$
c_0, c_1, c_2, and c_3	Parameters. of Muskingum-Cunge equation	[Dimensionless]
G	acceleration due to gravity	$[L.T^{-2}]$
H	In-stream water depth	[L]
I	Inflow discharge in the Muskingum scheme	$[L_3.T^{-1}]$
K	Muskingum transfer time between two adjacent river cells	[T]
N	Manning's roughness coefficient	$[T.L^{-1/3}]$
O	Outflow discharge in the Muskingum scheme	$[L^3T^{-1]}$
Q	Discharge	$[L^3.T^{-1}]$
q_l	lateral inflow per unit length	$[L^3.T^{-1}.L^{-1}]$
R	Hydraulic radius	[L]
Re	Reynolds number.	[Dimensionless]
S_f	friction slope (calculated using the Manning formula)	[Dimensionless]
S_o	bottom slope	[Dimensionless]
T	Time	[T]
u, v, w	Velocity components in the x, y, z directions	$[L.T^{-1}]$
V	Velocity	$[L.T^{-1}]$
A	Muskingum weighting factor	[Dimensionless]
x, y, z	Coordinates	[Dimensionless]
ΔS	change in storage within the reach during	$[L^3]$

2.1 Introduction

A wide variety of methods exist to quantify stream-aquifer interactions, including direct measurements, mass balance approaches, heat tracing and numerical methods (Kalbus et al., 2006).

Direct measurements can be carried out by using seepage meters coupled to mass balance (Landon et al., 2001) that are simple and relatively inexpensive, but a significant number of measurements are required to adequately characterize a given stream.

Mass balance approaches include differential stream gauging, hydrograph separation, solute and environmental tracers (Kalbus et al., 2006).

Heat tracing techniques assume that the temperature of ground water is more stable than that of surface water. Gaining reaches are thus characterized by relatively constant sediment

temperatures, where as losing reaches tend to present significant variability over short periods of time (Constantz et al., 2001).

A recent geophysical method for quantifying stream-aquifer exchanged fluxes at the local scale uses Fiber-optic distributed temperature sensing (FO-DTS) (Day-Lewis and Lane, 2006; Selker et al., 2006; Vogt et al., 2010).

At the regional scale, the aforementioned methods are not feasible to apply because they require the availability of consistent data along the river which is not always accessible at this scale.

This review will be focused on stream-aquifer interactions modeling based on numerical methods in order to identify the capabilities and limitations of each modeling methodology as well as the necessities required to complement stream-aquifer model's range of applicability at local and regional scale. The stream-aquifer interactions review follows a review on surface routing models which are of primary importance for simulating stream-aquifer interactions.

2.2 Surface routing modeling

Surface routing methodologies can be classified into two categories: (1) hydrodynamic routing methodologies; (2) hydrological routing methodologies (Arora et al., 2001).

In general, hydrodynamic routing methodologies are based on the 1D Saint-Venant equations (Barré de Saint-Venant, 1871). The Saint-Venant formulation includes a continuity equation (Eq. 2.5) which describes the balance between input, storage and output in a section of river, and a momentum equation (Eq. 2.6) which relates the change in momentum to the applied forces (Bathurst, 1988; Becker and Serban, 1990; Liggett, 1975).

The hydrological routing approaches are based on the continuity equation while empirical relationships are used to replace the momentum equation (Carter, 1960; Cunge, 1969; Dooge

et al., 1982; Sherman, 1932; Wilson, 1990). Examples of hydrological routing approaches include the Muskingum, Muskinum-Cunge and Unit Hydrograph methods.

A number of routing methodologies are reviewed in the following sections. These routing methodologies vary from fine scale to large scale applications.

2.2.1 Hydrodynamic routing modeling techniques

Navier-Stokes equations

The Navier-Stokes equations (Navier, 1822) of fluid are a formulation of Newton's law of motion for a continuous distribution of matter in the fluid state, they are central to applied research (Doering and Gibbon, 1995). The Navier-Stokes equations are a set of nonlinear partial differential equations that describe the flow of fluids. These equations are used to model the movement of air in the atmosphere, river hydraulics, ocean currents, water flow in pipes, as well as many other fluid flow phenomena.

The Navier-Stokes equations are based on the continuity equation (Eq. 2.1) and the momentum equation in the three dimensions x, y, z (Eq. 2.2, Eq. 2.3, Eq. 2.4)

$$\frac{\partial \rho}{\partial t} + \frac{\partial (\rho u)}{\partial x} + \frac{\partial (\rho v)}{\partial y} + \frac{\partial (\rho w)}{\partial z} = 0 \qquad \text{Eq. 2.1}$$

$$\frac{\partial (\rho u)}{\partial t} + \frac{\partial (\rho u^2)}{\partial x} + \frac{\partial (\rho uv)}{\partial y} + \frac{\partial (\rho uw)}{\partial z} = -\frac{\partial p}{\partial x} + \frac{1}{Re_r}\left[\frac{\partial \tau_{xx}}{\partial x} + \frac{\partial \tau_{xy}}{\partial y} + \frac{\partial \tau_{xz}}{\partial z}\right] \qquad \text{Eq. 2.2}$$

$$\frac{\partial (\rho v)}{\partial t} + \frac{\partial (\rho uv)}{\partial x} + \frac{\partial (\rho v^2)}{\partial y} + \frac{\partial (\rho vw)}{\partial z} = -\frac{\partial p}{\partial y} + \frac{1}{Re_r}\left[\frac{\partial \tau_{xy}}{\partial x} + \frac{\partial \tau_{yy}}{\partial y} + \frac{\partial \tau_{yz}}{\partial z}\right] \qquad \text{Eq. 2.3}$$

$$\frac{\partial (\rho w)}{\partial t} + \frac{\partial (\rho uw)}{\partial x} + \frac{\partial (\rho vw)}{\partial y} + \frac{\partial (\rho w^2)}{\partial z} = -\frac{\partial p}{\partial z} + \frac{1}{Re_r}\left[\frac{\partial \tau_{xz}}{\partial x} + \frac{\partial \tau_{yz}}{\partial y} + \frac{\partial \tau_{zz}}{\partial z}\right] \qquad \text{Eq. 2.4}$$

Where *x, y, z* are the coordinates, *t* is time, *p* is pressure, *u, v, w* are velocity components, ρ is density, τ is stress and R_e is the Reynolds number.

A number of complex models to simulate river flow using the Navier-Stokes equations may be found in literature (Abbott, 1979; Bradford and Katopodes, 1998; Naot and Rodi, 1982; Spanoudaki et al., 2009). However, these models that use the complete set of 3D Navier-Stokes equations are very complex and thus require a substantial amount of data and computer memory in order to obtain accurate solutions (Ma and Sikorski, 1993). The aforementioned raisons lead hydrodynamic modelers to use the 1D Saint-Venant equations or it's approximations in river flow modeling.

Saint-Venant equations

In 1843 Barré de Saint-Venant published a derivation of the incompressible Navier-Stokes equations that applies to both laminar and turbulent flows. The 1D Saint-Venant equations based on the continuity (Eq. 2.5) and momentum (Eq. 2.6) equations formalize the main concepts of river hydrodynamic modeling.

The basic derivation assumptions of the Saint Venant Equations (Abbott, 1979; Chow, 1959) are the following:

• The flow is one-dimensional, i.e. the velocity is uniform over the cross-section and the water level across the section is represented by a horizontal line.

• The streamline curvature is small and the vertical accelerations are negligible, so pressure can be considered as hydrostatic.

• The effects of boundary friction and turbulence can be accounted for through resistance laws analogous to those used for steady state flow.

• The average channel bed slope is small so that the cosine of the angle it makes with the horizontal may be replaced by unity.

The aforementioned hypotheses do not impose any restriction on the shape of the cross-section of the channel and on its variation along the channel axis.

The full derivation of the basic Saint-Venant equations can be found in a number of reviews (Chow, 1959; Cunge et al., 1980; Graff and Altinakar, 1996; Strelkoff, 1970).

$$\frac{\partial Q}{\partial x} + \frac{\partial A}{\partial t} - q_l = 0 \qquad \text{Eq. 2.5}$$

$$\underset{\mathbf{I}}{\frac{\partial V}{\partial t}} + \underset{\mathbf{II}}{V\frac{\partial V}{\partial x}} + \underset{\mathbf{III}}{g\frac{\partial h}{\partial x}} - \underset{\mathbf{IV}}{g\left(S_f - S_o\right)} = 0 \qquad \text{Eq. 2.6}$$

Where Q is discharge [$L^3.T^{-1}$], A is cross sectional area [L^2], x is distance along the longitudinal axes of the channel or floodplain [L], t is Time [T], q_l is lateral inflow per unit length [$L^3.T^{-1}.L^{-1}$], V is velocity [$L.T^{-1}$], h_r is flow depth [L] and g is acceleration due to gravity [$L.T^{-2}$], S_o is bottom slope (dimensionless), S_f is friction slope (dimensionless).

S_f is calculated using the Manning formula:

$$S_f = \left[\frac{nQ}{AR^{2/3}}\right]^2 \qquad \text{Eq. 2.7}$$

Where n is Manning's roughness coefficient [$TL^{-1/3}$], R is Hydraulic radius [L].

Term **I** represents the local inertia and reflects unsteady flow, term **II** represents the convective inertia and reflects both spatial variation of the flow ($\partial Q/\partial x$) and longitudinal change in the cross-section area, term **III** represents the pressure differential and reflects the change in depth in the longitudinal direction and term **IV** accounts for friction and bed slopes. Hydrodynamic models that include all the momentum terms of the Saint-Venant equation are called dynamic wave models.

Many numerical schemes have been used to solve the 1D Saint-Venant equations, these methods include explicit finite difference (Stoker, 1957b), method of characteristics (Abbott, 1966), finite differences methods (Cunge et al., 1980), and finite element schemes (Fread, 1985; Richard, 1976). Examples of widely used Saint-Venant models include Mike-11 (DHI, 2001), ISIS (Wallingford, 1997), FLDWAV (Fread and Lewis, 1998) and HEC-RAS (HEC, 2002).

Hydrodynamic models based on the complete Saint-Venant equations have the capability of accurately simulating the widest spectrum of waterway characteristics. Moreover, the calibration process is quite evident since the Saint-Venant hydraulic model contains only one parameter (Manning's roughness coefficient). Other advantages for using the full Saint-Venant formula are when downstream backwater effects are present, significant tributary inflows, or when upstream propagation of wave can occur from large tides and storm surges.

At large scale applications, one of the major challenges in hydrodynamic routing models based on the Saint-Venant equations is the lack of accurate data in the channel network such as channel geometry, slope, length, etc. That being said, only one reference was found with regards to the impact of degradation or simplification of channel geometry on the performance of the model (Hicks, 1996). This particular aspect will be addressed in chapters 3 of this thesis. Other limitations of the Saint-Venant equations include sharp discontinuities, such as the transition from subcritical flow to critical flow that can only be solved with a few numerical methods (Flipo, 2005).

The computational cost and scale factors motivated researchers to use simplified forms of the momentum equation (Eq. 2.6). Depending on which terms of the momentum equation terms are neglected, hydraulic models can be classified in Tab. 2.2 (Ponce and Simons, 1977). The most commonly simplified representations of the Saint-Venant equations are the kinematic

wave and the diffusive wave approximations. Hereafter only these two formulations are presented.

Tab. 2.2 Terms of the Saint-Venant momentum equation (Eq. 2.6) used in hydraulic modeling techniques

Hydraulic	**Considered momentum equation**	**References**
Dynamic wave	**I, II, III, IV**	(Fread and Lewis, 1998; HEC, 2002; Stoker, 1957a)
Diffusive wave	**III, IV**	(Dooge, 1973; Hayami, 1951; Lighthill and Whitham, 1955; Todini and Bossi, 1986)
Kinematic wave	**IV**	(Beven et al., 1987; Graham and Refsgaard, 2001; Hussein and Schwartz, 2003; Leavesley et al., 1983; Linsley, 1971; Wooding, 1965; Woolhiser and Liggett, 1967; Woolhiser et al., 1990b)
Steady dynamic wave	**II, III, IV**	(Tsai, 2003)
Gravity waves	**I, II, III**	(Gregory et al., 1998)

Diffusion wave equation

A simplified approximation of the Saint-Venant formulation combines the spatial derivative from the momentum equation with the continuity equation, which results in a second derivative term in the continuity equation (Dooge, 1973; Hayami, 1951; Lighthill and Whitham, 1955; Todini and Bossi, 1986). The second derivative term in the continuity equation causes the flood wave to spread upstream slightly and is commonly referred to as a diffusion analogy for the dynamic component of the momentum equation. The simplified form of the momentum equation (Eq. 2.6) is:

$$s_f - \frac{\partial h}{\partial x} = 0 \qquad \text{Eq. 2.8}$$

The diffusion wave equations are efficiently solved with a four point centered implicit finite difference solution techniques (Brankensiek, 1965) or explicit finite difference solution techniques (Harder and Armacost, 1966). The slope of water surface allows the diffusion

model to describe the attenuation (diffusion effect) of the flood at downstream extremity of the reach. It does not use the inertial terms of the momentum equation, therefore it is limited to moderately slow rising flood waves in channels of rather uniform geometry. An example on this approach is the surface-water flow model DAFLOW (Jobson and Harbaugh, 1999) that was coupled later on with MODFLOW (Harbaugh and McDonald, 1996).

Kinematic wave equation

The kinematic wave equation is also a simplified approximation of the Saint Venant equations. It approximates the Saint-Venant equations for computing flow through rectangular or non-prismatic channels. The kinematic-wave equation for in-stream flow routing can be written (Lighthill and Whitham, 1955):

$$\frac{\partial Q}{\partial x} + \frac{\partial A}{\partial t} = q_l \qquad \text{Eq. 2.9}$$

The kinematic wave approximation neglects the dynamic component of the flow which is represented by the derivative terms in the more complete form of the Saint-Venant momentum equation. It assumes that gravitational forces are balanced by frictional forces such that:

$$S_o = S_f \qquad \text{Eq. 2.10}$$

The kinematic wave models are widely used in applications to overland flow routing of runoff generated by precipitation (Beven et al., 1987; Graham and Refsgaard, 2001; Hussein and Schwartz, 2003; Leavesley et al., 1983; Linsley, 1971; Wooding, 1965; Woolhiser and Liggett, 1967; Woolhiser et al., 1990b). However, in theory this type of modeling should be limited to steep rivers applications where backwater effects are insignificant because flow disturbances only propagate in the downstream direction.

2.2.2 Hydrological routing modeling techniques

Hydrological routing techniques have been and continue to be an important tool to better understand the dynamical interactions within the water cycle. It is an essential component of integrated water resources management involving environment and ecology.

Regional scale hydrological modeling routing techniques have been used in a number of applications, for instance:

1- Integrated basin hydrology: Runoff Routing provides a basis for comparing and validating estimates of streamflow with observed hydrograph data. As most variables describing the state of the surface are not directly observable, river discharge is an appropriate measurement to assess model qualities (Nijssen et al., 2001).

2- Export from continental surface to the sea: The simulated fresh water flux into the oceans alters their salinity and may affect the thermohaline circulation (Wang et al., 1999; Wijffels et al., 1992).

3- Climate changes scenarios: Estimates of river discharge from climate change simulations can also be used to assess the impact of climate change on water resources and the hydrology of the major river basins (Arora et al., 2001; Milly et al., 2005; Oki and Kanae, 2006).

4- Influence of river discharge on freshwater ecosystems (Azevedo et al., 2010; Carpenter et al., 1992).

In general, hydrological routing approaches are based on the conservation of mass (Eq. 2.11) coupled with empirical relationships replacing the momentum equation.

Additionally, all the geomorphological characteristics and the hydraulic properties of river reaches are lumped into a number of more or less conceptual model parameters.

$$I - O = \frac{\Delta S}{\Delta t} \qquad \text{Eq. 2.11}$$

Where I and O are the upstream and downstream discharge respectively [$L^3.T^{-1}$], and ΔS [L^3] is the change in storage within the reach during a Δt time increment [T].

At the regional scale, the majority of hydrological models uses simplified hydrological techniques for flow routing that are generally based on linear/non-linear reservoir or Muskingum type routing methods (McCarthy, 1938), which is considered as one of the most popular hydrological routing approaches. Other examples include the cascade of linear reservoirs (Nash, 1958) and the Muskingum-Cunge (MC) approach (Cunge, 1969). Hydrological storage routing models offer the advantages of simplicity when backwater effects are insignificant. These hydrological models however do not simulate the corresponding in-stream water levels which are essential to accurately simulate the stream-aquifer interactions based on Darcy's equation.

The majority of regional scale hydrological models either assume a constant and uniform velocity (Coe, 1998; Miller et al., 1994; Oki and Sud, 1998) or constant flow velocities parameterized to the topographic gradient (Ducharne et al., 2003; Hagemann and Dumenil, 1998).

Muskingum method

The Muskingum channel routing method is based on two equations (Linsley et al., 1982). The first is the continuity equation or conservation of mass.

$$\frac{I_1 + I_2}{2}\Delta t - \frac{O_1 + O_2}{2}\Delta t = S_2 - S_1 \qquad \text{Eq. 2.12}$$

Where I_1 and I_2 are inflow discharges at time 1 and time 2, O_1 and O_2 are outflow discharges at time 1 and time 2, Δt is time difference between time 1 and time 2, S_1 and S_2 are values of reach storage at time 1 and time 2.

The second equation is a relationship between storage, inflow, and outflow of the reach.

$$S = k(\alpha I + (I - \alpha)O)$$ Eq. 2.13

where S is the reach storage, I = inflow discharge, O = outflow discharge, k is storage coefficient, α is weighting factor.

Combining equations 2.12 and 2.13 and simplifying results (Ponce and Yevjevich, 1978):

$$O_2 = C_1 I_1 + C_2 I_2 + C_3 O_1$$ Eq. 2.14

Where: $C_1 = (\Delta t / k) + 2\alpha) / C_0$ Eq. 2.15

$$C_2 = (\Delta t / k) - 2\alpha) / C_0$$ Eq. 2.16

$$C_3 = (2(1 - \alpha) - \Delta t / k) / C_0$$ Eq. 2.17

$$C_0 = \Delta t/k + 2(1 - \alpha)$$ Eq. 2.18

C_0, C_1, C_2, and C_3 are dimensionless parameters.

The Muskingum models are widely used for river routing applications because of the modest data requirement (Aldama, 1990; Birkhead and James, 2002; David et al., 2010; Drobot and Corbus, 1998; Gill, 1992; Tang et al., 1999).

The application of the Muskingum model to river and channel flood routing may have some limitations because of its inherent assumption of a linear relationship between channel storage and weighted flow (Mohan, 1997). Additionally it does not compute in-stream water levels associated with simulated discharge.

Muskingum-Cunge method

Cunge (1969) developed equations to estimate k and α from hydraulic properties of the reach. The mathematical derivation is condensed and presented by Ponce (1981). The equations for k and α Muskingum parameters are:

$$\alpha = \frac{1}{2}\left(1 - \frac{Q}{BS_O c\Delta x}\right) \quad \text{Eq. 2. 19}$$

$$k = \Delta x / c \quad \text{Eq. 2. 20}$$

Where c is flood wave celerity, Δx = distance increment, α is weighting factor, B is bottom width or average width, S_0 is bed slope.

The Muskingum-Cunge method have been widely applied for discharge routing albeit mass balance problems have been reported in several studies (Koussis, 1983; Perumal et al., 2001; Ponce and Chaganti, 1994; Ponce and Yevjevich, 1978; Tang et al., 1999; Todini, 2007).

2.3 Stream-aquifer modeling

2.3.1 Stream-aquifer connectivity and exchange directions

The streams and aquifer units are hydraulically connected (Winter, 1998). Their interactions are complex, difficult to measure, and affected by natural processes and human activities (Sophocleous, 2002; Winter, 1995). Stream-aquifer interactions occur in different landscapes and environments. Streamflow gain or loss can be persistent along a hydraulic year what means that the stream is either always gaining water from aquifer units (exfiltration process) or losing water towards aquifer units (infiltration process). In other environments, flow direction can vary along a stream, some reaches infiltrate towards aquifer units when the water table altitude in the vicinity of the reach is lower than the altitude of the in-stream water level while other reaches gain water from aquifer units when the altitude of the water table in the vicinity of the reach is higher than the altitude of the stream-water surface (Fig. 2.1). Furthermore, flow direction can change within a timeframe as a result of individual storms, rapid snowmelt, release of water and temporary flood peaks moving downwards the stream.

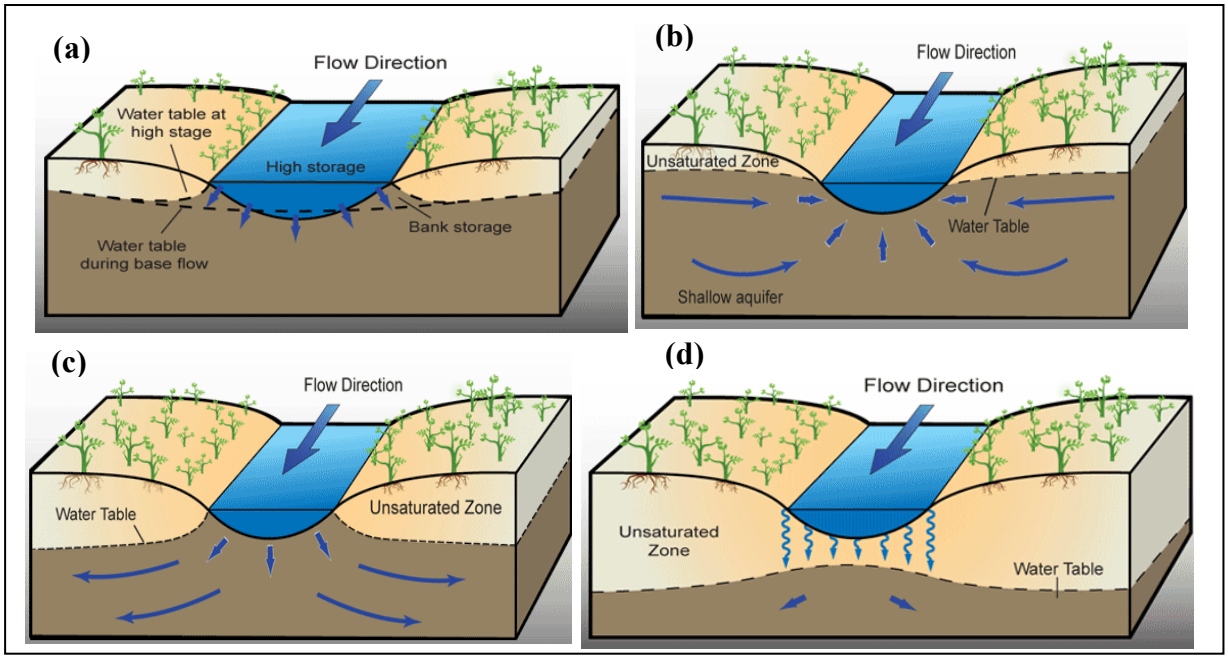

Fig. 2.1 (a) a contiguous fluctuating stream, with stream gaining during low-stage period and losing during high-stage period, (b) a gaining stream where in-stream water levels are lower than the surrounding watertable, (c) a contiguous losing stream, (d) a perched losing stream (graphics from Winter et al, 1998).

To summarize, stream-aquifer interactions connectivity can be classified on the basis of several key aspects outlined in Fig. 2.2.

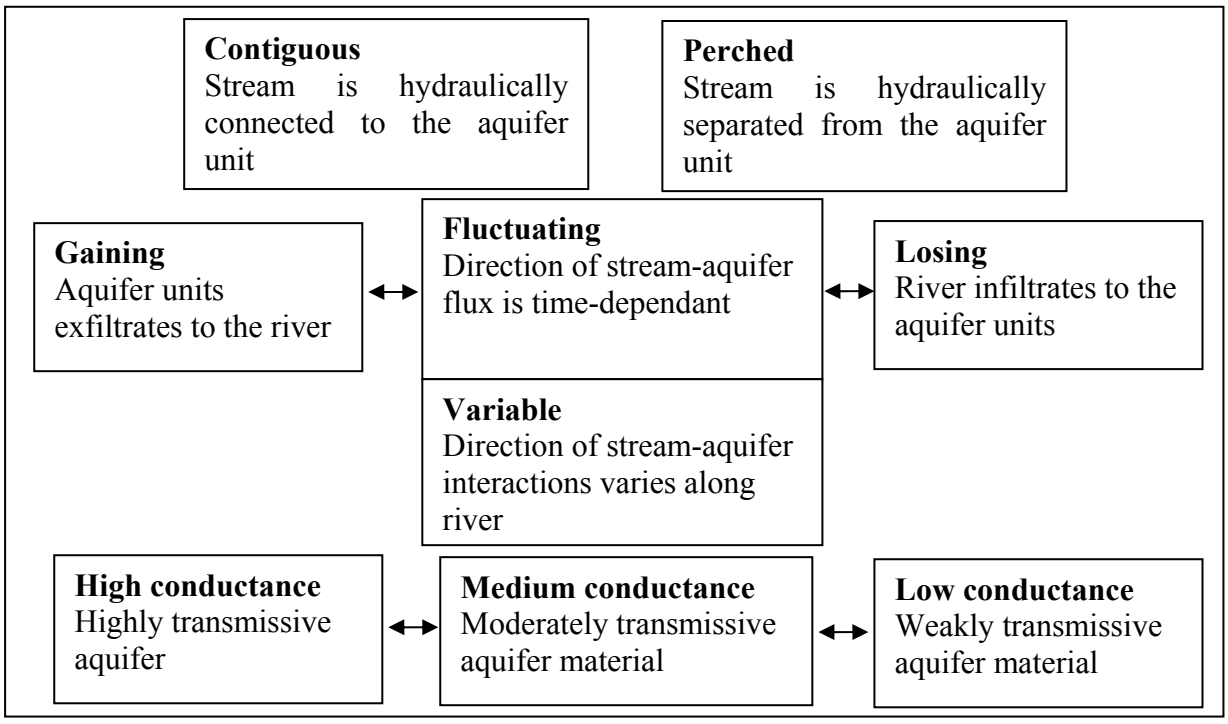

Fig. 2.2 Stream-aquifer categories of connectivity

In this framework, stream-aquifer interactions have been the focus of a number of studies, many of which have focused on 1D vertical river-aquifer exchange: either as groundwater sustaining base flow in gaining streams or as streamflow recharging groundwater in losing streams (Baillie et al., 2007; Cox and Stephens, 1988; Flipo et al., 2005; Gillespie and Perry, 1988; Goodrich et al., 1997; Harrington et al., 2002; Korkmaz et al., 2009; Ledoux et al., 1984; McDonnell et al., 1991; Pearce et al., 1986; Peters and Ratcliffe, 1998; Plummer et al., 2004; Ponce et al., 1999; Stephens, 1988; Waichler and Wigmosta, 2004).

Few other studies have shown that two-way exchanges have substantial implications for both water quantity and quality, including nitrate concentrations (Squillace, 1996; Whitaker, 2000). This two-way exchange process might occur in different sections of the river network and more importantly, a given river reach may be losing during high flow then suddenly becoming gaining as flow declines and the hydraulic gradient shifts towards the channel (Rushton, 2007; Saleh et al., 2010).

2.3.2 Importance of coupled stream-aquifer models for interdisciplinary investigations in hydrologic sciences

Stream-aquifer modeling tools have evolved rapidly in recent years (Jones et al., 2006; Panday and Huyakorn, 2004; Werner et al., 2006). Coupled hydro(geo)logical models capable of simulating stream-aquifer interactions are increasingly used to examine problems in hydrologic sciences (Ebel et al., 2009). Stream-aquifer coupling have enlarged visions on interdisciplinary investigations in hydrologic sciences (Loague et al., 2006).

It permitted to address scientific problems that were difficult to measure or observe, such as the quantification of flood recharge along river networks and how this compares to

phreatophyte[2] transpiration and groundwater exfiltration to the river (Morin et al., 2009), agricultural practices and scenarios related to nitrate contamination (Flipo et al., 2007a; Ledoux et al., 2007). A number of selected hydrologic problems addressed using models that fully couple stream-aquifer flow are listed in Tab. 2.3.

It also permitted to better understand where flood recharge is spatially highest along the river, and to characterize the temporal change after floods.

In these coupling techniques hydrodynamic surface routing models using the Saint-Venant equations require high resolution input data to parameterize the hydraulic model, which is usually not available in large scale applications.

To overcome this limitation, modelers use simplified hydraulic or hydrological routing techniques, where convective and local acceleration terms are neglected. This reduces the accuracy of in-stream water levels estimations when compared to methods that use the 1D Saint-Venant equations and eventually impacts the accuracy of stream-aquifer interactions.

[2] Phreatophyte is a deep-rooted plant that obtains a significant portion of the water that it needs from the phreatic zone (zone of saturation) or the capillary fringe above the phreatic zone.

Tab. 2.3 Selected hydrologic problems addressed using coupled stream-aquifer models

Area of interest	**References**
Agricultural practices	(Ledoux et al., 2007; Schoups et al., 2005)
Atmosphere–subsurface water and energy fluxes	(Maxwell and Miller, 2005)
Chemical and isotopic signatures	(Baillie et al., 2007; Squillace, 1996; Whitaker, 2000)
Contributions of aquifer units to surface flow and/or surface infiltration to aquifer units	(Baillie et al., 2007; Cox and Stephens, 1988; Gillespie and Perry, 1988; Goodrich et al., 1997; Harrington et al., 2002; Korkmaz et al., 2009; Ledoux, 1989; Lemieux et al., 2008; Marie and Hollett, 1996; Markstrom et al., 2008; Osterkamp et al., 1994; Pearce et al., 1986; Peters and Ratcliffe, 1998; Plummer et al., 2004; Ponce et al., 1999; Sanford et al., 2004; Sorman et al., 1997; Stephens, 1988; Waichler and Wigmosta, 2004)
Cumulative watershed effects	(Carr, 2006)
Dam problems	(Francis et al., 2010; Heppner and Loague, 2008)
Erosion & Sediment transport	(Ran et al., 2007)
Freshwater wetland systems and estuary exchange	(Graham and Refsgaard, 2001; Langevin et al., 2005; Panday and Huyakorn, 2004; VanderKwaak and Loague, 2001; Yeh and Huang, 2003)
Hydrogeomorphology and slope instability	(BeVille, 2007; Ebel and Loague, 2008; Hodge and Freeze, 1977; Mirus et al., 2007; Wilkinson et al., 2002)
Lake interactions with aquifers	(Hunt et al., 2008; Kollet and Maxwell, 2006; Smerdon et al., 2007; Winter, 1998)
Nitrate contamination and groundwater pollution	(Brooks and Lemon, 2007; Dent and Henry, 1999; Flipo et al., 2007a; Flipo et al., 2007b; Gomez et al., 2003; Haycock and Burt, 1993; Ledoux et al., 2007; Rassam et al., 2008; Refsgaard et al., 1999)
Quantifing streamflow components in quick flow and base flow	(Partington et al., 2009; Pionke et al., 1993)
Radionuclide contamination	(Bixio et al., 2002; Dent and Henry, 1999; Lienert et al., 1994; McLaren et al., 2000; Von Gunten et al., 1988; Waber et al., 1990)
Runoff generation	(Heppner, 2007; Kollet and Maxwell, 2006; Koster et al., 2000; Mirus et al., 2007; Morita and Yen, 2002; Qu and Duffy, 2007; VanderKwaak and Loague, 2001)
Solute transport	(Sudicky et al., 2008; VanderKwaak, 1999; VanderKwaak and Sudicky, 2000)
Stream-aquifer exchange	(Brookfield et al., 2008; Cardenas and Gooseff, 2008; Gunduz and Aral, 2005; Osman and Bruen, 2002; Weng et al., 2003)

2.3.3 Stream-aquifer interactions modeling: tackling the challenges

In spite of the evolution of the stream-aquifer modeling discipline in the last few years, many challenges still remain unsolved. Notable challenges in stream-aquifer modeling include spatial and temporal scale issues (Kollet and Maxwell, 2006; Loague and Corwin, 2007; Loague and VanderKwaak, 2004; Sudicky et al., 2005; Werner et al., 2006), initial conditions (Noto et al., 2008), absence or inadequacy of measured data to calibrate/control model outputs (Beven and Binley, 1992; Lefebvre et al., 2010; Uhlenbrook et al., 1999), equifinality[3] (Beven, 2006; Beven and Freer, 2001a; Ebel and Loague, 2006), insufficient computational power and conceptual and numerical difficulties (Jolly and Rassam, 2009).

Tab. 2.4 illustrates the diversity of equations and spatial dimension characteristics of selected coupled models employed for stream-aquifer modeling. The levels of complexity in these models are based on the type of equations and the spatial dimension (1D, 2D or 3D) used to describe surface water and groundwater flows (Tab. 2.4). Based on the discussion of Aral and Gunduz (2003) with regards to spatial scale issues, an approximate formulation of coupled stream and aquifer units may be successfully achieved using a multi-layer 2D horizontal model for the subsurface flow, preceeding a 1D model for stream flow, as in CASC2D (Julien et al., 1995), LISFLOOD (De Roo et al., 2000), MIKE-SHE (Refsgaard and Storm, 1995; Thompson et al., 2004), HEC-HMS/HEC-RAS (Knebl et al., 2005b), CAWAQS (Flipo et al., 2007a) and EauDyssée (Ledoux et al., 1984; Ledoux et al., 2007) . Other studies further encourage ground water modelers to start simple and to add complexity carefully as warranted by the complexity supported by the available data (Hill, 2006). The conclusion of

[3] Equifinality is a key concept to assess how uncertain hydrological predictions. In hydrological modeling, two models are equifinal if they lead to an equally acceptable or behavioral representation of the observed natural processes (Beven and Freer, 2001a).

Hill's study is that neither very simple nor very complex models are likely to provide the most accurate predictions.

Another significant conceptual obstacle is to determine the most effective technique for coupling the stream and aquifer continuum. According to Panday and Huyakorn (2004), several options for coupling stream and aquifer models are available including a fully coupled approach, in which the interaction flux is applied as a boundary condition to each model or a sequentially coupled approach in which the head for one system acts as a general-head boundary for the other system.

With regards to numerical difficulties, several techniques have been adapted to overcome this problem, including adaptive time steps (D' Haese et al., 2007; Park et al., 2008), non linear solvers (Hammond et al., 2005; Jones and Woodward, 2001; Knoll and Keyes, 2004) and parallel algorithms for solution (Kollet and Maxwell, 2006).

Tab. 2.4 Characteristics of type of equations and spatial dimensions for selected stream-aquifer models

Aquifers			**Streams**			**References**
Flow dimensions	**Zones**	**Solution**	**Flow dimensions**	**Equations**	**Solution**	
1D	Unsaturated	Empirical	1D	Empirical		(Moore and Grayson, 1991; Ross et al., 1979)
1D	Unsaturated	Numerical	1D	Kinematic	Numerical	(Alley et al., 1980; Smith and Woolhiser, 1971)
1D	Unsaturated	Analytical	1D	Kinematic	Numerical	(Engman and Rogowski, 1974; Woolhiser et al., 1990b)
1D	Unsaturated & saturated	Empirical	1D	Kinematic	Numerical	(Leavesley et al., 1983)
1D	Unsaturated & saturated	Empirical	1D	Empirical		(Beven and Kirkby, 1979)
2D	Unsaturated & saturated	Analytical	1D	Empirical		(Wigmosta and Burges, 1997)
2D	Unsaturated & saturated	Analytical	1D	Kinematic	Numerical	(Smith and Hebbert, 1983)
2D	Unsaturated & saturated	Numerical	1D	Kinematic	Numerical	(Beven et al., 1987)
2D	Unsaturated & saturated	Numerical	1D	Diffusion wave	Numerical	(Gunduz and Aral, 2005)
2D	Unsaturated & saturated	Numerical	1D	Saint-Venant	Numerical	(Abbott et al., 1986a; Akan and Yen, 1981a; Beven, 1977; Govindaraju and Kavvas, 1991)
2D	Unsaturated & saturated	Numerical	2D	Shallow water equations	Numerical	(Liang et al., 2007; Sparks, 2004)
2D	Unsaturated & saturated	Numerical	2D	Navier-Stokes	Numerical	(Bradford and Katopodes, 1998; Spanoudaki et al., 2009)
3D	Unsaturated & saturated	Numerical	1D	Continuity equation	Numerical	(Merrit and Konikow, 2000; Prudic et al., 2004)

3D	Unsaturated & saturated	Numerical	1D	Conceptual isochrones	Numerical	(Ledoux et al., 1984)
3D	Unsaturated & saturated	Numerical	1D	Empirical		(Binley et al., 1989; Wigmosta et al., 1994)
3D	Unsaturated & saturated	Numerical	1D	Kinematic wave	Numerical	(Graham and Refsgaard, 2001; Hussein and Schwartz, 2003; Sokrut, 2001)
3D	Unsaturated & saturated	Numerical	1D	Muskingum	Numerical	(David et al., 2010)
3D	Unsaturated & saturated	Numerical	1D	Muskingum-Cunge	Numerical	(Markstrom et al., 2008)
3D	Unsaturated & saturated	Numerical	1D	Diffusion wave	Numerical	(Jobson and Harbaugh, 1999; Morita and Yen, 2002; Panday and Huyakorn, 2004; Querner, 1997)
3D	Unsaturated & saturated	Numerical	1D	Saint-Venant	Numerical	(Flipo et al., 2005; Freeze, 1972; Kollet and Maxwell, 2006; Swain and Wexler, 1996; VanderKwaak, 1999; Yeh and Huang, 2003)

2.3.4 Scaling issues in stream-aquifer interactions modeling

Spatial scale is defined as the dimension at which entities, patterns, and processes can be observed and characterized to capture the important details of a hydrological or hydro(geo)logical process (Aral and Gunduz, 2003). It is an important issue in the assessment and management of stream-aquifer interactions.

In general, there are three main scales relating to stream-aquifer interactions modeling:

- Regional scale, where the stream is placed in context with the overall hydro(geo)logical setting of the catchment (> 100 km^2).
- Local scale, at the level of individual surface water features such as a lake or a stream reach (10 - 100 km).
- Site scale, where site specific studies provide insights into processes particularly at the stream-aquifer interface (1 m - 1 km).

Tab. 2.5 illustrates a range of selected hydro(geo)logical models applied at site scale, local scale and regional scale.

Each model has different levels of complexity and simulation capabilities ranging from models which simulate the complete land phase of hydrologic cycle at regional scale (e.g. MODHMS, MIKE SHE, MODCOU) to models that focus on local stream-aquifer water interactions (e.g. InHM). At regional scale applications, the majority of regional hydr(geo)logical models have limited capacity to simulate small-scale processes (e.g., near-stream groundwater pumping, bank storage effects, in-stream water level fluctuations) because these processes require a very fine discretization of the considered domain. The fine discretization required to capture such processes influences the computational efficiency. It is why alternative approaches are required to complement model's range of applicability (Werner et al., 2006). When large scale models are used to predict small scale events or when

small scale models are used to predict large scale events problems may arise (Aral and Gunduz, 2003). For example, if a more detailed site specific analysis is required at local or site scale then a finer discretization grid should be applied (e.g., 50-200 m) which is not always feasible in regional scale hydro(geo)logical models where discretization generally ranges from 1-4 km. Another issue to simulate fluxes at the regional scale is that hydro(geo)logical models are not very accurate at large scale (Lian et al., 2007). All the aforementioned factors confirm the necessity to identify an upscaling methodology in order to improve local scale stream-aquifer interactions at regional scale hydro(geo)logical models.

Tab. 2.5 range of selected hydro(geo)logical models applied at different scales.

Model	**Application Scale (km^2)**	**References**
MEFIDIS	0.013 – 290	(Nearing et al., 2005; Nunes et al., 2006a; Nunes et al., 2005; Nunes et al., 2006b)
InHM	0.1 – 100	(Loague and VanderKwaak, 2002; Loague and VanderKwaak, 2004; VanderKwaak, 1999; VanderKwaak and Loague, 2001; VanderKwaak and Sudicky, 2000)
MODHMS	10 – 420	(Barr and Barron, 2009; Beeson et al., 2004; Panday and Huyakorn, 2004)
KINEROS2	6.4 – 750	(Al-Qurashi et al., 2008; Michaud and Sorooshian, 1994b; Semmens et al., 2008; Smith et al., 1995; Wheater et al., 1991; Woolhiser et al., 1990a; Yatheendradas et al., 2008)
CASC2D	0.016 – 2300	(Jorgeson, 1999; Julien and Saghafian, 1991; Julien et al., 1995)
IHMM	10 – 50	(Georgakakos et al., 1988)
CAWAQS	Up to 2500	(Flipo, 2005; Flipo et al., 2007a; Flipo et al., 2005)
MIKE SHE	1 – 100000	(Abbott et al., 1986b; Abbott and Refsgaard, 1996; Andersen et al., 2001; Graham and Refsgaard, 2001; Olesen et al., 2000; Refsgaard, 2001; Refsgaard et al., 1998)
ArcEGMO	0.7 – 100000	(Becker et al., 2002)
MODCOU/ EauDyssée	Up to 100000	(Ambroise et al., 1995; Boukerma, 1987; Gomez et al., 2003; Habets et al., 1999b; Habets et al., 2010; Monteil et al., 2010; Thierion et al., 2010)
Hydro-BEAM	Up to 200000	(Kojiri et al., 1998; Park et al., 2000; Tamura and Kojiri, 2002; Tokai et al., 2002)
WATFLOOD	Up to 2000000	(Bingeman et al., 2006; Kouwen, 1988; Tao and Kouwen, 1989)

2.3.5 In-stream water levels fluctuations importance to stream-aquifer interactions

Time-dependent in-stream water levels fluctuations are acknowledged to influence the groundwater system and hydraulic gradients in regions surrounding the stream (Ataie-Ashtianti et al., 1999; Cooper, 1959; Glover, 1959; Reilly and Goodman, 1985; Winter, 1998).

In-stream water level fluctuations can arise from many natural and anthropogenic sources such as flood events, intense precipitation episodes, tidal oscillations, wave induced displacement, dam releases and associated reservoir drawdown. The increase in in-stream water levels due to one of the aforementioned factors frequently results in reversal stream aquifer units exchange, leading to losing water conditions for the stream network

(Friesz, 1996; Squillace, 1996).

In a study developed to simulate mass transport from a contaminant plume to a tidal estuary, comparison of models with and without tidal fluctuation (Yim and Mohsen, 1992) demonstrates that concentrations near the interface are less than ones obtained in simulations with tidal fluctuations enabled, velocity gradients are much greater, and more mass exchange from the aquifer to the estuary occurs.

In-stream water level variations have been also used to study large-scale hydraulic properties of fluvial aquifers (Bolster et al., 2001; Carrera and Neuman, 1986a; Loeltz and Leake, 1983; Pinder and Jones, 1969; Reynolds, 1987; Sophocleous, 1991). Moreover, Aquifer reaction to tidal fluctuations has been employed to calculate aquifer parameters (Erskine, 1991; Jha et al., 2003). In other studies, time varying surface water stage is frequently used to estimate aquifer hydraulic diffusivity (Ferris, 1951; Pinder and Jones, 1969; Reynolds, 1987; Swamee and Singh, 2003).

2.4 Conclusions

In this chapter an overview of available hydrosystems modeling with a specific focus on surface routing and stream-aquifer modeling techniques is presented with their relative advantages and limitations.

The routing techniques reviewed show that the final choice of a routing model is a trade off between a number of factors such as the temporal and spatial scale, the required accuracy, the type and availability of data, the available computational facilities and the extent of required information on water levels. Taking all the aforementioned factors into consideration, there is no universal superior routing model and choosing the appropriate routing approach depends to a great extent on the hydrological problem in question.

The review of stream-aquifer modeling techniques show that the rationale for selecting an appropriate stream-aquifer modeling technique is function of the application's objective and the model's suitability for modeling key aspects of the problem at hand. A more complex model does not necessarily make a better model, additional complexity is only justified if sufficient data are available for characterization of parameters, and if the problem will profit of the final resolution provided by additional complexity.

The review also illustrates the importance of regional hydro(geo)logic models capable of simulating coupled stream-aquifer interactions for conducting interdisciplinary investigations in hydrologic sciences. However, the majority of these regional models have limited capacity to simulate small-scale processes (e.g., near-stream groundwater pumping, bank storage effects, in-stream water level fluctuations, hyporheic exchange) because modeling these processes require a very fine discretization of the considered domain which is not always applicable in regional scale hydrological models.

The aforementioned factors addresse the necessity of identifying a methodology to improve the modeling of local scale stream-aquifer interactions in regional hydro(geo)logical models.

The following chapters will focus on identifying a methodology to compromise between local and regional scale modeling in order to complement regional hydrological models range of applicability. The regional hydrological model selected for this purpose is EauDyssée.

CHAPTER 3. PRINCIPLES AND FUNCTIONING OF THE HYDROLOGICAL PLATFORM EAUDYSSÉE AND THE HYDRAULIC MODEL HEC-RAS

Résumé en Français

Dans ce chapitre, nous présentons la version initiale de la plateforme de modélisation intégrée des hydrosystèmes EauDyssée, le modèle hydraulique HEC-RAS, ainsi que les critères statistiques que nous avons utilisé pour évaluer les résultantes obtenus dans cette thèse.

Nous nous focalisons sur la plateforme EauDyssée qui repose sur le couplage de modèles experts simulant le bilan hydrique, les écoulements de surface et souterrain, le transfert en zone non saturée, et les interactions nappe-rivière. Dans la version initiale d'EauDyssée, les échanges entre la nappe et la rivière sont simulés avec une cote d'eau imposée en rivière obtenue à partir d'un Modèle Numérique de Terrain (MNT). En conséquence ces cotes d'eau ne fluctuent pas en fonction de l'événement hydrologique ou du débit en rivière.

Abstract

In this chapter, the principles and functioning of the initial version of the hydrological platform EauDyssée and the hydraulic model HEC-RAS are presented. Additionally, we illustrate the statistical criteria used to evaluate the results of this thesis.

We particularly focus on the initial version of the platform EauDyssée which couples existing specialized models to address water resources and quality in regional scale river basins. It simulates the surface runoff, groundwater flow and stream-aquifer interactions using constant in-stream water levels that are obtained from a Digital Elevation Model (DEM) and imposed as constant boundary conditions along river networks. Hence, these in-stream water levels do not fluctuate as function of the simulated river discharge or the hydrological event.

Tab. 3.1 Chapter 3 list of symbols

Symbol	Description	Dimension
A	Flow area	$[L^2]$
AET	Actual Evapotranspiration	[L]
CQI	Depletion ratio of the aquifer feeding reservoir	[Dimensionless]
CQR	Depletion ratio of the surface runoff reservoir	[Dimensionless]
CRT	Mean value of soil water stock	[L]
$DCRT$	Minimum value of soil water stock	[L]
FN	Maximum value of infiltration in a time step	[L]
g	Acceleration due to gravity	$[L.T^{-2}]$
h_g	Piezometric head	[L]
h_r	In-stream water stage	[L]
I	Muskingum inflow discharge	$[L^3.T^{-1}]$
k	Muskingum transfer time between two adjacent river cells	[T]
$K_{c,f}$	Conveyance in the channel and floodplain	$[L^3.T^{-1}]$
kET	Evapotranspiration coefficient	[Dimensionless]
Kiz	Number of isochronal zones	[Dimensionless]
K_{riv}	Hydraulic conductance of the stream-aquifer interconnection for a unit length of reach	$[L^2.T^{-1}]$
n	Manning's roughness coefficient	[dimensionless]
Nk	Number of cells inside the isochronal zone	[Dimensionless]
Nr	Number of reservoirs in the Nash cascade	[Dimensionless]
NS	Nash-Sutcliffe coefficient	[Dimensionless]
O	Muskingum outflow discharge	$[L^3.T^{-1}]$
P	Precipitation	[L]
PET	Potential Evapotranspiration	[L]
Q	Discharge	$[L^3.T^{-1}]$
$q_{aquifer}$	Flow of water exchanged between a river cell and the aquifer cell beneath	$[L^3.T^{-1}]$
$Q_{c,f}$	Flow in main channel and floodplain	$[L^3.T^{-1}]$
QI	Infiltration	[L]
QII	Actual infiltration	[L]
$QImax$	Overflow level of aquifer feeding reservoir	[L]
q_l	lateral inflow per unit length	$[L^2.\ T^{-1}]$
$qlow$	Exchange of flowrate with the lower aquifer layer	$[L.T^{-1}]$
$Qmax$	Maximum magnitude of river infiltration towards aquifer units	$[L^3.T^{-1}]$
qr	Surface runoff volume into a river cell	[L]
$QRmax$	Overflow level of the surface runoff reservoir	[L]
$QRRj$	Surface runoff produced in cell j by the production function	[L]
$Qsur$	Exchanged flux with the surface	$[L.T^{-1}]$
Qup	Exchanged flux with the upper aquifer layer	$[L.T^{-1}]$
Qw	Volume of water outflowing from the balance reservoir	[L]
R	Hydraulic radius	[L]
Raq	Level of the aquifer feeding reservoir	[L]
Rb	Level of balance reservoir	[L]
$Rbmax$	Maximum level of balance reservoir	[L]
$Rbnew$	New level of balance reservoir	[L]
$RMSE$	Root mean squared error	[L or $L^3.T^{-1}$]
$Rsur$	Level of the surface runoff reservoir	[L]

S	Storage coefficient	[Dimensionless]
S_f	friction slope	[dimensionless]
S_o	Bottom slope	[dimensionless]
T	Storage constant of reservoir in NONSAT	[Dimensionless]
V	Velocity	[$L.T^{-1}$]
X_{obs}	Observed values used in the statistical evaluation of the model	[L or $L^3.T^{-1}$]
X_{sim}	Model simulated values compared to observed ones in the statistical evaluation of the model performance	[L or $L^3.T^{-1}$]
y	flow depth	[L]
Δh	Difference in piezometric heads	[L]
Δl	Distance between the centers of two cells	[L]
ΔS	Change in storage within the reach during a Δt time increment	[L^3]
Δt	Time step	[T]
$\Delta QII(t_0)$	Instantaneous volume given to the first reservoir in NONSAT	[L]
θ	Muskingum model weighting parameter	[Dimensionless]
ϕ	HEC-RAS discharge distribution factor	[dimensionless]

3.1 Introduction

In this study, we have at our disposal a regional hydrological model (EauDyssée) and a local hydraulic model (HEC-RAS).

The hydrological model EauDyssée addresses the different corposants of the water cycle, particularly the rainfall-discharge relationships at the regional scale by taking into consideration the surface and aquifer flow.

The hydraulic model HEC-RAS (HEC, 2002) performs one dimensional steady and unsteady flow calculations on a network of natural or man-made open channels. It simulates the water levels and discharge at each river cross section.

3.2 Principles and functioning of EauDyssée platform for hydrosystem modeling

The platform EauDyssée couples existing specialized models to address water resources and quality in regional scale river basins (Fig. 3.1).

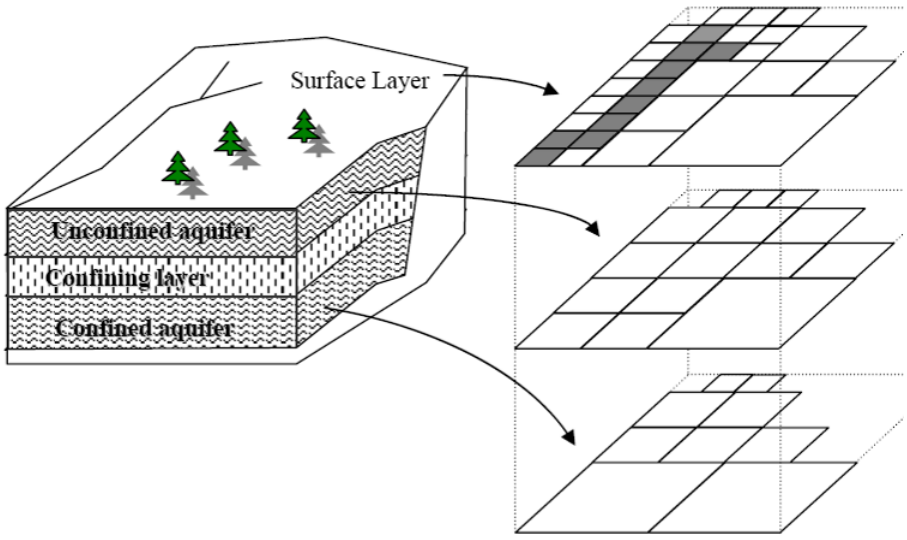

Fig. 3.1 Principle of the multi-layer schematization of EauDyssée

The core of the model is composed of four spatially distributed modules, corresponding to four components of the terrestrial water cycle: the surface mass balance component, the unsaturated component, the saturated zone or aquifer component and the river network component (Fig. 3.2). The core of the hydrogeological part of EauDyssée is based on the MODCOU (Ledoux et al., 1984) reshaping with an improved river routing module and an improved hydrogeological module based on NEWSAM (Ledoux et al., 1984). Interactions between modules have also been improved on an on- line coupling.

The former version of EauDyssée (MODCOU) has successfully predicted surface and groundwater flow in many basins of varying scales and hydrogeological settings: the Haute-Lys and Caramy basins (Ledoux, 1980); the HAPEX-MOBILHY study (Boukerma, 1987); the Fecht river basin (Ambroise et al., 1995); the Rhône basin (Golaz-Cavazzi, 1999; Habets et al., 1999b), the Seine basin (Gomez et al., 2003) and the Somme basin (Habets et al., 2010; Korkmaz et al., 2009). It is currently being implemented in the Rhine River (Thierion et al., 2010) and the Loire basin (Monteil et al., 2010).

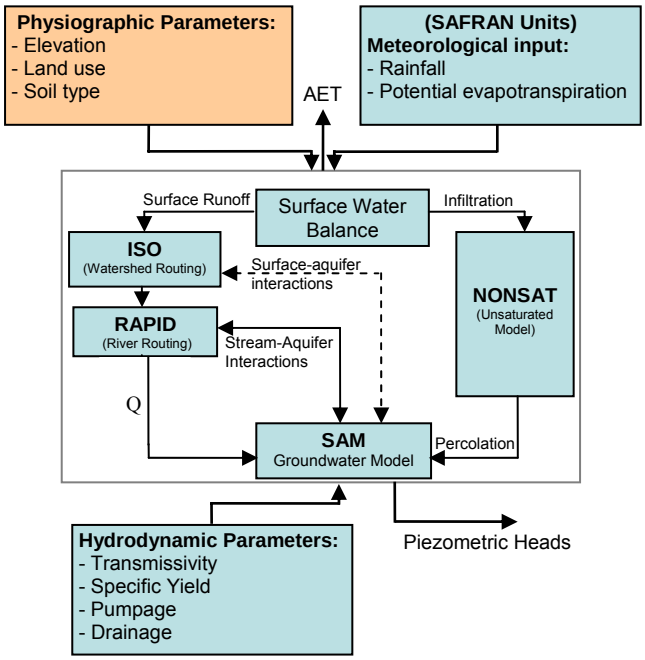

Fig. 3.2 EauDyssée platform components and simulated hydro(geo)logical layers

The platform is composed of the following components:

3.2.1 Surface component mass balance

The main functions of this component include the partition of precipitation into infiltration and surface runoff, and the transfer of surface runoff to the river network.

3.2.1.1 Production function

The surface domain is divided into production zones to which a 7-parameter model called production function (Fig. 3.3) is associated (Golaz-Cavazzi, 1999; Gomez et al., 2003). It computes the hydrological mass balance at a daily time step for each cell of the surface mesh. The input data consist in a meteorological database (precipitation and potential evapotranspiration) with a daily time step and a spatial resolution of 8 km×8 km. Data are derived from Météo-France SAFRAN database (Quintana-Seguí et al., 2008).

The final outputs are actual evapotranspiration (AET), soil water stock, the water flux that infiltrates to the aquifer system and the one corresponding to surface runoff.

The calibration of the production function parameters is carried out by comparing simulated discharge with measurements.

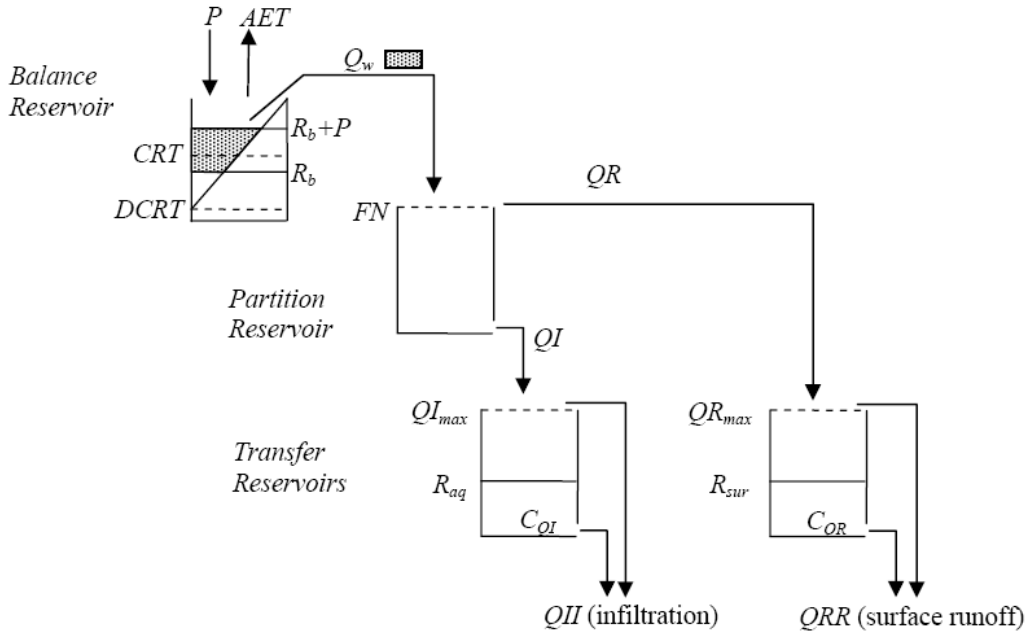

Fig. 3.3 Production function schematization (Ledoux, 1984)

The production function is composed of 4 reservoirs:

1 Balance Reservoir

The available water partitioned from this reservoir is function of precipitation, reservoir level (R_b), and two variables (*DCRT* and *CRT)*. *DCRT* represents the minimum value of soil water stock (mm) which determines the role of initial rainfall after a dry period. *CRT* represents the mean value of soil water stock. Both variables are conceptual and are used to calculate AET (Actual Evapotranspiration) on water mass balance cells. The calculations held in the balance reservoir are:

$$R_{bnew} = R_b + P - Q_w - AET \qquad \text{Eq. 3.1}$$

$$AET = min(PET,\ R_b + P - Q_w) \qquad \text{Eq. 3.2}$$

$$Qw = max(R_b + P - Rbmax,\ 0) + \Delta R\ (2RBA + \Delta R)/(4(CRT - DCRT)) \qquad \text{Eq. 3.3}$$

$$\Delta R = max(0, RHA–RBA)$$ Eq. 3.4

$$RHA = min(R_b+P, R_{bmax}) – DCRT$$ Eq. 3.5

$$RBA = max(DCRT, R_b) – DCRT$$ Eq. 3.6

$$R_{bmax} = 2(CRT–DCRT) + DCRT$$ Eq. 3. 7

Where R_{bnew} is the new level of balance reservoir [L], Q_w is the volume of water outflowing from the balance reservoir [L] and the other variables are temporary ones simplifying the writing of equations.

2 Partition Reservoir

This reservoir partitions the output received from the balance reservoir between the potential infiltration reservoir and the surface runoff reservoir. The distribution between potential infiltrating water (*QI*, [L]) and potential surface runoff (*QR*, [L]) is controlled by the parameter (*FN*, [L]) which stands for the maximum value of infiltration in a time step. These are expressed as follows:

$$QI = min(Q_w, FN)$$ Eq. 3.8

$$QR = max(0, Q_w – QI)$$ Eq. 3.9

Water joins surface runoff when the infiltration capacity of soil is overtopped. If the level of available water is not high enough to overtop the partitioning reservoir, then there will be no surface runoff and all the water will infiltrate.

3 Transfer Reservoirs

The transfer reservoirs include the infiltration reservoir that feeds the unsaturated zone or directly the aquifer units, and the surface runoff reservoir. The infiltration reservoir

introduces a delay between the potential infiltration (*QI*) and actual infiltration (*QII*). The reservoir is defined by the variables R_{aq}, *CQI* and QI_{max}.

Where, R_{aq} is the level of the reservoir, CQI is the discharge rate of the reservoir, QI_{max} is the overflow level of the reservoir.

The infiltration flux is calculated as follows:

$$R_{aq} = R_{aq} + QI \qquad \text{Eq. 3.10}$$

$$\text{If } R_{aq} < QI_{max} \text{ then } QII = C_{QI} * R_{aq} \qquad \text{Eq. 3.11}$$

$$\text{If } Raq > QI_{max} \text{ then } QII = (R_{aq} - QI_{max}) + C_{QI} * QI_{max} \qquad \text{Eq. 3.12}$$

$$R_{aqnew} = R_{aq} - QII \qquad \text{Eq. 3.13}$$

The amount of water available for surface runoff is calculated with exactly the same reservoir model than the one used to calculate infiltrating water.

3.2.1.2 Surface runoff routing: ISO module

The surface runoff partitioned by the production function is routed to the river network by the ISO module (Fig. 3.2). Each drainage area is divided into a number of isochronal zones equal to the number of time steps necessary for flow to reach the nearest river cell. The transfer times depend on topography and concentration time which is a parameter to be fit (Ledoux et al., 1984).

The flowrate of surface runoff into a river cell (*qr*) at any time (*t*) is described as follows:

$$qr_i(t) = \sum_{k=0}^{k=k_{iz}-1} \sum_{j=1}^{j=N_k} QRR_j(t - K.\Delta t) \qquad \text{Eq. 3.14}$$

Where K_{iz} is the number of isochronal zones, N_k is the number of cells inside the isochronal zone, QRR_j is the surface runoff produced in cell *j* by the production function.

3.2.2 Unsaturated zone component - NONSAT

The infiltrated water partitioned by the production function is transferred vertically to the groundwater table by the unsaturated-zone model NONSAT (Flipo et al., 2005; Golaz-Cavazzi, 1999; Gomez et al., 2003; Ledoux, 1980). This conceptual model consists in a succession of reservoirs (Fig. 3.4).

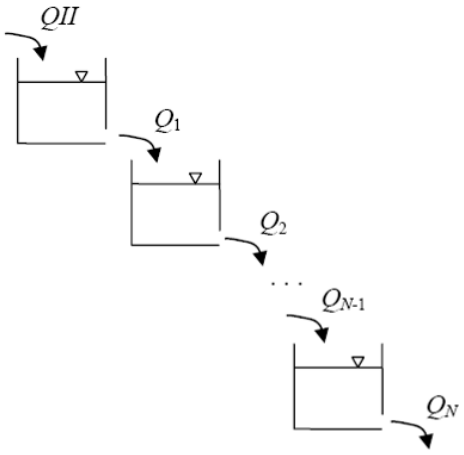

Fig. 3.4 Principle of the Nash model

The number of reservoirs is related to the distance between soil horizons and the saturated zone. This distance is initially calculated based on the hydraulic head distribution resulting from a steady state simulation using the mean annual infiltration as boundary conditions.

The outflow of the reservoir k is calculated as follows:

$$Q_k(t) = \frac{\Delta QII(t_0)}{\tau(k-1)} \cdot e^{-(t-t_0)/\tau} \cdot \left(\frac{t-t_0}{\tau}\right)^{k-1} \qquad \text{Eq. 3.15}$$

Where $\Delta QII(t_0)$ is an instantaneous volume given to the first reservoir at time $t=t_0$ [L^3], N is the number of reservoirs in the Nash cascade, τ is a storage constant of reservoir [dimensionless].

Flipo 2005 showed that it is important to take into account the evolution vadose zone. Thus, work is done to build a more dynamical definition of the vadose zone length to accurately

simulate water reaching the top of the aquifer units. Otherwise, transfer time in the vadose zone can be overestimated up to one order of magnitude (Philippe et al., 2010).

3.2.3 Saturated zone component: SAM (Simulation des Aquiferes Multicouches)

The SAM model (Ledoux et al., 1984, 1989) is a regional spatially distributed model that computes the temporal distribution of the piezometric heads of a multilayer aquifer system, using the diffusivity equation (de Marsily, 1986).

$$\frac{\partial}{\partial x}\left(T_x \frac{\partial h_g}{\partial x}\right) + \frac{\partial}{\partial y}\left(T_y \frac{\partial h_g}{\partial y}\right) = s\frac{\partial h_g}{\partial t} + Q_{sur} + Q_{up} + Q_{low} \qquad \text{Eq. 3.16}$$

Where h_g is the piezometric head [L], T is the transmissivity [$L^2.T^{-1}$], S is the storage coefficient [dimensionless], Q_{sur} is the exchanged flux with the surface [$L.T^{-1}$], Q_{up} is the exchange flux with the upper aquifer unit [$L.T^{-1}$] and Q_{low} is the exchanged of flowrate with the lower aquifer unit [$L.T^{-1}$].

In each aquifer, flows are bidimensionnal whereas they are vertically monodimensionnal in the aquitard between two horizontal layers. The multilayer model simulates confined and unconfined aquifer units. The variation through time of the head is modeled by nonlinear Boussinesq equaiton. It also computes exchange between aquifer units and rivers.

3.2.4 The regional river routing component RAPID

The in-stream discharge routing within the platform EauDyssée is conducted by a parallel computing-based river routing model called RAPID (David et al., 2010), Routing Application for Parallel Computation of Discharge, which is based on the Muskingum routing scheme (Eq. 2.12).

3.2.5 Stream-aquifer interactions

Stream-aquifer interactions are calculated in each river grid cell from the difference between hydraulic heads in the river cell and the underlying aquifer cell. Depending on the sign of this difference, surface water either infiltrates towards aquifer units, or groundwater exfiltrates towards the river network.

For large river basins such as the Seine River and the Loire River, cells representing the river have a length of 1 km and are thus usually greater than the dimensions of the stream. Therefore, the stream-aquifer interactions are simplified and controlled by a coefficient called river conductance that relates stream-aquifer flow to the difference between the in-stream water level and the groundwater head:

$$q_{aquifer} = K_{riv}\left(h_r - h_g\right) \qquad \text{Eq. 3.17}$$

Where $q_{aquifer}$ is the flow between stream and aquifer [$L^3.T^{-1}$], h_r is the in-stream water stage [L], h_g is the piezometric head in the aquifer unit [L] and K_{riv} is the hydraulic conductance of the stream-aquifer interconnection for a unit length of reach [$L^2.T^{-1}$].

In the current EauDyssée version, in-stream water levels are obtained from a Digital Elevation Model (DEM) and imposed as constant boundary conditions along the river network. Thus stream-aquifer interactions are only controlled by the fluctuation of the piezometric head in the aquifer units.

The magnitude of river infiltration towards aquifer units is controlled by a maximal value called Q_{max} [$L^3.T^{-1}.L^{-2}$]. If Q_{max} is equal to zero, infiltration from stream to aquifer unit is not authorized even if the in-stream water level is higher than the water table level. Q_{max} can be estimated either from field measurements based on local mass balance or through available literature on river's bed permeability (Lange, 2005). Typically Q_{max} varies from 0 $l.s^{-1}km^{-2}$ for

impermeable river beds to 500 $l.s^{-1}km^{-2}$ for high infiltration river beds such as the Rhine River (Thierion et al., 2010).

3.3 The hydraulic model HEC-RAS

The hydraulic model HEC-RAS (HEC, 2002) performs one dimensional steady and unsteady flow calculations on a network of natural or man-made open channels.

Basic input data required by the model include the channel network connectivity, cross-section geometry, reach lengths, energy loss coefficients, stream junctions information and hydraulic structures data. Cross sections are required at representative locations throughout a stream reach and at locations where changes in discharge, slope, shape or roughness occur. Boundary conditions are necessary to define the starting water depth at the stream system endpoints, i.e., upstream and downstream.

HEC-RAS solves the mass equation (Eq. 3.18) and the momentum equation (Eq. 3.19) using implicit finite difference approximations and Preissman's second-order scheme. The computation engine for the HEC-RAS 1-D unsteady flow simulator is based on the UNET model (Barkau, 1985).

$$\frac{\partial Q}{\partial x} + \frac{\partial A}{\partial t} - q_l = 0 \qquad \text{Eq. 3.18}$$

Where Q is the discharge [$L^3.T^{-1}$], A is the cross sectional area [L^2], x is the distance along the longitudinal axes of the channel or floodplain [L], t is Time [T], q_l is lateral inflow per unit length [$L^2.\ T^{-1}$].

$$S_f = S_0 - \frac{\partial y}{\partial x} - \frac{V}{g}\frac{\partial V}{\partial x} - \frac{1}{g}\frac{\partial V}{\partial t} \qquad \text{Eq. 3.19}$$

Where S_o is the bottom slope, S_f is the friction slope, V is the velocity [$L.T^{-1}$], y is the flow

depth [L], g is acceleration due to gravity [$L.T^{-2}$].

Because the primary direction of flow is oriented along the channel, two-dimensional flow field can often be accurately approximated by a one-dimensional representation. Off channels ponding areas can also be modeled with storage areas that exchange water with the channel. The two-dimensional characteristics of the interaction between the channel and floodplain flows are illustrated in Fig. 3.5. When there is a sudden rise in river water levels water moves laterally away from the main channel, inundating the floodplain and filling available storage areas. As the depth increases, the floodplain begins to convey water downstream, generally along a shorter path than the main channel, and when the river stage is falling, water moves towards the channel from the overbank supplementing the flow in the main channel.

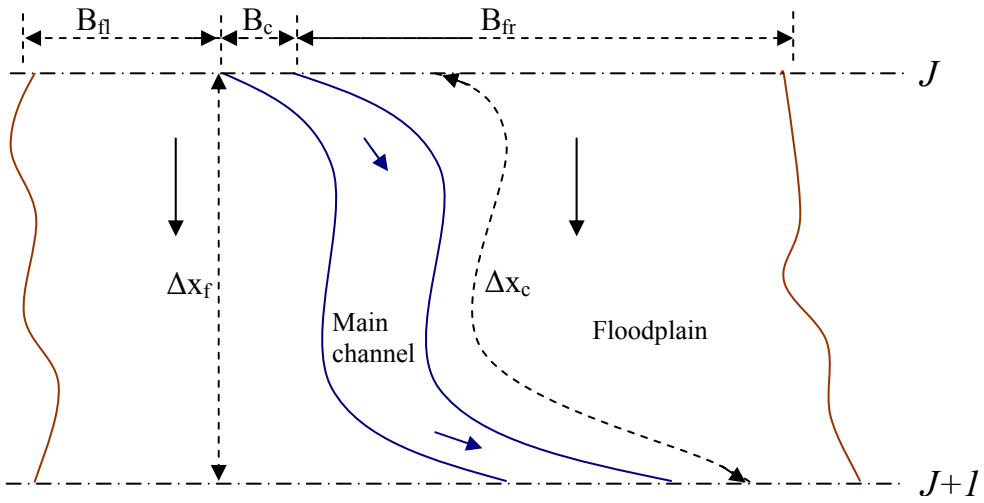

Fig. 3.5 Two-dimensional characteristics of the interaction between the channel and floodplain flows (USACE, 2002)

In HEC-RAS, the main channel and floodplain are described as two separate channels with unequal properties. The continuity and the momentum equations are written for each channel (Fread, 1974; Smith, 1978). To simplify the problem they assumed: 1) a horizontal water surface at each cross section normal to the direction of flow, 2) the exchange of momentum between the channel and the floodplain was negligible, 3) the discharge was distributed according to conveyance, i.e.:

$$Q_c = \phi Q \qquad \text{Eq. 3.20}$$

Where:

$$\phi = \frac{K_c}{K_c + K_f} \qquad \text{Eq. 3.21}$$

$$K = \frac{1}{n} AR^{2/3} \qquad \text{Eq. 3.22}$$

$$Q = KS^{1/2} \qquad \text{Eq. 3.23}$$

Where ϕ is the discharge distribution factor [dimensionless], Q_c is the flow in main channel [$L^3.T^{-1}$], Q is the total flow [$L^3.T^{-1}$], K is the conveyance (a measure of the carrying capacity of a channel), K_c is the conveyance in the channel, K_f is the conveyance in the floodplain, n is Manning's roughness coefficient (dimensionless), A is the flow area [L^2], R is the hydraulic radius [L].

With the above three assumptions, the one-dimensional equations of motion can be combined into a single set:

$$\frac{\partial A}{\partial t} + \frac{\partial(\phi Q)}{\partial x_c} + \frac{\partial[(1-\phi)Q]}{\partial x_f} = 0 \qquad \text{Eq. 3.24}$$

$$\frac{\partial Q}{\partial t} + \frac{\partial(\phi^2 Q^2 / A_c)}{\partial x_c} + \frac{\partial((1-\phi)^2 Q^2 / A_f)}{\partial x_f} + gA_c\left[\frac{\partial y}{\partial x_c} + S_{fc}\right] + gA_f\left[\frac{\partial y}{\partial x_f} + S_{ff}\right] = 0 \qquad \text{Eq. 3.25}$$

In which the subscripts *c* and *f* refer to the channel and floodplain, respectively. In HEC-RAS these equations are approximated using implicit finite differences, and the full nonlinear equations solved numerically using the Newton-Raphson iteration technique (Fread, 1974).

Expanding the earlier work of Fread and Smith (1974), Barkau (1982) manipulated the finite difference equations for the channel and floodplain and defined a new set of equations that were computationally more convenient. Using a velocity distribution factor, he combined the convective terms. Further, by defining an equivalent flow path, he replaced the friction slope terms with an equivalent force.

The equations derived by Barkau are the basis of UNET which was then Integrated in HEC-RAS as the unsteady flow simulator routine. The full equations and their derivations could be found in UNET Users Manual (Barkau, 1992).

3.4 Statistical criteria used to assess model performances

The performance of the models is statistically evaluated using criteria, that are standard deviation (Eq. 3. 26), Bias (Eq. 3.27), RMSE (Eq. 3.28), correlation coefficient (Eq. 3.29) and the Nash-Sutcliffe coefficient (Nash and Sutcliffe, 1970) (Eq. 3.30). These statistical criteria are used to summarize the quality of the simulation.

Standard deviation

The standard deviation is a statistical criterion used to measure the dispersion of a set of data from its mean. The more spread apart the data, the higher the deviation is. Standard deviation is calculated as the square root of variance:

$$\sigma_x = \sqrt{\frac{1}{N-1}\sum_{i=1}^{N}\left(X(t_i) - \overline{X}\right)^2} \qquad \text{Eq. 3. 26}$$

Bias

The bias of a model's simulation is the variation between calculated and observed values of the parameter being simulated. It is used to assess the overestimation or underestimation of simulations.

$$BIAS = 100\frac{\frac{1}{N}\sum_{i=1}^{N}\left(X_{sim}(t_i) - X_{obs}(t_i)\right)}{\overline{X}_{obs}} \qquad \text{Eq. 3.27}$$

Root Mean Square Error (RMSE):

The root mean square error is the average of squared differences between observed and calculated values. Thus RMSE always has the same unit as the data. It indicates the absolute spread of the data around the observed values.

$$RMSE = \sqrt{\frac{1}{N}\sum_{i=1}^{N}\left(X_{sim}(t_i) - X_{obs}(t_i)\right)^2} \qquad \text{Eq. 3.28}$$

Correlation Coefficient:

The correlation coefficient (ρ) indicates the strength and direction of a linear relationship between two random variables. It is often referred to as Pearson product moment correlation coefficient. The value of correlation coefficient varies between -1 and 1. A negative value indicates a negative linear correlation and a positive value a positive correlation whereas values near to 0 means that there is no or weak linear correlation between the two variables.

$$\rho = \frac{\sum_{i=1}^{N}\left(X_{obs}(t_i) - \overline{X}_{obs}\right)\left(X_{sim}(t_i) - \overline{X}_{sim}\right)}{\sqrt{\sum_{i=1}^{N}\left(X_{obs}(t_i) - \overline{X}_{obs}\right)^2}\sqrt{\sum_{i=1}^{N}\left(X_{sim}(t_i) - \overline{X}_{sim}\right)^2}} \qquad \text{Eq. 3.29}$$

Nash-Sutcliffe Coefficient:

The Nash-Sutcliffe coefficient is often used in hydrology, it measures the performance of the model against the overall in-stream mean discharge. The Nash value vary between -ω and 1 where a value of 1 represents a perfect model. A value of 0 indicates that the model predicts

no better than using the mean of the flows. Usually a model is considered to have "good" performance when Nash > 0.70.

$$Nash = 1 - \frac{\sum_{i=1}^{N} \left(X_{sim}(t_i) - X_{obs}(t_i) \right)^2}{\sum_{i=1}^{N} \left(X_{obs}(t_i) - \overline{X}_{obs} \right)^2} \qquad \text{Eq. 3.30}$$

Where N is the number of compared values, $X_{sim}(t_i)$ is the simulated value, $X_{obs}(t_i)$ is the observed value and $\overline{X}$ is the average of X time series.

3.4 Conclusions

In this chapter, the principles of functioning of the initial version of the hydrological platform EauDyssée and the hydraulic model HEC-RAS have been presented.

In the river component of the initial version of EauDyssée, in-stream water levels that are obtained from a Digital Elevation Model (DEM) are imposed as constant boundary conditions along river networks. The main reason behind this hypothesis is that the platform is mainly applied at regional scale basins where high resolution morphological data are not always accessible. Furthermore, the current hydrological routing model in the EauDyssée platform is based on the equations of Muskingum, hence it only simulates discharge through the river networks and does not simulate the associated water levels. In consequence, in-stream water levels does not fluctuate function of the hydrological event or the discharge routed in the river. Yet, the review of surface routing and stream-aquifer modeling techniques in chapter two show that in-stream water levels are of primary importance for the simulation of stream-aquifer interactions, river average velocity, flooding, low flows and water quality.

In this context, the next chapter will aim at establishing whether a reliable hydraulic flood routing model can be developed based on limited field data at regional scale, and eventually

identifying a methodology to improve the simulations of in-stream water levels and stream-aquifer interactions in EauDyssée.

CHAPTER 4. IMPACT OF IN-STREAM MORPHOLOGY ON SIMULATED DISCHARGE AND WATER LEVELS: SEREIN RIVER CASE STUDY

Résumé en Français

Les modèles de routage hydrologiques de débit continuent d'être les outils principaux pour le routage des débits à l'échelle des bassins versants. Cependant, la simulation des hauteurs d'eau nécessite des modèles (hydrauliques) déterministes. Un avantage fondamental des modèles de routage hydrauliques par rapport aux modèles hydrologique, en terme d'événements dynamiques, est que des données décrivant les hydrogrammes de débit et la hauteur d'eau entre des sites de jaugeage sont exploitées. De telles données sont importantes pour la simulation des interactions nappe-rivière (cf. chapitre 2).

A ce jour, les modèles hydrauliques à l'échelle régionale de bassin versant ne sont pas toujours utilisés pour deux raisons clés. Premièrement, ils peuvent être difficiles d'emploi d'un point de vue numérique. Deuxièmement, ils sont exigeants en données géométriques sur l'entière étendue du domaine modélisé.

Le premier problème n'est plus la préoccupation principale, puisque des recherches récentes ont abouti au développement de configurations de calcul robustes.

La nécessité d'utiliser de nombreuses données par les modèles hydrauliques est beaucoup plus limitante d'un point de vue pratique, puisque le routage de débit couvre de très longues étendues et que le coût d'obtention des données suffisantes sur la section peut être prohibitif.

Dans cette étude, la sensibilité d'un modèle hydraulique à la précision de la description géomorphologique des lits et à la géométrie réduite est évaluée pour identifier le meilleur compromis entre parcimonie et réalisme et identifier les facteurs morphologiques les plus importants pour obtenir une simulation satisfaisante des hauteurs d'eau.

Le principe des simulations est basé sur l'association entre un modèle hydraulique et un modèle hydrologique. Le modèle hydraulique utilisé est le modèle HEC-RAS, et les variables évaluées sont les débits et les hauteurs d'eau. Les apports latéraux sont simulés par la plateforme EauDyssée sous forme de lames d'eau écoulées depuis le bassin versant directement contributif. Les résultats ont été obtenus sur les biefs du Serein (affluent de l'Yonne) bien renseignés entre Dissangis et Beaumont (89 km).

A partir des résultats de ces tests, nous pouvons conclure qu'une simplification de la géométrie ne modifie pas significativement la simulation des débits. En revanche, une géométrie précise est nécessaire pour bien simuler les hauteurs d'eau, notamment dans les simulations nappe-rivière et la simulation des inondations.

Abstract

Hydrological routing models are the main tool for discharge routing at regional scale, while the simulation of river water levels require hydraulic models that are capable of simulating hydrodynamic events such as floods and overtopping frequency.

To date, hydrodynamic models are not widely used at the regional scale because they require high resolution morphological data that are not always accessible at regional scale, in addition to insufficient computational power and numerical difficulties when applied at regional scale.

The numerical difficulties are no longer the main concern, especially with the recent advances in the domain of numerical research.

In hydrodynamic models it is recognized that river flow characteristics are influenced by several morphological factors, amongst which, the channel slope and morphology. However, literature does not show to what extent these morphological factors influence the quality of the hydraulic model in predicting water levels and discharge hydrographs.

This chapter aims at establishing whether a reliable hydraulic model can be developed based on limited field data. A wide variety of "what if" river geometry scenarios are explored to determine the most appropriate simplified river representation geometry in areas where cross sections surveys are not available.

The validity of this approach has been illustrated by developing the Serein River hydraulic model (tributary of the Yonne River). The modelization methodology is based on the association between a hydraulic and hydrological model. The hydraulic model used is HEC-RAS (HEC, 2002) which is based on the Saint Venant equations solved using the four point implicit finite difference scheme. The calibration parameter involved in the development of the hydraulic model is the Manning's roughness coefficient (n). The hydrogeological model EauDyssée (explained in chapter 5) is used to simulate the lateral inflows of the Serein River subcatchments.

The results of this study show that hydraulic routing models based on the Saint Venant equations could be successfully used to determine discharge hydrographs in reaches where little channel geometry data are available, by approximating the modeled reach with simplified geometry. However, a hydraulic model based on approximate channel geometry does not always predict the associated water levels with possible consequences on stream-aquifer interactions and inundation zones. The results show that the accuracy of predicted water levels, maximum water depths rely on an accurate representation of channel geometry and bed level slopes along the river reach.

4.1 Introduction

The morphology of natural streams has attracted the attention of researchers since early 1900s (Lindley, 1919). Natural streams are characterized by variations in cross sections and bed slopes that occur over a range of spatial scales as result of several systematic and

statistical analysis of the river system such as discharge characteristics, quantity and characteristics of sediment load, and perimeter (bed and bank) sediments (Leopold et al., 1964).

The irregularities in bed slopes and cross-sectional shapes usually lead to rising irregularities of pressure and gravity forces in the flow direction, thus producing irregular driving forces (Chiu, 1972). Furthermore, irregularities of in-stream channel cross-section and channel slope are important in streams where the hydraulic behavior at low flow is dominated by backwater effects due to pool-riffle streams (Hey and Thorne, 1986; Miller and Wenzel, 1984). This effect is significant for low Froude numbers (which usually occur during low flows) and less important for high Froude numbers (Li et al., 1992). Moreover, the channel irregularities increase the range of flow velocities and water depths which occur in a stream reach (Western et al., 1994) thereby increasing the diversity of the physical habitats in the stream (Gubala et al., 1996; Rabeni and Jacobson, 1993). A recent study showed that irregularities in channel geometry throughout river networks are important to effectively manage flood propagation, sediment and nutrient transport, and river habitats at regional scale (Stewardson, 2005). Nevertheless, spatial and temporal variation in channel geometry is often difficult and expensive to measure at regional scale. This regional variation in the size and shape of river channels has been the core concern of fluvial geomorphologists and hydrologists for decades (Gordon, 1996; Snell and Sivapalan, 1995).

A number of techniques have been developed to estimate channel geometry indirectly, using catchment characteristics, hydrological information and climatic variables, which are easily measured and commonly available (Stewardson, 2005). In these techniques, regression relationships are developed between channel geometry and catchment characteristics (area, slope, vegetations etc), hydrology information (annual mean flow, two-year recurrence intervals) and climatic variables. These relationships are known as hydrologic geometry

models or regional geometry curves (Leopold and Maddock, 1953). Others have since used the bankfull discharge, instead of the mean discharge, as the independent variable in these downstream hydraulic geometry relations (Harman et al., 2008). Yet, there is no theoretical argument for the use of power functions (Rhoads, 1992), and this choice is rather based on empirical analysis (Leopold and Maddock, 1953). Recently, there have been efforts to develop hydraulic geometry relations for the distribution of cross-sectional hydraulic parameters within a reach based on surveys of multiple cross-sections. Some studies have examined the variability of channel geometry for studies of fluvial processes (Buhman et al., 2002; Western et al., 1997), others have developed hydraulic geometry relations for reach-averaged hydraulic parameters to assist stream habitat assessment (Jowett, 1998; Lamouroux and Capra, 2002; Lamouroux and Suchon, 2002; Singh and McConkey, 1989). This determination of hydraulic geometry relationships through river network analysis provides important inputs to regional scale hydrological models for predicting flood frequency and extent, pollutant transport as nutrient or sediment load e.g., (DeRose et al., 2005; Lu et al., 2004; McKergow et al., 2004; Prosser et al., 2001a).

A major advancement has been achieved in the late 1980's when geographic information extracted from Digital Elevation Models (DEM) were used to delineate watershed boundaries and stream networks (Jenson and Dominique, 1988). Although DEMs provide sufficient data for watershed delineation purposes and floodplain representation, they usually lack the accuracy required to represent stream channel cross-sectional morphology which is important for modeling in-stream hydrodynamic.

River morphological data are required to parameterize hydrodynamic models (Hateley et al., 2006). An important geomorphological factor for river hydrodynamic modeling is the correct identification of the bankfull stage and discharge. Bankfull stage corresponds with the discharge that fills a channel to the elevation of the active floodplain. Numerous methods

exist for bankfull stage identification including significant breaks in slope, changes in vegetation, and river top bank (Kilpatrick and Barnes, 1964; Leopold and Wolman, 1957; Nixon, 1959; Schumm, 1960; Williams, 1978) but this remains difficult and subjective (Johnson and Heil, 1996; Knighton, 1984; Williams, 1978).

In hydrodynamic models based on the Saint Venant equations, river flow is influenced by the aforementioned morphological factors. However, literature does not show to what extent these morphological factors impact the quality of the hydraulic model in predicting water levels and discharge hydrographs.

To investigate the influence of minimum field data available for the hydraulic model, the objective of this section is to examine the sensitivity of a hydraulic model to different river morphological data. In particular, the validity of using simplified geometry when surveyed cross sections are not available is explored, since one of the principal objectives of this thesis is to simulate water level and discharge hydrographs at regional scale, where surveyed cross sections are not always available.

4.2 Domain of application: Serein River

The Serein River is a sub tributary of the Seine River, its total length is 186 km. The source of the Serein is located in Saulieu (near to Morvan), and it meets the right bank of the Yonne at Bassou (Fig. 4.1). Within the studied reach, the Serein runs about 89 km starting from Dissangis and ending at Beaumont (confluence with the Yonne River). The control point where calibration is held is Chablis located in the middle of the reach, 55 km downstream from Dissangis (Fig. 4.1). The selection of this reach was based on the availability of unsteady flow simulations and high resolution morphological data.

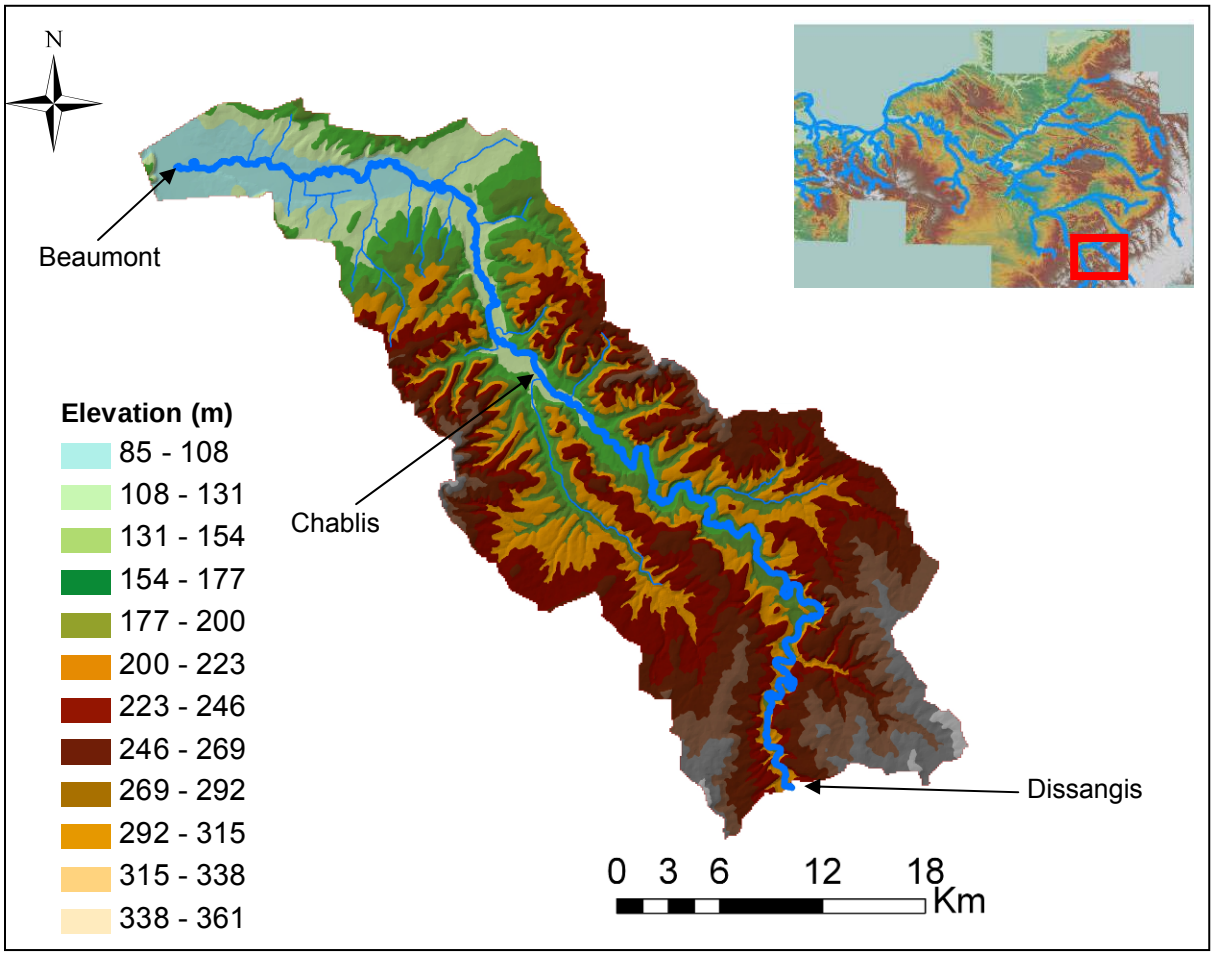

Fig. 4.1 Topography of the Serein watershed between Dissangis and Beaumont hydrometric stations, and location of Chablis hydrometric station where calibration was carried out

The Serein River has a simple hydrographic network with no major tributaries. Furthermore, no hydraulic structures are located within the studied reach which makes it less complicated to account for potential loss in energy grade line and water volume. The Serein River is well documented, what allows for maximum number of sensitivity analysis with fewer uncertainties, hence it allows to identify the importance of each hydraulic factor or boundary condition composing the hydraulic model, and furthermore identifying the influence of boundary conditions and geometry when simplified or degraded. The river geometrical profiles of the river were surveyed by the Direction Régionale de l'Environnement (DIREN). The observed discharge and water levels in three major hydrometric stations (Dissangis, Chablis, and Beaumont) are available for the use in boundary conditions and calibration. The

average observed discharges of the Serein River at major hydrometric stations are illustrated in Tab. 4.1.

Tab. 4.1 Observed discharge hydrographs at the main hydrometric stations of the Serein River

Location	Period	Average discharge ($m^3.s^{-1}$)	Catchment area (km^2)	Distance from Dissangis (km)
Dissangis	1997 – 2005	4.72	643	0
Chablis	1997 –2005	8.6	1120	55
Beaumont	1997 – 2005	11.43	1337	89

In terms of hydrology, the Serein River represents an important seasonal discharge fluctuation. High flows occur in winter and spring, with an average monthly rates ranging between 12.4 $m^3.s^{-1}$ and 17.5 $m^3.s^{-1}$, while a gradual decline is noticed in summer (July-September) with flow dropping to 1.14 $m^3.s^{-1}$ in August.

The interannual variation of mean and maximum annual discharge of the Serein River (Fig. 4.2 and Fig. 4.3) show the practicality of the hydrological year 2001, which is one among several important floods that occurred in the last two centuries (May 1836, May1856, September 1866, 21 January 1910, 28 April 1998 and March 2001).

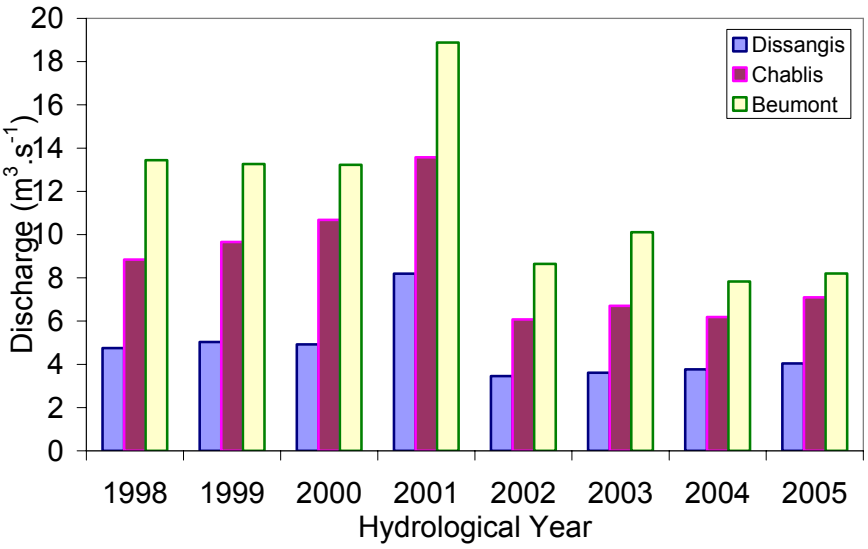

Fig. 4.2 Mean annual discharge in the three major hydrometric stations of the Serein River

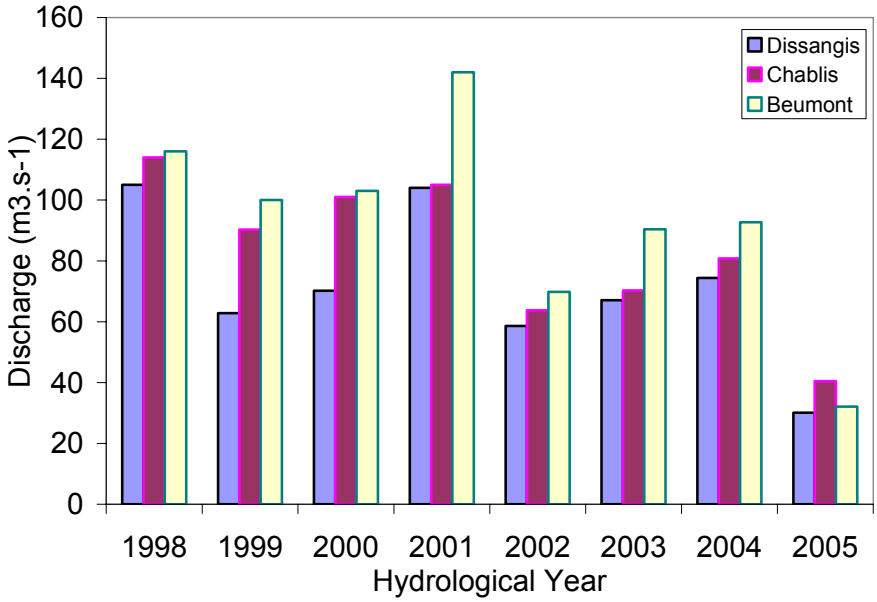

Fig. 4.3 Maximum observed discharges for a given hydrological year

4.3 The construction of the Serein River hydraulic model

The hydraulic model HEC-RAS (chapter 3) is used to construction of the Serein River model. A successful hydraulic simulation depends on the availability of accurate data such as river cross sections geometry and observed stage and discharge hydrographs in simulated river reaches. Fig. 4.4 illustrates the required input data to construct a hydraulic model, while the input data used to construct the Serein River model are summarized in Tab. 4.2

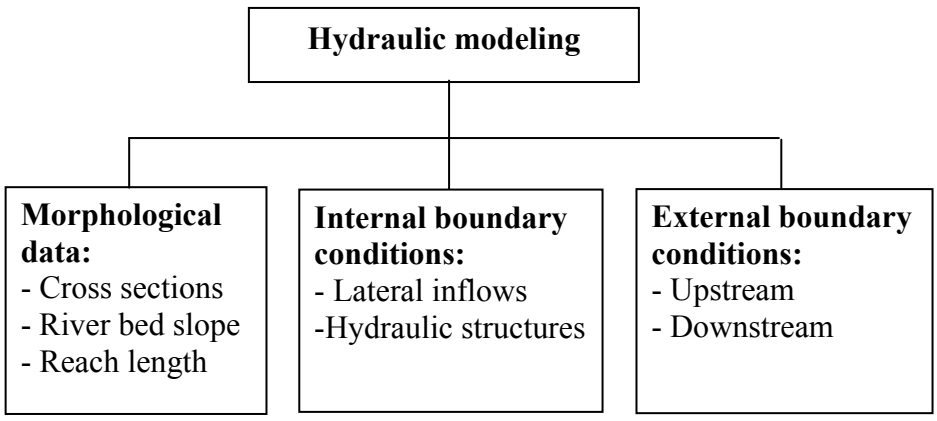

Fig. 4.4 Required input data to construct a hydraulic model

Tab. 4.2 Serein River hydrodynamic model input data

River Geometry	Upstream boundary condition	Downstream Boundary condition	Lateral inflows
20 surveyed cross sections	Observed discharge at Dissangis	Rating curve at Beaumont	Simulated by Eau-Dysée (Chapter 3)

Serein River morphological data

The Serein River geometry data is represented by 20 surveyed cross sections containing the main channel and floodplains. The sections were surveyed by the Direction Régionale de l'Environnement (DIREN) in 2007. The distances between surveyed cross sections vary from 1 km to 10 km (Fig. 4.5), this variation depends on where water surface elevations are required, sudden changes in river cross sectional properties and difficulties faced on the ground while surveying the river geometry. The widths of the floodplain vary from 100 to 600 meters according to the topographical characteristics of the area and the meanders along the river. Each cross section (shown in Annexe. A) is defined by a set of points surveyed perpendicularly to the main stream of the river and its floodplains, each point has an X, Y Lambert II system coordinates to which the elevation above the datum (sea level) is associated.

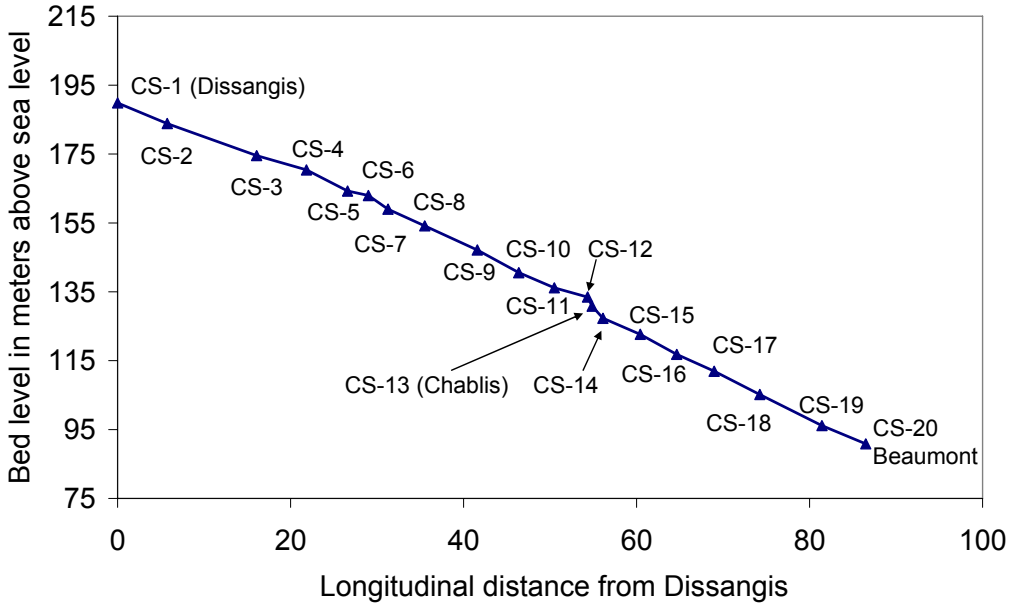

Fig. 4.5 Locations of the Serein River cross sections and main hydrometric stations

Serein River boundary conditions

The upstream boundary condition of the Serein model is defined by an observed mean daily discharge hydrograph at Dissangis (Fig. 4.6). The period of the input discharge hydrograph is from 1 August 1997 to 31 July 2005. The observed discharge hydrograph shows the two important flood events of April 1998 and March 2001 that occurred within the period of simulation.

The downstream boundary condition of the Serein River hydraulic model is an observed single value rating curve (monotonic function of stage and flow) at Beaumont (Fig. 4.7) provided by the DIREN.

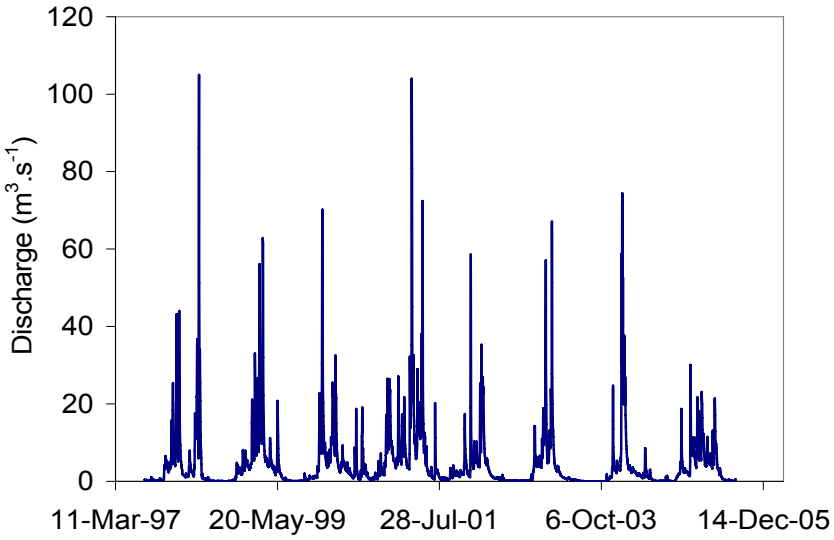

Fig. 4.6 Serein River observed discharge hydrograph at Dissangis used as an upstream boundary condition for the hydraulic model HEC-RAS

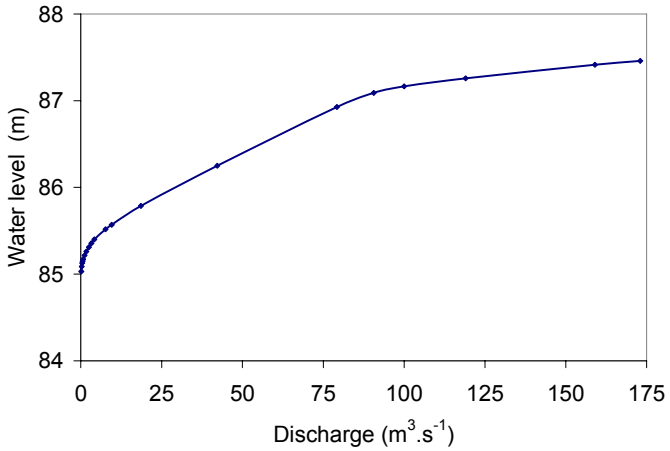

Fig. 4.7 Serein River observed rating curve at Beaumont used as upstream boundary condition

Sub-catchment lateral inflows

The catchment area of the Serein River between Dissangis and Beaumont is 694 km^2 (Fig. 4.8), which represents a catchment area larger than the upstream catchment area at Dissangis (643 km^2). The related lateral inflows are simulated by the hydrological model EauDyssée (Chapter 3). In this framework, runoff is simulated daily in each grid-cell of the contributing area (Fig. 4.8), as a term of water budget (using a production function). It is then routed daily by the ISO module (see section 3.2.1.2) to the 76 cells that represent the stream network (Fig. 4.8). The lateral inflows are thus daily discharge.

At this stage, stream-aquifer interactions are not taken into consideration because the focus is on assessing the sensitivity of the simulated water levels and discharges to the simplification of river geometry.

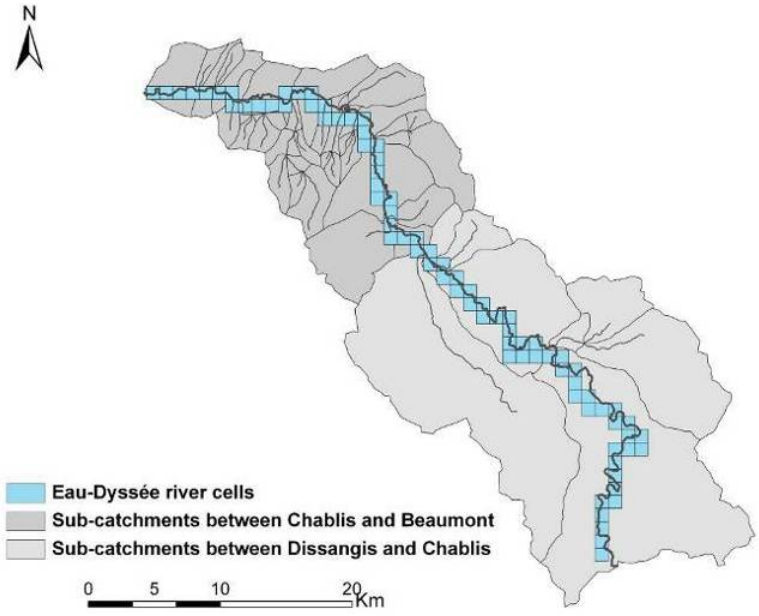

Fig. 4.8 Serein River sub-catchments and EauDyssée river cells between Dissangis and Beaumont

To spatially project the lateral inflows modeled by EauDyssée along the Serein River reach simulated by HEC-RAS, a linear relationship between the river cells of EauDyssée and the Serein River actual reach is developed. From this relationship, the discharge produced by each river cell (1 km * 1 km) is uniformly distributed over 1.3 km of the Serein River reach

by calculating a length equivalency factor between the high resolution river reach and the river grid-cell lengths.

4.3.1 Selection of the model's temporal and spatial computational factors

An important step in unsteady flow simulation models based on the 1D Saint-Venant equations is the proper selection of the time and spatial intervals (Δt , Δx) underlying the finite difference approximation (solved using a 4-point implicit scheme). These parameters influence the accuracy, convergence, robustness and stability of the numerical model (Fread and Lewis, 1993). If the values (Δt , Δx) are too small or randomly selected, the numerical computations can be inefficient to the extent of making the application too expensive or time consuming. If these values are too large, the resulting truncation error (the difference between the true solution of the partial differential Saint-Venant equations and the approximate solution of the (four-point implicit finite difference approximations) can cause significant errors in the computed discharges and corresponding water surface elevations. In this specific case, the errors may be large enough to make the computations totally unrealistic. Unrealistic solutions can cause computer program to abort when computed elevation result in negative depths. Unrealistic solutions can also result in significant irregularities (spurious spikes) in the computed hydrographs.

Temporal computational factor (Δt)

Through several years of experience with dynamic routing models applied to many case studies and using numerical convergence tests for a wide spectrum of unsteady flow applications, Fread (1993) developed an empirical selection criterion between the time step and the hydrograph time of rise:

$$\Delta t \approx \frac{T_r}{20} \qquad \text{Eq. 4.1}$$

Where Tr is the hydrographs time of rise (time from the significant beginning of increased discharge to the peak of the discharge hydrograph), in hours.

Fig. 4.9 illustrates the observed waves time of rise of the two major peaks (April 1998 & March 2001) occurring at the three gauging stations of the Serein River. The peak of April 1998 has a rising time of 19 hrs while the peak of March 2001 has a rising time of 21 hrs. According to the aforementioned equations, the computational time step was set to ~1hr in HEC-RAS simulations.

Other time step increments (0.5, 3, 4, 6, 12, 18, 24 hrs) were also tested for Δx set to 100 m. The comparison between the different time steps showed that the simulated water level and discharge hydrographs are not sensitive to the variation of Δt between 0.5 to 3 hours. However, the time of simulation was influenced, as smaller time steps required more time to complete the simulation. A time step larger than 4 hrs led to a slight numerical oscillation, while time steps larger than 5 hrs (6, 8, 12, 18 and 24 hrs) caused larger numerical oscillations and hence failure in the matrix solving.

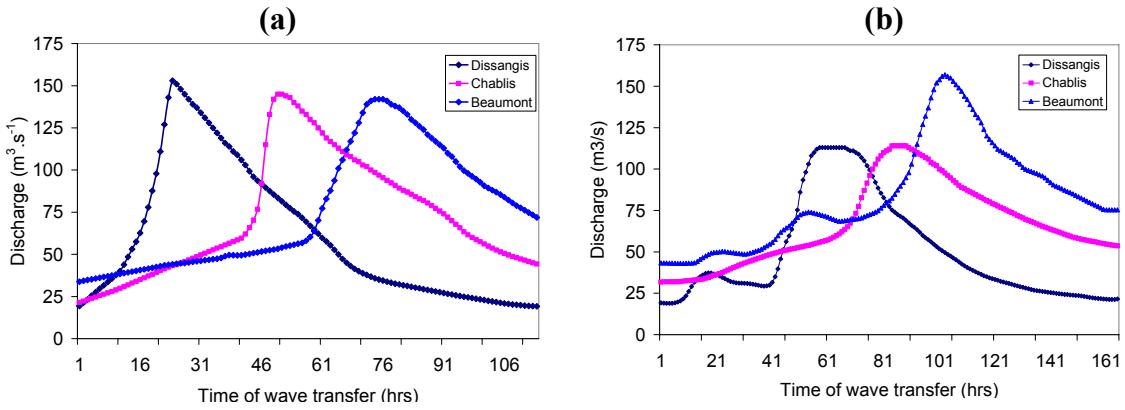

Fig. 4.9 Observed time of wave transfer and river rise of a) The April 1998 flood peak from Dissangis to Beaumont (flood attenuation), b) The March 2001 flood peak from Dissangis to Beaumont (flood amplification)

Spatial computational factor (Δx)

Cross sections are usually located along the river to describe the changes in geometry, discharge, slope, velocity, and roughness. There is no hard and fast guidance concerning the appropriate distance between cross sections. In the author's experience, large rivers (rivers with several thousand square kilometers of watershed) with mild slopes (less than 1.0 $m.km^{-1}$) can have a maximum cross-section spacing of approximately 750 m. On smaller streams with steeper slopes, closer spacing should be the rule. For urban situations, a section every 100 m or less is often needed (Dyhouse et al., 2003).

An empirical selection criterion between the time step and the hydrograph time of rise was developed by Fread (1993):

$$\Delta x \leq \frac{cT_r}{20} \qquad \text{Eq. 4.2}$$

Where T_r is the hydrographs time of rise in hours [T], c is the bulk wave speed or the celerity associated with an essential characteristic of the unsteady flow such as the peak or the center of the hydrograph $[L.T^{-1}]$.

In most applications the bulk wave speed is approximated as the kinematic wave speed. The kinematic wave celerity is approximated as:

$$c = kv \qquad \text{Eq. 4.3}$$

Where k is the kinematic wave ratio having values ranging from $4/3 \leq k \leq 5/3$ ($k \approx 1.5$ for most natural channels), v is flow velocity.

The peak flow velocity between Dissangis and Beaumont during the 1998 peak is 0.48 $m.s^{-1}$ and 0.6 $m.s^{-1}$ for the 2001 peak (Fig. 4.9).

Because the period of simulation (1997-2005) is too long when compared to classic hydraulic simulations and input hydrographs contain several peaks with wave transfer time fluctuating as function of the intensity and hydrological properties of the flood (Fig. 4.9), it was not evident to obtain numerical convergence depending on the above Δx, Δt selection criteria. To overcome that, a wide spectrum of convergence tests was conducted to select the most appropriate Δx. Large distance steps ($\geq 1000m$) created numerical oscillations and failure in matrix solution for high flow periods. The Δx of 250 m was found to be stable for both high and low flow simulations. However numerical oscillations occurred when conducting sensitivity analysis on Manning's roughness coefficient. The Δx of 100m was found to be the most stable spatial step and therefore adopted for all model simulations and sensitivity analysis.

4.3.2 Manning's roughness coefficient (*n*) calibration

Manning's *n* normally carries the most uncertainty in hydraulic modeling. In this study a wide range of possible Manning's roughness coefficients values for both the main channel and floodplain are investigated to calibrate the model.

The calibration of Manning's roughness coefficient (*n*) was investigated at Chablis hydrometric station where observed water levels and discharge hydrographs are available. The roughness coefficient was supposed to be uniform along the 89 km of the river. Sensitivity analysis was performed with *n* of the main channel ranging from 0.01 to 0.05 with an increment $\Delta n = 0.002$, and from 0.05 to 0.1 with $\Delta n = 0.01$ while the one of the floodplain ranged from 0.02 to 0.2 with $\Delta n = 0.01$.

The influence of Manning's *n* in the main channel is well illustrated when looking at the simulated rating curves (discharge vs. water levels) (Fig. 4.10). The increase of Manning's roughness coefficient in the main channel increases the simulated stage and attenuates the

associated peak discharge. These findings confirm the importance of appropriately selecting the Manning's roughness coefficient, especially when accurate water levels are needed (e.g. stream-aquifer interactions).

However, the variation of *n* in the floodplain did not influence the results at Chablis; this is due to the fact that no overtopping has occurred in Chablis section during the period of simulation. The slight overtopping upstream from Chablis seemed to have no influence on the simulated stage and discharge hydrographs at Chablis when using higher values of *n* in the floodplain.

The value of *n* equal to 0.028 for the main channel was found to be the optimal value in the Serein River model. Results for the discharges and water levels at Chablis are shown in Fig. 4.11 and Fig. 4.12. Moreover, the model exhibits satisfactory statistical criteria at Chablis with both correlation coefficients equal to 0.96 (Tab. 4.3).

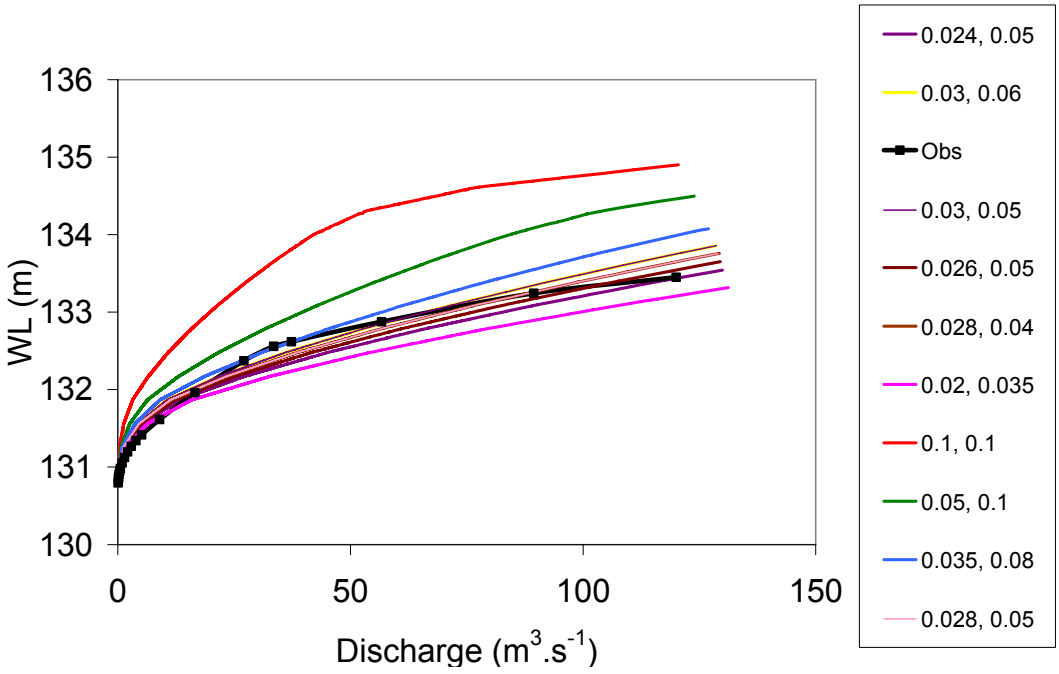

Fig. 4.10 Sensitivity of simulated rating curves at Chablis to the variation of a selected range of Manning's roughness coefficients (n) in the main channel (legend left values) and floodplain (legend right values)

Using different friction coefficients for different river segments between Chablis and Beaumont may improve the calibration, but as there are no reference points for this reach, no justification for the use of different individual friction values can be given.

In addition to simulated discharge and water levels, the outputs of the hydrodynamic model also include rating curves simulated at each river cross section along the Serein River (Annexe. A).

Tab. 4.3 Performance evaluation of the Serein River hydraulic Model at Chablis

	Average observed	**Average Simulated**	**Nash**	**Bias %**	**RMSE**	**Correlation coefficient**
Q	8.6 $m^3.s^{-1}$	8.37 $m^3.s^{-1}$	0.90	-2.67 %	3.72 $m^3.s^{-1}$	0.96
WL	131.49 m	131.57 m	0.89	0.06 %	0.14 m	0.96

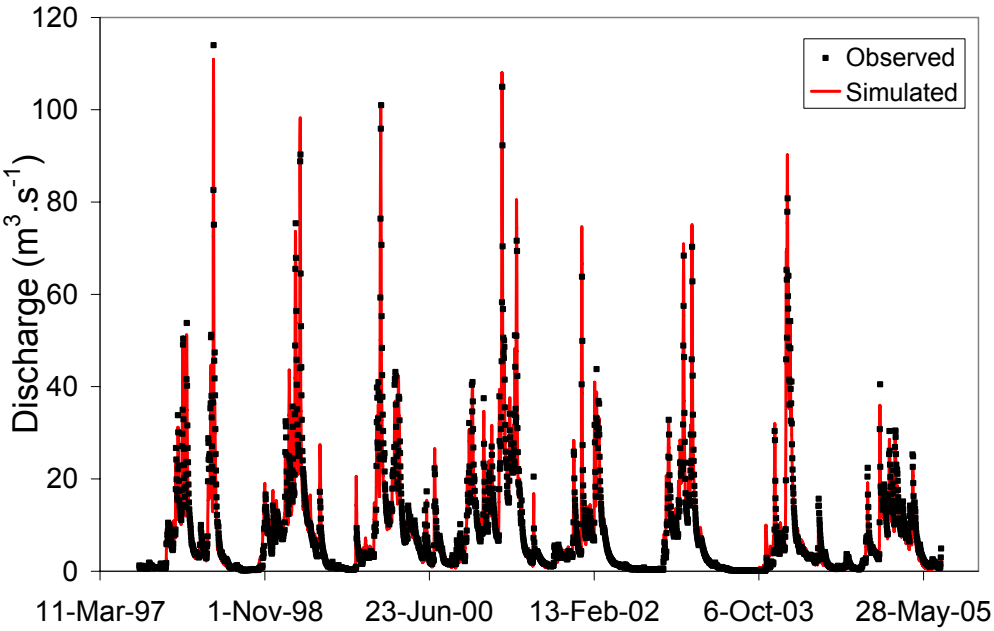

Fig. 4.11 Observed vs. simulated discharge hydrographs at Chablis hydrometric station (nchannel = 0.28, nfloodplain = 0.04)

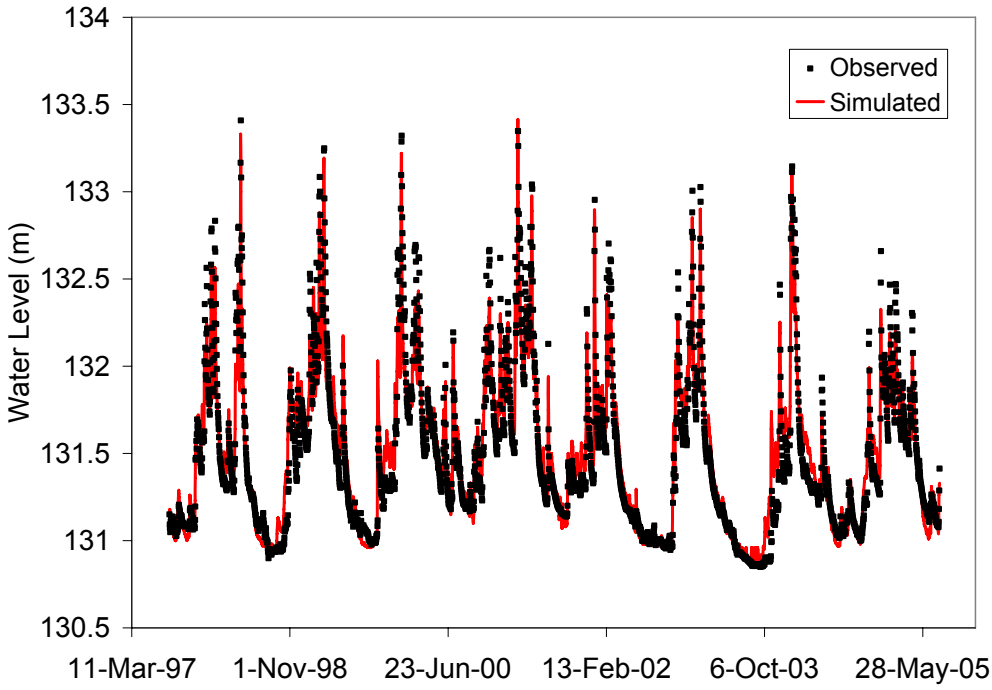

Fig. 4.12 Observed vs. simulated stage hydrographs at Chablis hydrometric station (nchannel = 0.28, nfloodplain = 0.04)

4.4 Impact of river morphology on river stage and discharge

In this section, several "what if" geometry scenarios are tested to assess the impact of morphological data on the simulated in-stream water levels and discharges (Tab. 4.4).

In this context, the cross sections shape and spatial sampling are both explored to determine the most appropriate simplified river representation geometry in areas where cross sections surveys are not available.

The analysis of geometry scenarios (Tab. 4.4) are classified into the following categories:

- Impact of spatial sampling of cross sections (GS-I, GS-II, GS-III).
- Impact of cross sections shape (GS-IV, GS-V).
- Effect of both shape and spatial sampling (GS-VI, GS-VII, GS-VIII).

In terms of spatial sampling, two methods are used to represent the river bed profiles in the Serein River. The first method consists of using the twenty surveyed bed levels (Fig. 4.13) while the second one consists of linearly interpolating the bed levels using only three known

bed levels located at Dissangis, Chablis and Beaumont (Fig. 4.13). These two methods induce different river bed slopes.

The change in the surveyed river bed levels generated by linear interpolation between the three major hydrometric stations varied between + 4 m along the river reach between Dissangis and Chablis, and -2 m along the river reach between Chablis and Beaumont (Fig. 4.14). The comparison illustrates the non uniformity of bed levels and longitudinal slopes along the Serein River.

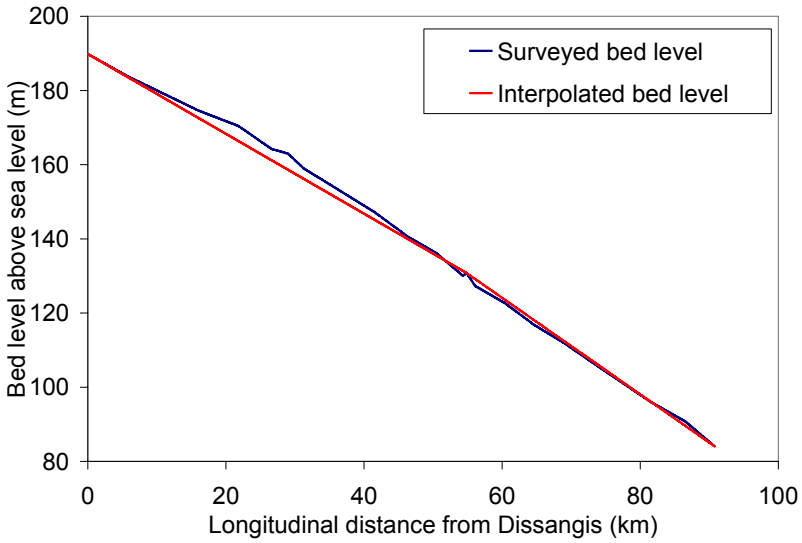

Fig. 4.13 Comparison between surveyed and interpolated bed levels of the Serein River

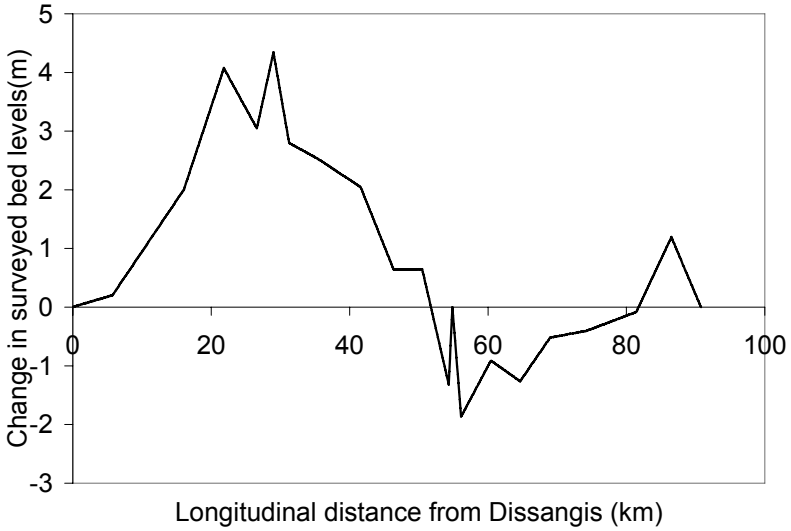

Fig. 4.14 The change in the river surveyed bed levels generated from the linear interpolation between the three major hydrometric stations bed levels located at Dissangis, Chablis and Beaumont

Tab. 4.4 “What if” geomtery scenarios tested on the Serein River hydrualic model

Scenario	River cross-section representation	Bed level	Objective
GS*-I	Removing all cross sections containing two conveying arms (islands).	Original surveyed bed levels.	Evaluate the importance of detailed river geometry at local and basin scale and its influence on simulation’s quality and numerical convergence of the hydraulic model.
GS-II	Only three surveyed cross sections (located at major hydrometric stations) are used to represent the geometry of the river.	Only three surveyed bed levels located at major hydrometric stations, remaining bed levels are linearly interpolated between the three known bed levels.	Importance of spatial distribution of cross sections.
GS-III	Generalizing only one irregular surveyed cross section along the river reach: a- Dissangis sections generalized along the river. b- Chablis sections generalized along the river. c- Beaumont sections generalized along the river.	Only three surveyed bed levels located at major hydrometric stations, remaining bed levels are linearly interpolated between the three known bed levels.	Importance of the description of an average cross-section if any.
GS-IV	Excluding the floodplain from the model and using only surveyed main channels to represent the river geometry. In case of overtopping, bank walls will be extrapolated vertically.	20 surveyed bed levels.	Examine the sensitivity of simulated water level peaks to the presence of floodplain. The test also aims at identifying the attenuation in water levels of a composed channel (main channel + floodplain) compared to that obtained by only using the main channel geometry.
GS-V	Replacing each irregular surveyed section by a trapezoidal section.	20 surveyed bed levels.	Test the sensitivity of simulated water levels and discharge hydrographs to the irregularities in main channel cross sections.
GS-VI	Representing the river geometry by a trapezoidal section obtained from average	Both spatial sampling methods are used, GS-VIa uses only three	

	surveyed information of 20 irregular sections.	surveyed bed levels located at major hydrometric stations while GS-VIb uses 20 surveyed levels.	Test the sensitivity of simulated water level and discharge hydrographs to the cross sectional shape representation of geometry and interpolated bed level slopes.
GS-VII	Representing the river geometry by a triangular section obtained from average surveyed information.	Only three surveyed bed levels located at major hydrometric stations, remaining bed levels are linearly interpolated between the three known bed levels.	
GS-VIII	Representing the river geometry by a rectangular section obtained from average surveyed information. Followed by the recalibration of Manning's n to improve results.	Only three surveyed bed levels located at major hydrometric stations, remaining bed levels are linearly interpolated between the three known bed levels.	

***GS = Geometry Scenario**

All geometry scenarios use the hydraulic computational parameters selected through calibration (section 4.5) and summarized in Tab. 4.5.

The results obtained from different "what if" scenarios are compared with observed water level and discharge hydrographs at Chablis. Furthermore, results are also compared longitudinally with the discharge, water levels and maximum water depth obtained by the reference simulation. The reference simulation refers to results obtained using the most documented river geomorphological data (Tab. 4.5). Results obtained from each geometry scenario are presented in the following subsections, (4.6.1 - 4.6.8) with a final synthesis of the overall results is represented in section 4.7.

Tab. 4.5 Hydraulic calibrated parameters used for the testing of river geometry

UBC	**Lateral inflows**	**DBC**	Δt	Δx	θ	n_c	n_f
Observed Discharge Hydrograph	76 EauDyssée cells	Rating Curve at Beaumont	1 hr	100 m	1	0.028	0.04

Where **UBC** is the upstream boundary condition, **DBC** is the downstream boundary condition, Δt is the computational time step, Δx is the computational distance step, θ is the implicit weighting factor, n_c is the main channel Manning's roughness coefficient and n_f is the floodplain Manning's roughness coefficient.

4.4.1 Scenario GS-I: Removing cross sections that contain two conveying arms (islands)

In this particular scenario, cross sections containing two conveying channels are removed from the geometry representation of the Serein River. The main objective of this test is to evaluate the influence of such cross sectional level of detail on the quality of the simulations and the effects on the numerical convergence of the model.

Four cross sections with islands are replaced in the model (Fig. 4.15):

- CS-4 located at 21.89 km from Dissangis.
- CS-5 located at 26.58 km from Dissangis.

- CS-9 located at 35.5 km from Dissangis.

- CS-10 located at 41.57 km from Dissangis.

The removed sections are replaced by interpolated sections obtained from adjacent sections.

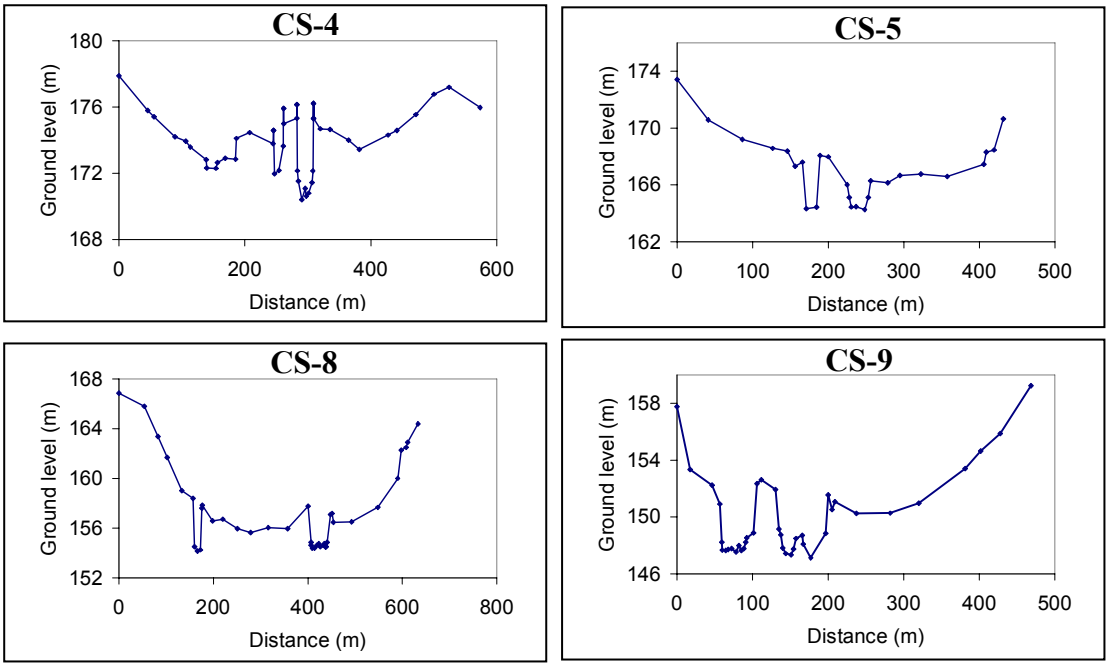

Fig. 4.15 Cross sections containing two conveying arms are removed from the morphological representation of the Serein River

The results obtained from this scenario show that the removal of the sections has no impact on the wave time of transfer and the simulated discharge hydrographs. Furthermore, simulated water levels and discharge hydrographs at Chablis are not influenced by the removal of these sections (Tab. 4.6).

Tab. 4.6 Fit between simulated and observed discharge and water levels at Chablis, addressed in terms of Nash efficiency and RMSE for GS- I scenario

Type of geometry	**Nash WL**	**Nash Q**	**RMSE WL (m)**	**RMSE Q ($m^3.s^{-1}$)**
GS-I	0.88	0.90	0.16	3.71
Reference simulation	0.89	0.90	0.14	3.72

The results also show that maximum water depths are only influenced locally in river reaches where cross sections are removed, this impact varies between 0.1 m and 1 m (Fig. 4.16).

In terms of numerical convergence, the model with no islands is more stable than the original model and it allowed us to use spatial computational steps that are equal or larger than 2 km. The test exhibits the importance of using accurate cross sections where water levels are required at site scale but for regional simulations the removal of the islands seems to be an acceptable approximate.

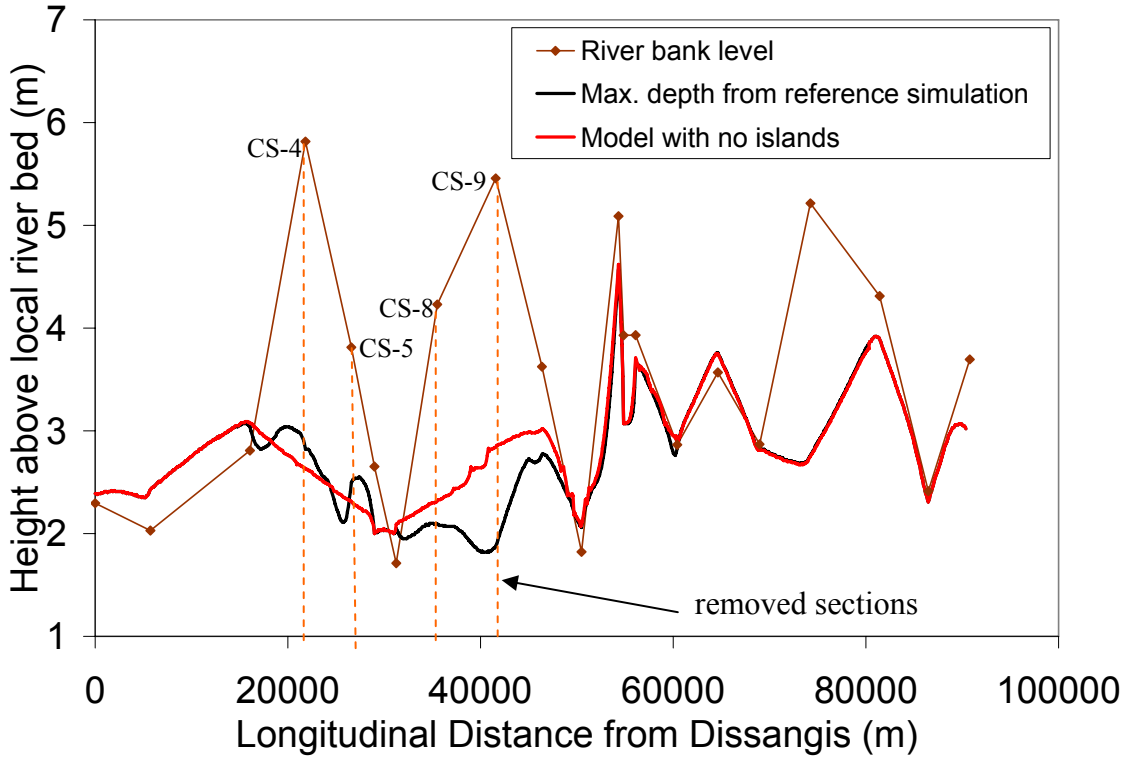

Fig. 4.16 Longitudinal comparison of maximum water depths between the simulation of reference and the obtained simulation using scenario GS-I river morphological representation

4.4.2 Scenario GS-II: Only three surveyed cross sections used to represent the geometry of the Serein River

This scenario evaluates the prediction accuracy of the hydraulic model when subsampling the river geometry with only three surveyed cross sections. These surveyed sections are located at major hydrometric stations (Dissangis, Chablis, and Beaumont) (Fig. 4.17). The linear interpolation proposed as preprocessing in HEC-RAS was used to generate additional cross sections between the three known surveyed sections with a spatial increment of 100 m along the Serein River. The bed levels of these interpolated cross sections were thus linearly interpolated between the three known bed levels of the surveyed sections.

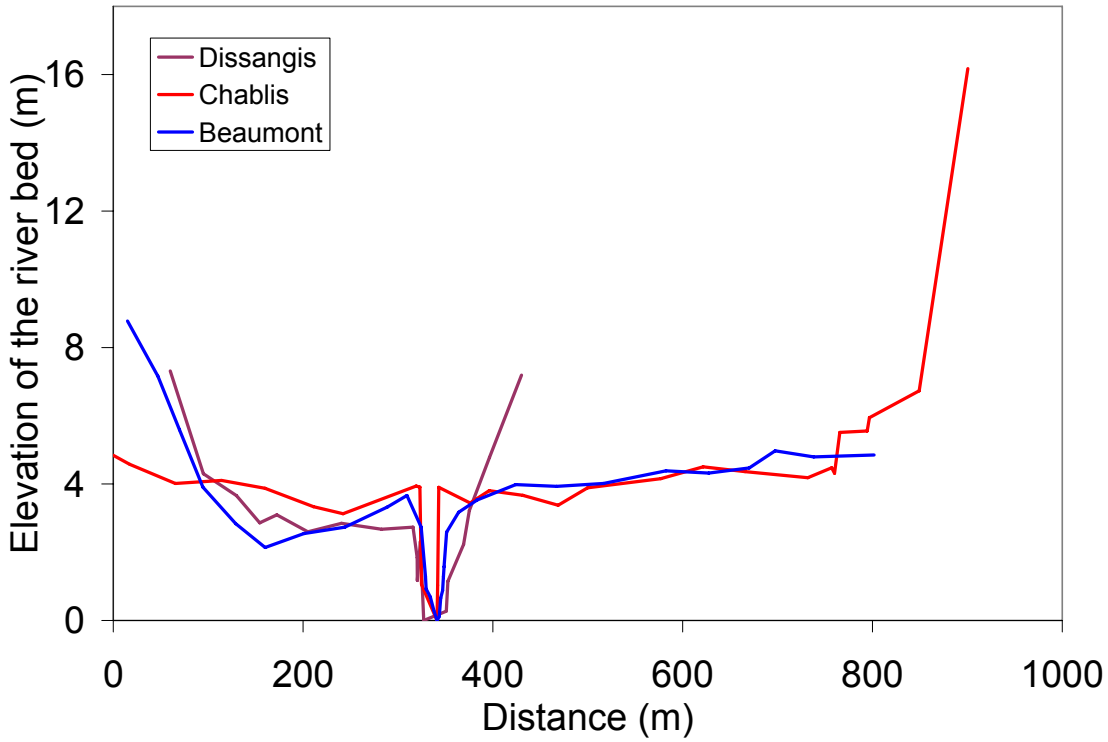

Fig. 4.17 Surveyed cross sections at Dissangis, Chablis and Beaumont

In terms of simulated water levels, the Nash and RMSE statistical criteria compared with observations at Chablis station are 0.86 and 0.18 m respectively, which are consistent with measurements (Tab. 4.7). However, the model did not accurately represent the maximum water depths when compared longitudinally to the maximum water levels obtained from the reference simulation (Fig. 4.18). The maximum water depths obtained from this scenario vary between 2 and 3 m with an average of 3.2 m, while in the reference simulation, the maximum water depths vary between 2 and 5 m with an average of 2.7 m. In certain river cross sections, simulated maximum water depths from this scenario are more than 1 m higher than the ones obtained in the reference simulation, especially upstream from the Chablis hydrometric station. This is due to the linearly interpolated bed levels and the uniformity of cross sections representing the river.

The results of this scenario show the importance of using several surveyed cross sections for a given river reach, especially where sudden change in cross section shape or bed level slope

occur. It also illustrates that comparing the simulation of the model with observations at one single point is not enough to evaluate the accuracy of the model.

Tab. 4.7 Fit between simulated and observed discharge and water levels at Chablis, addressed in terms of Nash efficiency and RMSE for GS- II scenario

Type of geometry	**Nash WL**	**Nash Q**	**RMSE WL (m)**	**RMSE Q ($m^3.s^{-1}$)**
GS-II	0.86	0.89	0.18	3.98
Reference simulation	0.89	0.90	0.14	3.72

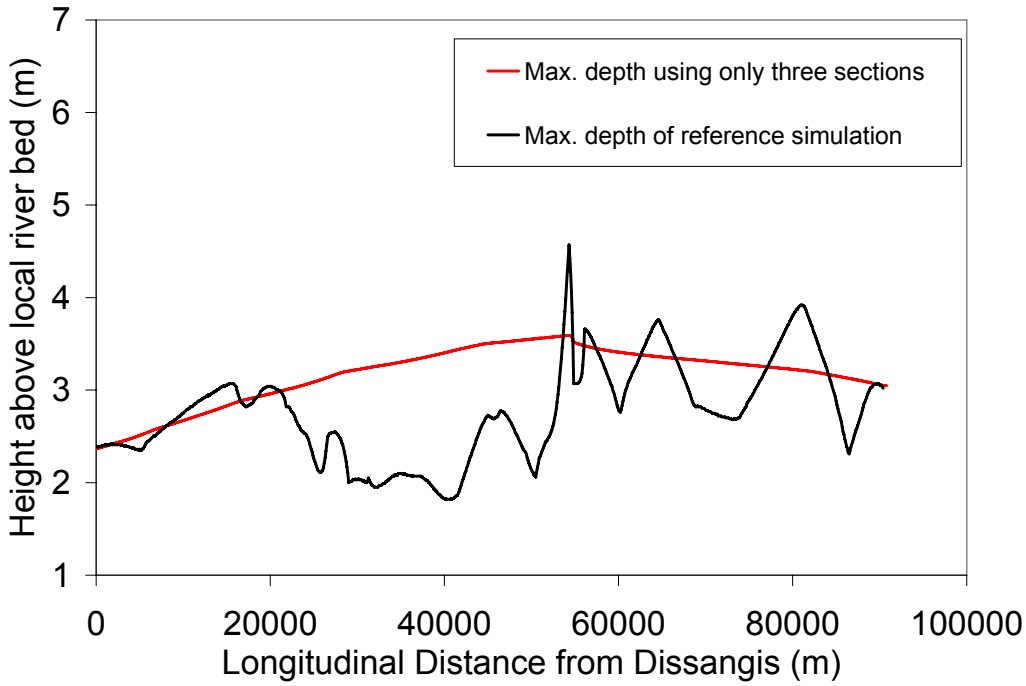

Fig. 4.18 Longitudinal comparison of maximum water depths between the simulation of reference and the obtained simulation using scenario GS-II river morphological representation

4.4.3 Scenario GS-III: Uniformly generalizing one surveyed cross section along the river reach

The scenario explores further the sensitivity of simulated water level and discharge hydrographs to the spatial sampling of cross sections using a single surveyed cross section. The single section is interpolated at constant distance steps (100 m) and generalized along the 89 km river reach. Three tests were conducted in this particular scenario, the first test was conducted by generalizing the surveyed cross section at Dissangis, the second test uses the surveyed cross section at Chablis, while the third test uses the surveyed section at Beaumont

(Fig. 4.17). In all three tests, bed levels are interpolated linearly between the surveyed bed levels of the three major hydrometric stations (Dissangis, Chablis, and Beaumont). The Comparison of wetted area and wetted perimeter characteristics of the three cross sections located in Dissangis, Chablis and Beaumont show that the Serein River cross sections do not depend on the catchment area they drain because they exhibit different morphologies (Fig. 4.19). The main river cross section at Dissangis which drains a basin area of 643 km^2 has larger conveying capacity and width than Chablis (1120 km^2) and Beaumont (1337 km^2), while the cross sections at Chablis and Beaumont have very close hydraulic properties for the main channel.

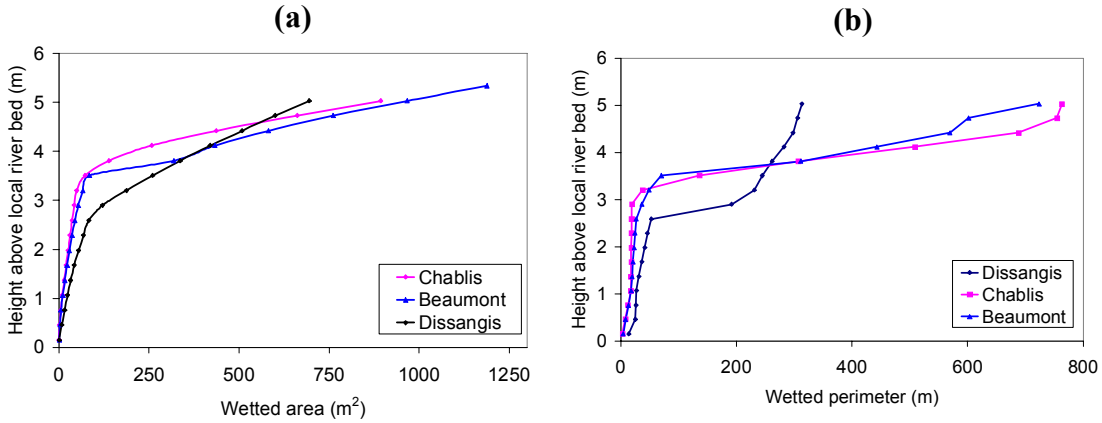

Fig. 4.19 Comparison between Dissangis, Chablis and Beaumont a) Cross sectional wetted area; b) Cross sectional wetted perimeter

Among the three simplified geometries, the best fit to observations in Chablis is obtained by generalizing the Beaumont cross-section (Fig. 4.20 & Tab. 4.8). More importantly, this comparison shows that using generalized geometry to represent the river has hardly no influence on simulated discharge while it sharply influences simulated water levels. This is because observed discharge hydrographs are used as upstream boundary conditions.

The average simulated water level in Chablis obtained by generalizing the Dissangis cross-section is 131.3 m which is equivalent to 0.5 m of water depth. This water depth is 0.4 cm lower than the average simulated water levels obtained by generalizing the Beaumont or

Chablis cross-sections of which the average water level is 131.7 m (0.9 m water depth) (Fig. 4.20).

The maximum simulated water levels in Chablis obtained by generalizing the Dissangis section is 133.21 m while the ones obtained by generalizing the Chablis and Beaumont cross-sections are 134.4 m and 134.35 m respectively (Fig. 4.20). This difference is due to the shape of the Dissangis cross-section which is twice wider than the Chablis and Beaumont cross sections. It has hence larger transfer capacity at lower water levels (Fig. 4.17).

Tab. 4.8 Fit between simulated and observed discharge and water levels at Chablis, addressed in terms of Nash efficiency and RMSE for GS- III scenario

Section generalized to represent the geometry	**Nash WL**	**Nash Q**	**RMSE WL (m)**	**RMSE Q ($m^3.s^{-1}$)**
Dissangis section	0.72	0.89	0.25	3.82
Chablis section	0.69	0.88	0.265	4.12
Beaumont section	0.80	0.90	0.21	3.75
Reference simulation	0.89	0.90	0.14	3.72

The longitudinal comparison of maximum water depths (Fig. 4.21) shows that the two simulations generalizing the sections of Chablis and Beaumont produce close maximum water depth levels, while the ones obtained by generalizing the Dissangis cross-section are lower. This is due to the fact that the cross sections at Dissangis have different geometric characteristics, as stressed earlier (Fig. 4.19).

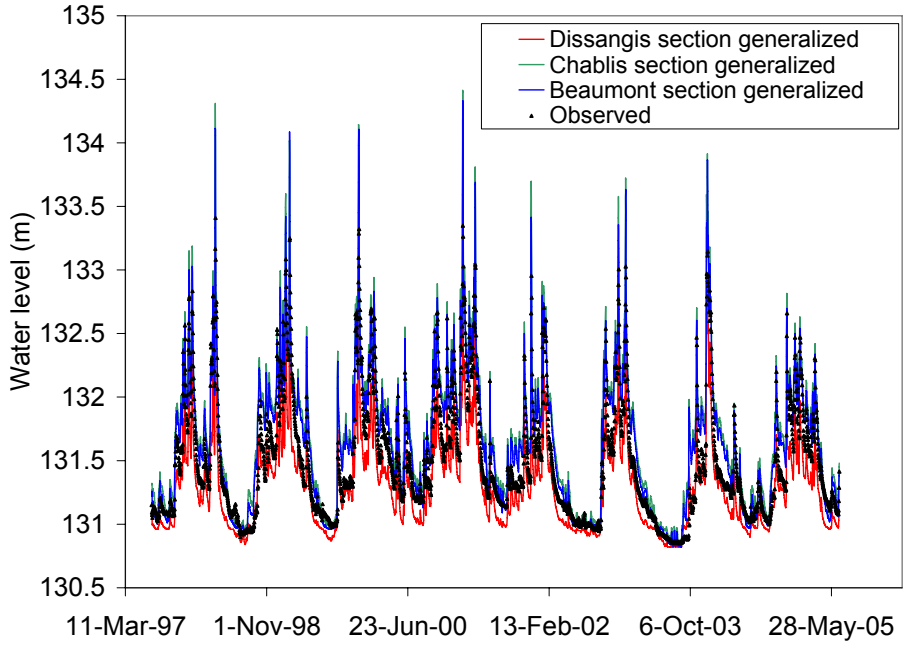

Fig. 4.20 Comparison of simulated water level hydrographs at Chablis using three geometry representation scenarios generalize along the river (Dissangis, Chablis and Beaumont)

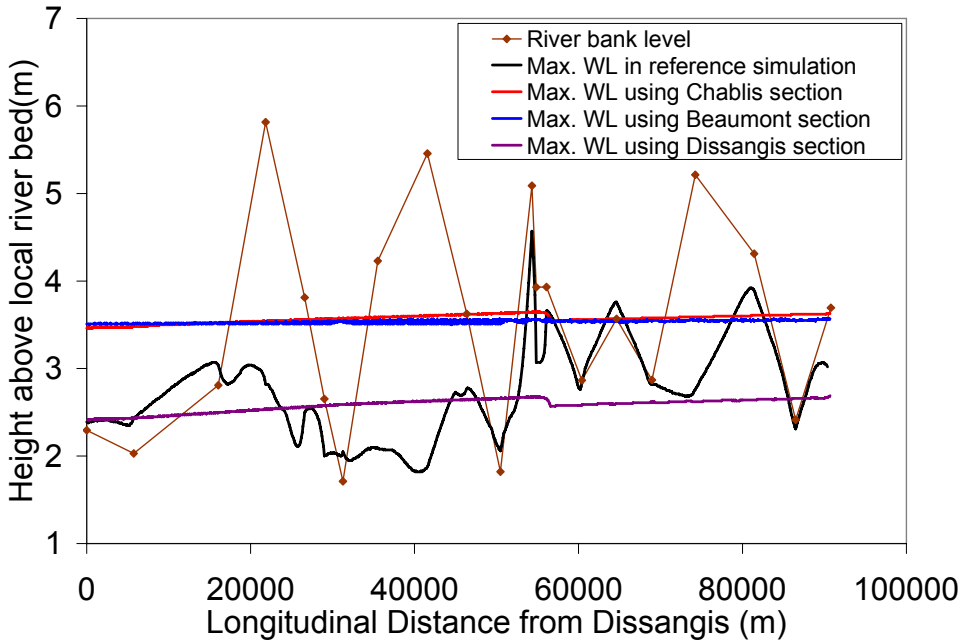

Fig. 4.21 Longitudinal comparison of maximum water depths using one surveyed section generalized along the Serein River (GS-III)

4.4.4 Scenario GS-IV: Excluding the floodplains from the geometry representation of the Serein River

In this scenario, only surveyed main channels are used for representing the geometry of the Serein River. All floodplains are removed from the river geometry. The main channel bank walls are extrapolated vertically if the water levels overtop the river bankfull level.

The objective of this scenario is to examine the sensitivity of simulated water level peaks to the presence of floodplain (composed channel) and to assess the attenuation of flood peaks by a river composed of a main channel and floodplain compared to the one of a main channel only.

The simulated water levels and discharges at Chablis are slightly influenced by the removal of floodplains from the representation of the geometry. The RMSE of water levels is reduced to 0.14 m compared to 0.16 m in the reference simulation, while the RMSE of discharge is reduced to 3.56 $m^3.s^{-1}$ compared to 3.72 $m^3.s^{-1}$ in the reference simulation. This slight improvement in results at Chablis is not due to the interaction between the main channel and floodplain in Chablis, because no overtopping occurred in Chablis station during the period of simulation. The slight influence on results is due to the influence of overtoppings and main channel floodplain interactions upstream and downstream from the Chablis section (Tab. 4.9).

Tab. 4.9 Fit between simulated and observed discharge and water levels at Chablis, addressed in terms of Nash efficiency and RMSE for GS- IV scenario

Type of geometry	**Nash WL**	**Nash Q**	**RMSE WL (m)**	**RMSE Q ($m^3.s^{-1}$)**
Scenario GS-IV	0.87	0.90	0.16	3.56
Reference simulation	0.89	0.90	0.14	3.72

The comparison was extended with section 18 (located 5.8 km from Dissangis) where overtopping has been simulated in the simulation of reference (Fig. 4.22). Observed water level hydrographs are not available in this section so the comparison was based on comparing two simulated hydrographs: the first is obtained using only the surveyed main channel geometry and vertical walls instead of floodplains, while the second one is obtained using the reference simulation (main channels connected to floodplains) (Fig. 4.22). The Results show the consequence of GS-IV on the 2001 peak water level which is attenuated from 186.4 m (2.6 m water depth) to 186.2 m (2.4 m water depth) when flood expansion is allowed to the

floodplain in this cross-section (Fig. 4.22 and Fig. 4.23 b). The 1998 peak water level is also attenuated by 12 cm in this particular cross-section (Fig. 4.23 a), which shows the influence of floodplain expansion in attenuating the peak water levels.

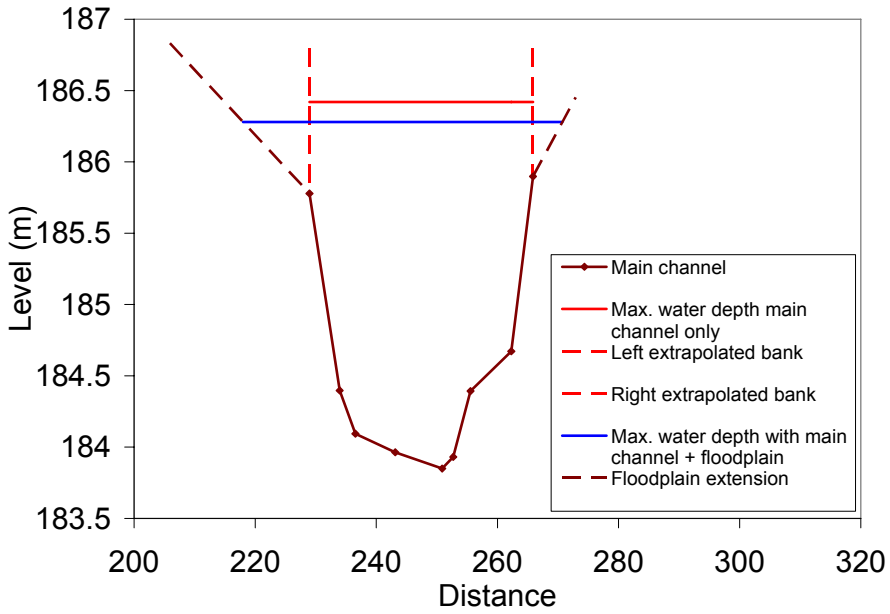

Fig. 4.22Comparison of maximum water depths between the simulation of reference and scenario GS-IV in cross section 18 during the 2001 flood

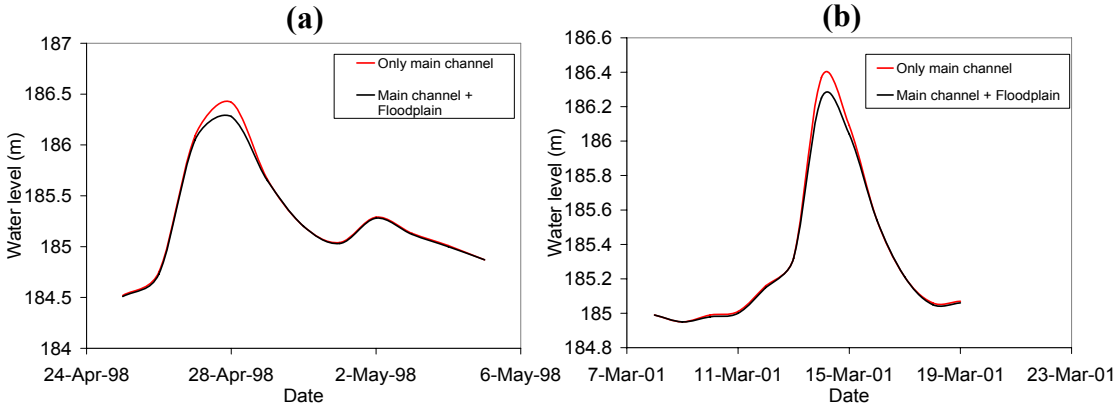

Fig. 4.23 Comparison of peak simulated water levels between the simulation of reference and GS-IV at section 18 (Fig. 4.22): a) April 1998 flood; b) March 2001 flood

Finally, the maximum water depths along the river reach were longitudinally compared in order to assess the influence of floodplains on the whole river reach (Fig. 4.24).

The influence of floodplain expansion in attenuating the peak water levels varies between 10 cm and 20 cm, particularly in the first 15 km reach nearby Dissangis and the 8 km reach upstream of Chablis where the main channel is not so deep (< 2.5 m) and where overtopping

occurs during high flow periods. The results exhibit the role of floodplain on water level attenuation when compared to the reference simulation of which slight overtopping occurred in certain reaches.

In this particular case study the impact of floodplains on simulated overtopping remains not very large but it might have important potential impacts in different flooding periods or other river case studies where overtopping is more important.

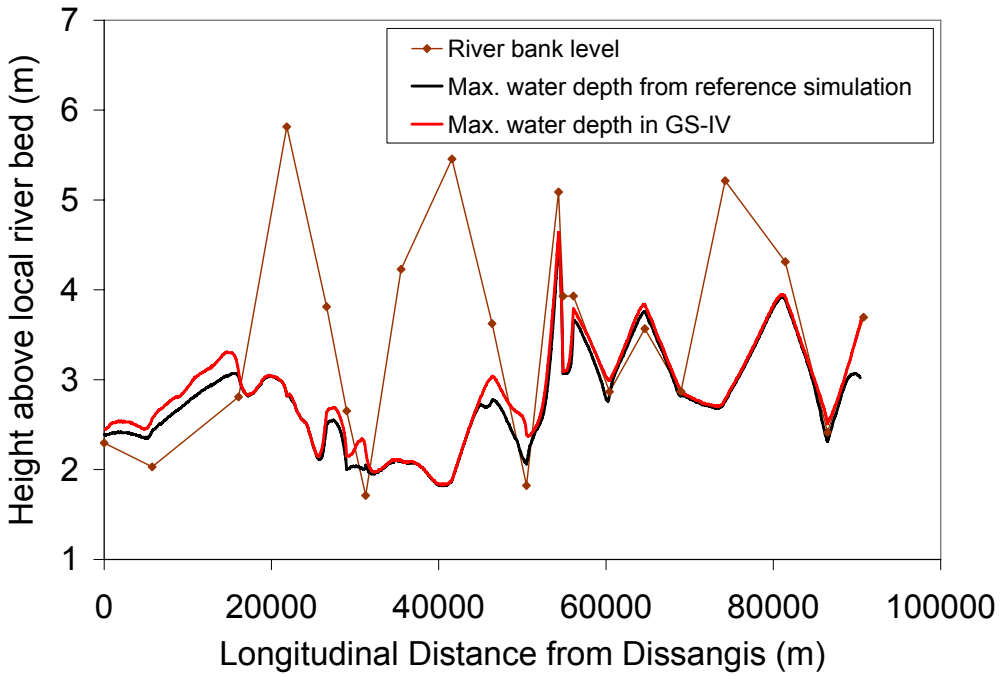

Fig. 4.24 Longitudinal comparison of maximum water depths along the Serein River (scenario GS-IV vs. simulation of reference)

4.4.5 Scenario GS-V: Replacing each irregular surveyed section by an equivalent regular trapezoidal section

After examining the influence of the floodplain's representation, we address here the sensitivity of simulated water levels and discharge hydrographs to the simplification of the main channel geometry. The surveyed main channels (irregular sections) are replaced by equivalent trapezoidal sections (regular sections). The wetted area, depth and bankfull width properties of each irregular section were used to define the bottom width and side slope of the trapezoidal section while the geometry of the floodplain is kept unchanged. An example of

this main channel modification is illustrated in a cross-section located at 74 km downstream from Dissangis (Fig. 4.25).

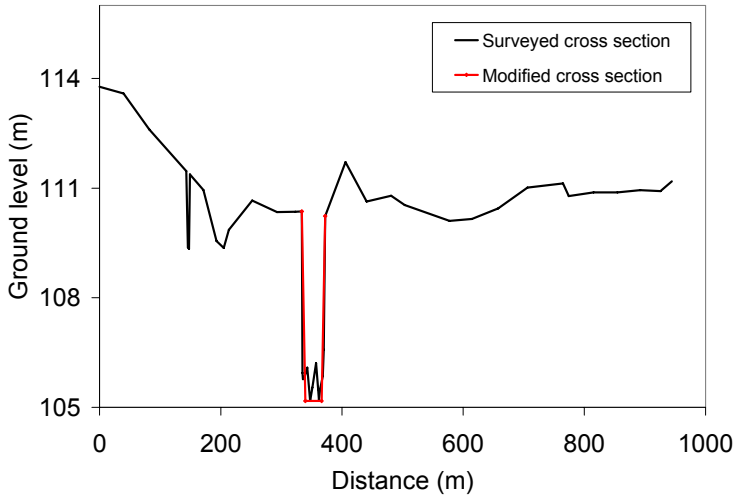

Fig. 4.25 River geometry scenario GS-V: example of main channel modification from irregular to regular shape in a cross-section located at 74 km downstream of Dissangis

The comparison between simulated and observed water levels at Chablis station shows that using this type of cross-sectional geometry with original surveyed bed levels reduces the Nash efficiency from 0.89 to 0.7 and increases the RMSE from 0.14 m to 0.26 m.

The discharge and water level hydrographs in other cross-sections are also compared at each cross section with the reference simulation using the Nash criterion (Fig. 4.26).

The results show that using this type of geometry to represent the river has no impact on simulated discharge while it sharply influences simulated water levels in many cross sections. The Nash statistical criterion for water levels is inferior to 0.5 in many cross sections downstream of Chablis while it is consistent with the reference simulation in other cross sections (> 0.7), particularly in ones upstream of Chablis (Fig. 4.26). The less accurate results (Nash < 0.2) are found in the cross-section located at 74 km downstream from Dissangis (Fig. 4.25 and Fig. 4.26).

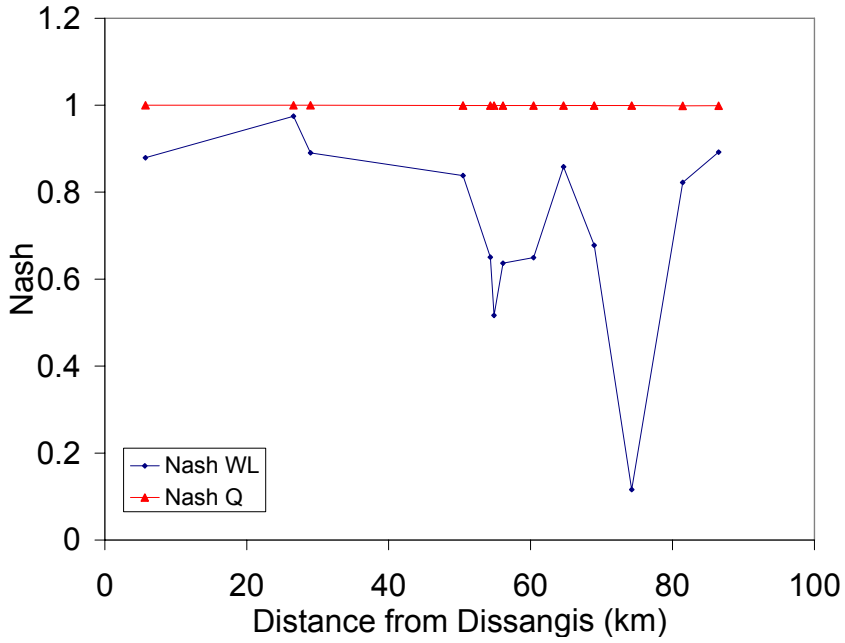

Fig. 4.26 Nash statistical index compared at each cross section between discharge and water level hydrographs obtained from the simulation of reference and ones obtained from using GS-V geometry

In this particular cross-section, the comparison of the simulated water levels hydrograph with the reference simulation (Fig. 4.27) shows the impact of cross sectional morphological modification on simulated water levels, especially during low flow periods where the water levels are, on average, 20 cm lower than the ones in the reference simulation. This is due to the fact that the lower the water level, the more important the friction is. Thus the description of the cross section geometry is crucial for low flow modeling. These cross-section bottom irregularities are neglected by the trapezoidal section which considers a plain bottom width.

The difference between the two simulations becomes less important when the water level rises towards the bank level (Fig. 4.27) because the difference between the two wetted areas characteristics decreases as the water level rises towards the bank level (Fig. 4.28).

The comparison of the wetted area characteristics between the original and modified sections (Fig. 4.28) shows that as the water level of the regular section approaches the bankfull level, the hydraulic characteristics of the regular section becomes equal to the hydraulic characteristics of the irregular sections:

If $Z_r = Z_{bf}$ Then $A_r \approx A_{ir}$ & $T_r \approx T_{ir}$

Where Zr is the water level in the regular channel, Z_{bf} is the bankfull water level, A is the wetted cross sectional area and T is the top width. Subscripts r and ir stand for regular and irregular sections, respectively.

An improvement in results might be obtained by varying the Manning's roughness coefficient vertically (Fread and Lewis, 1998).

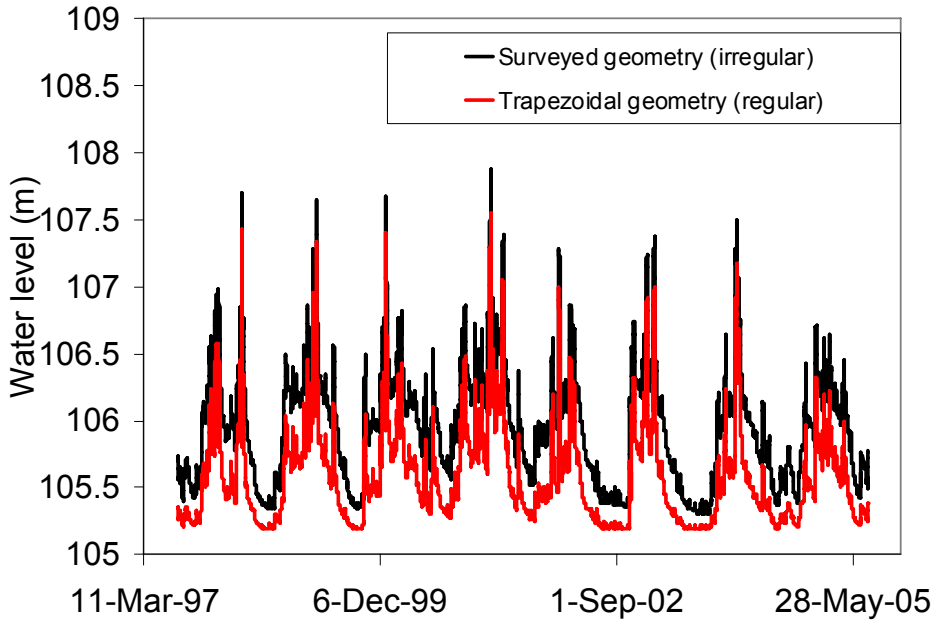

Fig. 4.27 Comparison of water levels obtained from regular and irregular geometrical shape of the cross-section located at 74 km downstream of Dissangis

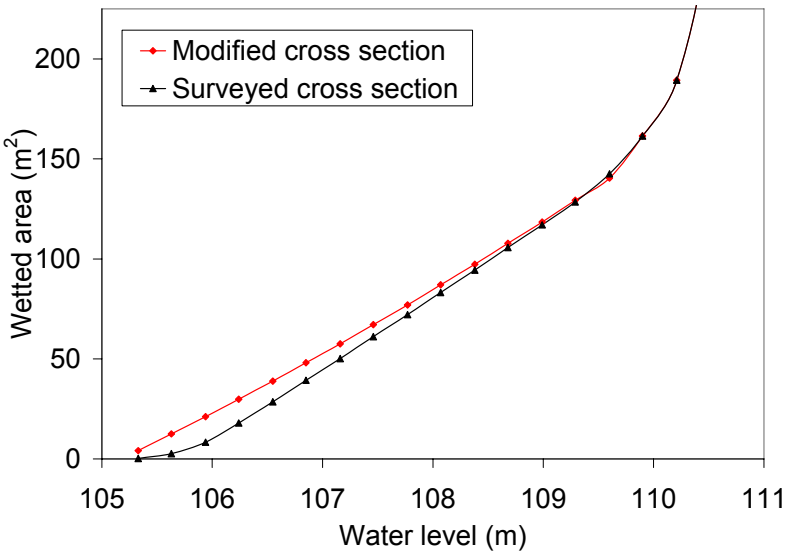

Fig. 4.28 Comparison of wetted area characteristics between surveyed irregular and modified regular cross section representation of the cross-section located at 74 km downstream of Dissangis (water levels are above sea level)

4.4.6 Scenario GS-VI: Representing the river geometry by a trapezoidal section obtained from average surveyed information of 20 surveyed cross sections

This scenario consists in using the average information obtained from the 20 surveyed cross sections (Annexe. A) to compose a uniform trapezoidal main channel section. Each main channel section is summarized in terms of depth, width and wetted area at bank full. The averages of these three variables define an average trapezoidal section (Fig. 4.29), which is then interpolated at constant distance increments of 100 m to represent the geometry of the Serein River. In this scenario, the original surveyed floodplains are used to complete the shape of the cross section.

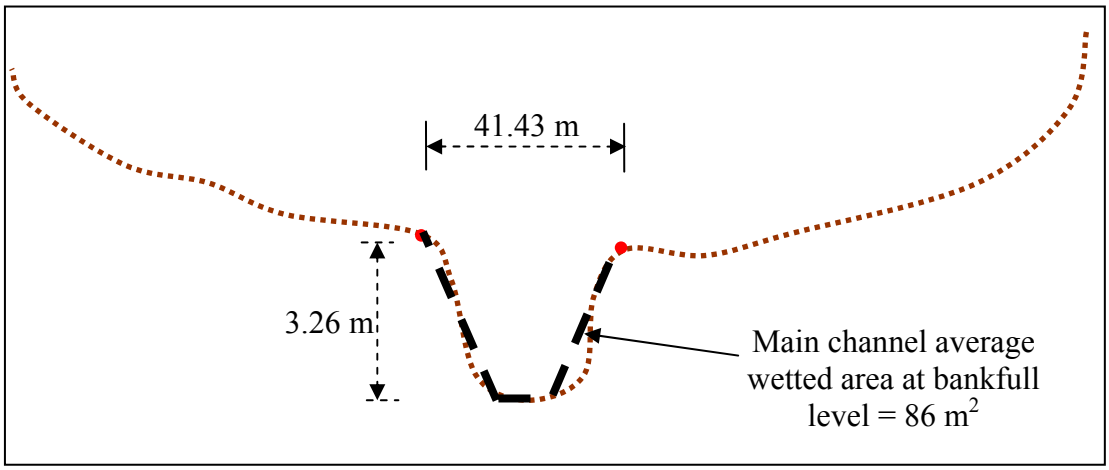

Fig. 4.29 Trapezoidal cross section obtained from average information on top width, wetted area and depth of 20 surveyed cross section (Scenario GS-VI)

Two methods are tested to represent the river bed profiles in the Serein River. The first method consisted of linearly interpolating the bed levels using only three known bed levels located at Dissangis, Chablis and Beaumont (Scenario GS-VIa), while the second method consisted of using the twenty surveyed bed levels (GS-VIb). These two methods induce different river bed slopes as illustrated in the previous section (Fig. 4.13).

The comparison between simulated and observed water levels at Chablis station (Tab. 4.10) shows that using this type of cross-sectional geometry with original surveyed bed levels (GS-VIb) reduces the Nash efficiency from 0.89 to 0.83 and increases the RMSE from 0.14 m to

0.19 m. However, using the same type of geometry but with interpolated bed levels (GS-VIa) reduces the Nash efficiency of simulated water levels from 0.83 to 0.61, while the RMSE is increased from 0.19 m to 0.3m. These results confirm that the bed levels have larger impact on the simulated water levels than the shape of the cross-section.

Tab. 4.10 Fit between simulated and observed discharge and water levels at Chablis, addressed in terms of Nash efficiency and RMSE for two versions of GS-VI scenario

Bed Level	**Nash WL**	**Nash Q**	**RMSE WL (m)**	**RMSE Q ($m^3.s^{-1}$)**
GS-VIa	0.61	0.89	0.30	4
GS-VIb	0.83	0.89	0.19	3.98
Reference simulation	0.89	0.90	0.14	3.72

The maximum water depths obtained from interpolated bed levels (GS-VIa) vary between 2.75 m and 3 m with an average of 2.9 m, while in the simulation based on surveyed bed levels (GS-VIb), the maximum water depths vary between 2.4 and 3.75 m with an average of 3.3 m (Fig. 4.30). In five river cross sections, the difference between simulated maximum water depths using surveyed bed levels and ones using interpolated bed levels is more than 1 m due to the linearly interpolated bed levels.

The results exhibit the effect of bed levels on the computed maximum water depths and thus on overtopping frequency as no overtopping was simulated when using interpolated bed levels with averaged trapezoidal sections (Fig. 4.30).

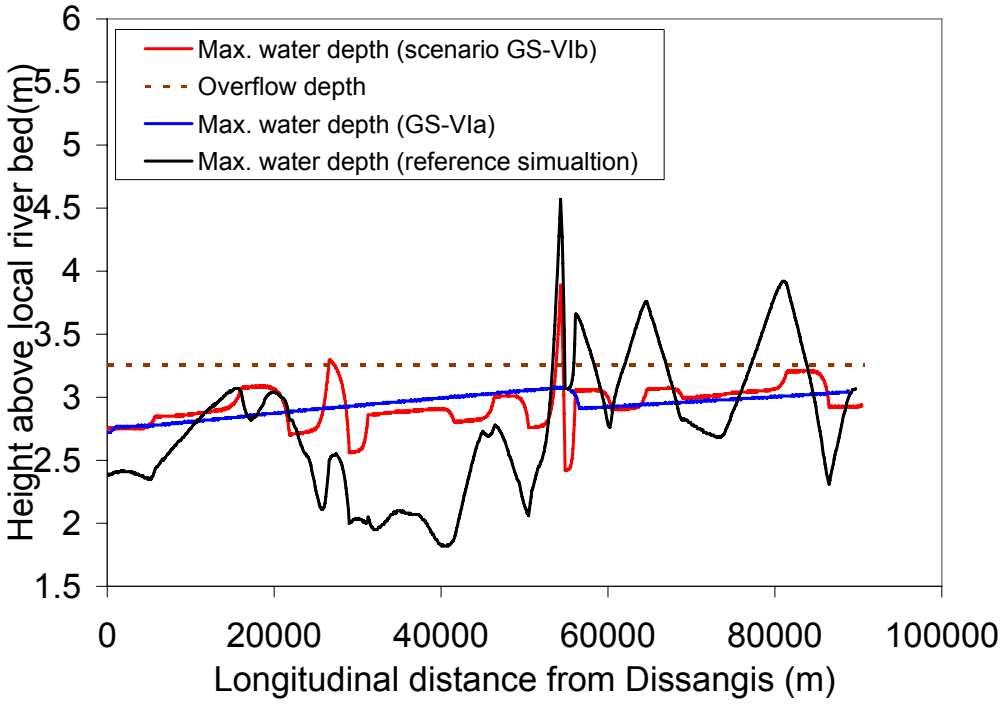

Fig. 4.30 Longitudinal comparison of maximum water depths along the Serein River (scenario GS-VIa and GS-VIb)

4.4.7 Scenario GS-VII: Representing the river geometry by a triangular section obtained from average surveyed information

In this scenario, a uniform triangular section is used to represent the river geometry (Fig. 4.31) instead of surveyed cross sections. The top width (41.43 m) and the depth (3.26 m) of the triangular section are obtained from the average depth and width of the 20 surveyed sections following the same methodology used in scenario GS-VIa. The only difference between this geometry representation (GS-VII) and the one used in GS-VIa is that the wetted area is not conserved because only two factors (section top width and depth) are used to identify the shape of the triangular section (Fig. 4.31), while in scenario GS-VIa three factors are used (depth, width and wetted area) to identify the characteristics of the uniform trapezoidal (Fig. 4.29). The bed level slopes are identified by linearly interpolating between the bed levels of the three major hydrometric stations (Dissangis, Chablis and Beaumont) while floodplains used in this scenario are surveyed ones.

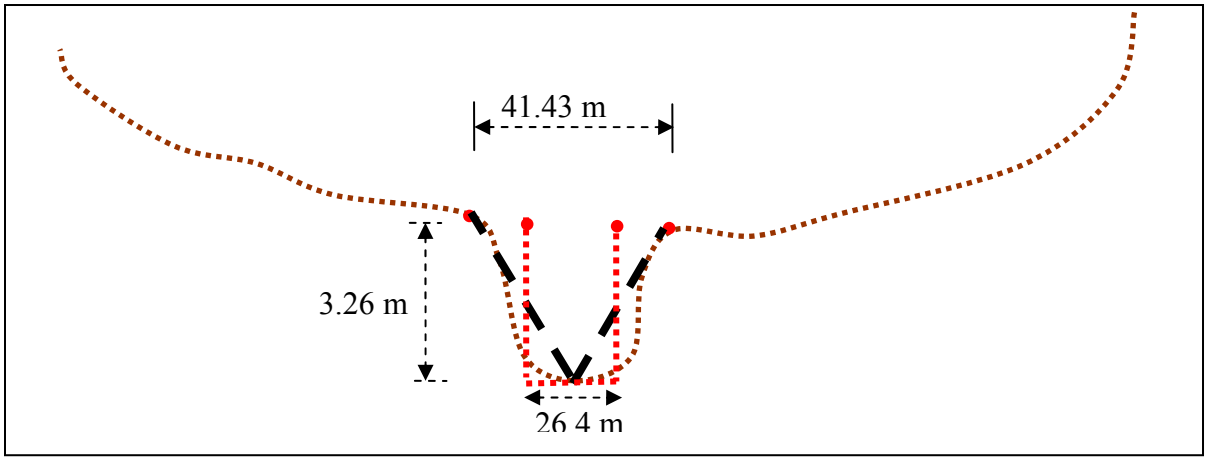

Fig. 4.31 Triangular cross section obtained from average information on top width and depth of 20 surveyed cross section (scenario GS-VII), and rectangular cross section obtained from average information on depth and wetted area (scenario GS-VIII)

The comparison between simulated and observed water levels at Chablis station (Tab. 4.11) shows that the Nash efficiency of simulated water levels is reduced to 0.56 compared to 0.61 in GS-VIa where the wetted area is used to define the trapezoidal section. The comparison demonstrates the influence of this geometry scenario on the accuracy of simulated water levels, while as usual, discharge hydrographs are not influenced by this scenario.

Tab. 4.11 Fit between simulated and observed discharge and water levels at Chablis, addressed in terms of Nash efficiency and RMSE for scenarios GS-VII and GS-VIa

Scenario	Nash WL	Nash Q	RMSE WL (m)	RMSE Q ($m^3.s^{-1}$)
GS-VII	0.56	0.89	0.31	3.85
GS-VIa	0.61	0.89	0.30	4
Reference simulation	0.89	0.90	0.14	3.72

The longitudinal comparison of maximum water depths between scenarios GS-VII, GS-VIa and the reference simulation (Fig. 4.32) shows that changing the cross sectional shape representation from trapezoidal to rectangular (i.e. not conserving the wetted area) increased the simulated maximum water depths by 0.5 m on average which eventually caused overtopping along the river reach and error in downstream discharge due to backwater effects. This scenario shows how a simple change in the cross sectional representation of the river can impact the simulations of water levels and maximum water depths.

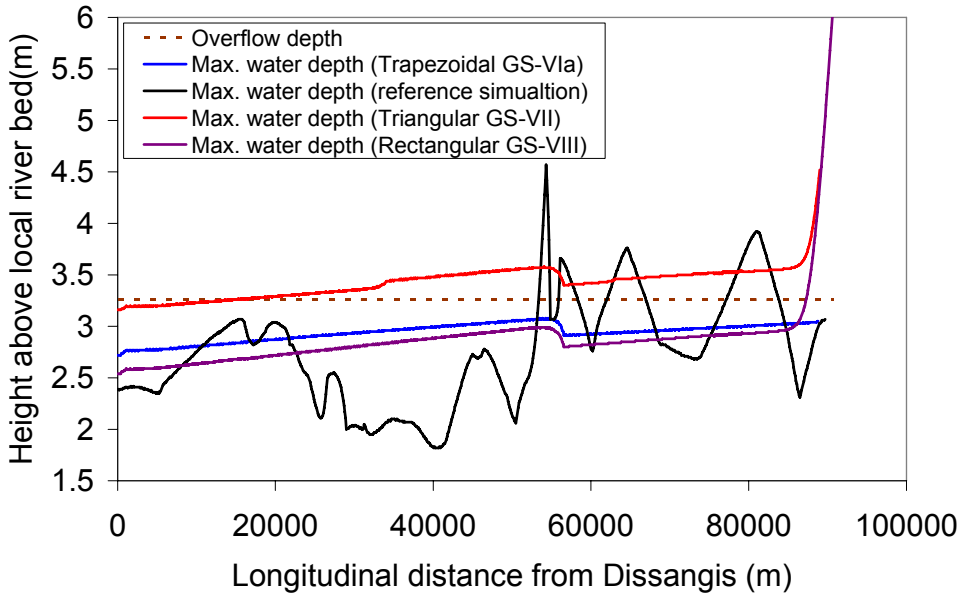

Fig. 4.32 Longitudinal comparison of maximum water depths along the Serein River between scenarios GS-VIa, GS-VII, GS-VIII and the reference simulation

4.4.8 Scenario GS-VIII: Representing the river geometry by a rectangular section obtained from average surveyed information

In this scenario a uniform rectangular channel is used to represent the river geometry, its dimensions are obtained by using the average depth (3.26 m) and average wetted area at bankfull level (86 m^2) of the 20 surveyed cross sections (Fig. 4.31). The bed level slopes are calculated with a linear interpolation between the bed levels of the three major hydrometric stations (Dissangis, Chablis and Beaumont), while floodplains used in this scenario are surveyed ones.

The comparison between simulated and observed water levels at Chablis station (Tab. 4.12) shows that the Nash efficiency of simulated water levels is reduced to 0.52 compared to 0.56 in GS-VII and 0.61 in GS-VIa. This comparison demonstrates the influence of this type of cross sectional representation on the accuracy of simulated water levels.

Tab. 4.12 Fit between simulated and observed discharge and water levels at Chablis, addressed in terms of Nash efficiency and RMSE for scenarios GS-VIII, GS-VII, GS-VIa and the reference simulation

Scenario	Nash WL	Nash Q	RMSE WL (m)	RMSE Q ($m^3.s^{-1}$)
GS-VIII	0.52	0.88	0.33	3.80
GS-VII	0.56	0.89	0.31	3.85
GS-VIa	0.61	0.89	0.30	4
Reference simulation	0.89	0.90	0.14	3.72

The longitudinal comparison of maximum water depths between scenarios GS-VIII, GS-VII, GS-VIa and the reference simulation is illustrated in Fig. 4.32. It shows that the difference between the maximum water depths obtained from this type of geometry and the reference simulation is more than 2 m in some parts of the river. Furthermore, using a rectangular cross-section to represent the river geometry reduces the simulated maximum water depths by 0.2 m on average compared to the trapezoidal cross-section (GS-VII), and 0.5 m compared to the triangular cross-section (GS-VIa).

The results also show that using a rectangular cross-section to represent the river geometry have caused a backwater effect that is more important than the ones obtained by using a triangular section.

The comparison between the last three scenarios shows that the trapezoidal cross-section is a better representation of river geometry than the triangular and rectangular cross-sections.

For this particular scenario, the Manning's roughness coefficient was recalibrated (Fig. 4.33 & Tab. 4.13). Higher values of Manning's roughness coefficients were used to improve the prediction of the model at Chablis. According to the Nash efficiency, the model prediction of water levels improved (Nash = 0.83) as Manning's *n* approaches a value of 0.05, which is 60 % higher than the calibrated *n* value using surveyed geometry. To validate the approach of recalibrating the Manning's roughness coefficient, the recalibrated maximum water profiles were longitudinally compared with the simulation of reference (Fig. 4.34). The comparison

shows that the model has been forced to correctly represent the water levels at Chablis and it is not valid for the whole river reach because maximum water depths are, on average, more than 2 m higher. The recalibrated model also produced backwater errors at the downstream end of the river reach that are 8 m higher than ones simulated when using a Manning's roughness coefficient of 0.03.

Tab. 4.13 Model performance at Chablis vs. Manning's roughness coefficients (scenario GS-VIII)

	n = 0.03	**n = 0.04**	**n = 0.05**	**n = 0.06**	**n = 0.07**
Nash WL	0.52	0.73	0.837	0.856	0.804
Nash Q	0.88	0.893	0.9	0.916	0.925

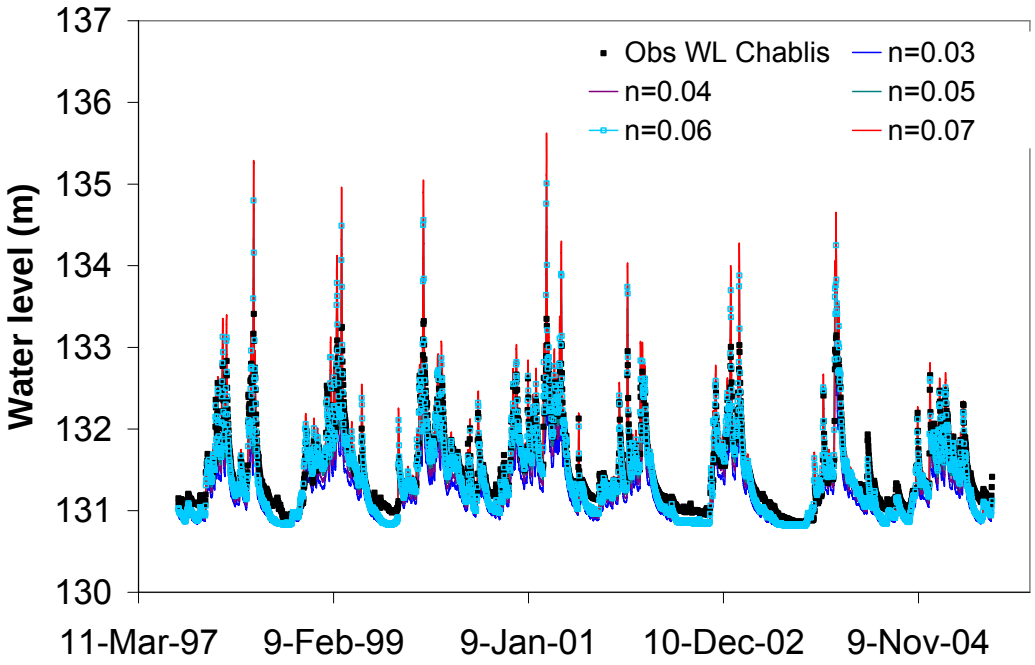

Fig. 4.33 Sensitivity of simulated water levels (scenario GS-VIII) to the variation of Manning's roughness coefficient

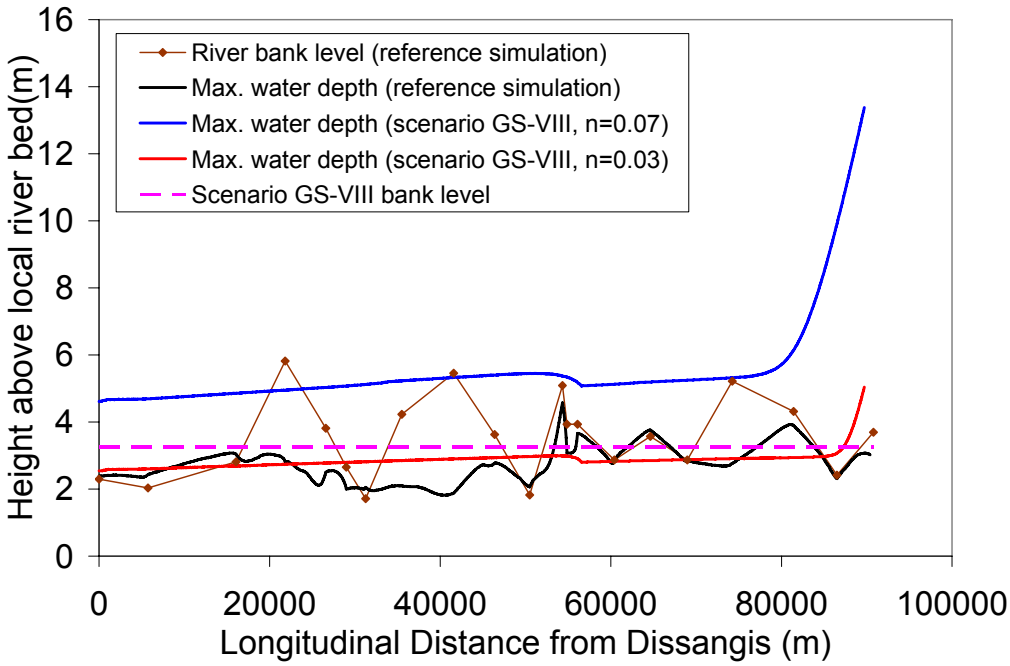

Fig. 4.34 Longitudinal comparison of maximum water depths along the Serein River using different values of Manning's roughness coefficients (Scenario GS-VIII)

4.5 Synthesis of geometry scenarios results

In general, the analysis of geometry scenarios represented in section 4.6 (Tab. 4.4) can be classified into the following categories:

- Impact of spatial sampling of cross sections (GS-I, GS-II, GS-III).
- Impact of shape of cross sections (GS-IV, GS-V).
- Impact of both shape and spatial sampling (GS-VI, GS-VII, GS-VIII).

In this section, a statistical comparison between simulations obtained from all geometry scenarios and observations at Chablis is presented for the whole period of simulation in order to make an overall synthesis of results. These comparisons are summarized in Tab. 4.14 and on Fig. 4.35 for discharge and Fig. 4.36 for simulated water levels.

The comparison of simulated discharge with observations at Chablis shows that simplified geometry could be successfully applied to route discharge in river reaches with insignificant impact on the quality of simulation. These findings are not surprising since observed river discharge was forced as upstream boundary conditions in the hydraulic model (Fig. 4.35),

thus the focus will be on characterizing the impact of simplified geometry on the quality of simulated water levels.

The statistical comparisons between simulated water levels using different geometry scenarios and observations at Chablis suggest that simulated water levels are consistent with measured data at Chablis (Nash > 0.7), except for scenarios GS-VII and GS-VIII of which the Nash efficiency is inferior to 0.6 (Fig. 4.36).

However, previous sections of this chapter illustrate that computed maximum water depths are longitudinally offset when compared to the reference simulation of which the maximum water depths vary between 2 m and 5 m with an average of 2.7 m. It was not possible to obtain consistent maximum water depths in the tested geometry scenarios primarily because of the approximated geometry and because the effective bed level is different from the actual bed level for certain scenarios. This exhibits the importance of spatial calibration in river reaches, as simulated water levels and discharges hydrographs can be accurate when compared at one control point but inaccurate in other parts of the river reach. It also illustrates the importance of calibrating hydraulic simulations to stage hydrographs and not only discharge hydrographs.

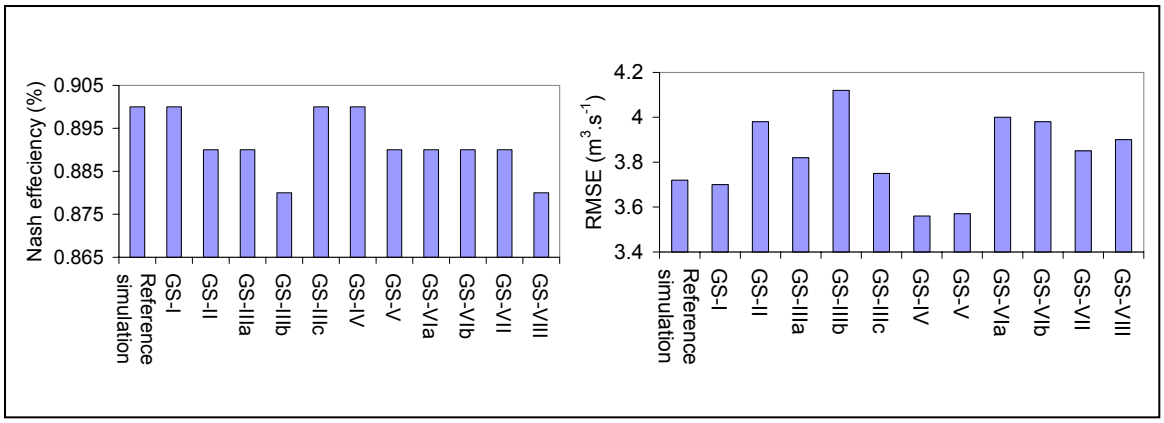

Fig. 4.35 Fit between simulated and observed discharge at Chablis, addressed in terms of Nash efficiency, RMSE, Bias and average for all geometry scenarios

Tab. 4.14 Fit between simulated and observed water levels and discharge at Chablis, addressed in terms of Nash efficiency, RMSE, Bias and average for all geometry scenarios

Scenario	Discharge		Water levels				
	Nash	RMSE ($m^3.s^{-1}$)	RMSE (m)	Bias (m)	Nash	Average* (m)	R (%)
Original geometry	0.90	3.72	0.14	0.06	0.89	131.57	0.96
GS-I	0.90	3.71	0.16	0.06	0.88	131.57	0.95
GS-II	0.89	3.98	0.18	-0.08	0.86	131.39	0.96
GS-IIIa	0.89	3.82	0.25	-0.15	0.72	131.30	0.96
GS-IIIb	0.88	4.12	0.27	0.16	0.69	131.70	0.95
GS-IIIc	0.90	3.75	0.21	0.10	0.80	131.63	0.95
GS-IV	0.90	3.56	0.16	0.07	0.87	131.58	0.96
GS-V	0.89	3.57	0.29	0.16	0.64	131.70	0.96
GS-Via	0.89	4	0.30	-0.19	0.61	131.24	0.96
GS-VIb	0.89	3.98	0.19	0.12	0.83	131.60	0.95
GS-VII	0.89	3.85	0.31	0.20	0.57	131.76	0.96
GS-VIII	0.88	3.9	0.33	-0.22	0.52	131.20	0.96

***Average observed water levels at Chablis is 131.5**

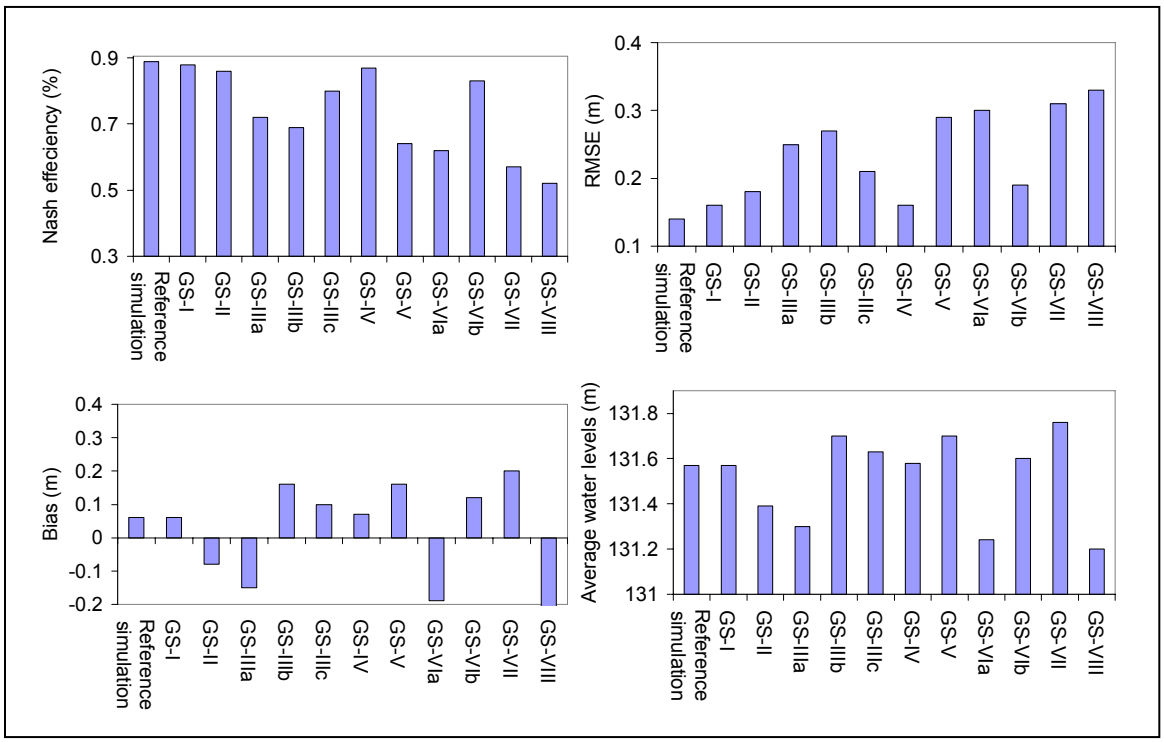

Fig. 4.36 Fit between simulated and observed water levels at Chablis, addressed in terms of Nash efficiency, RMSE, Bias and average for all geometry scenarios

In terms of spatial discretization and locations of surveyed cross sections along river reaches, the results of GS-I show that removing four surveyed cross sections that contain two conveying arms (islands) and replacing them with interpolated ones from adjacent cross sections has a local influence on the simulated water levels that varies between 0.1 m and 1 m. It has no impact on the overall wave time of transfer, simulated water levels and discharges in other parts of the river hence it is an acceptable approximate at regional scale that can allow for the use of computational steps that are equal or larger than 2 km.

To further test the impact of spatial discretization, only three surveyed cross sections (located at major hydrometric stations) were used to represent the geometry of the river reach while the remaining intermediate cross sections and bed levels were linearly interpolated between the three known bed levels (GS-II).

The results show that albeit the model simulates consistent water levels at Chablis (Nash = 0.86), it did not accurately represent the maximum water depths when compared longitudinally with the reference simulation. In this scenario, the simulated maximum water levels vary between 2 m and 3 m with an average of 3.2 m, while in the reference simulation, the maximum water depths vary between 2 and 5 m with an average of 2.7 m. In certain river cross sections, simulated maximum water depths obtained from this scenario are about 1 m higher than the ones obtained in the reference simulation, especially upstream from the Chablis hydrometric station. The results of this scenario illustrate the importance of using several surveyed cross sections for a given river reach, especially where sudden change in cross section shape or bed level slope occur.

During high flow events, the impact of floodplains geometry had minor influence on the overall system, mainly because slight overtopping occurred along the river reach within the period of simulation (scenario GS-IV). In areas where overtopping is important, the results show the importance of floodplain on the expansion of the flood and the peak water levels of

which attenuation levels varied between 10cm and 20 cm. This scenario offers interesting perspectives for flood mitigation and river channelization management.

During low flow events, irregularities in the river bed bottom have an important impact on simulated river stages, as simplifying the irregular river bed bottom to plain have, on average, attenuated the low flow water levels by 20 cm compared to ones in the reference simulation. This is because the lower the water level is, the more important is the friction and thus the description of the cross section geometry. This finding is important, especially in the simulations of stream-aquifer interactions where the river is sustained by aquifer units during low flow periods.

In terms of river bed levels, the results show how natural variations in bed levels and cross sections characteristics are large and, consequently, the effective bed used in limited geometry scenarios (interpolated bed levels) can be several meters different from the surveyed bed at a given point. This difference is not significant in terms of discharge routing over tens of kilometers. However, in the context of determining water levels at specific local scale, these differences are important. For instance, in GS-VIa using interpolated bed levels instead of surveyed ones for the same cross sectional representation have reduced the Nash efficiency of simulated water levels from 0.83 to 0.61, while the RMSE was increased from 0.19 m to 0.3 m. The maximum water depths obtained from interpolated bed levels vary between 2.75 m and 3 m with an average of 2.9 m, while in the simulation based on surveyed bed levels, the maximum water depths vary between 2.4 and 3.75 m with an average of 3.3 m for the same type of section. In certain river cross sections, the difference between simulated maximum water depths using surveyed bed levels and ones using interpolated bed levels is more than 1 m due to the linearly interpolated bed levels. The results exhibit the effect of bed levels on the computed maximum water depths and thus on overtopping frequency.

Finally, the cross sections shape impact on simulated water levels was characterized by comparing between water levels simulations based on using trapezoidal (GS-VI), triangular (GS-VII) and rectangular (GS-VIII) cross sections. The comparison of water levels with observed ones at Chablis station shows that the Nash efficiency of simulated water levels in GS-VIII is dropped to 0.52 compared to 0.56 in GS-VII and 0.61 in GS-VI.

The longitudinal comparison of maximum water depths between scenarios GS-VIII, GS-VII, GS-VI and the reference simulation shows that using a rectangular cross-section to represent the river geometry reduces the simulated maximum water depths by 0.2 m on average compared to the trapezoidal cross-section (GS-VII), and 0.5 m compared to the triangular cross-section (GS-VIa). Furthermore, using a simple rectangular or triangular cross-section to represent the river geometry has caused a backwater effect.

Trapezoidal cross sections are found to give more accurate results than triangular and rectangular ones, additionally, no backwater problems have occurred when using this particular shape of cross section.

4.6 Conclusions

The primary objective of this study was to establish whether a reliable hydraulic routing model could be developed based on limited field data. This study was carried out in the Serein River (tributary of the Yonne River), between the gauging stations of Dissangis et Beaumont, in a well surveyed reach (20 cross sections over 89 kms).

River discharge and stage are simulated by the hydraulic model HEC-RAS (1D Saint-Venant equations) solved using the four point implicit finite difference scheme while lateral inflows are simulated by the regional hydrogeological model EauDyssée.

The calibration parameter involved in the development of the hydraulic model was the Manning's roughness coefficient (n) which was first calibrated for a real channel morphology.

The results of the different geometry scenarios indicate that hydrodynamic models based on the Saint-Venant equations could be successfully used to determine discharge hydrographs in reaches where little channel geometry data are available, by approximating the modeled reach with simplified geometry. This result is not surprising since river discharge is mostly controlled by the upstream and lateral boundary conditions. However, a hydraulic model based on approximate morphological data does not accurately predict the associated water levels. For instance, in GS-VIa using interpolated bed levels instead of surveyed ones for the same cross sectional representation have reduced the Nash efficiency of simulated water levels at Chablis hydrometric station from 0.83 to 0.61, while the RMSE was increased from 0.19 m to 0.3 m. The maximum water depths obtained from interpolated bed levels vary between 2.75 m and 3 m with an average of 2.9 m, while in the simulation based on surveyed bed levels, the maximum water depths vary between 2.4 and 3.75 m with an average of 3.3 m for the same type of section. In five river cross sections, the difference between simulated maximum water depths using surveyed bed levels and ones using interpolated bed levels is more than 1 m due to the linearly interpolated bed levels. This exhibits the effect of bed levels on the simulated water levels, especially at the regional scale where DEM is used to identify the river geometry hence it is difficult to obtain an accurate river bed level representation.

In terms of river shape, the results show that irregularities in the river bed bottom have an important impact on simulated river stages, especially during low flow as simplifying the irregular river bed bottom to plain have, on average, attenuated the low flow water levels by 20 cm compared to ones in the reference simulation. This is because the lower the water level is, the more important is the friction and thus the description of the cross section geometry. This finding is important, especially in the simulations of stream-aquifer interactions where the river is sustained by aquifer units during low flow periods.

The study confirms that the accuracy of predicted water levels and maximum water depths simulated by a Saint-Venant model rely on an accurate representation of channel geometry and bed level slopes along the river reach.

That being said, a 1D Saint-Venant model is not suitable for simulating flow at regional scale where river morphology is not accessible. In spite of the aforementioned limitations, this type of hydrodynamic modeling remains crucial to accurately simulate in-stream water levels. To compromise between the scale issue, morphological data limitation and the importance to accurately simulate in-stream water levels, an original upscaling strategy will be developed. This strategy will allow for benefiting from high resolution hydraulic modeling outputs (e.g. Annexe. A) to describe fluctuating river stage function of routed discharge and potentially improve the regional scale simulation of stream-aquifer interactions in the integrated model EauDyssée.

CHAPTER 5. AN UPSCALING METHODOLOGY FOR SIMULATING RIVER STAGES AND STREAM-AQUIFER INTERACTIONS: OISE RIVER BASIN CASE STUDY

Résumé en Français

Dans ce chapitre, nous proposons une méthode de changement d'échelle dans laquelle la modélisation fine des processus hydrauliques à haute résolution permet d'améliorer la représentation des profils d'eau en rivière et les interactions nappe-rivière simulent à l'échelle régionale par la plateforme de modélisation intégrée des hydrosystèmes EauDyssée.

La méthodologie de changement d'échelle a été testée pour le bassin versant de l'Oise (sous bassin de le Seine) d'une superficie de 17000 Km^2, pour la période 1990-1995. Le modèle HEC-RAS a été utilisé pour la modélisation hydraulique basée sur les équations de Saint-Venant 1D pour un tronçon de l'Oise de 188 km. Le calage de ce modèle a été effectué en faisant varier le coefficient de Manning n (1/K) avec pour objectif de reproduire les courbes de tarage observées. L'efficacité du modèle hydraulique est évaluée par les critères statistiques classiques de Nash, RMSE, biais à 4 stations hydrométriques. Une courbe de tarage est définie à partir de la simulation hydraulique à la résolution du modèle HEC, tous les 200m en moyenne.

Ces courbes de tarage sont ensuite projetées comme conditions aux limites sur les mailles rivière du modèle régional EauDyssée (résolution de 1 km) afin de simuler la fluctuation du niveau d'eau en fonction du débit routé par le module de routage (RAPID). Les échanges entre les mailles rivière et les mailles aquifères (modèle SAM) sont ensuite estimés à partir d'une relation de type loi de Darcy se basant sur les gradients de charge verticaux entre la rivière et la nappe.

L'impact de la fluctuation des niveaux en rivière sur les isopièzes a été analysé par rapport à un état de référence pour lequel les niveaux en rivière sont fixes. L'analyse des résultats sur la période de simulation montre un écart moyen des niveaux piézométriques pouvant atteindre 1.9 m pour les mailles souterraines situées sous les mailles rivière.

Cet écart se réduit si l'on considère des mailles souterraines plus éloignées de la rivière. L'extension spatiale de cet écart moyen est plus importante dans la nappe de la Craie qui est confinée (jusqu'à 20 km de la rivière) que dans celle de l'Éocène qui est libre (3 km de la rivière).

Abstract

In this chapter, a coupling framework strategy is proposed to simulate stream-aquifer interactions. The methodology is based on an upscaling approach, which allows for benefiting from high resolution hydraulic modeling outputs to improve the simulation of fluctuating river stage in a regional scale hydro(geo)logical platfrom EauDyssée.

The hydro(geo)logical platfrom EauDyssée computes runoff and groundwater flows that are lateral inflow inputs of the hydraulic model. At the regional scale, the coupling between streams and aquifer units is ensured using rating curves calculated with the hydraulic model and discharges routed by the regional model. Then, during an Eau-Syssée simulation, differences between in-stream water stages and piezometric heads are used to calculate and quantify the exchanges between aquifer units and rivers.

This coupling framework strategy is applied on the Oise River basin, a 17 000 km^2 sub-basin of the Seine River basin, in Northern France.

The hydraulic model HEC-RAS (chapter 4) was used for simulating 188 km of the Oise stream network. Manning's roughness coefficient (n) was calibrated against discharges and water stages hydrographs measured at 4 hydrometric stations.

Upon calibrating the Oise River hydraulic model, the rating curves (discharge vs. water levels) derived at each cross-section by HEC-RAS are linearly projected along the river cells, and an equivalent rating curve at the center of this river grid-cell is calculated by inverse distance weight averaging with respect to the cell's center. Then, the resulting equivalent rating curve is sent as input boundary conditions for the QtoZ module which calculates the water level as function of the discharge routed by RAPID and sends it to the groundwater model (SAM) in order to simulate stream aquifer interactions.

Once the methodology is validated at the regional scale, the simulated regional river stages were almost as realistic as the ones from the local 1D hydraulic model.

The impacts of in-stream water level fluctuations on the aquifer system are characterized at local and regional scale by comparing with EauDyssée results obtained using constant in-stream water levels.

The variation in simulated piezometric heads caused by the in-stream water level fluctuations reach up to 1.9 m in aquifer units directly connected to the river cells, the impact decreases with distance to the stream.

The area influenced by fluctuating river stages extends across 3 to 20 km around the streams, depending on the hydrogeological setting (confined/unconfined) of the aquifer unit.

Substantial portions of this chapter are submitted for publishing in Journal of hydrology: Saleh, F., et al. 2010. (ref: HYDROL-S-10-01053)

5.1 Framework strategy to account for river stages fluctuations

To compromise between the spatial scale issue, morphological data limitation and the importance to accurately simulate in-stream water levels (stressed in previous chapters), a strategy is proposed to benefit from the results of the high resolution 1D channel flow model HEC-RAS (Fig. 5.1). Runoff and groundwater contribution to stream flow are first simulated

by EauDyssée at the regional scale considering an imposed water level in each river cell. The hydraulic model HEC-RAS is fed by the previous inputs as lateral inflows, and by observed discharges at the upstream limits of the simulated river network (Fig. 5.1). After calibration and validation against both river discharges and stages at control stations, unsteady flow simulations are used to derive functional relationships between river stages and discharges (rating curves) at each cross section of the river network.

The derived rating curves are then upscaled onto each river cell of the regional model's mesh. The river grid-cells rating curves are input data of the QtoZ module (Section 5.3.2), which provides a water level to the groundwater model SAM as function of the discharge routed by RAPID. Finally SAM uses water levels to simulate and quantify the exchange between the stream grid-cells and the aquifer grid-cells.

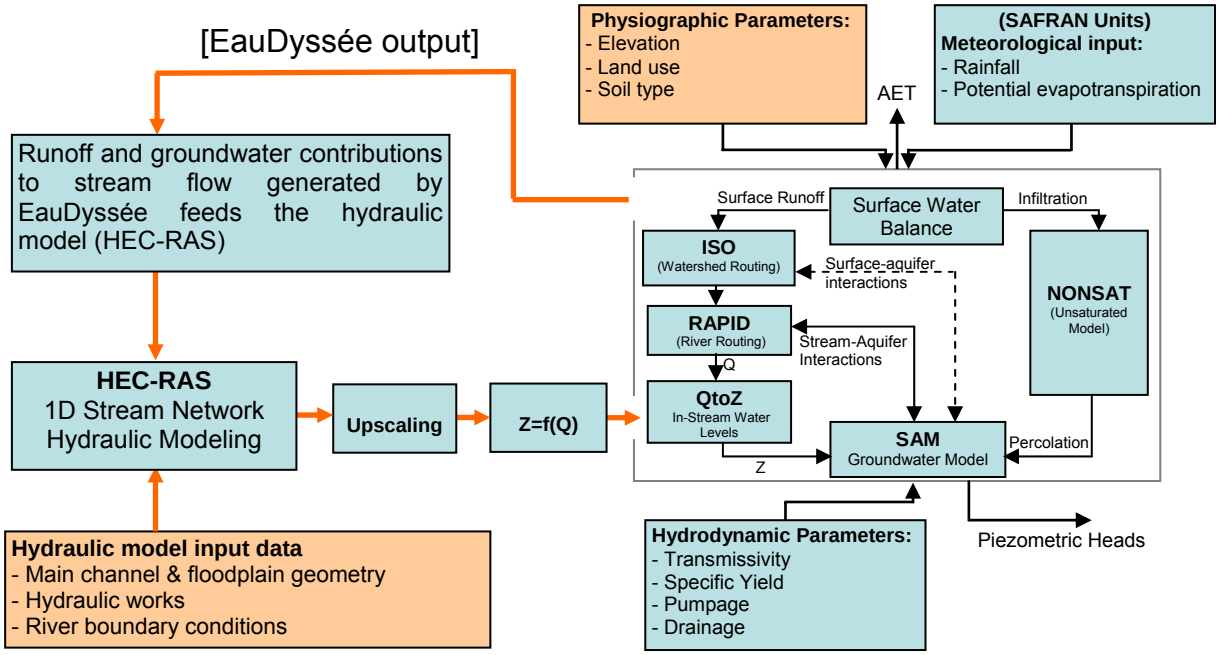

Fig. 5.1 Framework strategy for coupling results of local scale hydraulic modeling with regional hydrological modeling

5.1.1 Upscaling from local hydraulic modeling to regional hydrological modeling

Once the 1D hydraulic model is constructed, the derived rating curves from the local hydraulic model are upscaled toward the river grid-cells (1 km x 1 km in the application

described below) of the regional hydrological model. The cross-sections of the high resolution hydraulic model are linearly projected along the river cells, by calculating a length equivalency factor between the high resolution river reach and the river grid-cell lengths Fig. 5.2.

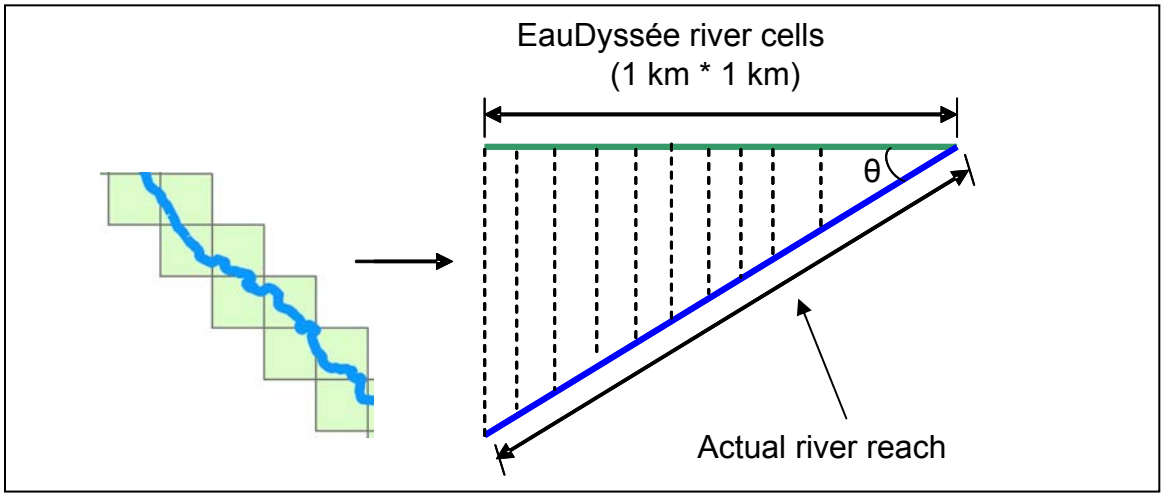

Fig. 5.2 Example of spatial projection of EauDyssée river cells discharge over a given river reach

Then, an equivalent rating curve at the center of each river grid-cell is calculated by inverse distance weight averaging with respect to the river cell center (Fig. 5.3):

$$h_r = \frac{\sum_{i=1}^{n}\left(\frac{z_i}{d_i}\right)}{\sum_{i=1}^{n}\left(\frac{1}{d_i}\right)} \qquad \text{Eq. 5. 1}$$

where h_r is the interpolated water level value in the center of the regional river grid-cell, z_i is the water level at each cross section of the hydraulic model within the river cell, and d_i is the distance between these cross-sections and the center of the river cell (Fig. 5.3). The algorithm estimates the water level value (h_r) at the center of the river grid-cell as function of the water level values of the nearest cross sections contained in a regional river cell (Fig. 5.3). The equation assumes that estimated water levels are more similar to nearby elevations

than to distant ones. Hence, the more distant a cross section is from the center of a river grid-cell, the less it influences the estimation of the water level in the center of the river grid-cell.

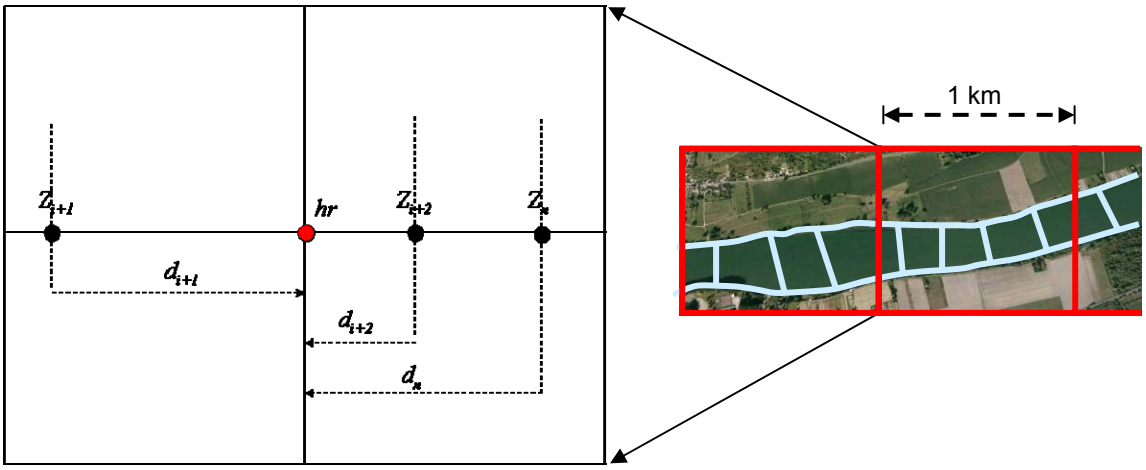

Fig. 5.3 Example of water level calculated at the center of the river grid-cell using the inverse distance weighted method

5.1.2 The QtoZ water level fluctuation module

The QtoZ module calculates the water level at a given river grid-cell as a function of the discharge routed by RAPID. The module has three options for calculating water level in each river grid-cell: a) fixed water level, b) water level estimated from a rating curve, c) water levels estimated using Manning's equations. The rating curves in option b are obtained from unsteady flow simulations, where discharge and water levels are integrated to form a rating curve.

Within the platform EauDyssée, the QtoZ module is coupled with the hydrological routing model RAPID and the groundwater model SAM (chapter 3). At each time step of the simulation, QtoZ receives discharge values from RAPID for each river grid-cell and calculates a water level which is sent to the groundwater model (SAM) in order to simulate stream aquifer interactions (Fig. 5.1).

5.2 Implementation of the EauDyssée stream-aquifer coupling framework strategy

The stream-aquifer coupling framework strategy is tested on the Oise River basin, described below, over a period of 5 years (1990 – 1995). This evaluation is practically composed of several steps: a) Running and calibrating the initial version of EauDyssée at regional scale using constant in-stream water levels (low frequency behavior) to generate runoff and groundwater contributions to the local scale hydraulic model, b) Calibrating the hydraulic model HEC-RAS to obtain rating curves along the high resolution river network, c) Upscaling these rating curves to the river cells of RAPID in the EauDyssée platform, d) Running and calibrating EauDyssée with river stage fluctuations enabled, e) Assessing the local and regional impact of in-stream water level fluctuations on the hydrogeological system) Conducting sensitivity analysis.

5.3 Domain of application: The Oise basin

The Oise River (France) is the largest tributary of the Seine River (65 000 km^2). Its total length is 340 km for a catchment area of 17 000 km^2 mainly distributed in four regions (Lorraine, Champagne-Ardenne, Picardie and Ile de France) and six departments (Meuse, Marne, Ardennes, Aisne, Oise, and Val d'Oise) (Fig. 5.4).

Its springs are located in the Belgian province of Hainaut at an altitude of 323 m above sea level. It crosses the border with France approximately 20 km downstream from its springs. It joins the Seine River at Conflans-Sainte-Honorine, 75 km downstream from Paris along the Seine River. The Oise River has several major tributaries, including the Serre and the Aisne (right bank), and the Thérain (left bank). These three major tributaries represent about 65% of its total drained area (Fig. 5.4).

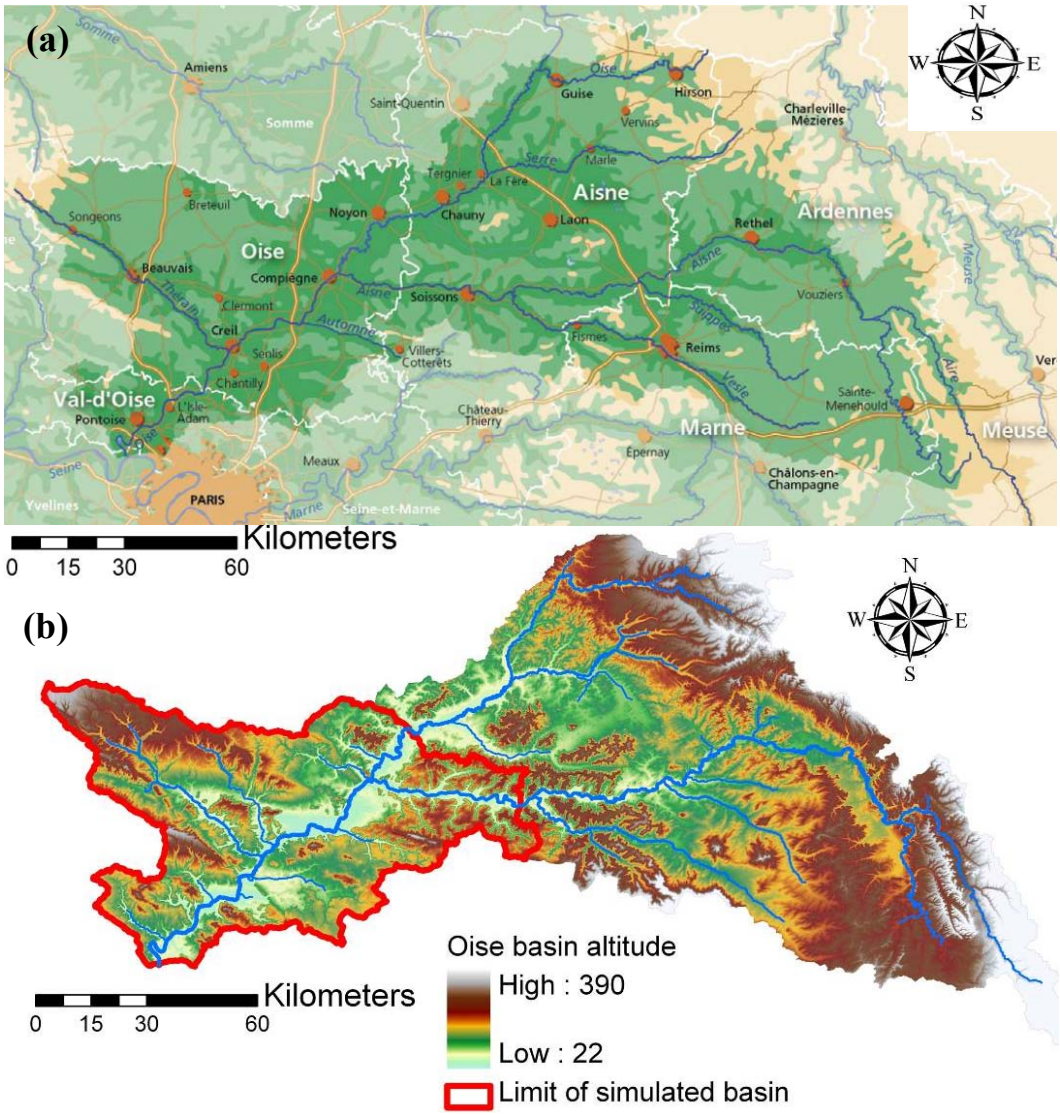

Fig. 5.4 a) Main cities of the Oise River basin, b) Oise River basin main tributaries and topography

The simulated part of the Oise River covers 131 km downstream from Sempigny to the confluence with the Seine River at Conflans-Sainte-Honorine (Fig. 5.4). It also includes part of the Oise's major tributaries, namely the Aisne downstream from Herant and the Thérain downstream from Beauvais. The total length of the simulated river network is 188 km. The hydrological regime of the Oise basin is pluvial, thus, floods are mainly caused by heavy rainfall events that lead to soil saturation. The average monthly precipitation is 60 mm.month^{-1} while the average annual precipitation is 735 mm.yr^{-1}. The dispersion of average monthly

rainfall from their mean varies in the range of +20 mm.month^{-1} during high rainfall months and -20 mm.month^{-1} during dry ones.

The average monthly discharge values at Sarron hydrometric station (14 200 km^2) are illustrated in Fig. 5.5. The river exhibits low flow rates from June to October with values ranging between 35 m^3.s^{-1} and 70 m^3.s^{-1}, and a mean of 112 m^3.s^{-1} at the Sarron hydrometric station. While high flow rates are generally observed between November and April with values ranging from 95 m^3.s^{-1} to 230 m^3.s^{-1}, the maximum observed discharge is 665 m^3.s^{-1}, registered in 5 February 1995 (Fig. 5.6).

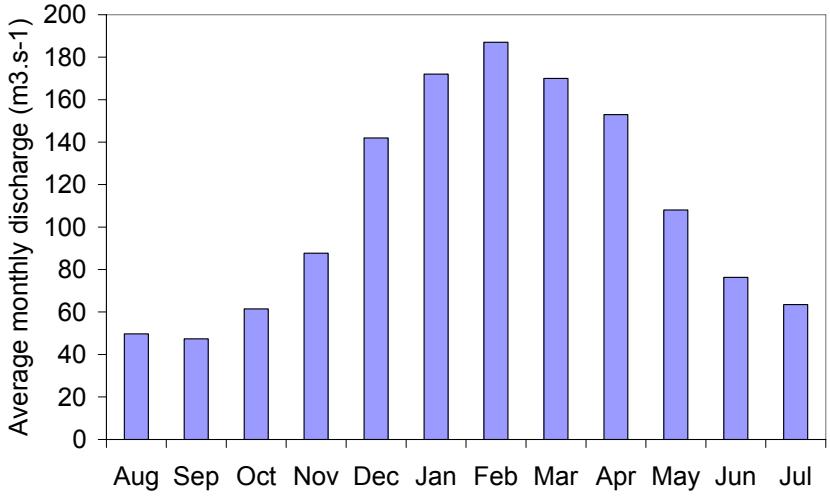

Fig. 5.5 Oise basin stream flow measurements at Sarron hydrometric station (14 200 km^2), average monthly discharge of 49 years (1960-2008)

Floods in the Oise basin are generally caused by successive events of high precipitation leading to soil saturation and higher water levels in aquifer units (Schornburgk and Pointet, 2003), these floods mainly take place between December and March. In the 20th century, the largest floods took place in February 1995, December 1993, December 1966, January 1926, and January 1920.

For instance, in 1993, high precipitation rates from the 1st to the 18th of December caused soil saturation, reaching high water levels in aquifer units. This period was followed by another intense precipitation event (140 mm) that lasted from the 19th to the 23rd of December. These

two successive rainfall events have caused a flood with a return period of 30 to 80 years depending on the inundated area.

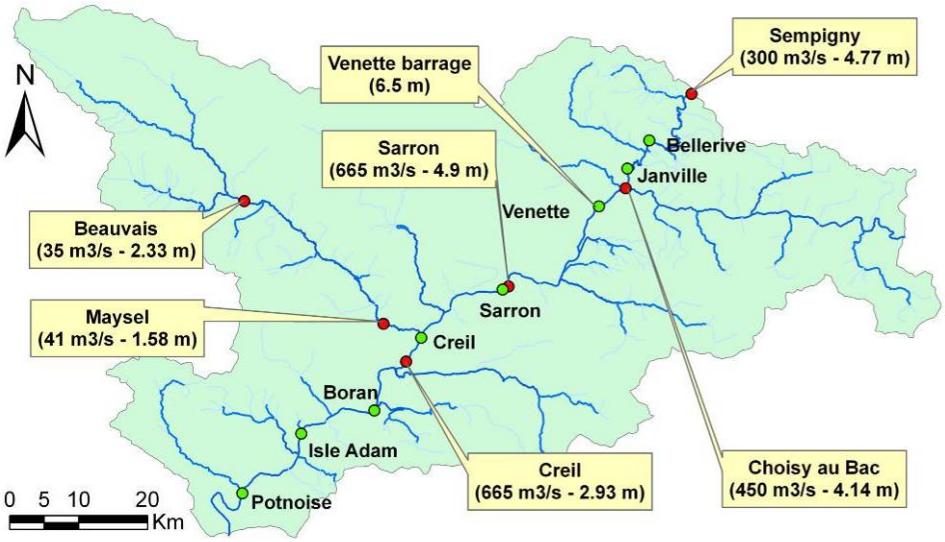

Fig. 5.6 Oise River basin hydrometric stations (in red), main navigational barrages (in green) and maximum observed discharges and water levels at selected hydrometric stations since 1900

The Oise River is amongst the most important navigational rivers in France, as freight traffic is about 4.6 million tones per year. The main stream of the Oise is controlled by a number of navigation dams or hydraulic works (Fig. 5.6). Notably, the reach between Compiegne and Val d'Oise is controlled by 5 navigation barrages: Venette, Verberie Sarron, Creil and Boran. The river bed slope in this reach is about 1 $m.km^{-1}$.

In terms of hydrogeology, the Oise river network is connected with two main geological formations: Eocene sands and limestones, and Cretaceous chalk (Fig. 5.7). For the simulated area, the Eocene aquifer unit connected to the Oise basin has an area of 3200 km^2 while the area connected to the Chalk aquifer unit is 5700 km^2.

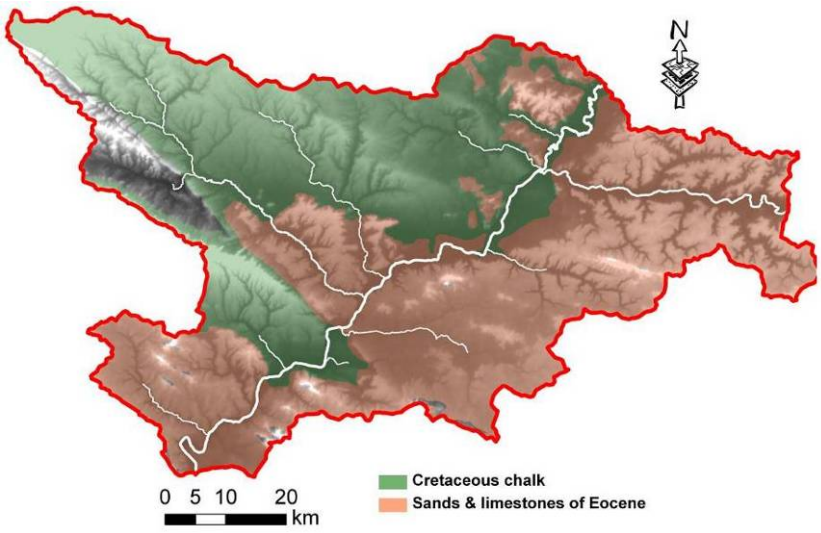

Fig. 5.7 Hydrogeological formations of the Oise basin

5.4 The Oise basin initial hydro(geo)logical model: low frequency behavior

Running and calibrating the initial EauDyssée version at regional scale to produce runoff and groundwater contributions to the hydraulic model

The Oise hydro(geo)logical model presented in this study was originally a regional model of the Seine basin (Gomez, 2002) for which constant in-stream water levels are imposed along all the stream network. The first step of this work consisted of running and recalibrating the initial version of the model in terms of parameter values. The objective of this recalibration is to improve the distribution of simulated piezometric heads and eventually improve the simulated runoff and groundwater contributions that will be boundary conditions of lateral inputs for the local hydraulic model.

5.4.1 The Oise basin hydro(geo)logical model description

The area of the Oise basin, where the upscaling methodology is applied, is composed of 1868 surface cells (1 km^2 – 16 km^2) and 120 meteorological (SAFRAN) cells of 64 km^2 (Fig. 5.8).

The surface input data of the Oise hydrological model consists in a meteorological database (precipitation and potential evapotranspiration) with a daily time step and a spatial resolution

of 8 km × 8 km. Data are derived from Météo-France SAFRAN database (Quintana-Segui et al., 2008).

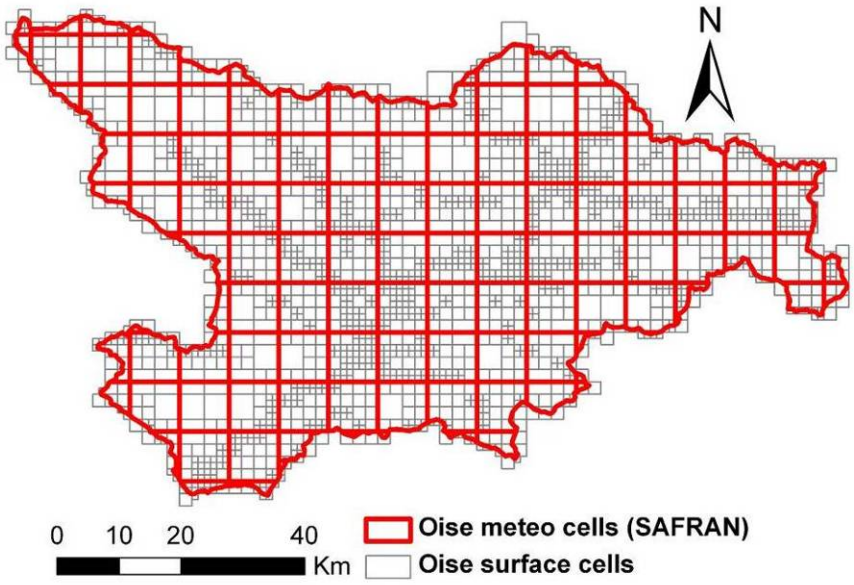

Fig. 5.8 Oise basin surface cells intersected with meteo France (SAFRAN) cells

Potential evaporation rates range from 745 to 900 mm.year^{-1} while precipitation rates range from 630 to more than 1000 mm.year^{-1} during the 5 years period of simulation. The highest precipitation rates (735 mm.yr^{-1}) are concentrated in the North-West districts of the basin, whereas the lowest intensity rates are measured in the center of the basin (Fig. 5.9).

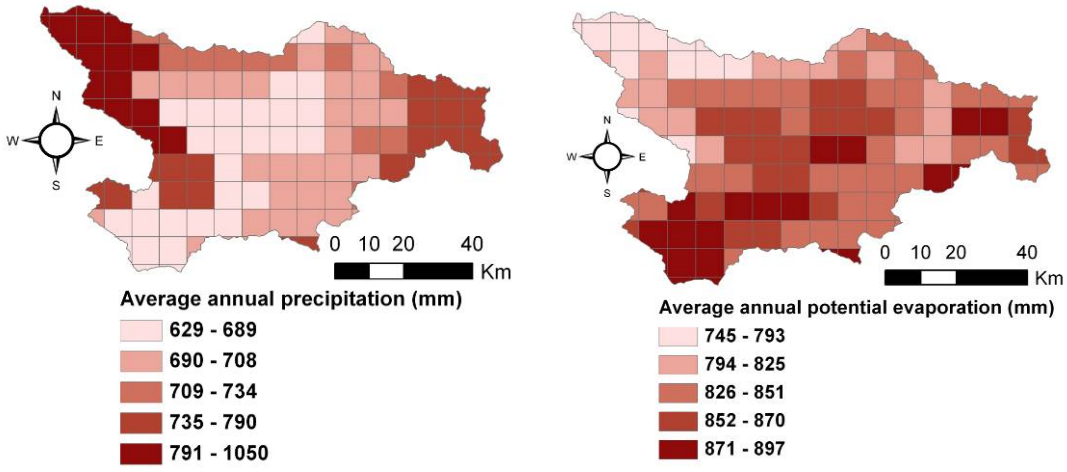

Fig. 5.9 Oise basin average annual precipitation and potential evaporation (1990-1995) rates obtained from SAFRAN database and used as input data for the Oise basin hydrological model

The hydrogeological part of the model is composed of 905 Eocene aquifer cells and 1053 Chalk aquifer cells (1 km^2 -16 km^2) (Fig. 5.10). The Chalk aquifer units are confined by the Eocene aquifer units. There are vertical exchanges between the two aquifer units.

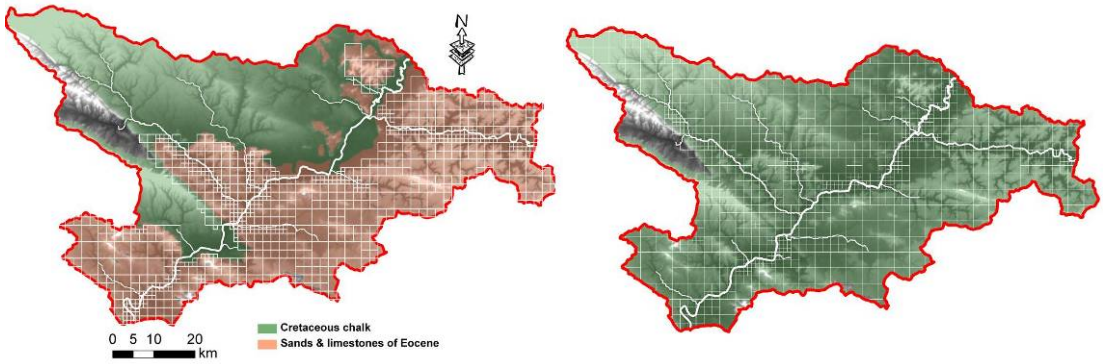

Fig. 5.10 Oise basin Eocene and Chalk aquifer unit cells (1 km^2 – 16 km^2)

5.4.2 Surface water budget characterization

Characterizing the water budget is an import step towards sustainable water management and modeling of river basins.

The average annual rainfall for the period from 1990 to 1995 is 735 mm. This rainfall is partitioned by the water balance component to actual evapotranspiration (516 mm), infiltration (120 mm) and runoff (99 m) (Fig. 5.11).

Computation of the water mass budget is performed by surface water mass balance component of the EauDyssée platform (chapter 3). The variables of the production function are similar to the ones calibrated by Gomez (2002) in the Seine basin.

The global water mass balance of the Oise basin hydro(geo)logical model is quantified using the following equation:

$$dR = P - AET - R - I \qquad \text{Eq. 5. 2}$$

Tab. 5.1 gives the definition of each term of Eq. 5.2. These terms are influenced by geomorphological and meteorological factors such as temperature which is known to impact the evaporative capacity of the basin.

Tab. 5.1 Water mass balance terms definition

Variable	Signification
dR	the variation of the surface and underground water resources
P	Precipitation
PET	Potential evapotranspiration
AET	Actual or effective evapotranspiration
R	Runoff
I	Infiltration

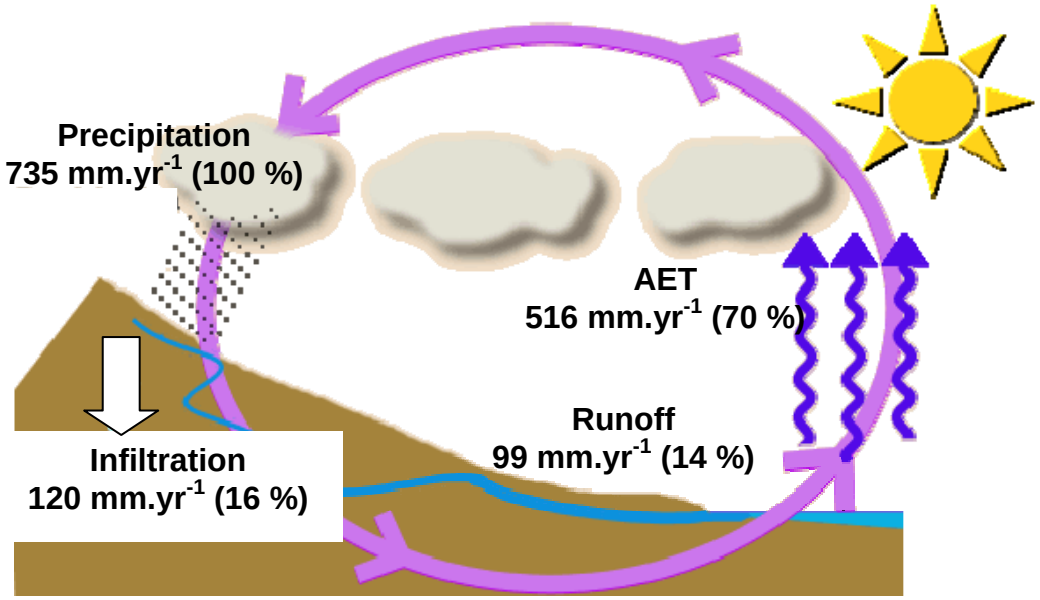

Fig. 5.11 Average yearly water mass balance for the Oise basin calculated over five years (1990-1995)

The annual partitioning of available water between actual evapotranspiration, infiltration and runoff varies significantly around the average values obtained from the five year simulation (Fig. 5.12). The difference between humid and dry periods is quite significant; examples amongst humid hydrological years are the 1993-1994 and 1994-1995 periods. During these two wet periods, the average annual rainfall is 825 mm and 865 mm respectively. This amount of rainfall is 15% higher than average rates. In consequence, the infiltration increases during the wet years, reaching 210 mm for the period of 1993-1994, which is equivalent to the total infiltration generated during three dry hydrological years between 1990 and 1993. The estimated annual infiltration for the 1994-1995 hydrological period (160 mm) is surprisingly lower than the one calculated for 1993-1994 (210 mm) even though the

precipitation intensity of the 1994-1995 hydrological year was higher. This can be justified by the fact that higher effective evapotranspiration rates were simulated during the 1994-1995 hydrological year which compensates the high rainfall rates of this period (Fig. 5.12).

The percentages of water distribution show that surface runoff represents around 10% of the rainfall during relatively dry periods whereas this percentage reaches 17% during high precipitation periods. As it is usually the case under oceanic climates, runoff rate partitioned by the water mass balance component is often inferior to the amount of infiltration rate which ranges from 10% to 24% (Fig. 5.13).

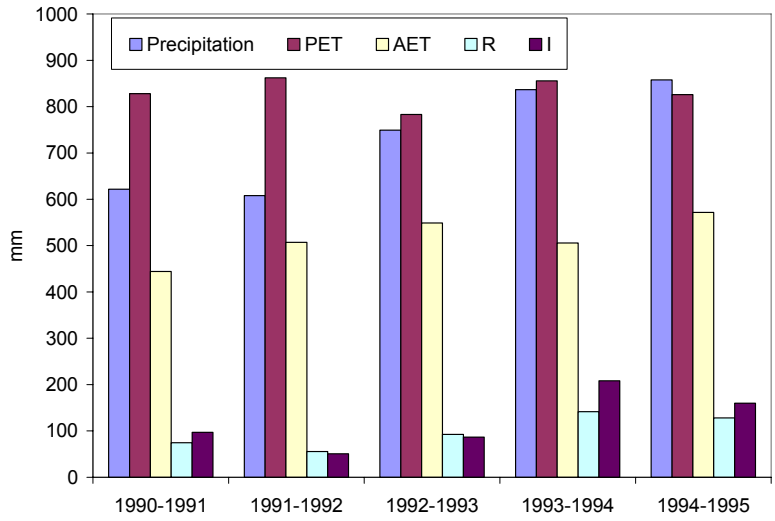

Fig. 5.12 Annual distribution of precipitation by the water balance component to actual evapotranspiration, infiltration and runoff for the period 1990-1995

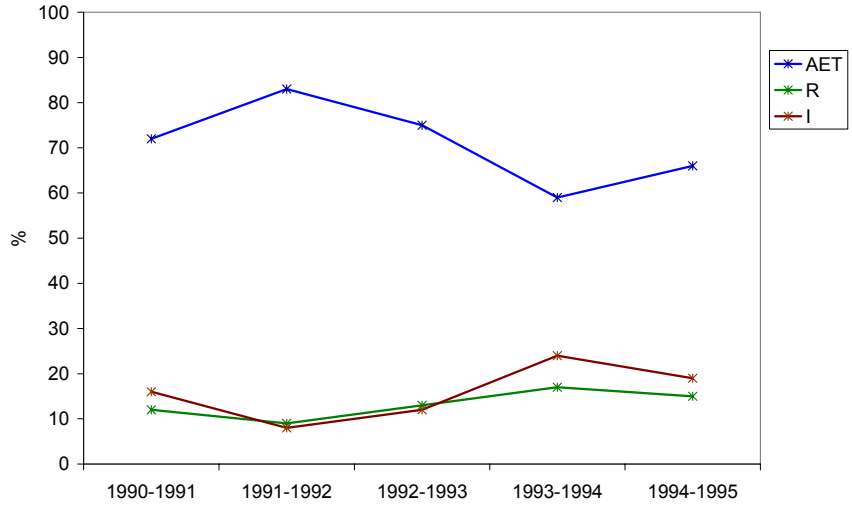

Fig. 5.13 Temporal evolution of water distribution percentage to actual evapotranspiration, infiltration and runoff for the period 1990-1995. AET+R+I = 100%

5.4.3 Hydro(geo)logical model initialization strategy

The hydrogeological module SAM needs proper initialization which aims at reaching equilibrium piezometric head distribution before running the model. Such equilibrium state is obtained via spinning up the model. Generally, the spin-up is done either by running the model for a long period or by looping the model runs within a given period of time until the model converges towards a steady state (Rodell et al., 2005). In this study, a spin-up is done for the period from 1 August 1989 through 31 July 1990 to initialize the water content of the unsaturated zone component before running the model for the period of interest (August 1, 1990 to July 31, 1995). The piezometric head initial conditions of the Eocene and Chalk units are illustrated in Fig. 5.14.

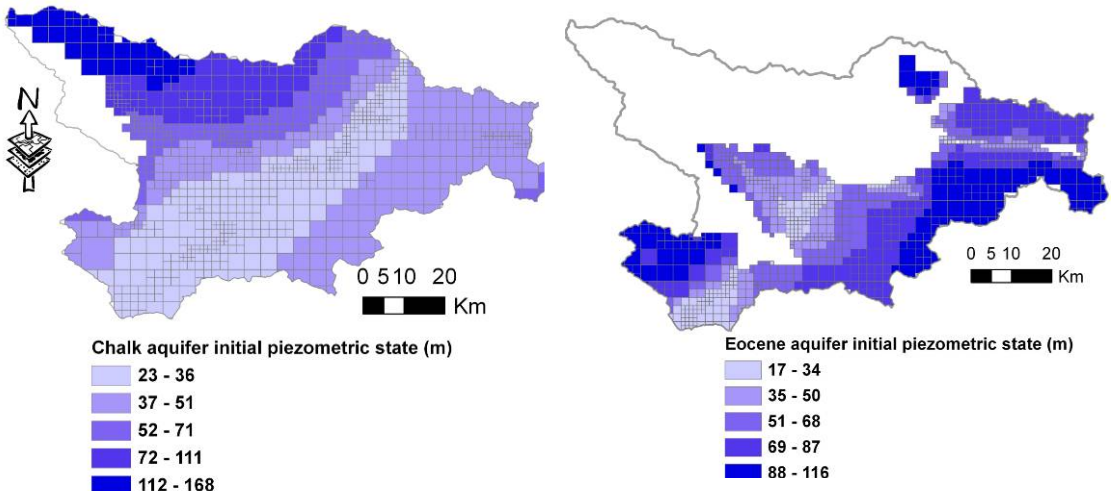

Fig. 5.14 Chalk and Eocene aquifer units initial piezometric heads obtained from the spin-up method

The initial conditions of the regional river routing model (RAPID) are similar to the ones used in the SIM-France study (David et al., 2010) (Fig. 5.15).

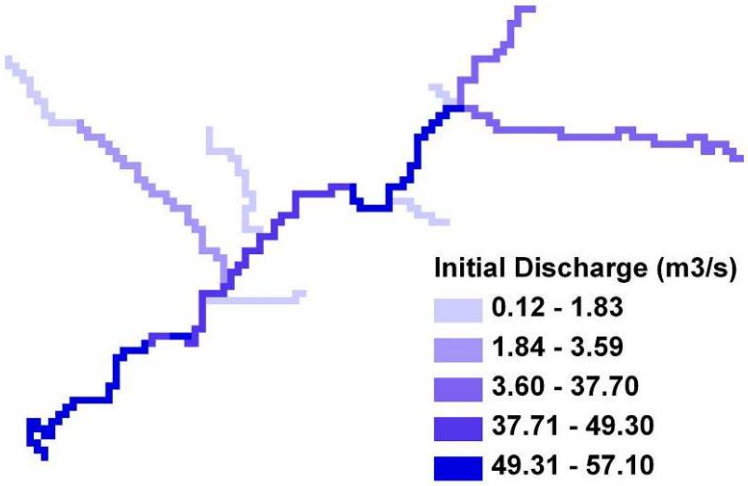

Fig. 5.15 Regional hydrological routing model (RAPID) initial conditions for the Oise stream network

5.4.4 Recalibration of the Oise initial hydro(geo)logical model: low frequency behavior

The hydrodynamic parameters of the Oise basin hydro(geo)logical model are similar to the ones previously applied by Gomez (2002) (Tab. 5.2) for constant in-stream water levels, except for storage and transmissivity coefficients of aquifer units that were recalibrated to improve the distribution of hydraulic heads in the simulated area of the Oise basin. The storage coefficient (dimensionless) is defined as the volume of water released from an aquifer per unit area per unit decline in the hydraulic head. It is an important factor in determining aquifer behavior and has a significant impact on both dewatering of the water table and pressure relief of confined aquifers. The transmissivity characterizes the ability of water to flow through a porous media.

Tab. 5.2 Hydrodynamic Characteristics of the Seine hydrogeological model

Hydrodynamic parameter	Parameter value
Eocene layer transmissivity ($L^2.T^{-1}$)	[7 10^{-4} ; 5.8 10^{-2}] $m^2.s^{-1}$
Eocene layer storage coefficient (dimensionless)	[9.9 10^{-5} – 10^{-1}]
Chalk layer transmissivity ($L^2.T^{-1}$)	[5.8 10^{-3} - 6.5 10^{-2}] $m^2.s^{-1}$
Chalk layer vertical transmissivity ($L^2.T^{-1}$)	[1.5 10^{-12} - 1.2 10^{-9}] $m^2.s^{-1}$
Chalk layer storage coefficient (dimensionless)	[9.9 10^{-5} - 7.8 10^{-2}]
Global concentration time of the basin (T)	17 days

In the initial model (Gomez, 2003), the simulated hydraulic heads in the Oise basin were either overestimated or underestimated due to an increase or decrease in hydraulic gradients. The recalibration process of the Oise hydro(geo)logical model consisted in partitioning the basin to local zones where hydraulic head time series exhibit the same behavior (Fig. 5.16). Furthermore, zone B was divided to smaller subzones (α, β and γ), in these subzones, the hydraulic head gradient between α and γ was decreased while hydraulic head gradient between α and β was increased in order to improve the hydraulic distribution in this particular zone.

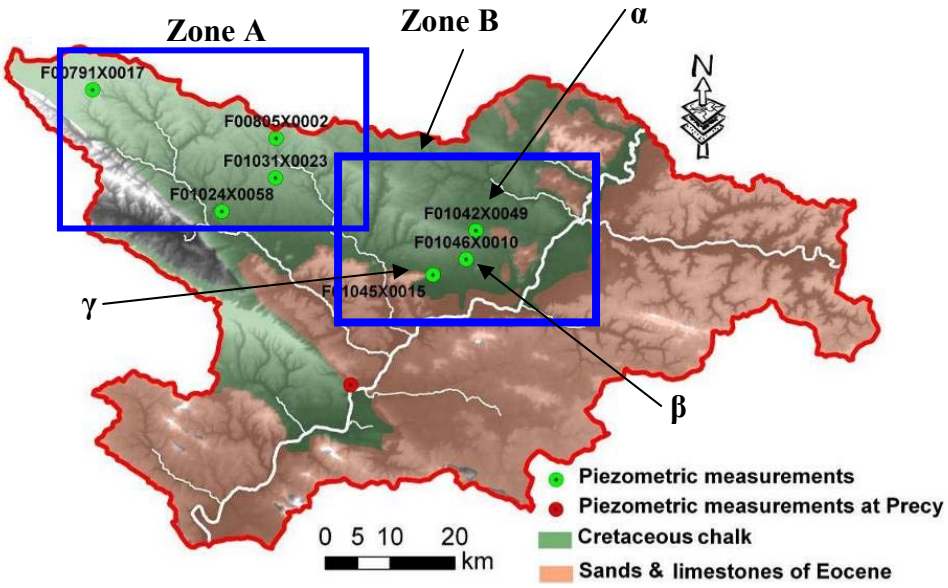

Fig. 5.16 Oise basin measured piezometric heads and local zones for calibration

The transmissivity and storage coefficients were locally calibrated by a trial-error approach, aiming at maximizing the fit between simulated piezometric heads against measured ones at seven piezometers located in the Chalk aquifer (Fig. 5.16) and grouped in different zones.

The transmissivity of the Chalk aquifer units were slightly modified in certain zones of the Oise basin, especially by lowering it in the A zone and for piezometers α and β (Fig. 5.17).

The storage coefficients were also adjusted in these zones to improve the dynamics and amplitude of the simulated piezometric heads, especially along the river network where the aquifer unit is mostly composed of alluvial deposits with peculiar properties. The comparison between initial state storage coefficients and the recalibrated ones for both Eocene and Chalk aquifer units of the Oise basin is illustrated in Fig. 5.18 and Fig. 5.19.

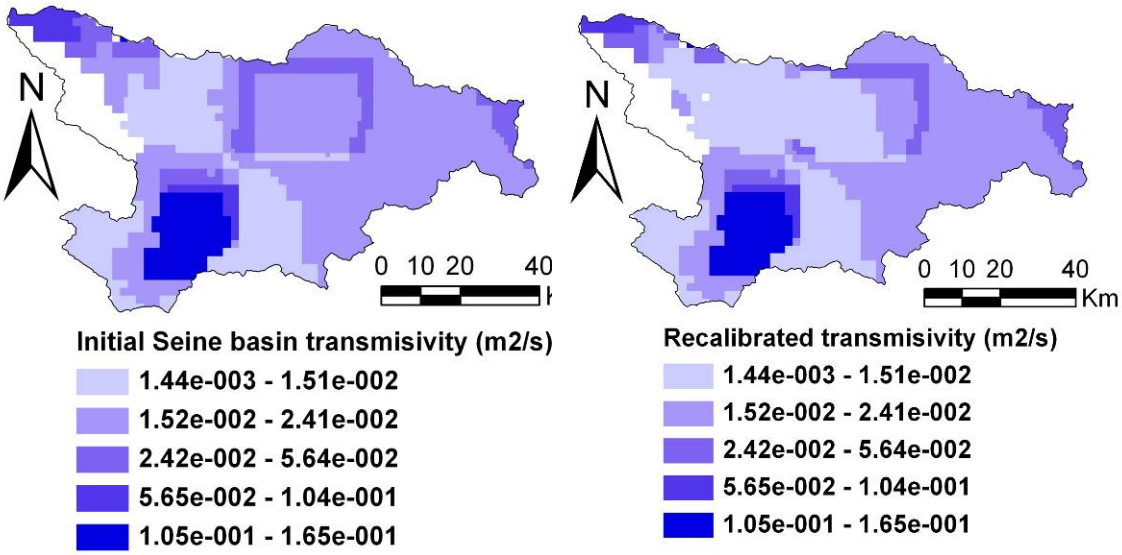

Fig. 5.17 Oise Chalk aquifer initial and recalibrated transmissivity

The calibration of the storage coefficients demonstrate that a local increase in the Chalk aquifer storage coefficients leads to a rise in simulated piezometric heads because the volume of water released from the storage in the aquifer is reduced. Moreover, fluctuations of simulated piezometric heads are impacted by the variation of storage coefficients, as an increase in storage coefficients dampens locally the simulated piezometric signal. A decrease in storage coefficients leads to a fall in simulated piezometric heads, especially when aquifer storage is depleted by exfiltration from the aquifer to the river.

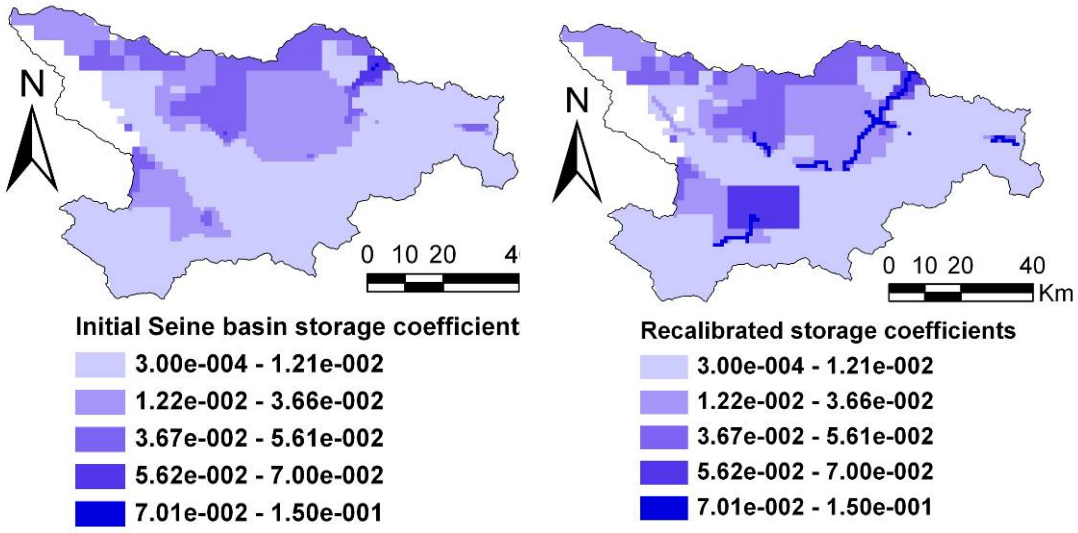

Fig. 5.18 Oise Chalk aquifer initial and recalibrated storage coefficients

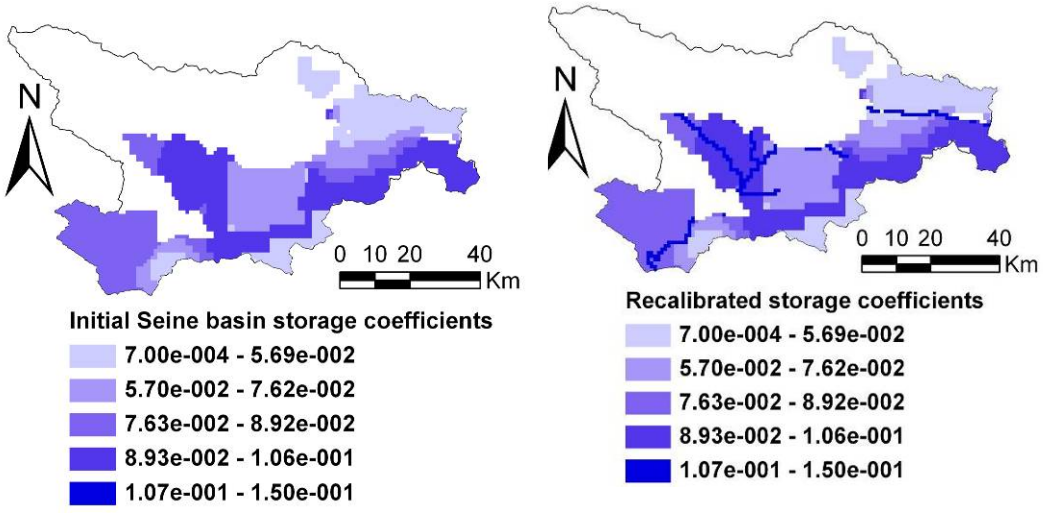

Fig. 5.19 Oise Eocene aquifer initial and recalibrated storage coefficients

The comparisons between recalibrated piezometric heads of the EauDyssée platform and the ones of the initial Seine regional model (2002) present a significant improvement of the model (Fig. 5.20). Furthermore, we compared the RMSE and correlation coefficient statistical criteria between the initial model and the recalibrated one (Tab. 5.3). The comparisons demonstrate the improvement of simulated piezometric heads in terms of piezometric levels and timing of peaks, owing that to the recalibration of storage and transmissivity coefficients.

Tab. 5.3 Comparison of statistical criteria between EauDyssée recalibrated piezometric heads and piezometric heads obtained in the Seine regional model

			Initial model			Recalibrated model		
Station code	**Number of observations (days)**	**Average observed (m)**	**Average simulated (m)**	**RMSE (m)**	**R (%)**	**Average simulated (m)**	**RMSE (m)**	**R (%)**
F00791X0017	1576	162.11	157.54	4.9	0.81	161.611	1.794	0.86
F00805X0002	1592	119.39	113.36	6.4	0.481	120.2	1.473	0.918
F01042X0049	1408	60.15	57.76	2.5	0.922	60.02	0.67	0.93
F01045X0015	225	38.5	49.36	10.9	NA	38.53	1.5	NA
F01024X0058	1576	77.35	73.88	4	0.941	75.1	3.042	0.813
F01046X0010	1606	51.46	47.25	4.5	0.779	50.9	1.82	0.716

Finally, the average aquifer piezometric heads were calculated for the whole period of simulation (Fig. 5.21). The steep piezometric gradients of both Chalk and Eocene aquifer units near to the main stream suggest that the movement of water is directed towards the Oise river and eventually the output of the basin. The figures also show that piezometric heads are generally correlated with topography for surface aquifer units.

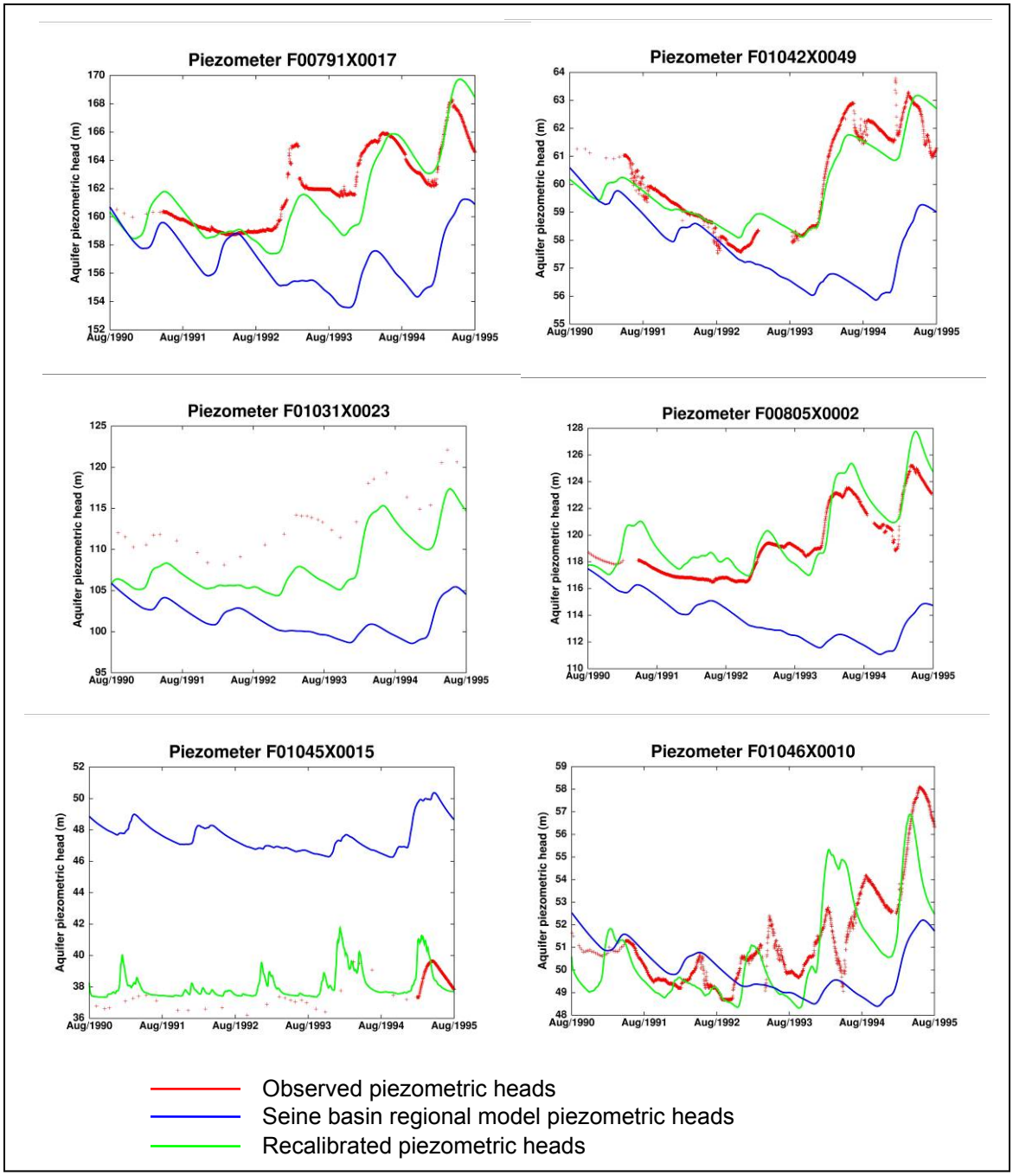

Fig. 5.20 Comparison between EauDyssée recalibrated piezometric heads of the Oise basin (in green), piezometric heads obtained in the Seine basin regional model (in blue) developed by Gomez (2002) and observations (in red)

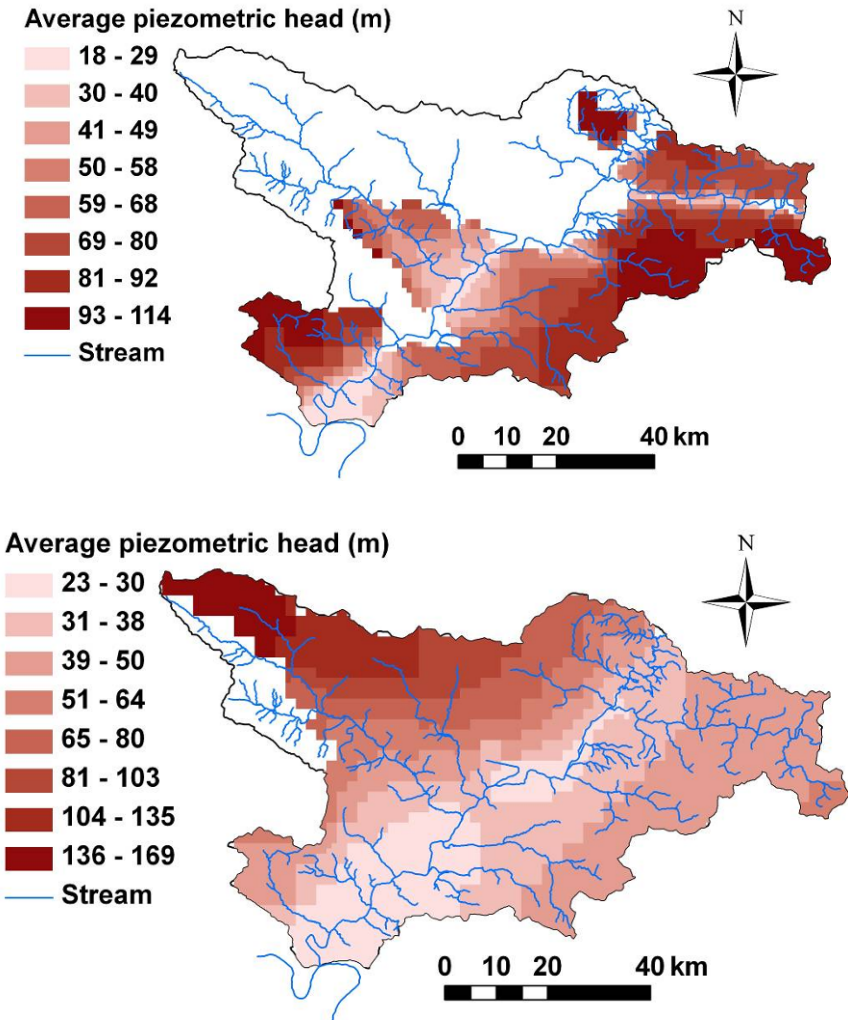

Fig. 5.21 Average simulated piezometric heads for the period 1990-1995 a) Eocene aquifer units, b) Chalk aquifer units

Oise regional river routing model calibration

The *k* Muskingum parameter of RAPID (section 3.2.4) was determined using a relative transfer time that is computed for each river cell based on topography (Golaz-Cavazzi, 1999). Multiplied by a global concentration time of the basin (17 days) that was fitted by Gomez (2003), it provides the time needs to reach the outlet of the basin starting from a surface cell. Subtracting the transfer times of two neighboring river cells gives the time needed to flow from the upstream cell to the downstream one, which is the in-stream *k* parameter of the Muskingum model (Monteil et al., 2010). Based on this technique, the distribution of *k* for the Oise basin varies from 500 to 5000 seconds for a spatial discretization of 1 km, the

average k is 2443 seconds (equivalent to an average river velocity of 0.4 $m.s^{-1}$) which is consistent for such river network (Fig. 5.22). The minimum and maximum values of k were cut-off at 500 and 5000 to avoid numerical divergence of the code EauDyssée. The other parameters of the regional river routing model are similar to the ones developed in the SIM-France model (David et al., 2010).

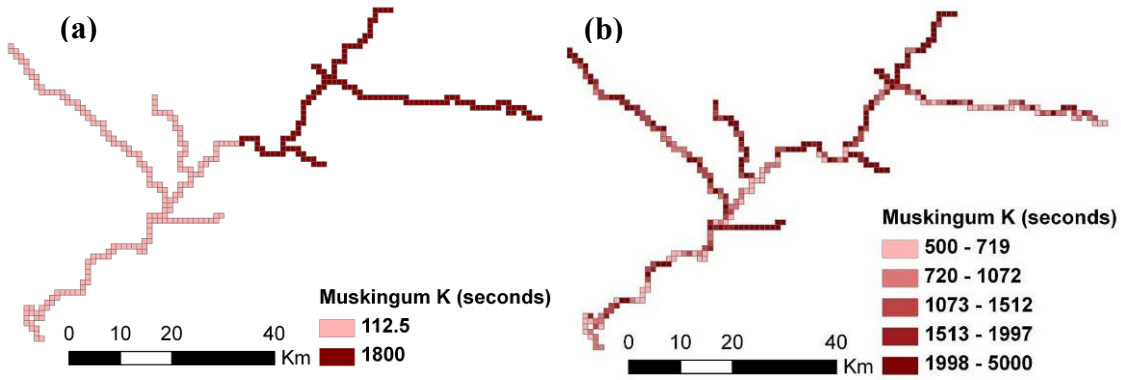

Fig. 5.22 The k parameter of RAPID along the Oise stream network a) SIM-France model (David et al., 2010), b) Determined using the relative transfer time methodology

Upon recalibrating the initial Oise hydro(geo)logical model, simulated runoff and groundwater contributions will be used to construct the Oise River hydraulic model, this step will be detailed in the following section of this chapter.

5.5 The construction of the Oise River hydraulic model

The hydraulic model HEC-RAS (section 3.4) is used to model the Oise River between Sempigny and the confluence with the Seine River (Fig. 5.6). The total length of simulated river reaches is 188 km for which river cross sections are surveyed by the Direction Régionale de l'Environnement (DIREN) (Fig. 5.23).

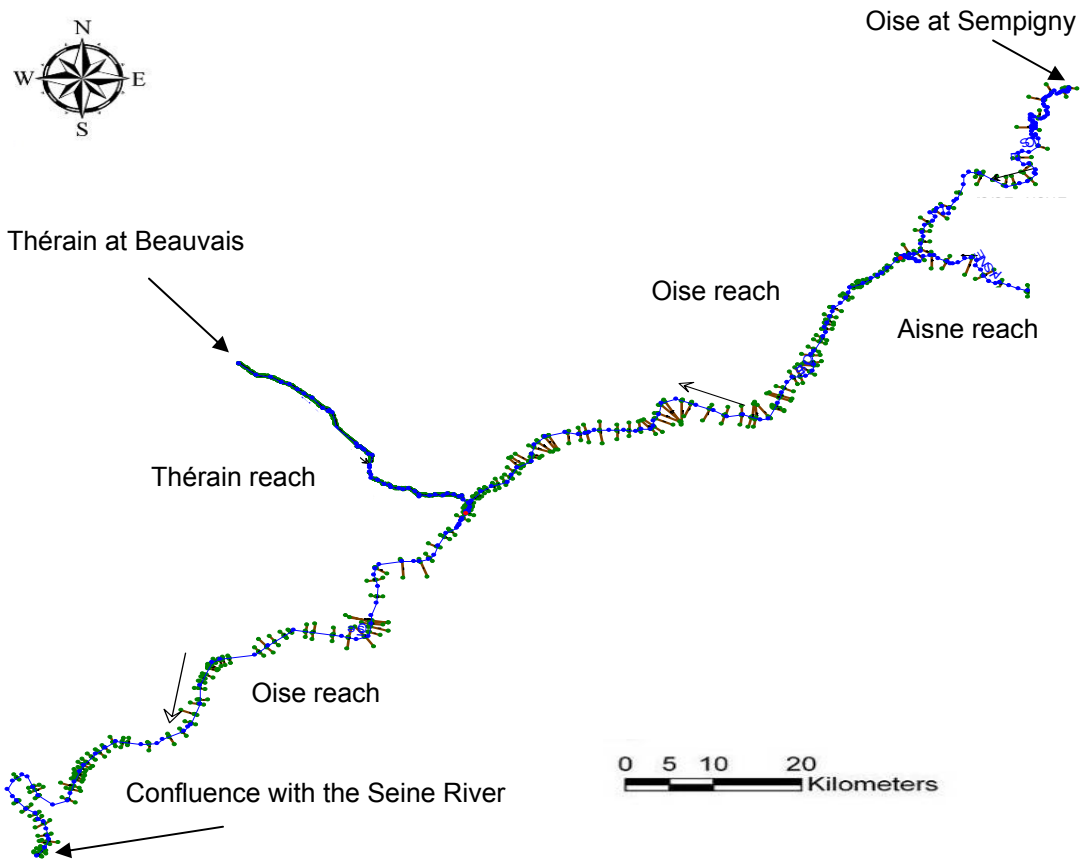

Fig. 5.23 Surveyed cross sections along the Oise River network

The input data used to construct the hydrodynamic model are composed of:

- River morphological representation: Cross sections each 200 m on average
- Upstream boundary conditions: Observed discharge hydrographs
- Downstream boundary conditions: Manning's equation
- Surface lateral inflows: Observed + Runoff simulated by EauDyssée
- Groundwater contributions: Simulated by EauDyssée

The upstream boundary condition of the Oise hydraulic model is defined by observed mean daily discharge hydrographs at Sempigny (Oise reach), Herant (Aisne reach) and Beauvais (Thérain reach) (Fig. 5.24). The period of the input discharge hydrograph is from 1 September 1990 to 31 August 1995. The observed discharge hydrographs demonstrate the

two important flood events of February 1995 and January 2003 that occurred within the period of simulation (Fig. 5.25).

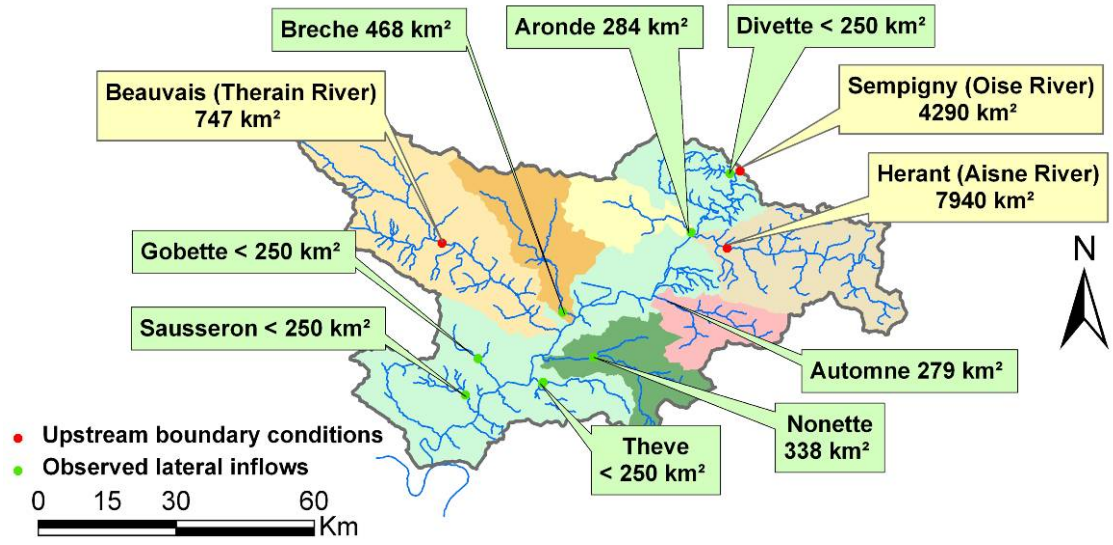

Fig. 5.24 Location of the Oise basin boundary conditions and observed sub-catchments flow used to construct the Oise hydrodynamic model

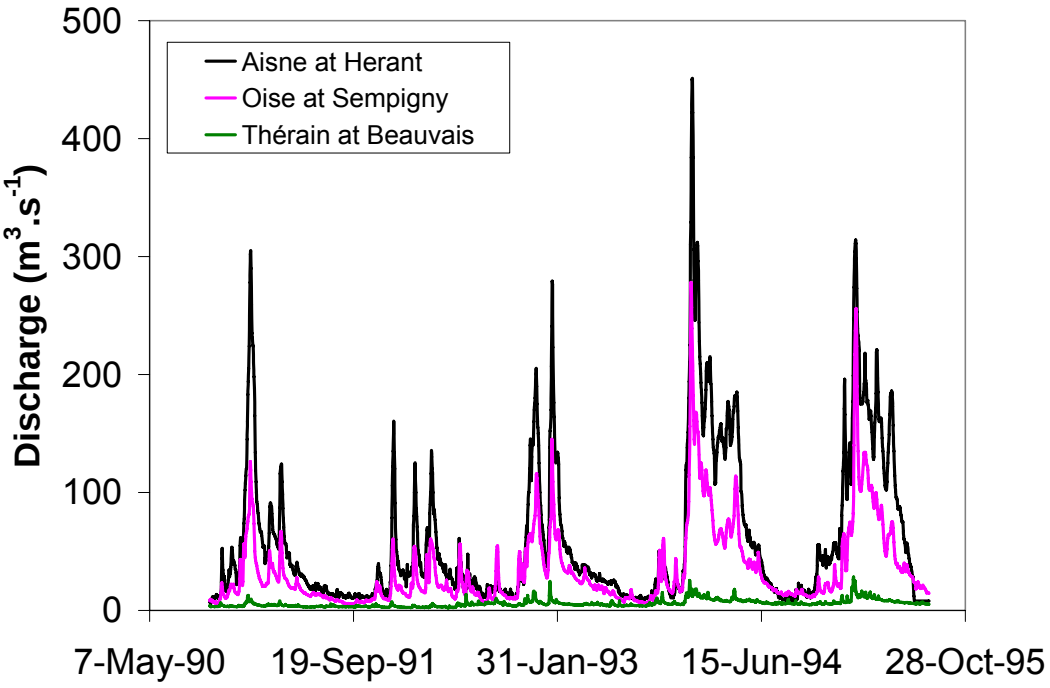

Fig. 5.25 Oise River observed discharge hydrographs at Sempigny, Herant and Beauvais used as upstream boundary conditions for the hydraulic model HEC-RAS.

Observed lateral inflows of the Oise sub-catchments (Divette, Automne, Nonette, Theve, Esches, Sausseron) are directly integrated into the hydraulic model while non observed ones in addition to groundwater contributions are simulated by the EauDyssée Platform river cells. In this framework, runoff and groundwater contributions simulated by EauDyssée at each river grid-cell are spatially projected along the river reach by calculating a length equivalency factor between the high resolution river reach and the river grid-cell lengths (Fig. 5.26 and section 5.2 of this chapter).

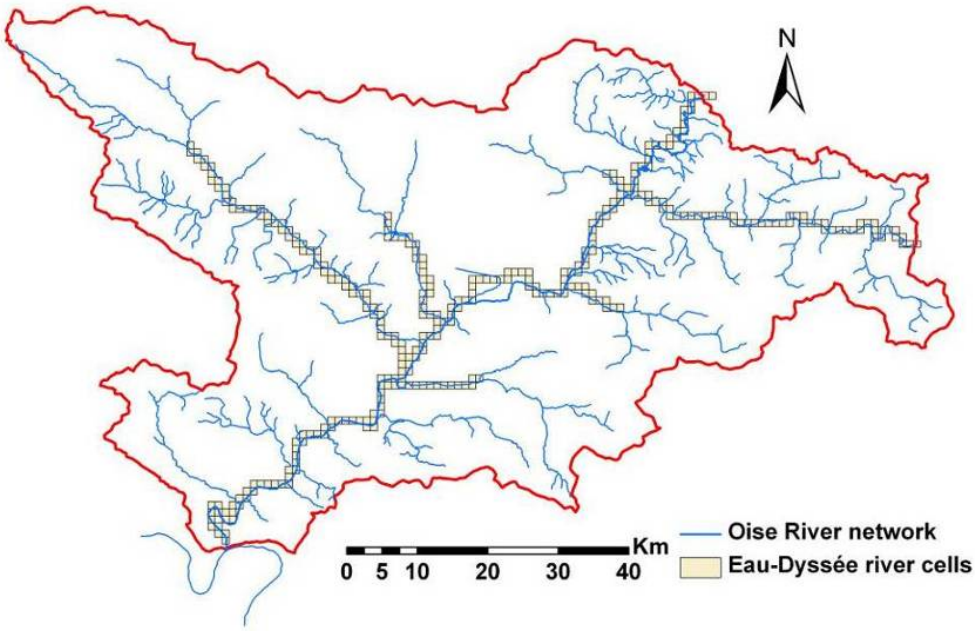

Fig. 5.26 Oise stream network and EauDyssée river cells (1 km * 1 km)

5.5.1 Oise hydraulic model calibration of Manning's roughness coefficient

The Manning's roughness coefficient (n) [$T.L^{-1/3}$] represents the energy loss due to the water friction with the bed surface's roughness. An increase of Manning's roughness coefficient in the main channel has the following impacts on the hydraulic response: a) local increase in water stage b) decrease of discharge peak as the flood wave moves downstream, c) increase of travel time. The calibration of Manning's roughness coefficient was performed by a trial-error approach, aiming at maximizing the fit between simulated discharge and water levels

against observations at four gauging stations (Sarron, Maysel, Creil and Auvers sur Oise) (Fig. 5.27). The performance of the Oise hydraulic model was evaluated by a number of statistical criteria (Tab. 5.4).

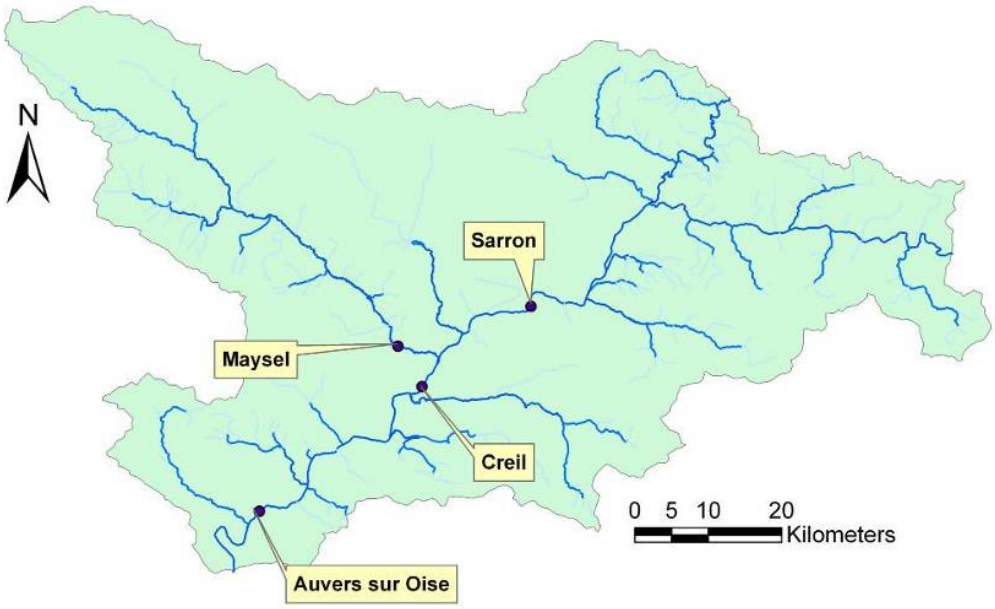

Fig. 5.27 Oise hydraulic model calibration stations

Optimal values of Manning's roughness coefficients vary between 0.026 for the main reaches to 0.032 for the Oise tributaries which is consistent with standard values for such rivers (Chow, 1959). Roughness coefficient for the floodplain was fixed at 0.04 and had minor influence on the model's performance. Example of calibration results are shown at Sarron for discharge and water level (Fig. 5.28).

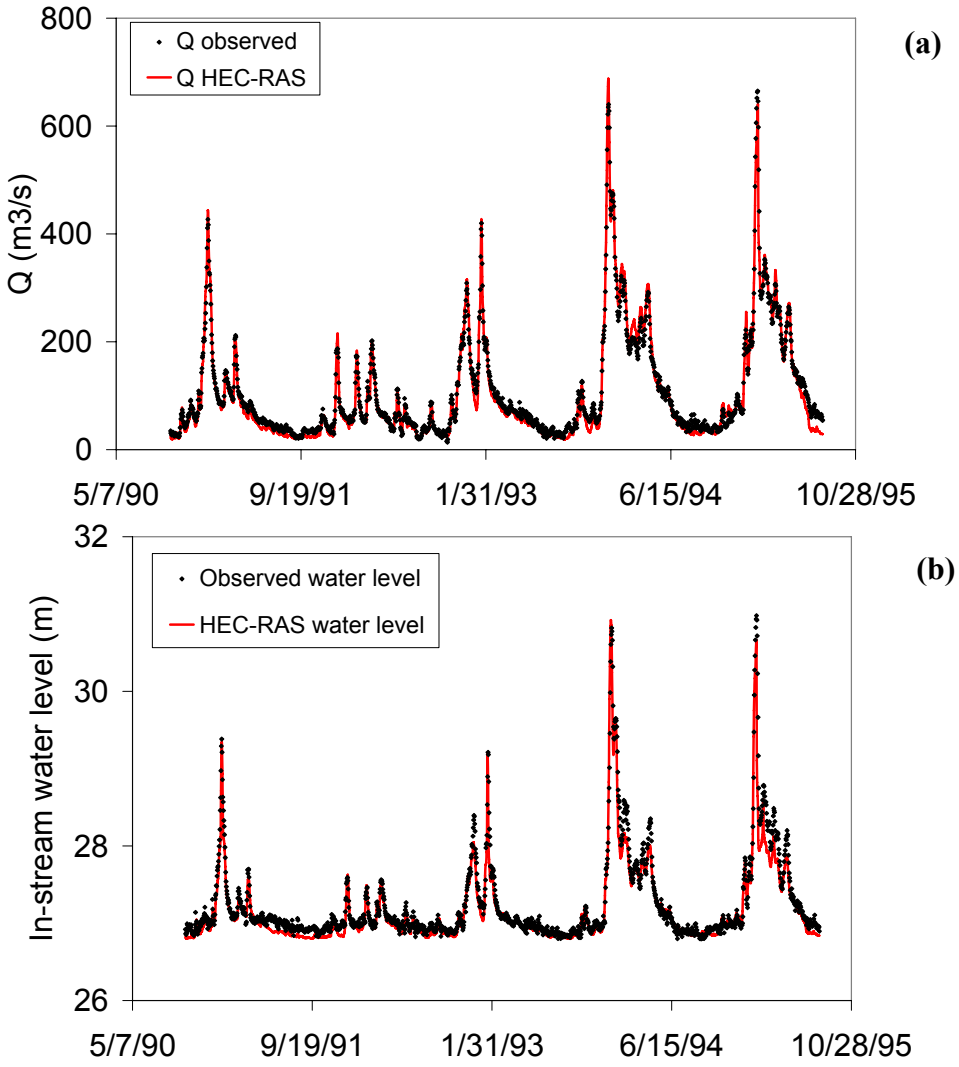

Fig. 5.28 Comparison of observations and simulations at the Sarron hydrometric station over 5 years, obtained from the high resolution hydraulic model HEC-RAS: a) river discharge, b) river stage

Upon calibrating the hydraulic model, we tested the importance of feeding the hydraulic model with runoff and groundwater contributions calculated by EauDyssée (Fig. 5.29). The resulting simulated discharge by the hydraulic model HEC-RAS is lower than the one estimated with regional inflows (groundwater and surface inputs from the basin). For instance, at Auvers sur Oise, the underestimation is in average of 19 % (Fig. 5.29).

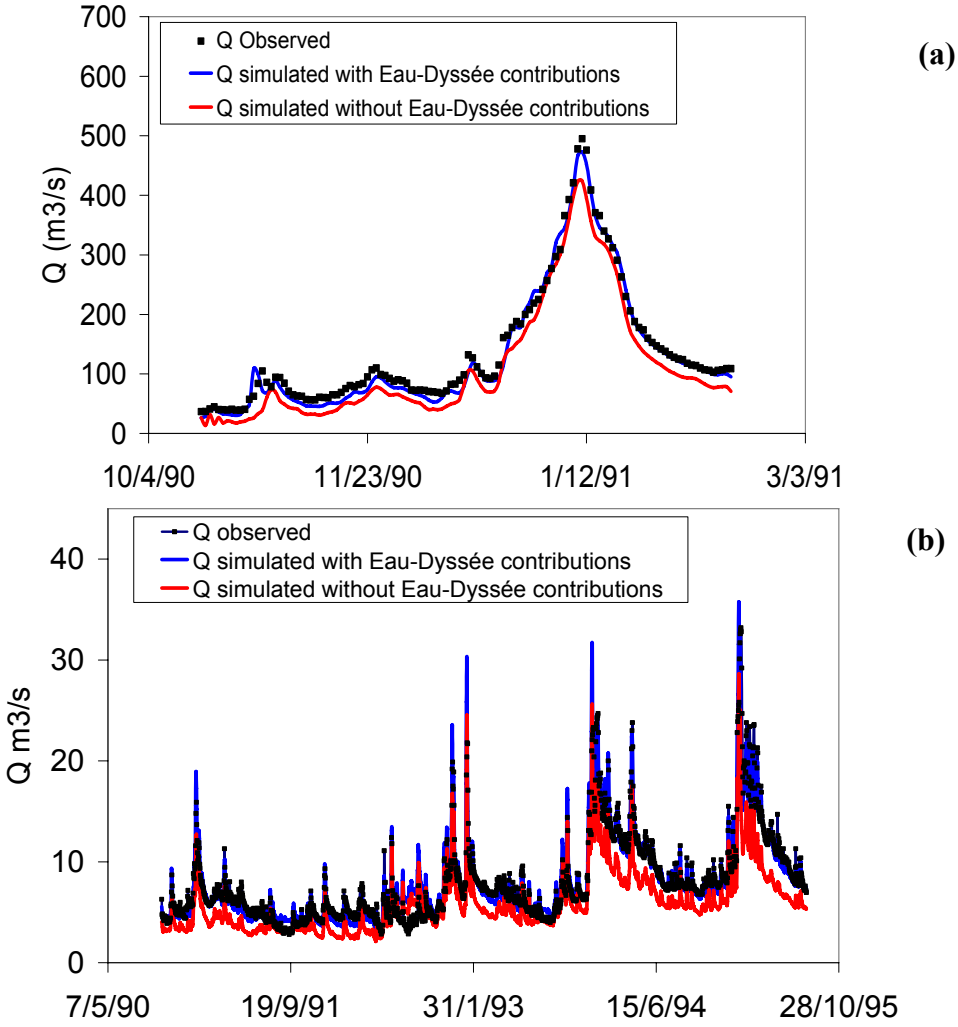

Fig. 5.29 HEC-RAS simulated discharge hydrographs compared to observations at a) Auvers sur Oise, b) Maysel hydrometric stations with and without runoff and groundwater contributions from EauDyssée.

Once the hydraulic model is calibrated, rating curves (discharge vs. water levels) are extracted at each river cross section. These rating curves are upscaled to the resolution of a regional scale hydrogeological model, where they are used to deduce river stage from the simulated discharge at each time step and in each river grid-cell.

Tab. 5.4 Summary of HEC-RAS performances at the four available hydrometric stations. The statistical criteria are computed at the daily time step

Station	Period	Discharge					Water level				
		Nash	Bias (%)	RMSE (m^3s^{-1})	σ_{obs}	σ_{sim}	RMSE (m)	Bias (%)	ρ	σ_{obs}	σ_{sim}
Sarron	1990-1995	0.97	-4.0	12	99.7	103.7	0.17	-0.26	0.96	0.6	0.54
Maysel	1990-1995	0.91	0.15	1.35	4.4	4.3	NA	NA	NA	NA	NA
Auvers	1990-1991	0.98	-4.0	13.4	105	107	NA	NA	NA	NA	NA
Creil	1990-1991	NA	NA	NA	NA	NA	0.09	0.07	0.94	0.24	0.25

NA: No available observations to compare with

5.5.2 Local to regional scale upscaling example

Upon calibrating the Oise River hydraulic model, the rating curves (discharge vs. water levels) derived at each cross-section by HEC-RAS are linearly projected along the river cells, by calculating a length equivalency factor between the high resolution river reach and the river grid-cell lengths.

Fig. 5.30 illustrates a local to regional upscaling example for a given river cell (1 km * 1 km). This particular river cell contains three projected rating curves located at three distances from the center of the river cell (253.3 m, 506.5 m, 761.6 m). An equivalent rating curve at the center of this river grid-cell is calculated by inverse distance weight averaging with respect to the cell's center (Eq. 5.1). Then, the resulting equivalent rating curve is sent as input boundary conditions for the QtoZ module which calculates the water level as function of the discharge routed by RAPID and sends it to the groundwater model (SAM) in order to simulate stream aquifer interactions (Fig. 5.30).

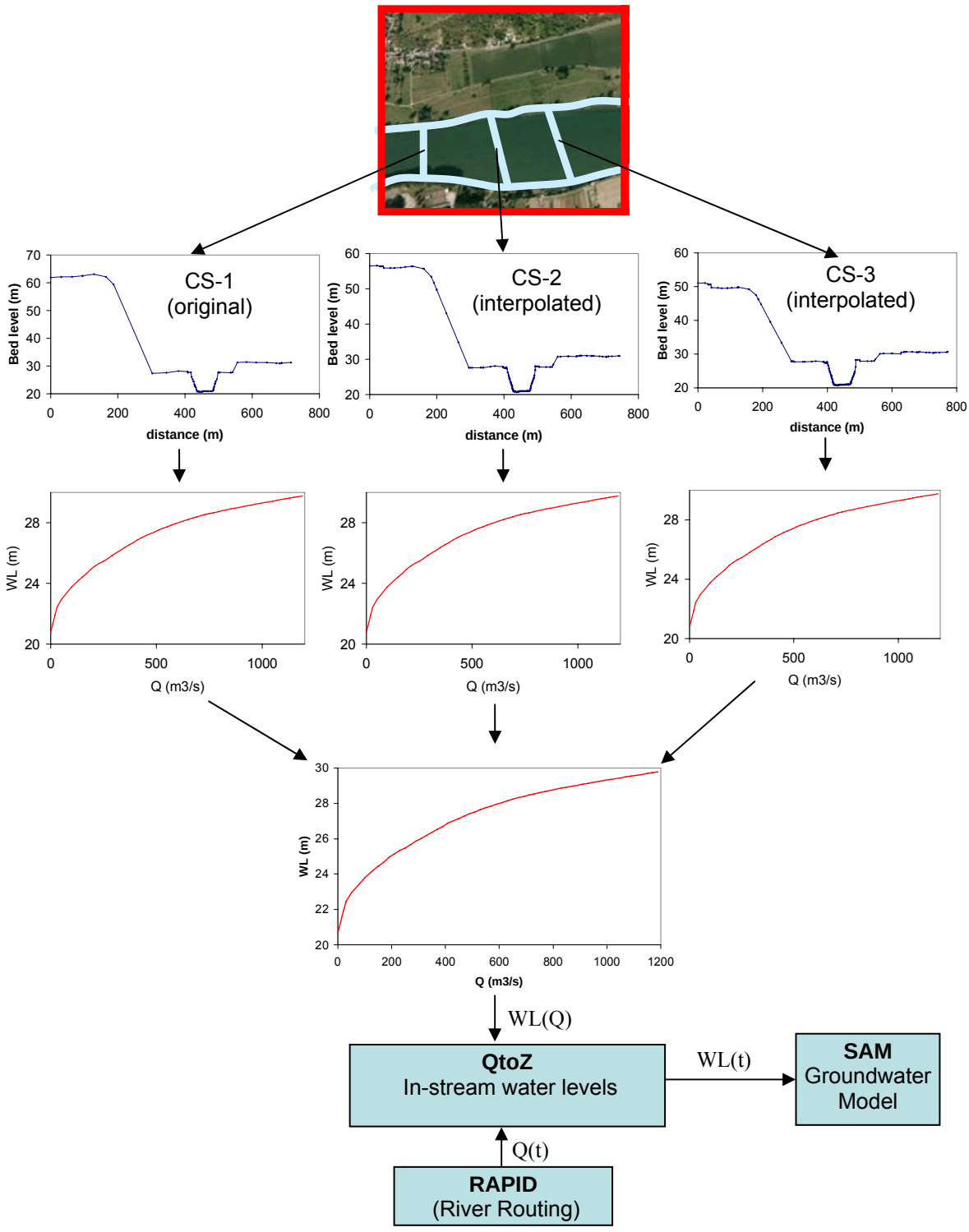

Fig. 5.30 local to regional scale uspcaling example in a given river grid-cell

5.6 EauDyssée simulations after applying the upscaling methodology

5.6.1 Simulated discharge and river stage by the regional hydro(geo)logical model EauDyssée

Discharge and water level hydrographs are simulated by the regional model EauDyssée after implementing the new methodology of in-stream water level fluctuations.

In-stream discharges and water levels simulated by EauDyssée are visually in agreement with observations in terms of hydrograph shape and timing of peaks albeit the model tends to overestimate discharge peaks due to overestimation produced by the Seine regional model upstream of the simulated area (e.g. at Sarron, Fig. 5.31). Indeed in-stream boundary conditions for the Oise and its tributaries are given by EauDyssée applied over the whole Seine basin (Gomez et al., 2003), whereas we used observed hydrographs for the HEC-RAS simulation. To prove that overestimation is due to upstream boundary condition discharge, we have imposed observed discharge hydrographs similar to the ones used to construct the hydraulic model (HEC-RAS) upstream boundary conditions instead of discharge hydrographs produced by the regional Seine model (Fig. 5.25). The comparison between the two simulations demonstrates the impact of upstream boundary conditions on the quality of simulated discharge and water levels, especially during high flow periods (Fig. 5.31). Nevertheless, the Nash and bias criteria of the simulated discharge at Sarron station remain satisfactory when using boundary conditions given by EauDyssée applied over the whole Seine basin, equal to 0.85 and 6%, respectively (Tab. 5.5).

The overestimation in the Seine regional model upstream of the simulated area is most likely due to a not optimal calibration of the upstream production units.

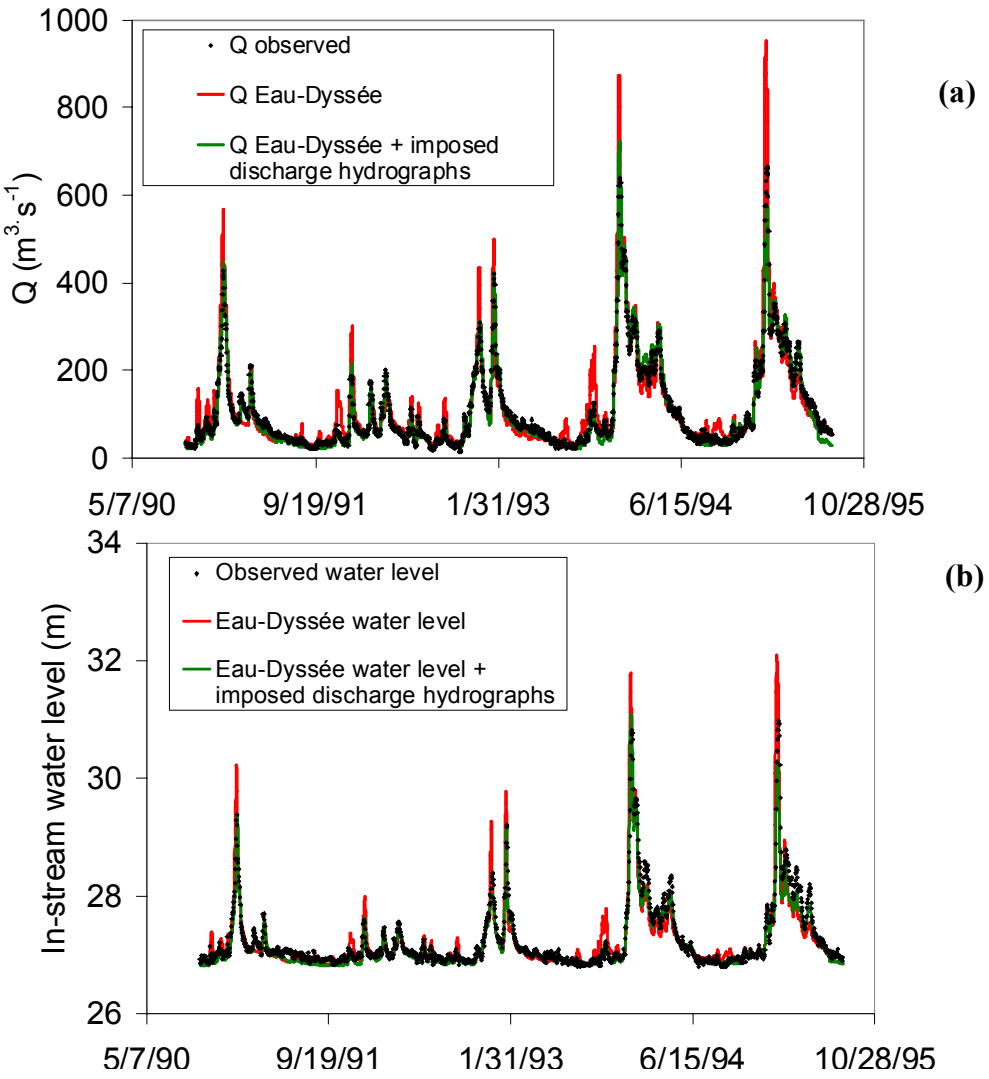

Fig. 5.31 Comparison between observations, EauDyssée simulations using observed boundary conditions imposed at the upstream and simulations using boundary conditions given by EauDyssée applied over the whole Seine basin: a) river discharge, b) river stage at the Sarron hydrometric station over 5 years

Tab. 5.5 Summary of EauDyssée performances at the four available hydrometric stations. The statistical criteria are computed at the daily time step

Station	Period	Discharge			Water level				
		Nash	Bias (%)	RMSE (m^3s^{-1})	RMSE (m)	Bias (%)	ρ	σ_{obs}	σ_{sim}
Sarron	1990-1995	0.85	6	18	0.2	0.4	0.93	0.6	0.78
Maysel	1990-1995	0.78	0.23	1.85	NA	NA	NA	NA	NA
Auvers	1990-1991	0.83	5.8	20	NA	NA	NA	NA	NA
Creil	1990-1991	NA	NA	NA	0.14	0.21	0.90	0.24	0.32

NA: No available observations to compare with

5.6.2 EauDyssée hydrogeological model simulations: high frequency behavior

Upon applying the upscaling methodology for taking into account in-stream water level fluctuations, the EauDyssée hydrogeological model was recalibrated to account for the effect of high frequency river signals on aquifer units.

The transmissivity and storage coefficients were locally modified in zones adjacent to the main stream where in-stream water levels fluctuations were enabled to improve the dynamics and amplitude of the simulated piezometric heads (Fig. 5.18 and Fig. 5.19).

In this context, storage coefficients of both Eocene and Chalk aquifer units in direct contact with the main river cells were set at 0.15 to dampen the high impact of in-stream water level fluctuations on underlying aquifer cells (Fig. 5.18 and Fig. 5.19).

This recalibration is conducted by comparing simulated and observed piezometric heads at Precy (Fig. 5.32). The Precy piezometer is located in the Chalk aquifer within a distance of 1.5 km from the river cell. It is the nearst available piezometer to the stream in the simulated area and the only one available for comparison.

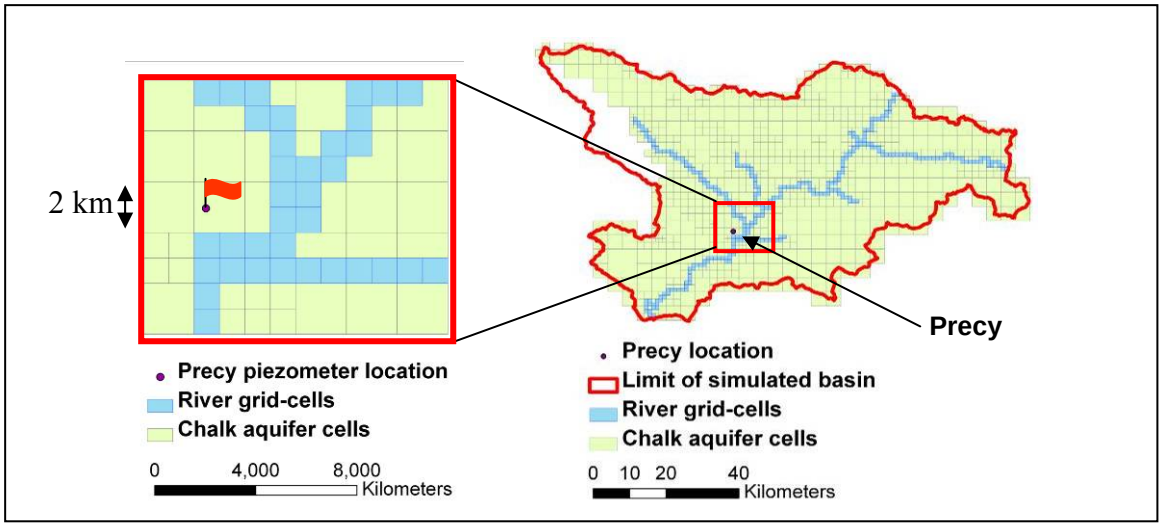

Fig. 5.32 Measured piezometric heads located at Precy sur Oise

In the river cell directly draining the Precy piezometer, the amplitude of the simulated river stage variations exceeds 6 m during the last two years of simulation, when river stage

fluctuations are enabled (Fig. 5.33). This leads to a 1 m rise of the piezometric head in the Precy piezometer, which is more realistic than the 0.15 m rise obtained neglecting in-stream water level fluctuations as previously simulated by Gomez (2002) (Fig. 5.34). Furthermore, best improvements of the simulated piezometric head are obtained for the rising and falling limbs of 1994 and 1995 flood hydrographs.

The next stage will be to characterize the local and regional impact of high frequency river signals on the overall system.

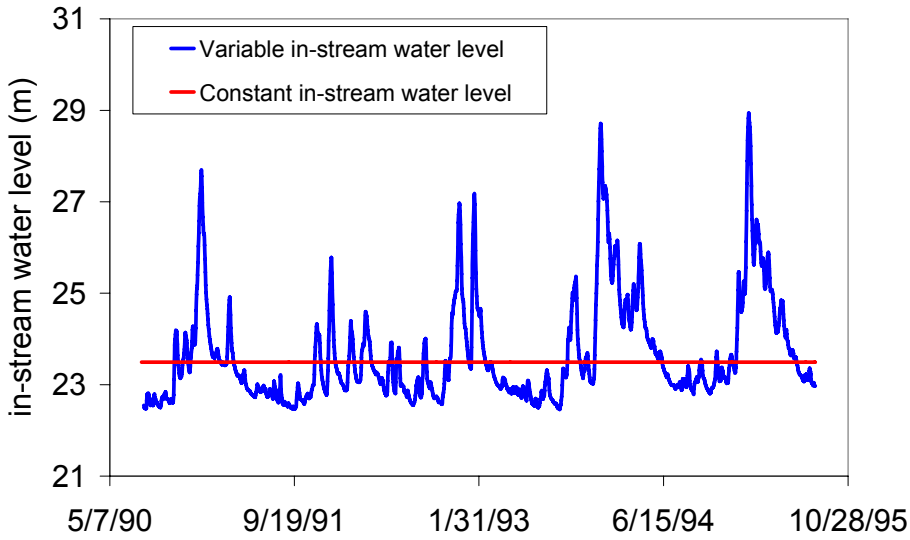

Fig. 5.33 Constant and variable in-stream water level located in the river cell draining the aquifer cell containing the Precy piezometer (Fig. 5.32)

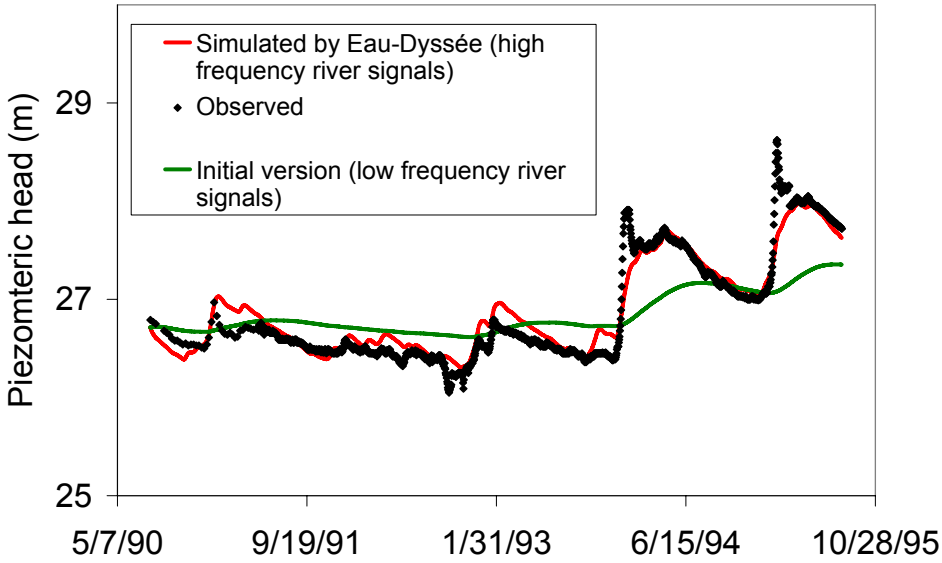

Fig. 5.34 Comparison between the simulations of the recalibrated version of EauDyssée (high frequency behavior) and the initial version (low frequency behavior) at Precy

5.7 Impact of in-stream water level fluctuations on stream-aquifer interactions at local and regional scale

In this part of the study, the impacts of in-stream water level fluctuations and Q_{max} (section 3.2.5) on the aquifer system are characterized at local and regional scale comparing four EauDyssée simulations summarized in Tab. 5.6.

Tab. 5.6 Overview of the main EauDyssée simulations to characterize the impact of in-stream water level fluctuations on stream-aquifer interactions

Simulation name	C0	C100	V0	V100
In-stream water level	Constant	Constant	Variable	Variable
Q_{max} (l s^{-1})	0	100	0	100

5.7.1 Stream-aquifer exchanges

5.7.1.1 Local scale analysis

Impact of water level fluctuations. This analysis is conducted by comparing simulated and observed piezometric heads at Precy that are impacted by in-stream water levels.

The results of comparing V0 with C0 and V100 with C100 show that each flood wave initiates an infiltration process from streams to aquifer units, leading to a significant increase in the piezometric head at Precy (Fig. 5.35). Taking into account water level fluctuations allows for simulating this aquifer unit recharge processes by the stream network.

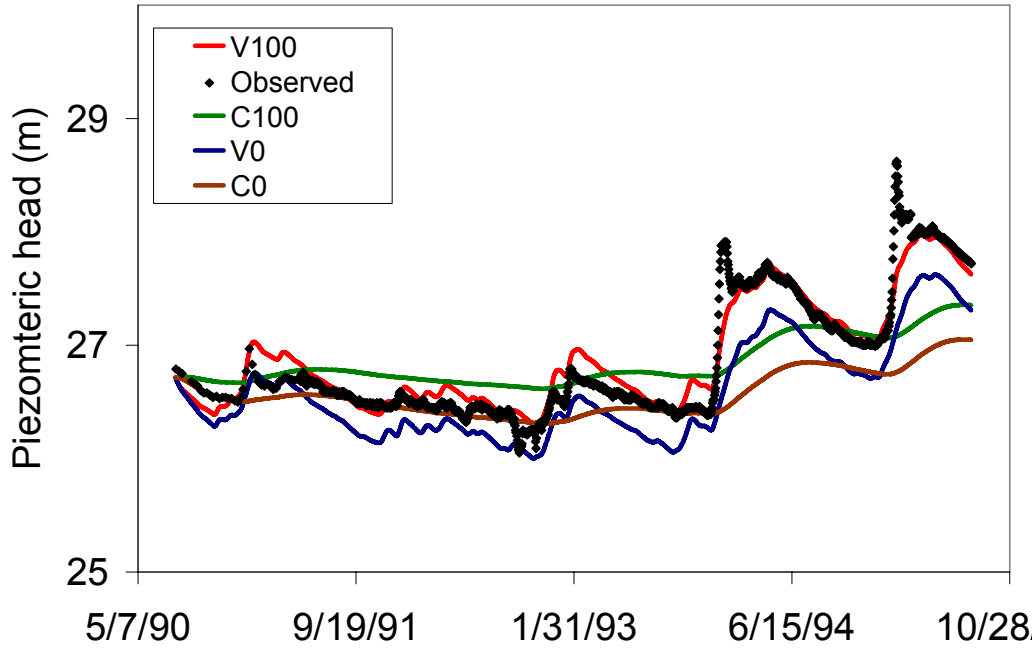

Fig. 5.35 Simulated ground-water levels in the Chalk aquifer cell containing the Precy piezometer using: a) variable and constant in-stream water levels for Q_{max} values varying between 0 and 100 $l.s^{-1}$ (Tab. 5.7)

Additionally, we compared simulated piezometric heads of scenarios V100 & C100 located at different spatial distances from the main stream: 1) At aquifer cells underlying the river cell, 2) At aquifer cells located at 3.5 km from the center of the river grid-cell (Fig. 5.36). In response to a 6 m increase in the main river cell, the peak increase in the V100 simulated Chalk aquifer piezometric head underlying the river cells is about 2 m, and 0.6 m in aquifer cells located at 3.5 km from the stream (Fig. 5.36b), while fluctuations are in the range of few centimeters when constant in-stream water levels are imposed (C100) (Fig. 5.36a).

The local analysis held to assess the local effect of river stage fluctuations on simulated piezometric heads shows that response of ground water levels to in-stream water level fluctuation is attenuated with distance from the stream. At greater distances from the stream, ground-water heads rise less rapidly, with a lower amplitude, going back to the undisturbed conditions (constant in-stream water level) more rapidly.

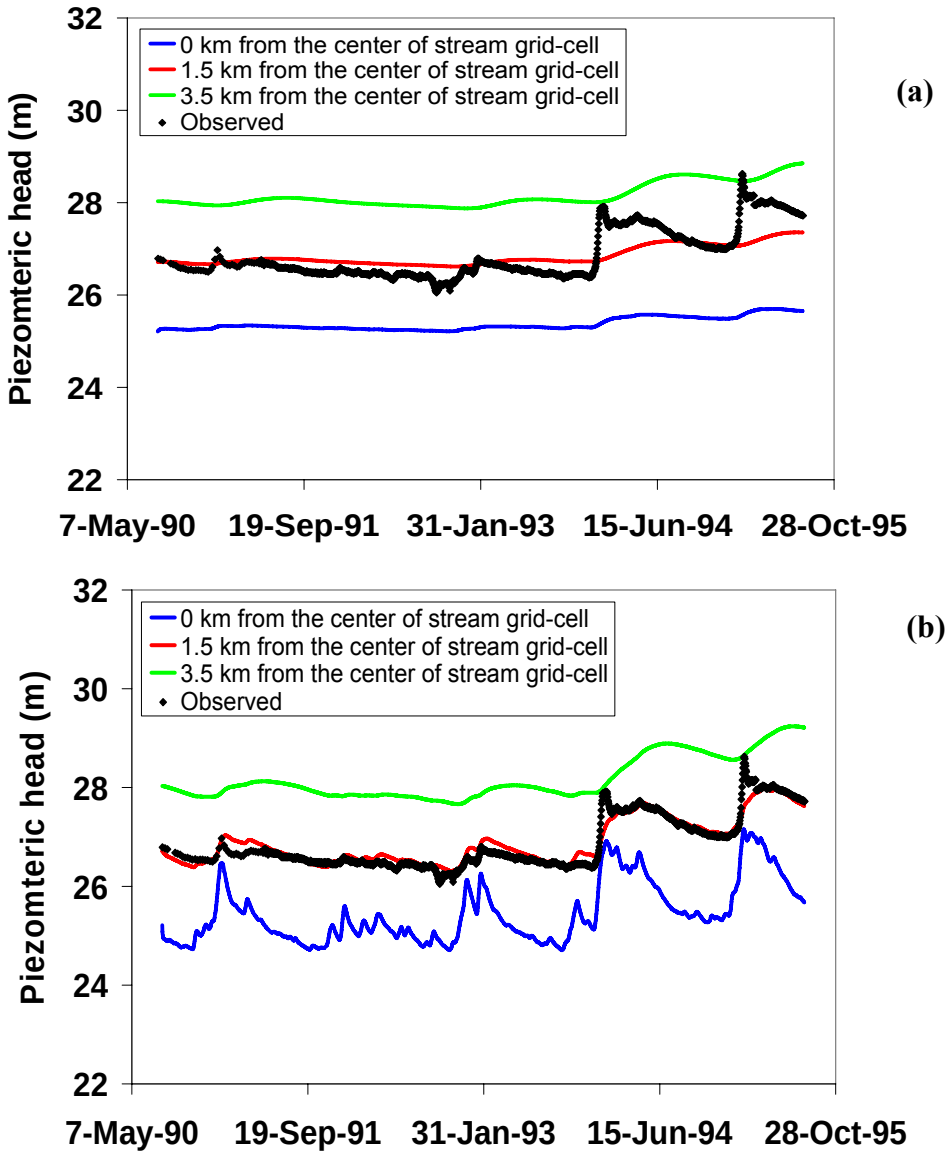

Fig. 5.36 Simulated Chalk aquifer unit piezometric heads located at three distances from the in-stream grid-cell: 1) underlying the river cell, 2) at 1.5 km from the center of the main stream (Precy piezometer) , 3) at 3.5 km from the main stream, using: a) Constant in-stream water levels (C100), b) Variable in-stream water levels (V100)

Impact of Q_{max}. The local impact of Q_{max} on stream-aquifer interactions is also explored. A sensitivity analysis of piezometric head distribution to Q_{max} is performed for both constant and variable in-stream water levels, with values of Q_{max} varying from 0 $l.s^{-1}$ (infiltration is not authorized) to 500 $l.s^{-1}$ in each river cell. The resulting simulated hydraulic heads are locally compared to observations in the Precy piezometer (Tab. 5.7). Results show that the impact of Q_{max} on simulated piezometric heads is significant up to a value of 100 $l.s^{-1}$, which

leads to the best fit to observed piezometric head, especially when the variable river stage is enabled (Fig. 5.35). Results show that rising Q_{max} beyond 100 $l.s^{-1}$ has negligible impact on simulated aquifer heads (Tab. 5.7)

Tab. 5.7 Local impact of Q_{max} on simulated aquifer piezometric heads compared with measurements at Precy piezometer

Q_{max} ($l.s^{-1}km^{-2}$)	In-stream water level	Average observed heads (m)	Average simulated heads (m)	BIAS (m)	RMS E (m)	ρ	σ_{obs} (m)	σ_{sim} (m)
0	Variable	26.9	26.6	-0.30	0.36	0.95	0.56	0.46
0	Constant	26.9	26.6	-0.30	0.52	0.83	0.56	0.20
50	Variable	26.9	26.8	-0.10	0.2	0.96	0.56	0.50
50	Constant	26.9	26.7	-0.20	0.43	0.85	0.56	0.22
100*	**Variable**	**26.9**	**26.9**	**0.03**	**0.16**	**0.97**	**0.56**	**0.50**
100	Constant	26.9	26.8	-0.025	0.4	0.86	0.56	0.22
150	Variable	26.9	26.9	0.081	0.18	0.97	0.56	0.48
150	Constant	26.9	26.9	0.012	0.39	0.86	0.56	0.22
250	Variable	26.9	27	0.099	0.18	0.97	0.56	0.49
250	Constant	26.9	27	0.028	0.39	0.86	0.56	0.22
500	Variable	26.9	27	0.099	0.18	0.97	0.56	0.49
500	Constant	26.9	27	0.028	0.39	0.86	0.56	0.22

* best simulation

Fig. 5.35 confirms the quality of the simulated piezometric heads when enabling variable river stage and river recharge to the aquifer (with Q_{max} = 100 $l.s^{-1}$). In this case, the river starts recharging underlying aquifer cells when river stage rises above the aquifer head which leads to a significant increase in simulated piezometric heads at local scale.

Furthermore, the exchanged flux between the stream and aquifer units for both C100 and V100 simulations are compared in the aquifer cell adjacent to Precy and underlying the river cell (Fig. 5.37). In the C100 simulation, exfiltration rates from aquifer units to the river were quasi-constant at about 0.2 $m^3.s^{-1}$ while infiltration from the river to aquifer units did not occur even during high flow periods, i.e. river is always gaining. This is due to the fact of imposing a constant in-stream water level in river grid-cells.

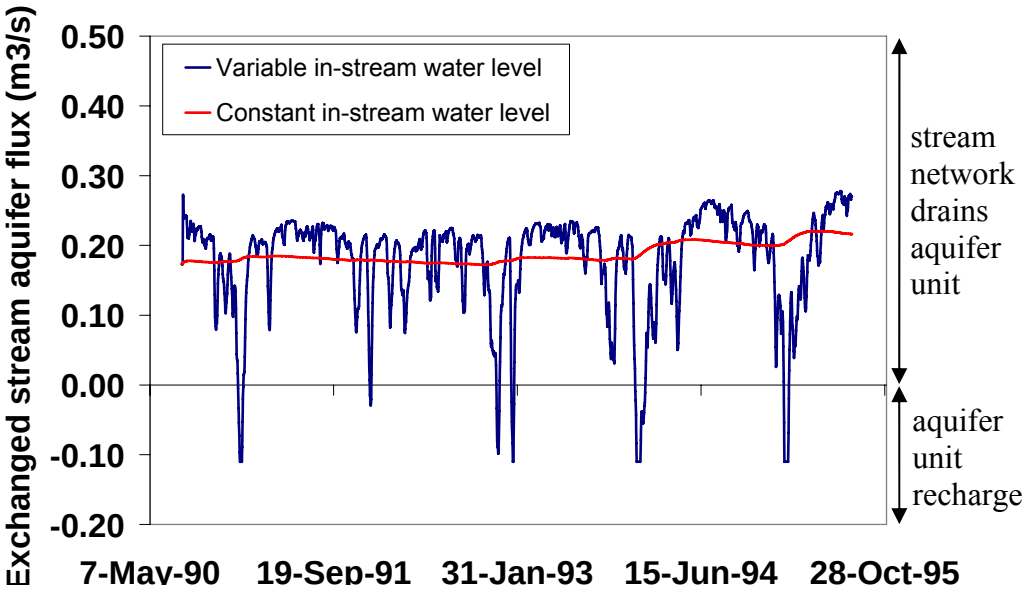

Fig. 5.37 Comparison of exchanged stream-aquifer flux for constant and variable in-stream water levels (C100 vs. V100) (Negative when stream recharges the aquifer, and positive when water flows from the aquifer towards the stream)

In the V100 simulation, the increase of in-stream water levels resulted in reversal of the stream-aquifer unit interaction from gaining to losing conditions (Fig. 5.37). These reversals have an impact on stream-aquifer processes. The impact of in-stream water level fluctuations on the dynamics and magnitude of exchanged flux is important when compared to constant in-stream water levels.

Impact of river conductance (K_{riv})

A sensitivity analysis is conducted to evaluate the effect of river hydraulic conductance (Eq. 3.17) on the simulation of stream-aquifer interactions and piezometric heads in aquifer units beneath the river cells.

This sensitivity analysis is carried out by varying K_{riv} between 0.05 and 1 $m^2.s^{-1}$, while Q_{max} equals 100 $l.s^{-1}$ (Tab. 5.8).

The impact of K_{riv} on simulated piezometeric heads and exchanged flux is locally compared with observations in the Precy piezometer.

The results show that increasing K_{riv} by a factor of 10 from its original calibrated value (0.1 $m^2.s^{-1}$) increases the average exfiltration rate from 0.18 to 0.27 $m^3.s^{-1}$ over the simulated area (Fig. 5.38). This exfiltration rate increase lowers the average simulated piezomteric heads at Precy from 26.9 m (K_{riv} = 0.1 $m^2.s^{-1}$) to 25.5 m (K_{riv} = 1 $m^2.s^{-1}$) (Fig. 5.39 and Tab. 5.8). Results also show that K_{riv} does not have a significant impact on the infiltration process because the later is controlled by Q_{max}.

In terms of K_{riv} impact on the dynamics of simulated piezomteric heads, results show that higher values of K_{riv} produce an increase in the rising and falling limbs of simulated piezomteric heads, because higher K_{riv} values mean higher hydraulic conductivity of stream-bed which increases the impact of in-stream water level fluctuations on the aquifer system (Fig. 5.39). Important is to notice that for high K_{riv} values, the slope of the rising limbs is not in agreement with the observed one. This might be due to the fact that the limbs are not due to water level fluctuation but more to the saturation of the chalk aquifer that might have a double porosity.

This sensitivity analysis shows to what extent it is important to accurately select the K_{riv} values, it also shows the interest of the developed upscaling methodology that permitted to investigate the effect of this physical factor on the system, which was not possible in the initial version of EauDysée.

Tab. 5.8 Local impact of river conductance on simulated aquifer piezometric heads compared with measurements at Precy piezometer.

K_{riv} ($m^2.s^{-1}$)	**Average simulated Piezomteric heads (m)**	**BIAS (m)**	**RMSE (m)**	ρ	σ_{obs} **(m)**	σ_{sim} **(m)**
0.05	27.7	0.85	0.88	0.92	0.56	0.53
0.1	**26.9***	**0.03**	**0.16**	**0.97**	**0.56**	**0.50**
0.15	26.5	-0.39	0.42	0.96	0.56	0.49
0.25	26.1	-0.77	0.80	0.94	0.56	0.50
0.5	25.7	-1.12	1.15	0.91	0.56	0.50
1	25.5	-1.33	1.36	0.89	0.56	0.51

* equals the observed average piezomteric head

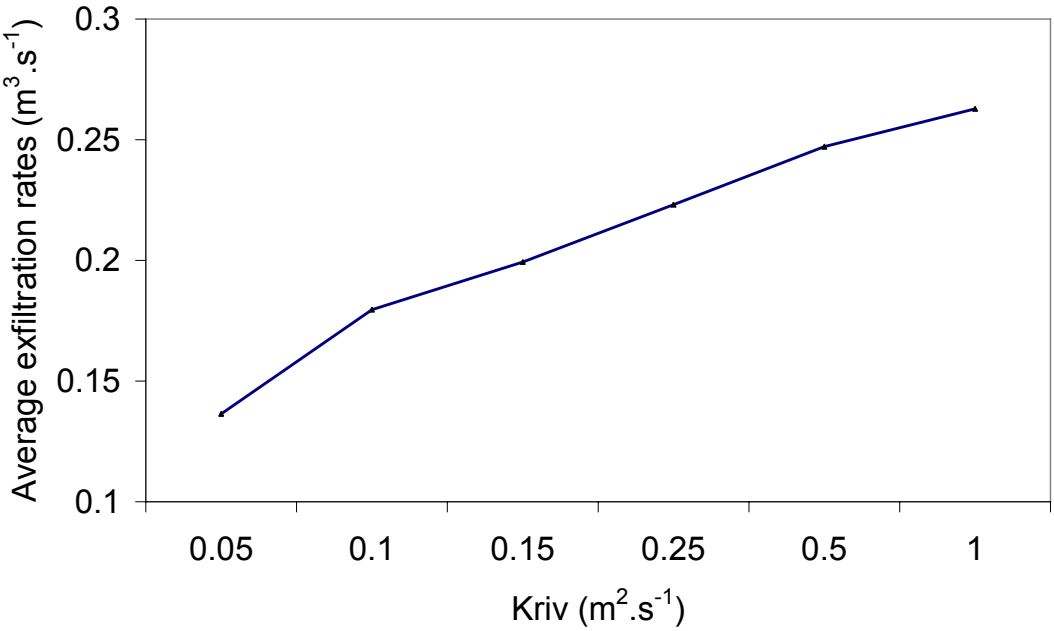

Fig. 5.38 Impact of K_{riv} on average exfiltration rates in the river cell adjacent to Precy piezometer

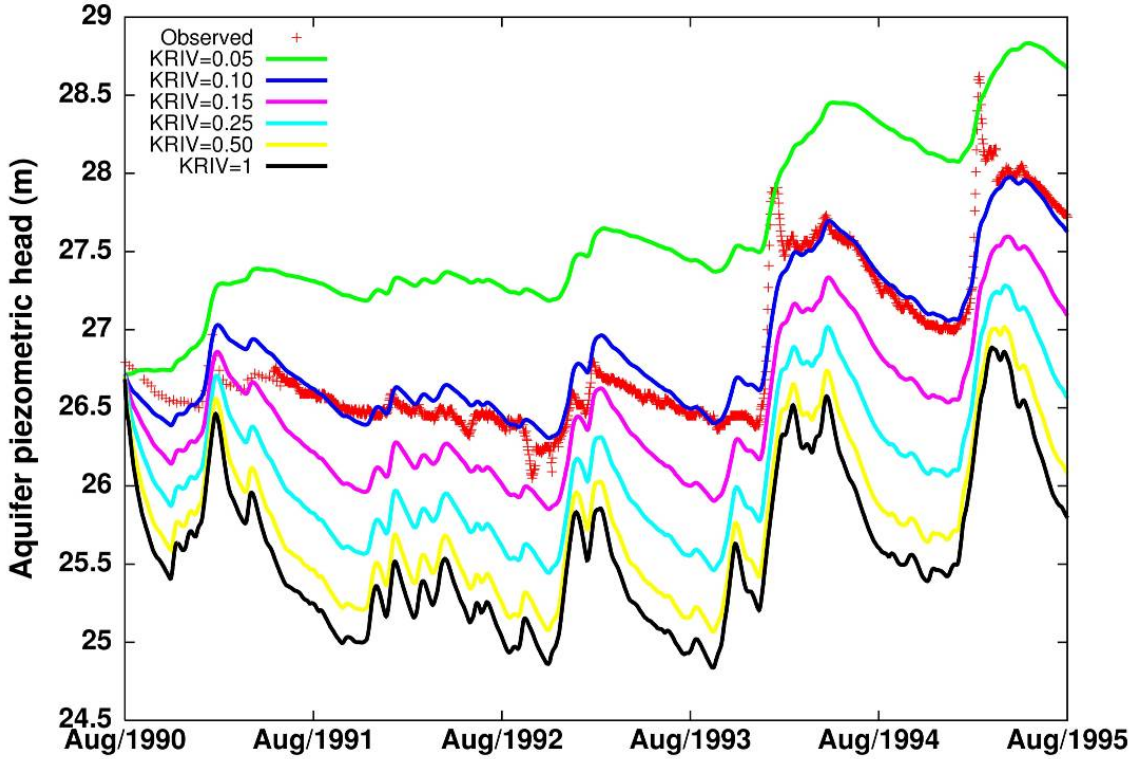

Fig. 5.39 Simulated ground-water levels in the Chalk aquifer cell containing the Precy piezometer using variable in-stream water levels for K_{riv} values varying between 0.05 and 1 $m^2.s^{-1}$ (Tab. 5.8)

5.7.1.2 Regional scale analysis

Effect of high frequency in-stream water stage fluctuations. In this section, the spatial impact of stream water level fluctuations on piezometric head distribution in adjacent aquifer units is characterized at each aquifer cell by calculating the temporal mean absolute differences (MAD) between the piezometric heads (Eq. 5.3) with and without taking into account high frequency in-stream water level fluctuations and given a Q_{max} of 100 $l.s^{-1}$ (i.e. comparing V100 & C100).

$$MAD = \frac{1}{N}\sum_{i=1}^{N}\left|H_{fix}(t_i) - H_{\text{var}}(t_i)\right| \qquad \text{Eq. 5.3}$$

Where, $H_{fix}(t_i)$ is the simulated piezometric head at a given time (Δt) using a constant in-stream water level , $H_{\text{var}}(t_i)$ is the simulated piezometric head using variable in-stream water levels and N is the number of time steps.

The spatial distribution of *MAD* varies from a few centimeters to more than 1.9 m in aquifer grid-cells close to the main stream (Fig. 5.40). As locally shown (Fig. 5.36), the influence of fluctuating water levels on piezometric head decreases with distance to the stream. The area influenced by river stage fluctuations extends over 3 km around the river for the Eocene aquifer unit and over 20 km for the Chalk aquifer unit (Fig. 5.40). The influence of river stage fluctuations is broader in the Chalk aquifer unit because it is confined by the overlying Eocene aquifer unit. In terms of storage capacity, the one of the Chalk aquifer unit is three time lower than the ones of the Eocene aquifer unit (in average 0.035 and 0.09 respectively), what leads to a smaller wave attenuation with distance for the Chalk aquifer unit.

The standard deviation between piezometric heads of both V100 and C100 scenarios was also characterized (Fig. 5.41). The variation of simulated piezometric heads from their means range from a few centimeters to more than 1 m in aquifer grid-cells near to the main stream.

Similarly to the previous MAD criterion, the standard deviation of simulated piezometric heads decreases with distance to the main stream. The standard deviation values in the Eocene aquifer units are relatively higher than the ones in the Chalk aquifer because the Eocene units are unconfined and directly connected with river cells.

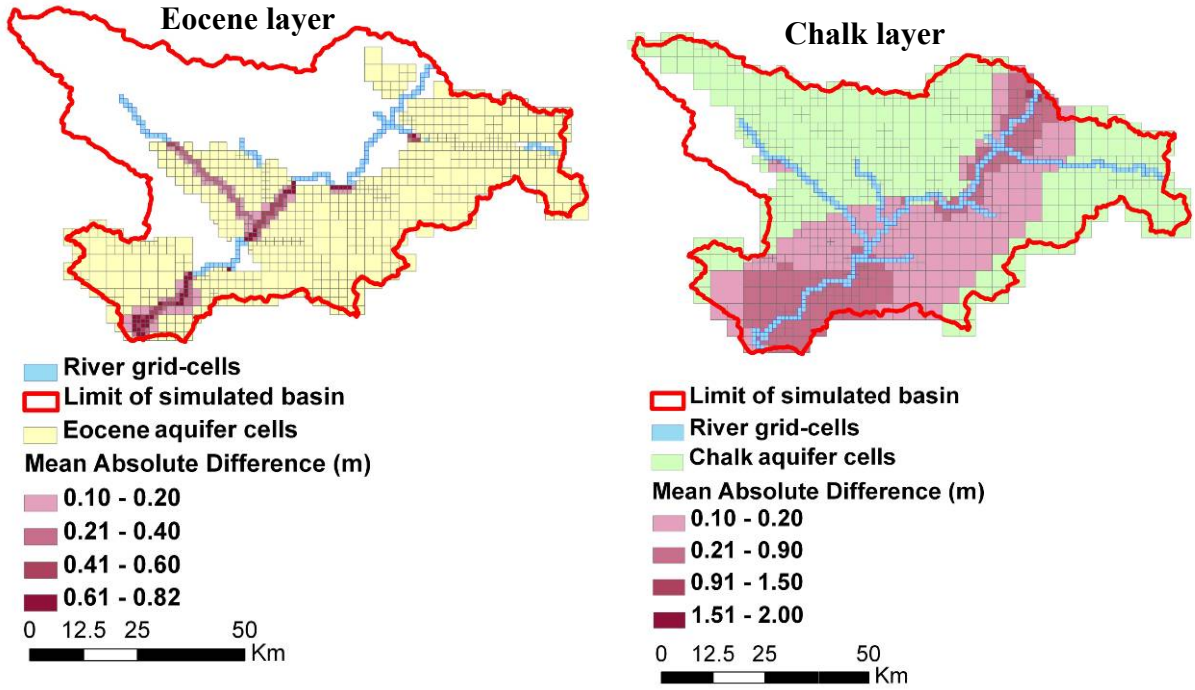

Fig. 5.40 : Mean absolute difference between piezometric heads of two simulations based on constant and variable in-stream water levels (1/Aug/1990 – 31/Jul/1995)

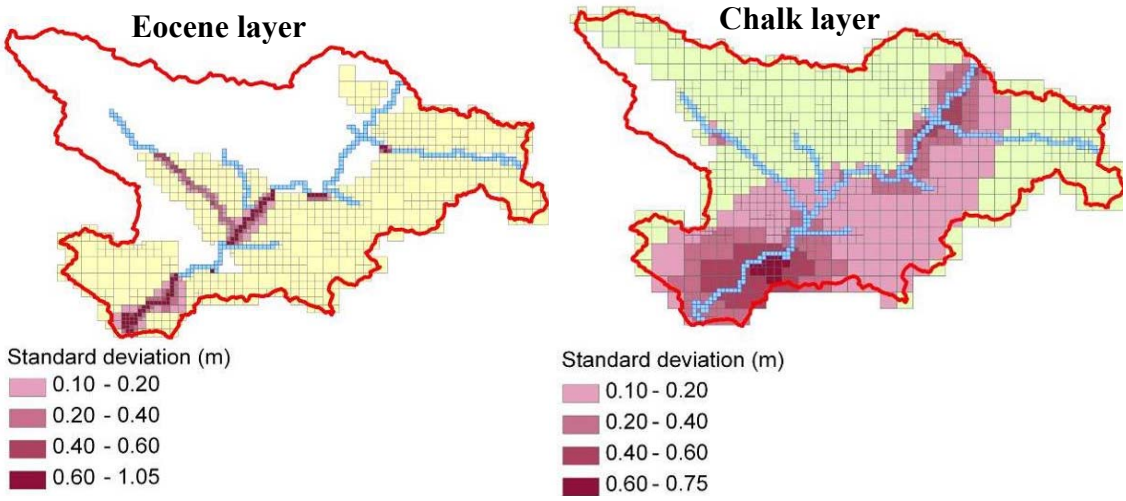

Fig. 5.41 Standard deviation between piezometric heads of two simulations based on constant and variable in-stream water levels (1/Aug/1990 – 31/Jul/1995)

Sensitivity to Q_{max}. To assess the impact of river infiltration to aquifer units at the regional scale, simulated piezometric heads distant from the main streams for scenarios V0 and V100 are compared with the observed ones when available (Fig. 5.16 & Fig. 5.42). The comparison demonstrates that river infiltration has a negligible impact on piezometric head distribution at the regional scale.

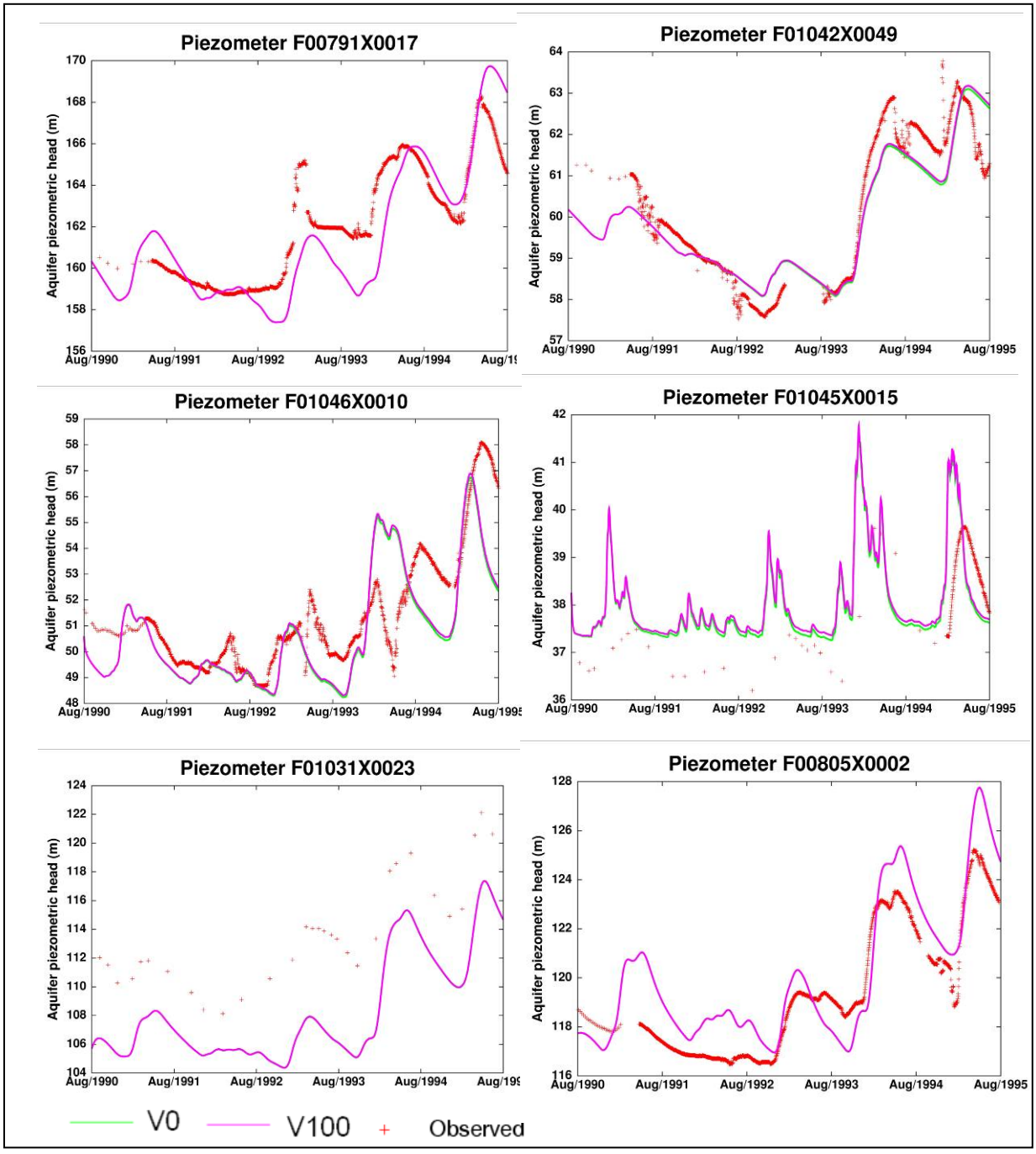

Fig. 5.42 Comparison of aquifer piezometric heads simulated by EauDyssée with variable river stage (using two values of Q_{max}) to observations in 6 piezometers (located in Fig. 5.16)

5.8 Quantification of stream-aquifer exchange

A wide variety of methods exist to quantify stream-aquifer exchange, including mass balance approaches, heat tracing, direct measurements and numerical methods (Kalbus et al., 2006; Lange, 2005).

Mass balance approaches, include a variety of procedures that range from differential stream gauging and hydrograph separation methods to solute and environmental tracers (Kalbus et al., 2006).

Heat tracing techniques assume that the temperature of ground water is more stable than that of surface water. Gaining reaches are thus characterized by relatively constant sediment temperatures, where as losing reaches tend to present significant variability over short periods of time (Constantz et al., 2001).

A recent geophysical method for quantifying stream-aquifer exchanged fluxes at the local scale includes Fiber-optic distributed temperature sensing (FO-DTS) (Day-Lewis and Lane, 2006; Selker et al., 2006; Vogt et al., 2010).

Direct measurements can be carried out by using seepage meters (Landon et al., 2001) that are simple and relatively inexpensive, but a significant number of measurements are required to adequately characterize a given stream. Other approaches use observed hydraulic head fluctuations within piezometers close by the stream to assess increase or decrease of the aquifer water storage, from which the infiltration/exfiltration rate of water is derived (Blasch et al., 2004; Sanford, 2002). These methods are widely used in flood-water infiltration studies. However, they require the availability of consistent data along the river which is not always the case at the regional scale.

For the Oise River, exchanged fluxes between streams and aquifer units are assessed based on simulations for four different scenarios (Tab. 5.6) during the period of simulation (1/Aug/1990 – 31/Jul/1995) (Eq. 5.4):

Net exchanged flux = Aquifer exfiltration – River infiltration Eq. 5.4

Therefore, a positive net exchanged flux means that the overall exfiltrated volume of water by the aquifer units is higher than river infiltration, and vice versa.

The net exchange is positive for all simulations, which means that overall, the aquifer system sustains the river network.

To assess the impact of Q_{max} on the exchanges between streams and aquifer units, scenarios V0 & V100 are compared (Fig. 5.43). The comparison shows that the infiltration flux from the rivers to the aquifer units has almost no impact on the net stream-aquifer exchanges. The main impact is a dynamical one due to the volume of the infiltrated flux from river to aquifer unit during in-stream high flow periods which eventually involves a longer transfer time in aquifer units near to the river network that corresponds to an increase of the stored water in the aquifer system.

To globally assess the impact of in-stream water level fluctuations on exchanged stream-aquifer flux, scenarios V100 & C100 are compared. The comparison (Fig. 5.43) shows that fluctuations of in-stream water level slightly modifies the net stream-aquifer exchanges (from 37.8 $mm.yr^{-1}$ to 37.7 $mm.yr^{-1}$). The exchanged flux from aquifer units to streams slightly increases, while the exchanged one from stream to aquifer units also increases leading to a net exchange of 37.7 $mm.yr^{-1}$, which remains almost unchanged for the two scenarios. But the intensity of exchanges is 2 times higher for V100 than C100 showing the importance of taking into account water levels fluctuations for simulating high frequency aquifer system response.

Finally, the mean monthly stream-aquifer exchange dynamics is analyzed based on scenario V100 (Fig. 5.44). The minimum of net exchanges occurs in October (2.6 mm.month^{-1}) which corresponds to low water piezometric level and to the beginning of the hydrological year. From October to January infiltrated water from rivers towards aquifer units increases from 0.18 mm.month^{-1} to 0.31 mm.month^{-1}. While January corresponds to the maximum of infiltration (3.2 l.s^{-1}.km^{-1} of river stretch), it appears on Fig. 10b that the recharge of the aquifer system is not only due to infiltration from the river network but to the recharge from the impluvium so that high water piezometric level is only reached in March when the flux from aquifer units to rivers is maximum (3.8 mm.month^{-1}). During the rising of piezometric level in aquifer units, the infiltrated flux from rivers to aquifer units decreases, reaching a minimum of 0.1 mm.month^{-1} in March. During spring, the net exchanges are maximum and the exfiltration from the aquifer system prevails. During summer the river network mostly drains the aquifer system which leads to the low water piezometric level in late August. Interesting is that the later in the summer, the more the summer storms impact the water content of the aquifer system because infiltrated water from rivers to aquifer units increases from 0.1 mm. month^{-1} in May to 0.15 mm. month^{-1} in September. This is important for pollutant transfer at the basin scale because late summer is the warmest period when bacterial activity is maximal. Hence, doubling the exchange flux can have an impact on nitrate elimination for instance.

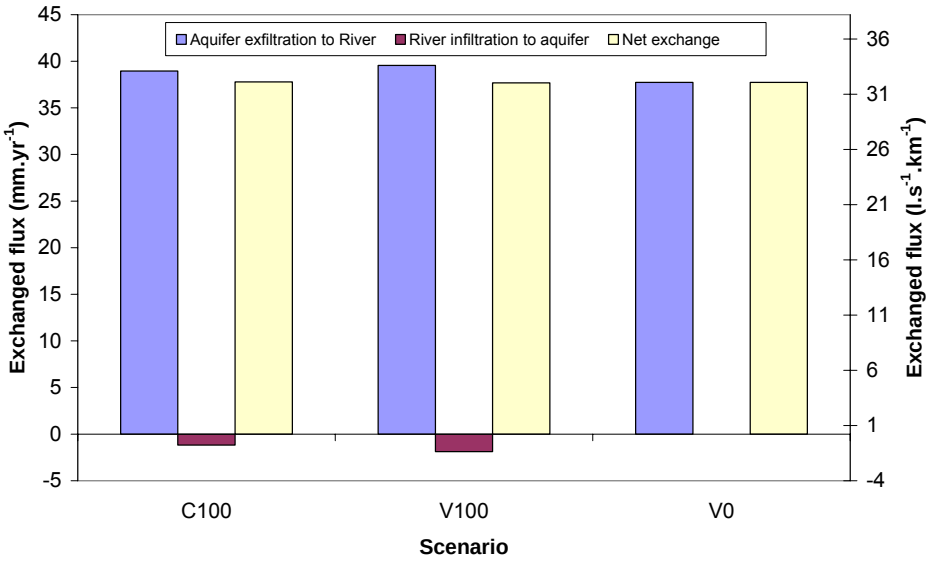

Fig. 5.43: Comparison of the net river-aquifer flux and its components between the four simulations of Tab. 5.6. The fluxes are expressed in cumulated volume over the 4-year simulation period ($mm.yr^{-1}$) and the mean linear stream-aquifer exchanged flux for each 1 km of stream network ($l.s^{-1}.km^{-1}$).

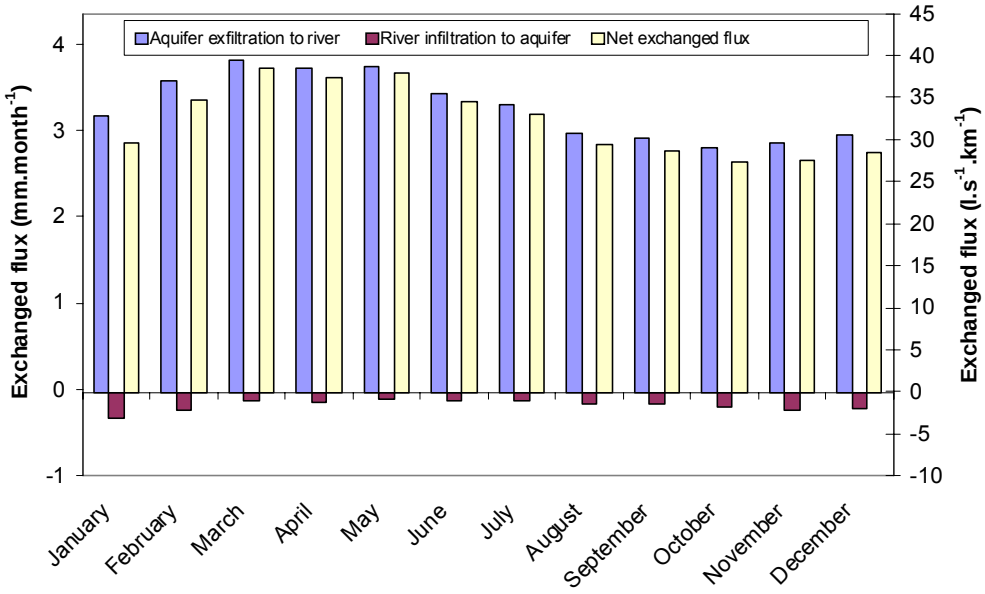

Fig. 5.44 Average monthly linear exchanged flux ($mm.month^{-1}$) and the mean linear stream-aquifer exchanged flux ($l.s^{-1}.km^{-1}$) for each 1 km for scenario V100

5.9 Conclusions

In this chapter, a 1D physically-based hydraulic model was used as a spatial and temporal interpolator of river stages and river discharges along a whole river network. The resulting rating curves, which provide a continuous description of reality given the available information, are upscaled to the coarser resolution of a regional scale hydrogeological model,

where they are used to deduce river stage from the simulated discharge at each time step and in each river grid-cell.

The approach was tested for a 188-km river network in the Oise River basin. The simulated regional river stages were almost as realistic as the ones from the local 1D hydraulic model, which eventually allowed for a better stream-aquifer simulation.

The simulated fluctuating river stages (high river frequency behavior) leads to inversing the direction of stream-aquifer flow, hence initiating an infiltration process that leads to a significant increase in simulated piezometric heads located in underlying aquifer units.

Within the period of simulation, the infiltrated flux from the rivers to the aquifer units caused by high river frequency signals had slight impact on the net annual stream-aquifer exchanges (from 37.8 $mm.yr^{-1}$ to 37.7 $mm.yr^{-1}$). The main impact was a dynamical one due to the volume of the infiltrated flux from river to aquifer unit during high in-stream flow periods, which eventually involves a longer transfer time in aquifer units near to the river network that corresponds to an increase of the stored water in the aquifer system. In this context, although the impact of high river frequency signals on the net exchanged flux was small, it permitted to quantify the water content in the stream-aquifer interface which is the principal zone where pollutants are eliminated.

The stream-aquifer exchange was also quantified on monthly basis. The lowest mean monthly stream-aquifer exchanged flux occurred in October (2.6 $mm.month^{-1}$), which corresponds to low water piezometric levels and to the beginning of the hydrological year. From October to January, the infiltrated water from rivers towards aquifer units increases from 0.18 $mm.month^{-1}$ to 0.31 $mm.month^{-1}$.

During the spring, the mean monthly net exchanges are maximum and the exfiltration from the aquifer system prevails.

During the summer the river network mostly drains the aquifer system which leads to low water piezometric levels in late August. Interesting is that the later in the summer, the more the summer storms impact the water content of the aquifer system because infiltrated water from rivers to aquifer units increases from 0.1 $mm.month^{-1}$ in May to 0.15 $mm.month^{-1}$ in September. This is particularly important for pollutant transfer at the basin scale because late summer is the warmest period when bacterial activity is maximal. Hence, doubling the exchange flux can have an impact on nitrate elimination for instance.

In terms of spatial impact, the area influenced by high frequency river signals extends across 3 to 20 km around the streams, depending on the hydrogeological setting (confined/unconfined) of the aquifer unit. The fluctuations of simulated piezometric heads from their means range from a few centimeters to more than 1 m in aquifer grid-cells near to the main stream. The impact of these high frequency river signals on simulated piezometric heads decreases with distance to the stream.

This study confirms that surface and groundwater models should not be treated separately because they are connected components of the hydrosystem, especially in large sedimentary basins as the one of the Oise River. The upscaling method offers an efficient way to improve the physics of the stream-aquifer interactions at the regional scale, with a limited computational burden owing to the pre-computation of the rating curves.

CHAPTER 6. CONCLUSIONS AND FUTURE WORK

The present work contributes to the development of the integrated hydrosystem model EauDyssée applied to the Seine River basin. The main objective was to provide a realistic simulation of river stage and discharge at the regional scale, in order to improve the simulation of stream-aquifer interactions and better assess piezometric heads.

Two operating regimes for hydraulic heads are considered. The first one is a low frequency behavior of hydraulic heads at large scale. At this scale, the basin filters the rainfall signal for which the temporal variability is highly reduced by the signal filtering effect of the flow through the soil, the unsaturated zone and the aquifer unit. The second regime is a temporal frequency behavior of hydraulic heads due to fast in-stream water levels fluctuation. This regime impacts the stream-aquifer interactions and the aquifer system at local scale near the river with a high frequency response.

The initial version of EauDyssée was a low frequency behavior, while this study is focused on high frequency behavior that was taken into consideration through developing an upscaling framework under unsteady-state conditions. The outputs from this framework were compared to the initial version in order to quantify the improvements carried out by considering this physical process in the model.

This work started with an overview of available surface routing and integrated hydrosystem models with a special focus on stream-aquifer interactions modeling techniques. The review of the surface routing techniques shows that the final choice of a surface routing model is a trade off between a number of factors such as the temporal and spatial scale, the required accuracy, the type and availability of data, the available computational facilities and the extent of required information on water levels. This shows that there is no universal superior

routing model and choosing the appropriate routing approach depends to a great extent on the hydrological problem in question.

On the other hand, the review of stream-aquifer modeling techniques shows the importance of regional hydro(geo)logical models that are capable of simulating coupled stream-aquifer interactions and conducting interdisciplinary investigations in hydrological sciences. However, the majority of these regional models has limited capacity to simulate small-scale processes (e.g., near-stream groundwater pumping, bank storage effects, in-stream water level fluctuations, hyporheic exchange) because modeling these processes require a very fine discretization of the considered domain which is not always applicable in regional scale hydrological models. This particular limitation addresses the necessity of identifying a methodology to improve the modeling of local scale stream-aquifer interactions within regional hydrogeological models. The review also shows that in-stream water levels are of primary importance for the simulation of stream-aquifer interactions, the estimation of low flow discharge and the water quality.

Upon reviewing the integrated models of the hydrosystems, the regional hydrological model EauDyssée was selected to simulate the hydrosystem with a special focus on the surface routing and stream-aquifer interaction component. The later is simulated with imposed constant in-stream water levels because river morphological data are not always accessible in regional scale applications. To quantify the impact of morphological data on in-stream water levels and discharge simulations, an investigation using different simplified geometry scenarios was carried out in the Serein River (tributary of the Yonne River), between the gauging stations of Dissangis and Beaumont, in a well surveyed reach (20 cross sections over 89 kms).

River discharge and stage are simulated by the hydraulic model HEC-RAS (1D Saint-Venant equations) solved using the four point implicit finite difference scheme while lateral inflows are simulated by the regional hydrological model EauDyssée.

The results of the different geometry scenarios show that certain cross sectional representation (e.g. trapezoidal shape) produces water levels that are consistent with measured data in certain locations of the river reach. However, the maximum water depths are longitudinally offset, primarily because of the approximated geometry and because the simplified bed levels are different from the actual bed levels. During low flow, the results show that irregularities in the river bed bottom have an important impact on simulated river stages, as simplifying the irregular river bed bottom to plain have, on average, attenuated the low flow water levels by 20 cm compared to ones in the reference simulation. This is because the lower the water level is, the more important is the friction and thus the description of the cross section geometry. This finding is important, especially in the simulations of stream-aquifer interactions where the river is sustained by aquifer units during low flow periods.

In terms of river bed level, the results show that using interpolated bed levels instead of surveyed ones for a trapezoidal cross-section have reduced the Nash efficiency of simulated water levels at Chablis hydrometric station from 0.83 to 0.61, while the RMSE was increased from 0.19 m to 0.3 m. The maximum water depths obtained from interpolated bed levels vary between 2.75 m and 3 m with an average of 2.9 m, while in the simulation based on surveyed bed levels, the maximum water depths vary between 2.4 and 3.75 m with an average of 3.3 m for the same type of section. In five river cross sections, the difference between simulated maximum water depths using surveyed bed levels and ones using interpolated bed levels is more than 1 m due to the linearly interpolated bed levels. This exhibits the effect of bed levels on the simulated water levels, especially at the regional scale where DEM is usually

used to identify the river geometry hence it is difficult to obtain an accurate river bed level representation.

This confirms that the accuracy of predicted water levels and maximum water depths simulated by a Saint-Venant model rely on an accurate representation of channel geometry and bed level slopes along the river reach.

That being said, a 1D Saint-Venant model is not suitable for simulating flow in areas where river morphology is not accessible. In spite of these limitations, this type of hydrodynamic modeling remains crucial to accurately simulate in-stream water levels. To compromise between the spatial scale issue, morphological data limitation and the importance to accurately simulate in-stream water levels, an original upscaling strategy is developed, with which a 1D Saint-Venant hydraulic model is used as a spatial and temporal interpolator of river stages and river discharges along a whole river network. The resulting rating curves are upscaled to the coarser resolution of a regional scale hydrogeological model, where they are used to deduce river stage from the simulated discharge routed with a simple Muskingum model at each time step and in each river grid-cell.

The approach was validated in a 188-km river network in the Oise River basin. The simulated regional river stages were almost as realistic as the ones from the local 1D hydraulic model.

The simulated fluctuating river stages (high frequency behavior) leads to inversing the direction of stream-aquifer flow, hence initiating an infiltration process that leads to a significant increase in simulated piezometric heads located in underlying aquifer units.

Within the period of simulation, the infiltrated flux from the rivers to the aquifer units caused by high river frequency signals had slight impact on the net annual stream-aquifer exchanges (from 37.8 $mm.yr^{-1}$ to 37.7 $mm.yr^{-1}$). The main impact was a dynamical one due to the volume of the infiltrated flux from river to aquifer unit during high in-stream flow periods,

which eventually involves a longer transfer time in aquifer units near to the river network that corresponds to an increase of the stored water in the aquifer system. In this context, although the impact of high river frequency signals on the net exchanged flux was small, it permitted to quantify the water content in the stream-aquifer interface which is the principal zone where pollutants are eliminated.

The stream-aquifer exchange was also quantified on monthly basis. The lowest mean monthly stream-aquifer exchanged flux occurred in October (2.6 $mm.month^{-1}$), which corresponds to low water piezometric levels and to the beginning of the hydrological year. From October to January, the amount of infiltrated water from rivers towards aquifer units increases from 0.18 $mm.month^{-1}$ to 0.31 $mm.month^{-1}$. During spring, the mean monthly net exchanges are maximum and the exfiltration from the aquifer system prevails. In summer the river network mostly drains the aquifer system which leads to low water piezometric levels in late August. Interesting is that the later in the summer, the more the summer storms impact the water content of the aquifer system because infiltrated water from rivers to aquifer units increases from 0.1 $mm.month^{-1}$ in May to 0.15 $mm.month^{-1}$ in September. This is particularly important for pollutant transfer at the basin scale because late summer is the warmest period when bacterial activity can be maximal. Hence, doubling the exchange flux can have an impact on nitrate elimination for instance.

In terms of spatial impact, the area influenced by high frequency river signals extends across 3 to 20 km around the streams, depending on the hydrogeological setting (confined/unconfined) of the aquifer unit. The fluctuations of simulated piezometric heads from their means range from a few centimeters to more than 1 m in aquifer grid-cells near the main stream. The impact of these high frequency river signals on simulated piezometric heads decreases with distance to the stream.

This study confirms that surface and groundwater models should not be treated separately because they are connected components of the hydrosystem, especially in large sedimentary basins as the one of the Oise River. The upscaling method offers an efficient way to improve the physics of the stream-aquifer interactions and better assess soil water content at the regional scale, with a limited computational burden owing to the pre-computation of the rating curves. Thus, it offers interesting perspectives to better address the impacts of environmental changes on hydrosystems, such as climate change (Ducharne et al., 2007; Ducharne et al., 2010), irrigation, or nitrate contamination from agricultural practices (Flipo et al., 2007a; Gomez et al., 2003; Ledoux et al., 2007) and wetlands which are often located at the contact zone between groundwater and in-stream waters (Curie et al., 2009; Devito et al., 1996; Kehew et al., 1998).

The functional curves approach could also be generalized to account for variable river velocity in regional scale hydrological models (Lucas-Picher et al., 2003). The advantage of the proposed method would be to benefit from the complete physics offered by the hydraulic model (Saint-Venant equations) and from high resolution morphological data, but with a significant spare of computational time in the regional model, owing to the pre-computation of the functional curves. The approach could even be further generalized to account for floods and inundations assessment in regional hydrological models (Knebl et al., 2005a), by defining functional curves derived from 2D hydraulic modeling.

The proposed approach also offers an interesting way to benefit from river stage remote-sensing measurements (Alsdorf et al., 2007; Biancamaria et al., 2010; Neal et al., 2009) to constrain hydrological modeling, with increasing coverage, precision, and temporal resolution.

This methodology also offers interesting perspectives for coastal aquifers applications, where tidal fluctuation is an important driving force for groundwater flow, and dynamic interactions

between groundwater and seawater are important (Guo et al., 2010; Sun et al., 2008). In this context, Aquifer reaction to tidal fluctuations has been employed to calculate aquifer parameters (Erskine, 1991; Jha et al., 2003).

Other coastal applications include the impact of coastal land reclamation on ground water level and the sea water interface (Guo and Jiao, 2007).

The in-stream water level variations can also be used to study hydraulic properties of fluvial aquifers at large scale (Bolster et al., 2001; Carrera and Neuman, 1986a; Loeltz and Leake, 1983; Pinder and Jones, 1969; Reynolds, 1987; Sophocleous, 1991).

In other studies, time varying surface water stage is frequently used to estimate aquifer hydraulic diffusivity (Ferris, 1951; Pinder and Jones, 1969; Reynolds, 1987; Swamee and Singh, 2003).

Furthermore, this methodology allows to account for smaller scale processes, such as simulating the mixing in the hyporheic zone (Arntzen et al., 2006; Ryan et al., 2004), biogeochemical processing (Cardenas, 2009) nutrient cycling (Kim et al., 1992; Kim et al., 2000) and nutrient release from sediment pore fluids during low flow conditions, especially in estuarine environments (Linderfelt and Turner, 2001; Westbrook et al., 2005).

ANNEXE A: SEREIN RIVER MORPHOLOGICAL DATA VS. SIMULATED RATING CURVES

Left: X-axis: Distance from left bank (m), Y-axis: Ground level (m), PK: Distance from Dissangis (m)
Right: X-axis: Discharge ($m^3.s^{-1}$), Y-axis: Water level (m)

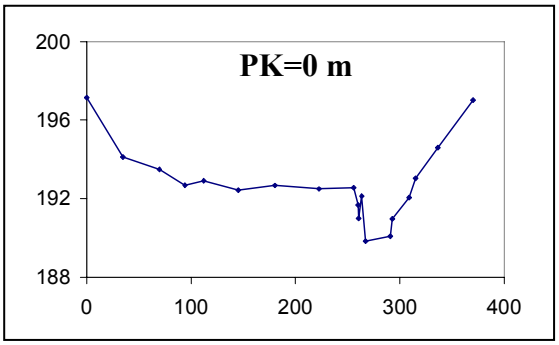

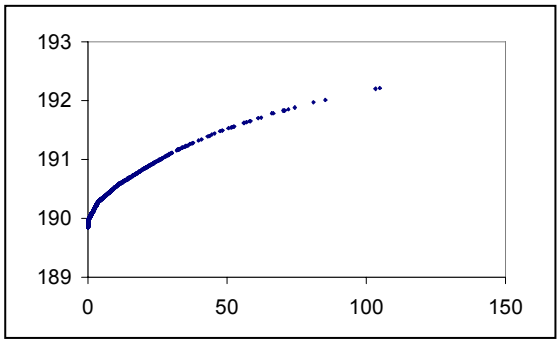

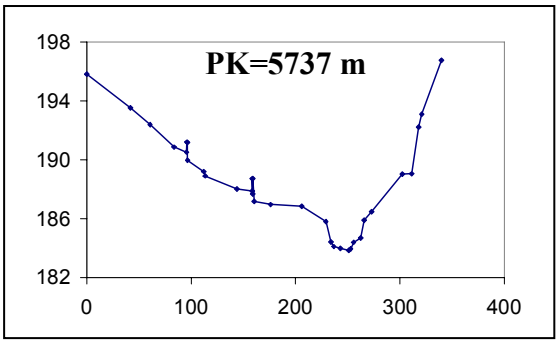

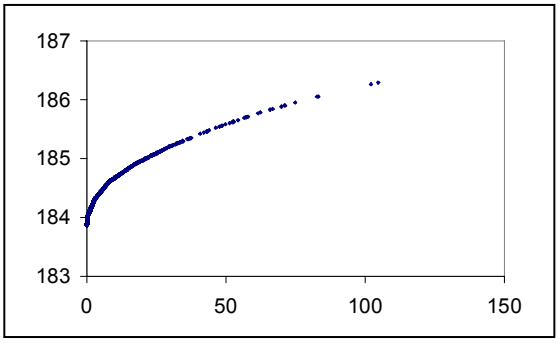

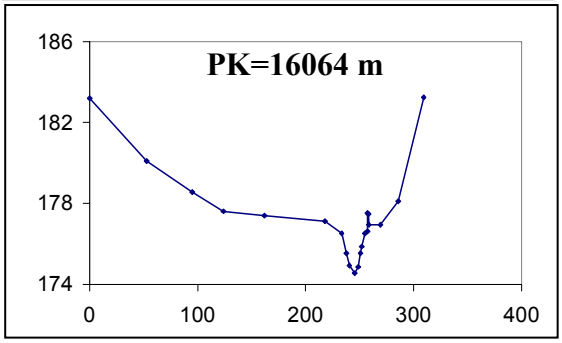

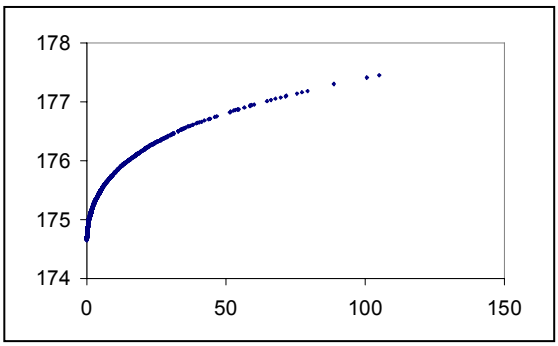

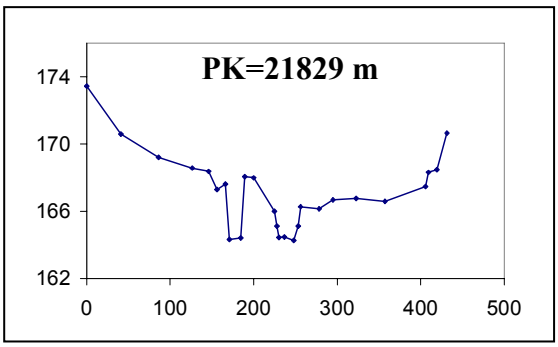

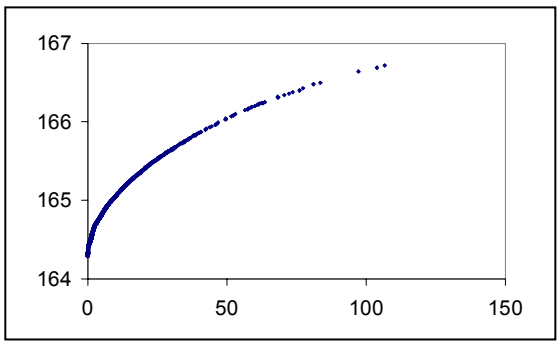

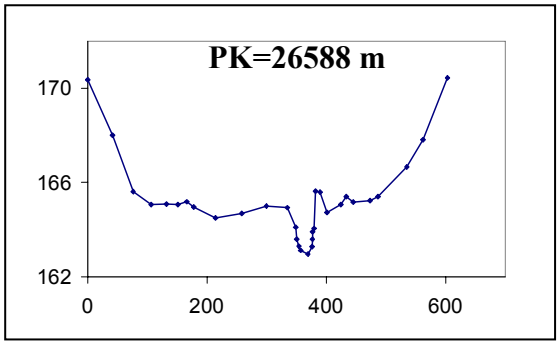
PK=26588 m
170
166
162
0
200
400
600

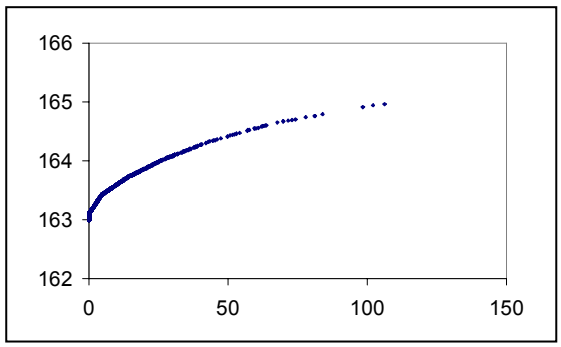
166
165
164
163
162
0
50
100
150

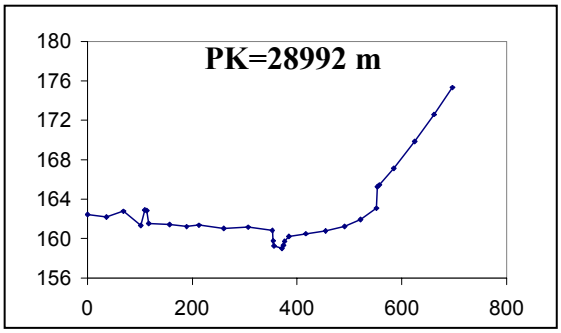
PK=28992 m
180
176
172
168
164
160
156
0
200
400
600
800

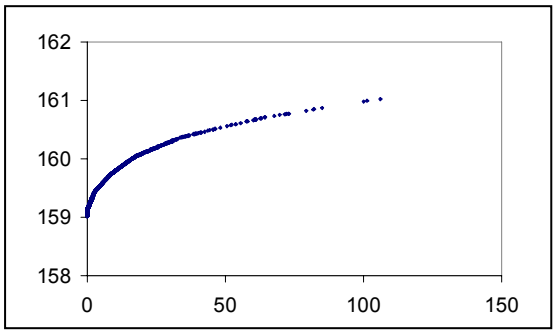
162
161
160
159
158
0
50
100
150

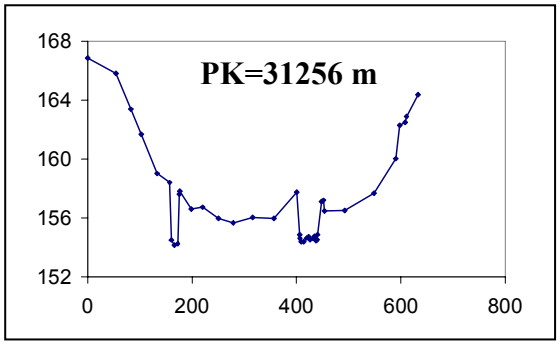
PK=31256 m
168
164
160
156
152
0
200
400
600
800

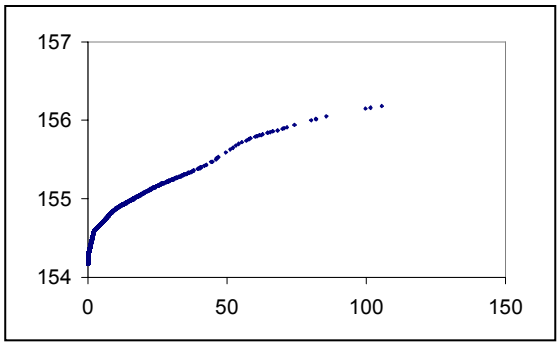
157
156
155
154
0
50
100
150

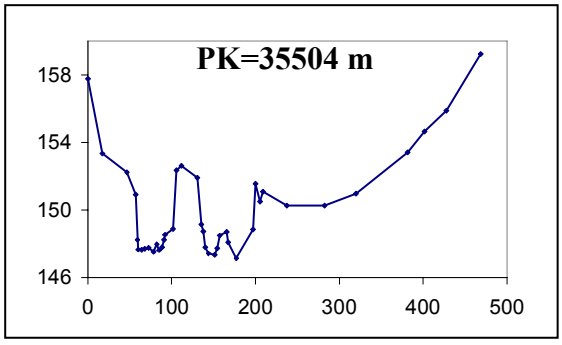
PK=35504 m
158
154
150
146
0
100
200
300
400
500

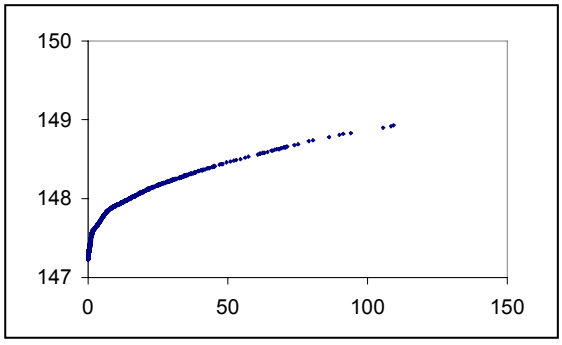
150
149
148
147
0
50
100
150

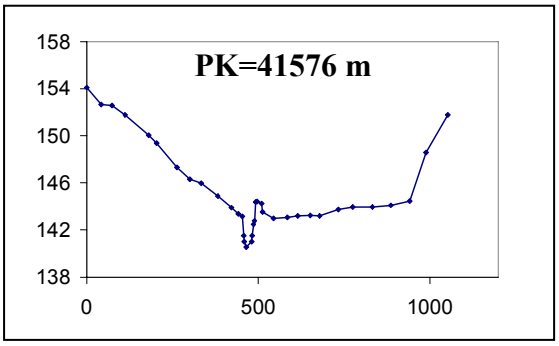
PK=41576 m
158
154
150
146
142
138
0
500
1000

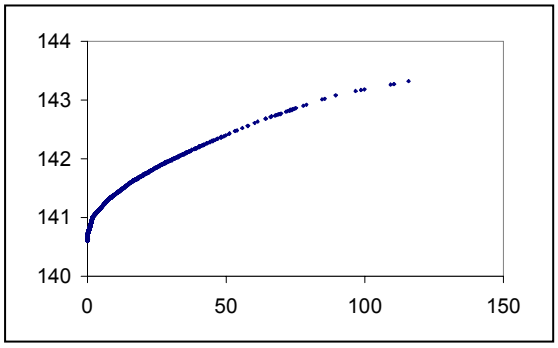
144
143
142
141
140
0
50
100
150

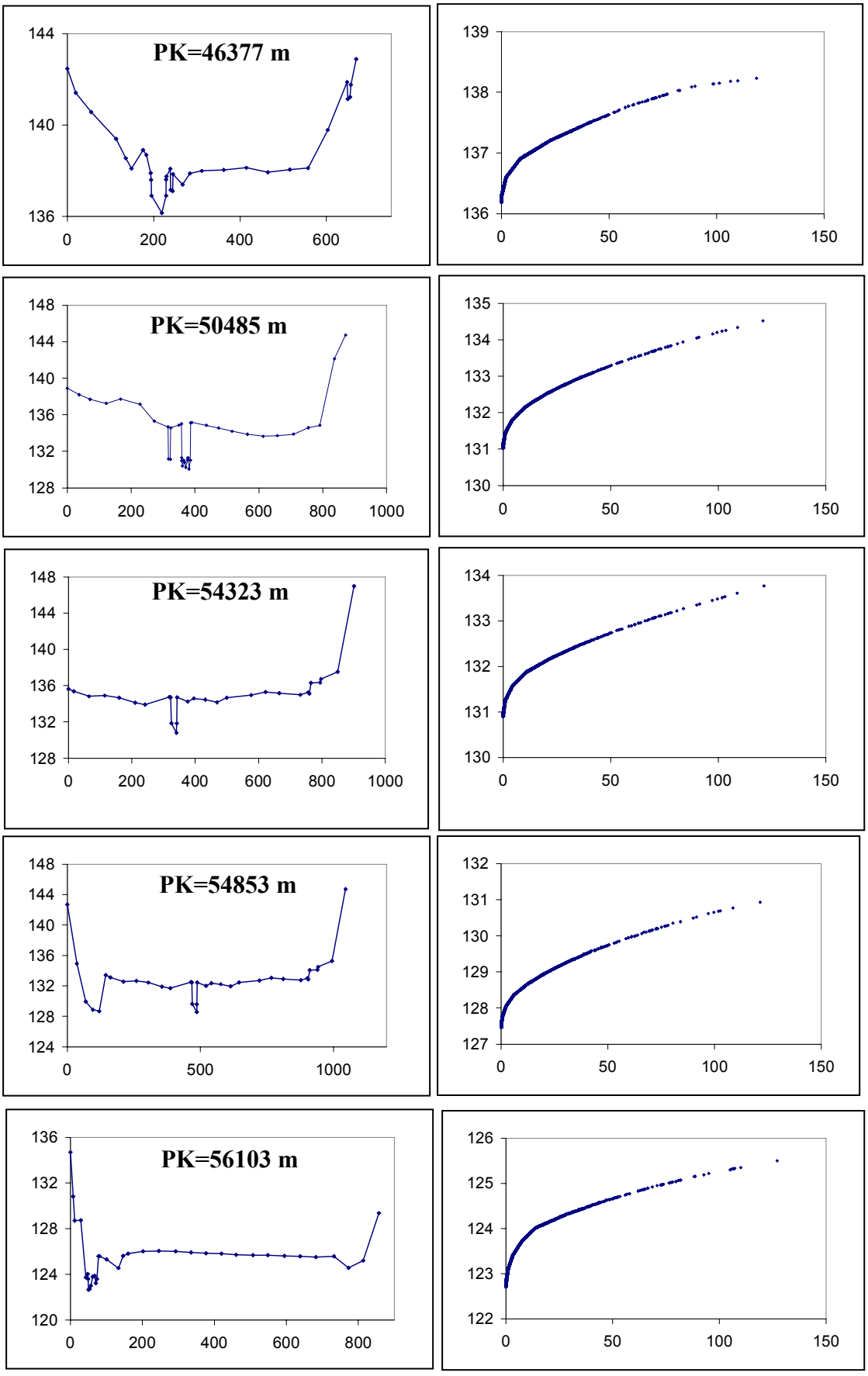
PK=46377 m
PK=50485 m
PK=54323 m
PK=54853 m
PK=56103 m

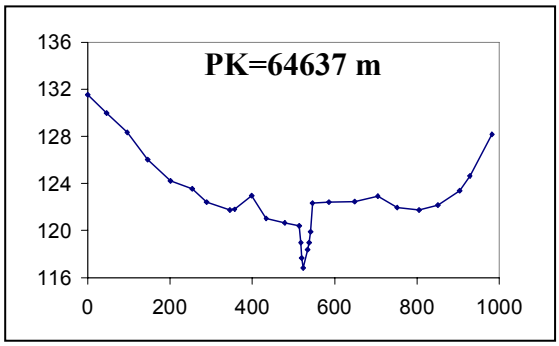
PK=64637 m
136
132
128
124
120
116
0
200
400
600
800
1000

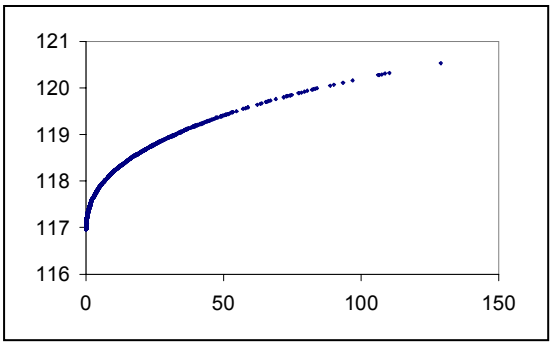
121
120
119
118
117
116
0
50
100
150

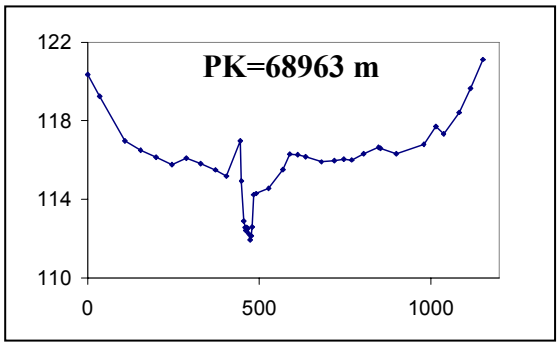
PK=68963 m
122
118
114
110
0
500
1000

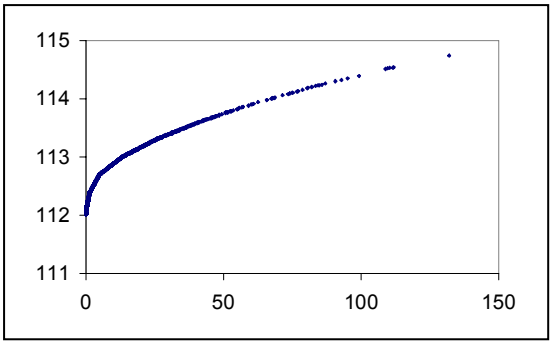
115
114
113
112
111
0
50
100
150

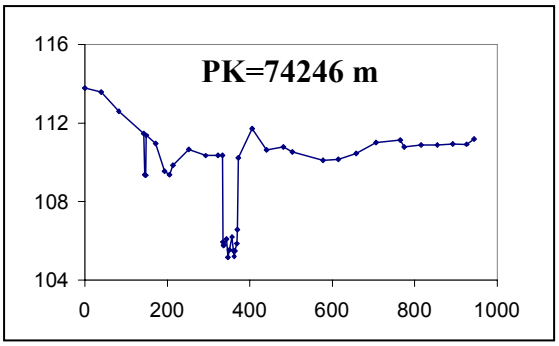
PK=74246 m
116
112
108
104
0
200
400
600
800
1000

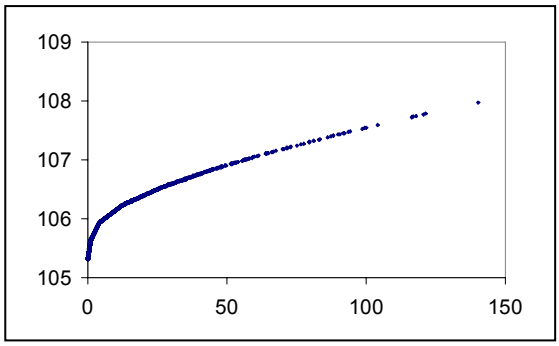
109
108
107
106
105
0
50
100
150

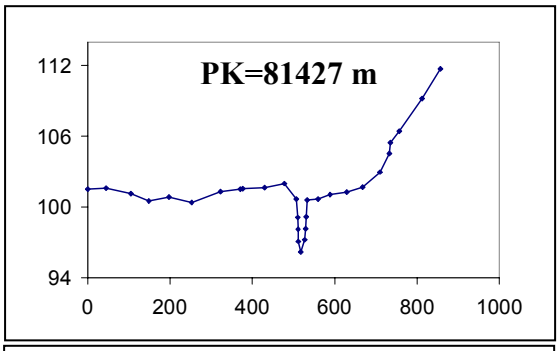
PK=81427 m
112
106
100
94
0
200
400
600
800
1000

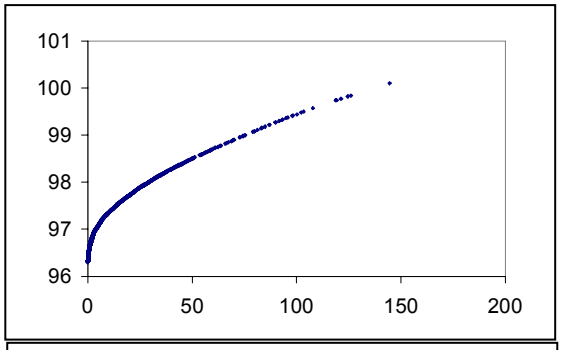
101
100
99
98
97
96
0
50
100
150
200

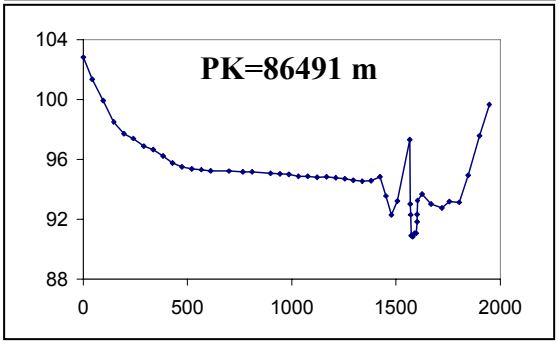
PK=86491 m
104
100
96
92
88
0
500
1000
1500
2000

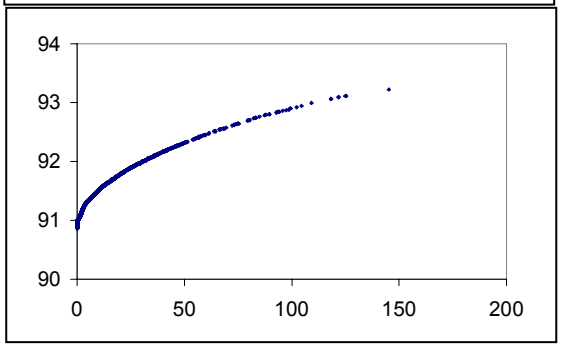
94
93
92
91
90
0
50
100
150
200

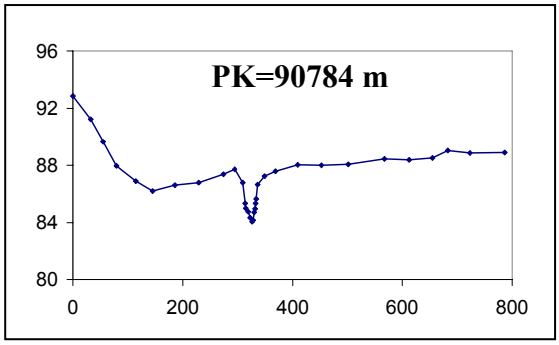
PK=90784 m
96
92
88
84
80
0
200
400
600
800

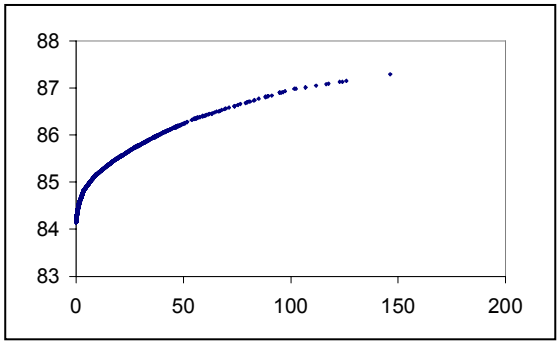
88
87
86
85
84
83
0
50
100
150
200

ANNEXE B: RESUME LONG DE LA THESE EN FRANÇAIS

Apport de la modélisation hydraulique pour une meilleure simulation des tirants d'eau et des échanges nappe-rivière à l'échelle régionale

Cette thèse s'inscrit dans le développement de la plateforme EauDyssée de modélisation intégrée des hydrosystèmes régionaux, au sein du bassin pilote de la Seine. L'objectif principal est de contribuer à une meilleure simulation des niveaux des cours d'eau à l'échelle régionale afin d'améliorer la simulation des interactions nappe-rivière et de mieux quantifier les niveaux piézométriques dans les aquifères. Il s'agit donc de construire le lien entre débits et niveaux d'eau dans une modélisation des écoulements en rivière à l'échelle régionale.

Comme détaillé dans le **Chapitre 2**, la modélisation des écoulements en rivière peut être classifiée en deux catégories : la modélisation hydrologique et la modélisation hydraulique. A l'échelle régionale, les principaux outils sont les modèles hydrologiques, qui propagent le débit dans le réseau hydrographique sur des bases simples (ex. Muskingum, Muskingum-Cunge). Ces modèles sont généralement ciblés sur le routage du débit, sans tenir compte des niveaux d'eau, du fait de l'intérêt prioritaire pour les ressources en eau à l'échelle régionale ou globale. Au contraire, les modèles hydrauliques déterministes (ex. Navier–Stokes 3D, Saint-Venant) sont couramment utilisés pour simuler les relations entre débit et niveau d'eau à l'échelle locale. L'intérêt principal est alors de caractériser les événements dynamiques ou les phénomènes d'inondation.

L'avantage fondamental des modèles de routage hydraulique par rapport aux modèles hydrologiques vient de leur résolution physique des processus, qui rend compte des liens débit/niveau d'eau, et implique une haute résolution le long du réseau de drainage, ce qui permet d'exploiter les données intermédiaires (sections transversales et/ou courbes de tarage). A ce jour, les modèles hydrauliques restent cependant peu utilisés à l'échelle régionale du

bassin versant. En effet, ils requièrent des données géométriques sur l'intégralité du réseau hydrographique modélisé, si bien que le coût d'obtention de données suffisantes peut être prohibitif ; ils peuvent aussi poser des problèmes de stabilité numérique, potentiellement plus fréquents dans un grand domaine avec de nombreuses confluences et points singuliers ; ils sont enfin plus exigeants en puissance de calcul que les modèles hydrologiques.

En conséquence de cette analyse, la démarche de cette thèse fut de combiner les capacités de deux types de modèles d'écoulement ci-dessus, ce qui amène à répondre aux questions scientifiques suivantes :

- Quelle est la capacité d'un modèle hydraulique à géométrie simplifiée pour simuler les niveaux d'eau et les débits à l'échelle régionale ?
- Comment faire le lien entre un modèle hydraulique local et un modèle hydrologique régional ?
- Quel est l'impact local et régional de la fluctuation des niveaux d'eau en rivière sur les niveaux piézométriques et les échanges nappe-rivière ?

Dans ce contexte, nous nous somme appuyés sur deux modèles représentatifs :

1- Le modèle hydrologique régional EauDyssée (**Chapitre 3**) permet de modéliser les principales composantes du cycle continental de l'eau, en particulier le rôle des écoulements de surface et souterrain sur les relations pluies-débit à l'échelle. Ce modèle s'articule autour d'une plateforme qui permet le couplage de modèles experts simulant le bilan hydrique, les écoulements de surface et souterrain, le transfert en zone non saturée, et les interactions nappe-rivière, qui sont estimées à partir d'une relation de type loi de Darcy, en fonction des gradients de charge verticaux entre la rivière et la nappe

Dans la version initiale d'EauDyssée, les échanges entre la nappe et la rivière sont simulés avec une cote d'eau fixe, obtenue à partir d'un Modèle Numérique de Terrain (MNT). Ces

cotes ne fluctuent donc pas en fonction du débit, alors que la dynamique des niveaux des cours d'eau a des impacts reconnus sur la vitesse des écoulements, la dynamique des débordements, et les interactions nappe-rivière.

2- Le modèle hydraulique HEC-RAS (Hydrologic Engineering Centers River Analysis System, USACE, 2002 ; **Chapitre 3.3**) est un logiciel de modélisation hydraulique monodimensionnelle à surface libre. Il permet de simuler les écoulements permanents et non permanents, le transport de sédiments et certaines fonctions facilitant la conception d'ouvrages hydrauliques. Il permet également d'analyser les débits et les niveaux d'eau dans le lit des rivières et de déterminer les zones inondables. Ce modèle résout l'ensemble dynamique des équations de Saint-Venant par la méthode des différences finies, à partir de données morphologiques de rivière, notamment les sections transversales et la pente de fond des cours d'eau. La rugosité du lit de la rivière est représentée par le coefficient de Manning n, sur lequel porte le calage hydrodynamique du modèle.

Dans les deux applications décrites ci-dessous, le modèle hydraulique est forcé par le débit observé à l'amont, par une courbe de tarage observée à l'aval, et par les apports latéraux simulés par le modèle hydrologique EauDyssée. Le calage est effectué manuellement, en sélectionnant les valeurs de n qui permettent la meilleure reproduction des niveaux d'eau observés. La qualité des simulations est évaluée par les critères statistiques classiques de Nash, RMSE et biais aux stations hydrométriques de contrôle.

Pour répondre à la première question scientifique de cette thèse, le **Chapitre 4** vise à évaluer la sensibilité du modèle hydraulique HEC-RAS à la précision de la description géomorphologique du lit mineurs et de la pente du fond de rivière. Le but est de définir le meilleur compromis entre parcimonie et réalisme, en d'identifiant les facteurs morphologiques les plus importants pour obtenir une simulation satisfaisante des tirants d'eau à l'échelle régionale.

Cette étude est menée sur le Serein (affluent de l'Yonne), dans un bief bien renseigné (20 sections transversales sur 89 km) entre les stations hydrométriques de Dissangis et Beaumont.

Le principe consiste à comparer différents scénarios de géométrie simplifiée, portant sur le nombre (de 20 à 3) et la forme (irrégulière, trapézoïdale, rectangulaire ou triangulaire) des sections transversales. Cette analyse montre que ces simplifications de la géométrie n'altèrent pas significativement la simulation des débits, mais qu'une géométrie précise est nécessaire pour simuler précisément les niveaux d'eau. En conclusion, si un modèle hydraulique Saint-venant 1D est indispensable pour effectuer des simulations fiables des niveaux d'eau en fonction de données géométriques précises, ce type de modélisation hydrodynamique ne permet pas une simulation précise des niveaux d'eau à partir d'une géométrie simplifiée.

Pour trouver un bon compromis entre l'échelle d'application, l'importance d'effectuer des simulations précises et fiables des niveaux d'eau, et la disponibilité des données morphologiques, une méthode de changement d'échelle est proposée en **Chapitre 5**. Le principe est d'utiliser la modélisation des processus hydrauliques à haute résolution par le modèle HEC-RAS, pour améliorer la représentation des niveaux d'eau et des interactions nappe-rivière à l'échelle régionale dans la plateforme de modélisation EauDyssée.

Cette méthodologie a été validée dans un sous-bassin versant de l'Oise, d'une superficie de 4500 km^2, sur la période 1990-1995. Le domaine de surface est constitué de 1868 mailles (de 1 km^2 à 16 km^2), dont 202 mailles rivière de 1 km^2 qui représentent le réseau hydrographique. Le domaine souterrain comprend deux couches souterraines qui représentent les nappes de l'Éocène et de la Craie, avec des mailles de 1 km^2 à 16 km^2. La couche de la Craie est confinée par l'Éocène et il y a des échanges verticaux entre ces deux couches. Le modèle hydrogéologique développé par Gomez (2002) dans l'application régionale du bassin de la Seine a d'abord été recalé, en séparant deux régimes de fonctionnement. Nous avons commencé par recaler les coefficients d'emmagasinement et les transmissivités qui contrôlent

le comportement à basse fréquence des charges hydrauliques, dans lequel la variabilité des niveaux piézométriques de la nappe est due aux fluctuations climatiques. Le deuxième régime se caractérise par un comportement à haute fréquence temporelle des niveaux piézométriques, qui est dû aux fluctuations des niveaux d'eau en rivière. Nous avons pu améliorer la restitution de ce régime en recalant les coefficients d'emmagasinement dans les mailles souterraines situées sous les mailles rivière, ainsi qu'un coefficient de transfert nappe-rivière (Q_{max}).

Une fois le modèle hydrogéologique recalé, il a permis de simuler les apports latéraux pour la modélisation hydraulique par HEC-RAS d'un tronçon de l'Oise de 188 km, où 420 sections transversales sont disponibles. Le calage du modèle HEC-RAS a été validé en 4 stations hydrométriques de contrôle, ce qui a permis de simuler des courbes de tarage (reliant débit et niveau d'eau) *a priori* réalistes à la résolution de ce modèle, c'est-à-dire tous les 200m en moyenne. Ces courbes de tarage ont ensuite été moyennées à la résolution des mailles rivières du modèle hydrologique régional (1 km²) afin de pouvoir en déduire la fluctuation du niveau d'eau en fonction du débit simulé par le module de routage régional. Les échanges entre les mailles rivière et les mailles aquifères peuvent alors être estimés en fonction des gradients de charge verticaux entre la nappe et la rivière, dont le niveau, représentatif de la charge, n'est plus fixe.

L'impact de la fluctuation des niveaux en rivière sur les isopièzes a été analysé par rapport à un état de référence pour lequel les niveaux en rivière sont constants, ce qui correspond donc à la version originale de la plateforme EauDyssée. À l'échelle locale, nous avons comparé les niveaux piézométriques simulés avec les observations d'un unique piézomètre suffisamment proche de la rivière (Précy sur Oise). L'analyse des résultats montre que ces fluctuations en rivière ont des impacts importants sur les dynamiques des niveaux piézométriques. Par exemple, une fluctuation des niveaux d'eau en rivière de 5 mètres produit une modification

des niveaux piézométriques qui peut atteindre 1.5 m, alors que la variation piézométrique correspondante n'est que de 15 cm dans la version de référence où la cote des cours d'eau est fixe. A l'échelle régionale, l'analyse des résultats sur la période de simulation montre un écart moyen des niveaux piézométriques pouvant atteindre 1,9 m pour les mailles souterraines situées sous les mailles rivière. Cet écart se réduit si l'on considère des mailles souterraines plus éloignées de la rivière. L'extension spatiale de cet écart moyen est plus importante dans la nappe de la Craie qui est confinée (jusqu'à 25 km de la rivière) que dans celle de l'Éocène qui est libre (6 km de la rivière).

Ces résultats démontrent l'efficacité de la méthode de changement d'échelle proposée pour simuler les niveaux d'eau et mieux évaluer les interactions nappe-rivière à l'échelle régionale avec un faible coût de calcul pour le modèle régional. En revanche, le problème crucial du manque de données à l'échelle régionale n'est pas levé par cette démarche, dont le principal avantage est la finalement d'exploiter au mieux l'information disponible, que ce soient des courbes de tarage observées, des modèles hydrauliques existants, ou même une cote fixe en absence de meilleure information, ce qui permet d'enrichir graduellement le modèle hydrologique régional et traiter les zones de manière flexible et de mieux exploiter

La suite de ce travail consistera donc à généraliser cette méthodologie à l'échelle du bassin de la Seine, en exploitant les sorties de modèles hydrauliques existants, ou par interpolation de courbes de tarage observées. En parallèle, cette méthode pourrait aussi être étendue pour relier d'autres paramètres hydrauliques au débit, notamment la vitesse des écoulements et le volume d'eau débordé pendant les crues, qui peuvent tous deux rétroagir sur le débit.

En conclusion, ce travail offre des perspectives intéressantes dans différent domaines (**Chapitre 6**):

- simulation de processus jusque là négligés par le modèle EauDyssée : risques d'inondation à l'échelle régionale (Knebl et al., 2005) ; fonctionnement de la zone hyporhéique, où l'eau du

cours d'eau s'infiltre et se mélange à l'eau interstitielle des sédiments (Arntzen et al., 2006; Ryan et al., 2004) ; élimination des nitrates dans les zones humides, qui sont souvent situées à la zone de contact entre les nappes souterraines et la rivière (Curie et al., 2009; Devito et al., 1996; Kehew et al., 1998) ; relargage de polluants comme les nitrates par des processus biogéochimiques (Cardenas, 2009; Flipo et al., 2007a; Gomez et al., 2003; Ledoux et al., 2007),

- estimation de l''impact du changement climatique sur le fonctionnement des hydrosystèmes : risques de crue et étiage, évolution des niveaux piézométriques et des processus hydrodynamique et bioégochimiques associés (Ducharne et al., 2007; Ducharne et al., 2010),

- simulation des aquifères côtiers, où la fluctuation des marées est importante pour l'écoulement des eaux souterraines, et où les interactions dynamiques entre les eaux souterraines et l'eau de mer sont importantes (Guo et al., 2010; Sun et al., 2008).

Mots clés: Interactions nappe-rivière, hydrologie, hydrogéologie, Changement d'échelle, Plateforme EauDyssée, morphologie des rivières

REFERENCES

Abbott, M.B., 1966. An introduction to the method of characteristics. Elsevier, New York.

Abbott, M.B., 1979. Computational hydraulics: Elements of the theory of free surface flows. Pitman, London.

Abbott, M.B., Bathurst, J.C., Cunge, J.A., E., O.C.P. and J., R., 1986a. An introduction to the European Hydrological System -Système Hydrologique Européen, SHE. 2. Structure of a physically-based, distributed modeling system. Journal of Hydrology, 87: 61-77.

Abbott, M.B., Bathurst, J.C., Cunge, J.A., O'Connell, P.E. and Rasmussen, J., 1986b. An introduction to the European Hydrological System -Système Hydrologique Européen, SHE. 2. Structure of a physically-based, distributed modeling system. Journal of Hydrology, 87: 61-77.

Abbott, M.B. and Refsgaard, J.C., 1996. Distributed Hydrological Modelling. Kluwer Academic, Dordrecht.

Akan, A.O. and Yen, B.C., 1981a. Mathematical model of shallow water flow over porous media. Journal of the Hydraulics Division, ASCE, 107(HY4): 479–494.

Al-Qurashi, A., McIntyre, N., Wheater, H. and Unkrich, C.L., 2008. Application of the Kineros2 rainfall-runoff model to an arid catchment in Oman. Journal of Hydrology, 355(1-4): 91.

Aldama, A.A., 1990. Least-squares parameter estimation for Muskingum flood routing. Journal of Hydraulic Engineering, 116(4): 580.

Alley, W.M., Dawdy, D.R. and Schaake, J.C., 1980. Parametric-deterministic urban watershed model. Journal of Hydraulics Division, American Society of Civil Engineers, 106: 679–690.

Alsdorf, D., Rodriguez, E. and Lettenmaier, D., 2007. Measuring surface water from space. Reviews of Geophysics, 45(2): RG2002.

Ambroise, B., Perrin, J.L. and Reutenauer, D., 1995. Multi-criterion validation of a semi-distributed conceptual model of the water cycle in the Fecht catchment (Vosges Massif, France). Water Resources Research, 31(6): 1467–1481.

Andersen, J., Refsgaard, J.C. and Jensen, K.H., 2001. Distributed hydrological modelling of the Senegal River Basin -- model construction and validation. Journal of Hydrology, 247(3-4): 200.

Anderson, E.I., 2003. An analytical solution representing groundwater–surface water interaction. Water Resources Research, 39(3): 1071.

Aral, M.M. and Gunduz, O., 2003. Scale effects in large scale watershed modeling. In: V.P. Singh and R.N. Yadava (Editors), International Conference on Water and Environment. WE, Allied Publishers, India, pp. 37–51.

Arnold, J.G., Allen, P.M. and Bernhardt, G., 1993. A comprehensive surface-groundwater flow model. Journal of Hydrology, 142: 47–69.

Arntzen, E., Geist, D. and Dresel, E., 2006. Effects of fluctuating river flow on ground¬water/surface water mixing in the hyporheic zone of a regulated, large cobble bed river. River Research and Applications, 22: 937–946.

Arora, V.K., Seglenieks, F., Kouwen, N. and Soulis, E., 2001. Scaling aspects of river flow routing. Hydrological Processes, 15(3): 461-477.

Ataie-Ashtianti, B., Volker, R. and Lockington, D., 1999. Tidal effects on sea water intrusion in unconfined aquifers. Journal of Hydrology, 216: 17–31.

Azevedo, I.C., Bordalo, A.A. and Duarte P, M., 2010. Influence of river discharge patterns on the hydrodynamics and potential contaminant dispersion in the Douro estuary

(Portugal). Water Research, 2010, vol. 44, no10, pp. 3133-3146 [14 page(s) (article)] (1 p.1/4).
Baillie, M.N., Hogan, J.F., Ekwurzel, B., Wahi, A.K. and Eastoe, C.J., 2007. Quantifying water sources to a semiarid riparian ecosystem, San Pedro River, Arizona. Journal of Geophysical Research, 112: G03S02.
Barkau, R.L., 1985. A Mathematical Model of Unsteady Flow Through a Dendritic Network, Colorado State University, Collins, CO.
Barkau, R.L., 1992. UNET, One-Dimensional Unsteady Flow Through a Full Network of Open Channels. Computer Program, St. Louis, MO.
Barr, A. and Barron, O., 2009. Application of a coupled surface water-groundwater model to evaluate environmental conditions in the Southern River catchment. CSIRO: Water for a Healthy Country National Research Flagship.
Barré de Saint-Venant, 1871. Théorie du mouvement non permanent des eaux, avec application aux crues des rivières et à l'introduction des marées dans leur lit. C.R. [Comptes Rendus des Séances de l'Académie des Sciences. Paris.] 73, 147-154, 237-240.
Bathurst, J.C., 1988. Flow processes and data provision for channel flow models. Modelling Geomorphological Systems. John Wiley and Sons New York.
Becker, A., Klocking, B., Lahmer, W. and Pfutzner, B., 2002. The Hydrological Modelling System ArcEGMO In Mathematical Models of Watershed Hydrology. In: V.P. Singh and D.K. Frevert (Editors), Water Resources Publications, Littleton, Colorado, pp. 891.
Becker, A. and Serban, P., 1990. Hydrological models for water-resources systems design and operation. WMO Operational Hydrology Report No. 34.
Beeson, P., Duffy, C., Springer, E. and Panday, S., 2004. Integrated hydrologic models for closing the water budget. Whitewater River Basin, Kansas. Eos Trans. AGU, 85(47), Fall Meeting Supplement, Abstract H34B-05.
Beven, K., 1977. Hillslope hydrographs by the finite element method. Earth Surface Processes and Landforms, 2: 13–28.
Beven, K., 2006. A manifesto for the equifinality thesis. Journal of Hydrology, 320(1-2): 18.
Beven, K. and Kirkby, M.J., 1979. A physically-based variable contributing area model of basin hydrology. Hydrological Sciences Bulletin. 24: 43–69.
Beven, K.J. and Binley, A.M., 1992. The future of distributed models: model calibration and uncertainty prediction. Hydrological Processes, 6: 279-298.
Beven, K.J., Calver, A. and Morris, E.M., 1987. The Institute of Hydrology distributed model. Report 98, Institute of Hydrology, Wallingford.
Beven, K.J. and Freer, J., 2001a. Equifinality, data assimilation, and uncertainty estimation in mechanistic modelling of complex environmental systems. Journal of Hydrology, 249: 11–29.
BeVille, S.H., 2007. Physics-based simulation of near-surface hydrologic response for the Lerida Court landslide in Portola Valley, California, Stanford University, Stanford.
Biancamaria, S. et al., 2010. Preliminary characterization of SWOT hydrology error budget and global capabilities. Journal of Selected Topics in Earth Observations and Remote Sensing, 3(1): 6-19.
Bingeman, A.K., Kouwen, N., ASCE, M. and Soulis, E.D., 2006. Validation of the hydrological processes in a hydrological model. Journal of Hydrologic Engineering, ASCE, 11(5): 451-463.
Binley, A.M., Beven, K. and Elgy, J., 1989. A physically-based model of heterogeneous hillslopes. II. Effective hydraulic conductivities. Water Resources Research, 25: 1227–1233.

Birkhead, A.L. and James, C.S., 2002. Muskingum river routing with dynamic bank storage. Journal of Hydrology, 264(1-4): 113.

Bixio, A. et al., 2002. Modeling groundwater-surface water interactions including effects of morphogenetic depressions in the Chernobyl exclusion zone. Environmental Geology, 42(2-3): 162-177.

Blasch, K. et al., 2004. Processes controlling recharge beneath ephemeral streams in southern Arizona. In: J.F. Hogan, F.M. Phillips and B.R. Scanlon (Editors), Ground-water Recharge in Desert Environments. American Geophysical Union, Washington, DC, pp. 69–76.

Bolster, C.H., Genereux, D.P. and Saiers, J.E., 2001. Determination of specific yield for the Biscayne Aquifer with a canal-drawdown test. Ground Water, 39(5): 768–777.

Boukerma, B., 1987. Modélisation des écoulements superficiels et souterrains dans le sud Ouest de la France: Approche du bilan hydrique., Ecole Nationale Supérieure des Mines de Paris.

Bradford, S.F. and Katopodes, N.D., 1998. Nonhydrostatic model for surface irrigation. Journal of Irrigation and Drainage Engineering, 124 (4): 200–212.

Brankensiek, D.L., 1965. An Implicit Flood Routing Method. Hydraulics Division Speciality Conference, American Society of Civil Engineers, Tucson, Arizona.

Brookfield, A.E., Sudicky, E.A. and Park, Y.-J., 2008. Analysis of Thermal Stream Loadings In A Fully-Integrated Surface/Subsurface Modelling Framework. IAHS-AISH Publication, 321: 117–123.

Brooks, P.D. and Lemon, M.M., 2007. Spatial variability in dissolved organic matter and inorganic nitrogen concentrations in a semiarid stream, San Pedro River, Arizona. Journal of Geophysical Research - Biogeosciences, 112: G03S05.

Buhman, D.L., Gates, T.K. and Watson, C.C., 2002. Stochastic variability of fluvial hydraulic geometry: Mississippi and Red Rivers. Journal of Hydraulic Engineering, ASCE, 128(4): 426–437.

Cardenas, M.B., 2009. Stream-aquifer interactions and hyporheic exchange in gaining and losing sinuous streams. WATER RESOURCES RESEARCH, 45(W06429): 13.

Cardenas, M.B. and Gooseff, M.N., 2008. Comparison of hyporheic flow under uncovered and covered channels based on linked surfaceground-water simulations. Water Resources Research, 44: W03418.

Carpenter, S.R., Fisher, S.G., Grimm, N.B. and Kitchell, J.F., 1992. Global Change and Freshwater Ecosystems. Annual Review of Ecology and Systematics, 23(1): 119-139.

Carr, A.E., 2006. Physics-based simulations of hydrologic response and cumulative watershed effects, Stanford University, Stanford.

Carrera, J. and Neuman, S.P., 1986a. Estimation of aquifer parameters under steady-state and transient conditions: I. Background and statistical framework. Water Resources Research, 22(2): 199–210.

Carter, R.W., and R. G. Godfrey, 1960. Storage and flood routing. US Geological Survey Water Supply Paper, 1543-B:93.

Chiu, C.-L., 1972. Stochastic methods in hydraulics and hydrology of streamflow. 1(1): 61-84.

Chow, V.T., 1959. Open Channel Hydraulics. McGraw Hill Company Inc., New York.

Coe, M., 1998. A linked global model of terrestrial hydrologic processes: Simulation of modern rivers, lakes and wetlands. Journal of Geophysical Research, 103: 8885-8899.

Constantz, J., Stonestrom, D., Stewart, A., Niswonger, R. and Smith, T.R., 2001. Analysis of streambed temperatures in ephemeral channels to determine streamflow frequency and duration. Water Resources Research, 37(2): 317–328.

Cooper, H., 1959. A hypothesis concerning the dynamic balance of fresh water and salt water in a coastal aquifer. Journal of Geophysics, 64: 461–467.
Cooper, H.H. and Rorabaugh, M.I., 1963. Groundwater movements and bank storage due to flood stages in surface streams. USGS Water Supply Paper, 1536-J: 343-366.
Cox, W.B. and Stephens, D.B., 1988. Field study of ephemeral stream-aquifer interaction., Proceedings of the FOCUS Conference on Southwestern Ground Water Issues. National Water Well Association, Dublin OH, pp. 337-358.
Cunge, J.A., 1969. On the Subject of a Flood Propagation Computation Method, (Muskingum Method). Journal of Hydraulic Research, 7(2): 205-230.
Cunge, J.A., Holly, F.M. and Verwey, A., 1980. Practical aspects of computational river hydraulics. Pitman Publishing Ltd. London, (17 CUN).
Cunningham, A.B. and Sinclair, P.J., 1979. Application and analysis of a coupled surface and groundwater model. Journal of Hydrology, 43: 129-148.
Curie, F., Ducharne, A., Sebilo, M. and Bendjoudi, H., 2009. Denitrification in a hyporheic riparian zone controlled by river regulation in the Seine River basin (France). Hydrological Processes, 23: 655-664.
D' Haese, C.M.F., Putti, M., Paniconi, C. and Verhoest, N.E.C., 2007. Assessment of adaptive and heuristic time stepping for variably saturated flow. International Journal for Numerical Methods in Fluids, 53(7): 1173-1193.
David, C., Habets, F. and Maidment, D.R., 2010. Rapid applied to the SIM-France model. Submitted to Journal of Hydrological Processes (revision phase).
Day-Lewis, F.D. and Lane, J.W., 2006. Using a Fiber-Optic Distributed Temperature Sensor to Understand Ground-Water/Surface-Water Interaction. U.S. Geological Survey Water Resources Discipline - Wester Region Research Seminar Series, November 30, 2006.
de Marsily, G., 1986. Groundwater Hydrology for Engineers. Academic Press, New-York.
De Roo, A.P.J., Wesseling, C.G. and Van Deursen, W.P.A., 2000. Physically based river basin modelling within a GIS: the LISFLOOD model. Hydrological Processes(14): 1981-1992.
Dent, C.L. and Henry, J.C., 1999. Modelling nutrient-periphyton dynamics in streams with surface-subsurface exchange. Ecological Modelling, 122(1-2): 97.
DeRose, R.C. et al., 2005. Regional patterns of riparian vegetation, erosion and sediment transport in the Ovens River Basin. CSIRO Land and Water Client Report, Canberra.: 26.
Devito, K.J., Hill, A.R. and Roulet, N., 1996. Groundwater-surface water interactions in headwater forested wetlands of the Canadian Shield. Journal of Hydrology, 181(1-4): 127.
DHI, 2001. MIKE11 Hydrodynamic Reference Manual, DHI Water & Environment, Horshølm, Denmark.
Doering, C.R. and Gibbon, J.D., 1995. Applied Analysis of the Navier-Stokes Equations. Cambridge University Press, 232 pp.
Dooge, J.C.I., 1973. Linear Theory of Hydrologic Systems, USDA, Tech. Bull.1468, U.S. Department of Agriculture, Washington, D.C.
Dooge, J.C.I., Strupczewski, W.G. and Napiórkowski, J.J., 1982. Hydrodynamic derivation of storage parameters of the Muskingum model. Journal of Hydrology, 54(4): 371.
Drobot, R. and Corbus, C., 1998. Muskingum Model for Large Major Beds Rivers, XIXth Conference of the Danube Countries on Hydrological Forecasting and Hydrological Bases of Water Management, Osijek, Croatia, pp. 59-66.

Ducharne, A. et al., 2007. Long term prospective of the Seine river system: Confronting climatic and direct anthropogenic changes. Science of the Total Environment, 375: 292-311.

Ducharne, A. et al., 2003. Development of a High Resolution Runoff Routing Model, Calibration and Application to Assess Runoff from the LMD GCM. Journal of Hydrology, 280: 207-228.

Ducharne, A. et al., 2010. Climate change impacts on Water Resources and Hydrological Extremes in Northern France, proceedings of XVIII International Conference on Water Resources, Barcelona.

Dyhouse, G., Hatchett, J. and Benn, J., 2003. Floodplain Modeling using HEC-RAS. Haestad Press, Waterbury, CT. USA.

Ebel, B.A. and Loague, K., 2006. Physics-based hydrologic-response simulation: Seeing through the fog of equifinality. Hydrological Processes, 20: 2887–2900.

Ebel, B.A. and Loague, K., 2008. Rapid simulated hydrologic response within the variably saturated near surface. Hydrological Processes, 22: 464–471.

Ebel, B.A., Mirus, B.B., Heppner, C.S., VanderKwaak, J.E. and Loague, K., 2009. First-order exchange coefficient coupling for simulating surface water-groundwater interactions: parameter sensitivity and consistency with a physics-based approach. Hydrological Processes, 23(13): 1949-1959.

Engman, E.T. and Rogowski, A.S., 1974. A partial area model for storm flow synthesis. Water Resources Research, 10: 464–472.

Erskine, A.D., 1991. The effect of tidal fluctuation on a coastal aquifer in the UK. Ground Water, 29(4): 556–562.

Ferris, J.G., 1951. Cyclic fluctuations of water level as a basis for determining aquifer transmissibility. In: IAHS (Editor), Proceedings of the International Union of Geodesy and Geophysics, pp. 148–155.

Flipo, N., 2005. Modélisation intégrée des transferts d'azote dans les aquifères et les rivières: Application au bassin du Grand Morin. Doctorat Hydrologie et Hydrogéologie Quantitatives, CIG- Centre d'informatique géologique, ENSMP.

Flipo, N., Even, S., Poulin, M., Théry, S. and Ledoux, E., 2007a. Modeling nitrate fluxes at the catchment scale using the integrated tool CAWAQS. Science of the Total Environment, 375: 69-79.

Flipo, N., Jeannée, N., Poulin, M., Even, S. and Ledoux, E., 2007b. Assessment of nitrate pollution in the Grand Morin aquifers (France): combined use of geostatistics and physically-based modelling. Environmental Pollution, 146(1): 241-256.

Flipo, N., Poulin, M., Even, S. and Ledoux, E., 2005. Hydrological part of CAWAQS (CAtchment WAter Quality Simulator): fitting on a small sedimentary basin., Proceedings of the SIL, Lahti. Verh. Internat. Verein. Limnol., pp. 768-772.

Francis, B.A., Francis, L.K. and Cardenas, M.B., 2010. Water table dynamics and groundwater–surface water interaction during filling and draining of a large fluvial island due to dam-induced river stage fluctuations. Water Resources Research, 46: W07513.

Fread, D.L., 1974. Numerical Properties of Implicit Four-Point Finite Difference Equations of Unsteady Flow, U.S. Department of Commerce, NWS, NOAA.

Fread, D.L., 1985. Channel Routing', Hydrological Forecasting. Edit by M.G.Anderson and T.P.Burt, 437-503.

Fread, D.L. and Lewis, J.M., 1993. Selection of DX and DT computational Steps for Four-Point Implicit Nonlinear Dynamic Routing Models, San Francisco.

Fread, D.L. and Lewis, J.M., 1998. NWS FLDWAY MODEL, Hydrologic Research Laboratory, Office of Hydrology, National Weather Service, NOAA.

Freeze, R.A., 1971. Three-dimensional, transient, saturated–unsaturated flow in a groundwater basin. Water Resources Research, 7(347–366).
Freeze, R.A., 1972. Role of subsurface flow in generating surface runoff: 1. Base flow contributions to channel flow. Water Resources Research, 8(3): 609-623.
Friesz, P., 1996. Geohydrology of stratified drift and stream flow in the deerfield river basin, northwestern massachusetts. Water Resources Investigations, 96(4115): 1–17.
Georgakakos, K.P., Rajaram, H. and Li, S.G., 1988. On Improved Operational Hydrologic Forecasting of Streamflows," IIHR Report No. 325, Iowa Institute of Hydraulic Research, The University of Iowa, Iowa City, Iowa, 162.
Gill, M.A., 1992. Numerical solution of Muskingum equation. Journal of Hydraulic Engineering - ASCE, 118(5): 804.
Gillespie, J.B. and Perry, C.A., 1988. Channel infiltration from floodflows along the Pawnee River and its tributaries, west-central Kansas. U.S. Geological Survey Water-Resources Investigations Report 88-4055, 30 p.
Glover, R., 1959. The pattern of fresh-water flow in a coastal aquifer. Journal of Geophysical Research, 64: 457–459.
Golaz-Cavazzi, C., 1999. Modélisation hydrologique à l'échelle régionale appliquée au bassin du Rhône Comparaison de deux modes de calcul des bilans hydriques de surface et étude de sensibilité à une perturbation des forçages climatiques, Ecole Nationale Supérieur des Mines de Paris.
Gomez, E., 2002. Modélisation intégrée du transfert de nitrate à l'échelle régionale dans un système hydrologique. Application au bassin de la Seine., Ecole Nationale Supérieure des Mines de Paris.
Gomez, E. et al., 2003. Un outil de modélisation intégrée du transfert des nitrates sur un système hydrologique: application au bassin de la Seine. La Houille Blanche, No. 3/2003.
Goodrich, D.C. et al., 1997. Linearity of basin response as a function of scale in a semiarid watershed. Water Resources Research, 33(12): 2951-2965.
Gordon, N.D., 1996. The Hydraulic Geometry of the Acheron River, Victoria, Australia. Unpublished Report by the Centre for Environmental Applied Hydrology, The University of Melbourne, Australia.
Govindaraju, R.S. and Kavvas, M.L., 1991. Dynamics of moving boundary overland flows over infiltrating surfaces at hillslopes. Water Resources Research, 27: 1885–1898.
Graff, W. and Altinakar, M.S., 1996. Ecoulement non permanent et phenomenes de transport. Presse Polytechnique et Universitaires Romandes, Lausanne.
Graham, D.N. and Refsgaard, A., 2001. MIKE SHE: A Distributed, Physically based Modelling System for Surface Water/Groundwater Interactions, MODFLOW 2001 and other modelling Odysseys Conference, Colorado.
Gregory, D., Shutts, G.J. and Mitchell, J.R., 1998. A new gravity-wave-drag scheme incorporating anisotropic orography and low-level wave breaking: Impact upon the climate of the UK Meteorological Office Unified Model. Quarterly Journal of the Royal Meteorological Society, 124(546): 463.
Gubala, C.P., Eilers, J.M. and Bemert, J.A., 1996. The relationships between river channel morphology, complexity and aquatic habitat, Proceedings of 2nd IAHR Symp. Habitat Hydraulics, Ecohydraulics 2000, 1996, INRS-Eau with FQSA, IAHR, Québec, pp. B299-B306.
Gunduz, O. and Aral, M.M., 2005. River Networks and Groundwater Flow: Simultaneous Solution of a Coupled System. Journal of Hydrology, 301(1-4): 216-234.
Guo, H. and Jiao, J.J., 2007. Impact of coastal land reclamation on ground water level and the sea water interface. Ground Water, 45(3): 362.

Guo, H., Jiao, J.J. and Li, H., 2010. Groundwater response to tidal fluctuation in a two-zone aquifer. Journal of Hydrology, 381(3-4): 364.
Habets, F. et al., 1999b. Simulation of the water budget and the river flows of the Rhone basin. Journal of Geophysical Research, 104(D24): 31145-31172.
Habets, F. et al., 2010. Multi-model simulation of a major flood in the groundwater-fed basin of the Somme River (France). Journal of Hydrology and Earth System Sciences, 4(1): 99-117.
Hagemann, S. and Dumenil, L., 1998. A parameterization of lateral water flow for the global scale. Journal of Climate Dynamics, 14: 17-41.
Hammond, G.E., Valocchi, A.J. and Lichtner, P.C., 2005. Application of Jacobianfree Newton-Krylov with physics-based preconditioning to biogeochemical transport. Advances in Water Resources, 28: 359–376.
Harbaugh, A.W. and McDonald, M.G., 1996. User's Documentation for MODFLOW-96, an Update to the U.S. Geological Survey Modular Finite-Difference Ground-Water Flow Model. U.S. Geological Survey, Open-File Report 96-485.
Harder, J.A. and Armacost, L.V., 1966. Wave propogation in rivers. Hydraulic Engineering Laboratory, report No. 1, Serien 8, University of California, Berkeley.
Harman, C., Stewardson, M. and DeRose, R., 2008. Variablity and uncertainty in reach bankfull hydraulic geometry. Journal of hydrology, 351: 13-25.
Harrington, G.A., Cook, P.G. and Herczeg, A.L., 2002. Spatial and temporal variability of ground water recharge in central Australia: A tracer approach. Ground Water, 40(5): 518-528.
Hateley, L. et al., 2006. Sediment and nutrient modeling in the Far North Queensland NRM region. Volume 1. In: The use of SedNet and ANNEX models to guide GBR catchment sediment and nutrient target setting (Ed) A.L. Cogle, C. Carroll and B.S. Sherman. Department of Natural Resource and Water. QNRM06138.
Hayami, S., 1951. On the propagation of flood waves. Bulletin of the Disaster Prevention Research Institute, Kyoto Univ., Japan, 1, 1-16.
Haycock, N.E. and Burt, T.P., 1993. Role of floodplain sediments in reducing the nitrate concentration of subsurface run-off: a case study in the Cotswolds, UK. Hydrological Processes, 7: 287–295.
HEC, 2002. River analysis system (HEC-RAS) user's manual. Hydrologic Engineering Center (HEC), U.S. Army Corps of Engineers, Davis, California.
Henderson, R.D., Day-Lewis, F.D. and Harvey, C.F., 2009. Investigation of aquifer-estuary interaction using wavelet analysis of fiber-optic temperature data. Geophysical Research Letters, 36(6): L06403.
Heppner, C.S., 2007. A dam problem: characterizing the upstream hydrologic and geomorphologic impacts of dams, Stanford University, Stanford.
Heppner, C.S. and Loague, K., 2008. A dam problem: simulated upstream impacts for the Searsville Watershed. Journal of Ecohydrology, 1: 408-424.
Hey, R.D. and Thorne, C.R., 1986. Stable channels with mobile gravel beds. Journal of Hydraulic Engineering, ASCE, 112(8): 671–689.
Hicks, F.E., 1996. Hydraulic flood routing with minimal channel data: Peace River, Canada. Canadian Journal of Civil Engineering, 23: 525-535.
Hill, M.C., 2006. The practical use of simplicity in developing ground water models. Ground Water, 44(6): 775-781.
Hodge, R.A. and Freeze, R.A., 1977. Groundwater flow systems and slope stability. Canadian Geotechnical Journal, 14: 466-476.
Hunt, R.J., Walker, J.F., Westenbroek, S. and Doherty, J., 2008. Hydrologic climate change from a deterministic view: Using GSFLOW to simulate climate change in a northern

temperate climate, 2nd USGS Modeling Conference. U.S. Geological Survey., Orange Beach, Ala.
Hussein, M. and Schwartz, F.W., 2003. Modelling of flow and contaminant transport in coupled stream–aquifer systems. Journal of Contaminant Hydrology, 65(1–2): 41–64.
Jenson, K. and Dominique, J.O., 1988. Extracting topographic structure from digital elevation data for geographical information system analysis. Photogram etric Engineering and Remote Sensing, 54(11): 1593-1600.
Jha, M.K., Kamii, Y. and Chikamori, K., 2003. On the estimation of phreatic aquifer parameters by the tidal response technique. Water Resources Management, 17(1): 69–88.
Jobson, H.E. and Harbaugh, A.W., 1999. Modifications to the diffusion analogy surface water flow model (Daflow) for coupling to the modular finite-difference groundwater flow model (Modflow). United States Geological Survey, Open File Report: 99-217.
Johnson, P.A. and Heil, T.M., 1996. Uncertainty in Estimating Bankfull Conditions. Water Resources Bulletin, Journal of the American Water Resources Association, 32(6): 1283-1292.
Jolly, I.D. and Rassam, D.W., 2009. A review of modelling of groundwater-surface water interactions in arid/semi-arid floodplains, 18th World IMACS / MODSIM Congress, Cairns, Australia.
Jones, J.E. and Woodward, C.S., 2001. Newton-Krylov-multigrid solvers for large-scale, highly heterogeneous, variably saturated flow problems. Advances in Water Resources, 24: 763–774.
Jones, J.P., Sudicky, E.A., Brookfield, A.E. and Park, Y.J., 2006. An assessment of the tracer-based approach to quantifying groundwater contributions to streamflow. Water Resources Research, 42(W02407.1-W02407).
Jorgeson, J.D., 1999. Peak flow analysis using a two dimensional watershed model with radar precipitation data, Colorado State University, Fort Collins, Colorado.
Jowett, I.G., 1998. Hydraulic geometry of New Zealand rivers and its use as a preliminary method of habitat assessment. Regulated Rivers. Research and Management, 14: 451-466.
Julien, P.Y. and Saghafian, B., 1991. CASC2D Users Manual, Civil Engineering report, Dept. of Civil Engineering, Colorado State University, Fort Collins, CO 80523.
Julien, P.Y., Saghafian, B. and Ogden, F.L., 1995. Raster-Based Hydrologic Modeling of Spatially-Varied Surface Runoff. Water Resources Bulletin, 31(3): 523-536.
Kalbus, E., Reinstorf, F. and Schirmer, M., 2006. Measuring methods for groundwater–surface water interactions: a review. Hydrol Earth Syst Sci, 10(6): 873–887.
Kehew, A.E. et al., 1998. Hydrogeochemical Interaction Between a Wetland and an Unconfined Glacial Drift Aquifer Southwestern Michigan. Ground Water, 36(5): 849.
Kilpatrick, F.A. and Barnes, H.H.J., 1964. Channel Geometry of Piedmont Streams as Related to Frequency of Floods. Professional Paper 422-E. US Geological Survey, Washington, DC.
Kim, B., Jackman, A. and Triska, F., 1992. Modeling biotic uptake by periphyton and transient hyporheic storage of nitrate in a natural stream. Water Resources Research, 28(10).
Kim, K., Anderson, M.P. and Bowser, C.J., 2000. Enhanced dispersion in groundwater caused by temporal changes in recharge rate and lake levels. Advances in Water Resources, 23(6): 625-635.
Knebl, M.R., Yang, Z.L., Hutchison, K. and Maidment, D.R., 2005a. Regional scale flood modeling using NEXRAD rainfall, GIS, and HEC-HMS/RAS: a case study for the

San Antonio River Basin Summer 2002 storm event. Journal of Environmental Management, 75: 325-336.
Knebl, M.R., Yang, Z.L., Hutchison, K. and Maidment, D.R., 2005b. Regional scale flood modeling using NEXRAD rainfall, GIS, and HEC-HMS/RAS: a case study for the San Antonio River Basin Summer 2002 storm event. Journal of Environmental Management, 75(4): 325.
Knighton, D., 1984. Fluvial Forms and Process. Edward Arnold, London.
Knoll, D.A. and Keyes, D.E., 2004. Jacobian-free Newton-Krylov methods: a survey of approaches and applications. Journal of Computational Physics, 193: 357–397.
Kojiri, T., Tokai, A. and Kinai, Y., 1998. Assessment of river basin environment through simulation with water quality and quantity. Annuals of Disaster Preventation Research Institute, 41(2): 119-134.
Kollet, J. and Maxwell, R., 2006. Integrated surface–groundwater flow modeling: A free-surface overland flow boundary condition in a parallel groundwater flow model. Advances in Water Resources, 29: 945-958.
Korkmaz, S., Ledoux, E. and Önder, H., 2009. Application of the coupled model to the Somme river basin. Journal of Hydrology, 366(1-4): 21.
Koster, R.D., Suarez, M.J., Ducharne, A., Praveen, K. and Stieglitz, M., 2000. A catchment-based approach to modeling land surface processes in a GCM - Part 1: Model structure. Journal of Geophysical Research, 105(D20): 24809-24822.
Koussis, A.D., 1983. Accuracy criteria in diffusion routing: a discussion. Journal of hydraulic Division. ASCE, 109(5): 803–806.
Kouwen, N., 1988. WATFLOOD: A Micro-Computer based Flood Forecasting System based on Real-Time Weather Radar. Canadian Water Resources Journal, 13(1): 62-77.
Lamouroux, N. and Capra, H., 2002. Simple predictions of instream habitat model outputs for target fish populations. Journal of Freshwater Biology, 47(8): 1543–1556.
Lamouroux, N. and Suchon, Y., 2002. Simple predictions of instream habitat model outputs for habitat guilds in large streams. Journal of Freshwater Biology, 47(8): 1531–1542.
Landon, M.K., Rus, D.L. and Harvey, F.E., 2001. Comparison of Instream Methods for Measuring Hydraulic Conductivity in Sandy Streambeds. Ground Water, 39(6): 870.
Lange, J., 2005. Dynamics of transmission losses in a large arid stream channel. Journal of Hydrology, 306(1-4): 112-126.
Langevin, C.D., Swain, E.D. and Wolfert, M.A., 2005. Simulation of integrated surface-water/ground-water flow and salinity for a coastal wetland and adjacent estuary. Journal of Hydrology, 314(1-4): 212-234.
Leavesley, G.H., Lichty, R.W., Troutman, B.M. and Saindon, L.G., 1983. Precipitation-runoff modeling system user's manual. Water Re-sources Investigation Report, US Geological Survey.
Ledoux, E., 1980. Modélisation intégrée des écoulements de surface et des écoulements souterrains sur un bassin hydrologique, Ecole Nationale Supérieure des Mines de Paris.
Ledoux, E., Girard, G. and Villeneuve, J.P., 1984. Proposition d'un modèle couplé pour la simulation conjointe des écoulements de surface et des écoulements souterrains sur un bassin hydrologique. La Houille Blanche: 101-110.
Ledoux, E., Girard, G., De Marsily, G., Villeneuve, JP., Deschenes, J., 1989. Spatially distributed modeling: conceptual approach, coupling surface water and groundwater. In: Morel-Seytoux HJ, editor. Unsaturated flow in hydrologic modeling, theory and practice. NATO ASI Ser. CNorwell, Massachussett: Kluwer Academic: 435-454.

Ledoux, E. et al., 2007. Agriculture and Groundwater Nitrate Contamination in the Seine Basin. The STICS-MODCOU modelling chain. Science of the Total Environment, 375(33-47).
Lefebvre, E., Flipo, N., de Fouquet, C. and Poulin, M., 2010. Geostatistics for assessing the efficiency of distributed physically-based water quality model. Application to nitrates in the Seine River. Hydrological Processes (Accepted).
Lemieux, J.-M., Sudicky, E.A., Peltier, W.R. and Tarasov, L., 2008. Dynamics of groundwater recharge and seepage over the Canadian landscape during the Wisconsinian glaciation. Journal of Geophysical Research, 113: F01011.
Leopold, L.B. and Maddock, T., 1953. The hydraulic geometry of stream channels and some physiographic implications. U.S. Geological Survey Paper, 252: 1–57.
Leopold, L.B. and Wolman, M.G., 1957. River Channel Patterns: Braided, Meandering and Straight. U.S. Geological Survey Professional Paper 282-B, 51p.
Leopold, L.B., Wolman, M.G. and Miller, J.P., 1964. Fluvial Processes in Geomorphology. W.H. Freeman, San Francisco, California, USA.
Li, S.G., Venkataraman, L. and McLaughlin, D., 1992. Stochastic theory for irregular stream modelling. I: Flow resistance. Journal of Hydraulic Engineering, 118(8): 1079-1090.
Lian, Y. et al., 2007. Coupling of hydrologic and hydraulic models for the Illinois River Basin. Journal of Hydrology, 344(3-4): 210.
Liang, D., Falconer, R.A. and Lin, B., 2007. Coupling surface and subsurface flows in a depth averaged flood wave model. Journal of Hydrology, 337(1-2): 147.
Lienert, C., Short, S.A. and Gunten, H.R., 1994. Uranium infiltration from a river to shallow groundwater. Geochimica et Cosmochimica Acta, 58(24): 5455.
Liggett, J.A., 1975. Basic equations of unsteady flow, in Unsteady Flow in Open Channels, K. Mahmood, and V. Yevjevick (Eds.), Vol. I, Fort Collins, Colorado,Water Resources Publications, pp. 29-62.
Lighthill, M.J. and Whitham, G.B., 1955. On kinematic waves. I. Flood movement in long rivers, Proceedings of the Royal Society of London., Piccadilly, London. A229(1178):281–316.
Linderfelt, W. and Turner, J., 2001. Interactions between shallow groundwater, saline surface water and nutrient discharge in a seasonal estuary: the swan-canning system. Hydrological Processes, 15: 2631–2653.
Lindley, E.S., 1919. Regime channels, Proceedings of Punjab Engineering Congress.
Linsley, R.K., 1971. A critical review of currently available hydrologic models for analysis of urban stormwater runoff. Palo Alto, Calif.: Hydrocomp International.
Linsley, R.K., Kohler, M.A. and Paulhus, J.L.H., 1982. Hydrology for Engineers, Third Edition. McGraw-Hill, New York.
Loague, K. and Corwin, D.L., 2007. Scale issues. In The Handbook of Groundwater Engineering, Delleur JW (ed.). CRC Press; 25D1–25D21.
Loague, K. et al., 2006. Physics-based hydrologic-response simulation: foundation for hydroecology and hydrogeomorphology. Hydrological Processes, 20: 1231–1237.
Loague, K. and VanderKwaak, J.E., 2002. Simulating hydrologic response for the R-5 catchment:comparison of two models and the impact of the roads. Hydrological Processes, 16: 1015–1032.
Loague, K. and VanderKwaak, J.E., 2004. Physics-based hydrologic response simulation: Platinum bridge, 1958 Edsel, or useful tool. Hydrological Processes, 18: 2949–2956.
Loeltz, O.J. and Leake, S.A., 1983. A method for estimating groundwater return flow to the lower Colorado river in the Yuma Area. USGS Water Resources Investigation Report 83-4220.

Lu, H., Moran, C.J., Prosser, I.P. and DeRose, R., 2004. Investment prioritization based on broad scale spatial budgeting to meet downstream targets for suspended sediment loads. Water Resources Research, 40: W09501.

Lucas-Picher, P., Arora, V., Caya, D. and Laprise, R., 2003. Implementation of a large-scale variable velocity river flow routing algorithm in the Canadian Regional Climate Model (CRCM). Atmosphere - ocean, 41(2): 139-153.

Ma, K.L. and Sikorski, K., 1993. A distributed 3D Navier-Stokes solver in Express. Energy & Fuels, 7(6): 897.

Marie, J.R. and Hollett, K.J., 1996. Determination of hydraulic characteristics and yield of aquifers underlying Vekol Valley, Arizona, using several classical and current methods. U.S. Geological Survey Water-Supply Paper 2453.

Markstrom, S.L., Niswonger, R.G., Regan, R.S., Prudic, D.E. and Barlow, P.M., 2008. GSFLOW - Coupled ground-water and surface-water flow model based on the integration of the precipitation-runoff modeling system (PRMS) and the modular ground-water flow model (MODFLOW-2005). U.S. Geological Survey Techniques and Methods, 6(D1)(240).

Maxwell, R.M. and Miller, N.L., 2005. Development of a coupled land surface and groundwater model. Journal of Hydrometeorology, 6: 233–247.

McCarthy, G.T., 1938. The Unit Hydrograph and Flood Routing. Unpublished manuscript presented at a conference of the North Atlantic Division, U.S. Army Corps of Engineers.

McDonnell, J.J., Stewart, M.K. and Owens, I.F., 1991. Effect of catchment-scale subsurface mixing on stream isotopic response. Water Resources Research, 27(12): 3065–3073.

McKergow, L.A., Prosser, I.P., Hughes, A.O. and Brodie, J., 2004. Sources of sediment to the Great Barrier Reef World Heritage Area. Marine Pollution Bulletin, 51: 200–211.

McLaren, R.G. et al., 2000. Flow and transport in fractured tuff at Yucca Mountain: numerical experiments on fast preferential flow mechanisms. Journal of Contaminant Hydrology, 43: 211–238.

Merrit, L.M. and Konikow, L.F., 2000. Documentation of a computer program to simulate lake-aquifer interaction using the MODFLOW ground-water flow model and the MOC3D solute transport model. United States Geological Survey, Water-Resources Investigation Report 00-4167.

Meyboom, P., 1961. Estimating ground-water recharge from stream hydrographs. Journal of Geophysical Research, 66(4): 1203-1214.

Michaud, J.D. and Sorooshian, S., 1994b. Comparison of simple versus complex distributed runoff models on a midsized semi arid watershed. Water Resources Research, 30(3): 593–606.

Miller, B.A. and Wenzel, H.G., 1984. Low flow hydraulics in alluvial channels. Dept. of Civil Engineering, University of Illinois at Urbana-Champaign.

Miller, J.R., Russell, G.L. and Caliri, G., 1994. Continental-Scale river flow in climate models. Journal of Climatology, 7: 914-928.

Milly, P.C.D., Dunne, K.A. and Vecchia, A.V., 2005. Global pattern of trends in streamflow and water availability in a changing climate. Nature Geoscience, 438(7066): 347–350.

Mirus, B.B., Ebel, B.A., Loague, K. and Wemple, B.C., 2007. Simulated effect of a forest road on near-surface hydrologic response: redux. Earth Surface Processes and Landforms, 32: 126–142.

Mohan, S., 1997. Parameter estimation of nonlinear muskingum models using genetic algorithm. Journal of hydraulic engineering, 123(2): 137-142.

Monteil, C. et al., 2010. Assessing the contribution of the main aquifer units of the Loire Basin to river discharge during low flow, Proceedings of XVIII International Conference on Water Resources, Barcelona.
Moore, I.D. and Grayson, R.B., 1991. Terrain-based catchment partitioning and runoff prediction using vector elevation data. Water Resources Research, 27: 1177–1191.
Morin, E. et al., 2009. Flood routing and alluvial aquifer recharge along the ephemeral arid Kuiseb River, Namibia. Journal of Hydrology, 368(1-4): 262.
Morita, M. and Yen, B.C., 2002. Modeling of conjunctive two dimensional surface-three dimensional subsurface flows. Journal of Hydraulic Engineering, ASCE, 128(2): 184-200.
Naot, D. and Rodi, W., 1982. Calculation of secondary currents in channel flow. Journal of Hydraulic Devision- ASCE, 108(HY8): 948-968.
Nash, J.E., 1958. IUGG General Assembly of Toronto, UGG General Assembly of Toronto, vol. III, IAHS Publ, pp. 114–121.
Nash, J.E. and Sutcliffe, J.V., 1970. River flow forecasting through conceptual models, 1-A discussion of principles. Journal of Hydrology, 10(3): 282–290.
Navier, C.L.M.H., 1822. Memoire sur les lois du mouvement des fluides. Mem. Acad. Sci. Inst. France, 6, 389-440.
Neal, J. et al., 2009. A data assimilation approach to discharge estimation from space. Hydrological Processes, 23 (25): 3641-3649.
Nearing, M.A. et al., 2005. Modeling response of soil erosion and runoff to changes in precipitation and cover. Catena, 61(2-3): 131-154.
Nijssen, B., O'Donnell, G.M., Lettenmaier, D.P., Lohmann, D. and Wood, E.F., 2001. Predicting the Discharge of Global Rivers. Journal of Climate, 14: 3307–3323.
Nixon, M., 1959. A Study of Bankfull Discharges of Rivers in England and Wales, Proceedings of the Institution of Civil Engineers, pp. 157-175.
Noto, L.V., Ivanov, V.Y., Bras, R.L. and Vivoni, E.R., 2008. Effects of initialization on response of a fully-distributed hydrologic model. Journal of Hydrology, 352(1-2): 107.
Nunes, J.P., de Lima, J.L.M.P., Singh, V.P., de Lima, M.I.P. and Vieira, G.N., 2006a. Numerical modelling of surface runoff and erosion due to moving rainstorms at the drainage basin scale. Journal of Hydrology, 330(3-4): 709-720.
Nunes, J.P., Vieira, G., Seixas, J., Gonçalves, P. and Carvalhais, N., 2005. Evaluating the MEFIDIS model for runoff and soil erosion prediction during rainfall events. Catena, 61(2-3): 210-228.
Nunes, J.P., Vieira, G.N. and Seixas, J., 2006b. MEFIDIS - A Physically-based, Spatially-Distributed Runoff and Erosion Model for Extreme Rainfall Events. In: Singh VP, Frevert DK (Eds.), Watershed Models. CRC press, Boca Raton. 291-314.
Oki, T. and Kanae, S., 2006. Global Hydrologic Cycle and World Water Resources. Science, 313(5790): 1068–1072.
Oki, T. and Sud, Y.C., 1998. Design of Total Runoff Integrating Pathways (TRIP) - A global river channel network. Earth Interactions 2., available at http://EarthInteractions.org.
Olesen, K.W., Refsgaard, A. and Havnø, K., 2000. Restoring River Ecology, A Complex Challenge, International Conference on New Trends in Water and Environmental Engineering for Safety and Life, Capri, Italy.
Osman, Y.Z. and Bruen, M.P., 2002. Modelling stream-aquifer seepage in an alluvial aquifer: an improved loosing-stream package for MODFLOW. Journal of Hydrology, 264(1-4): 69.

Osterkamp, W.R., Lane, L.J. and Savard, C.S., 1994. Recharge estimates using a geomorphic/distributed-parameter simulation approach, Amargosa River basin. Water Resources Bulletin, 30(3): 493-507.

Panday, S. and Huyakorn, P.S., 2004. A fully coupled physically-based spatially-distributed model for evaluating surface/subsurface flow. Advances in Water Resources, 27(4): 361.

Park, J., Kojiri, T., Ikebuchi, S. and Oishi, S., 2000. GIS based hydrological comparison and run-off simulation of a river basin. Fresh Perspectives on Hydrology and Water Resources in Southeast Asia and the Pacific: 143-156.

Park, Y.J., Sudicky, E.A., Panday, S., Sykes, J.F. and Guvanasen, V., 2008. Application of implicit sub-time stepping to simulate flow and transport in fractured porous media. Advances in Water Resources, 31(7): 995.

Partington, D.J. et al., 2009. Using a fully coupled surface water - groundwater model to quantify streamflow components, Proceedings of the 18th World IMACS and MODSIM09 International Congress.

Pearce, A.J., Stewart, M.K. and Sklash, M.G., 1986. Storm runoff generation in humid headwater catchments: 1. where does the water come from? Water Resources Research, 22(8): 1263-1272.

Perumal, M., O'Connell, P.E. and Raju, R., 2001. Field Applications of a Variable-Parameter Muskingum Method. Journal of Hydraulic Devision- ASCE, 6(3): 196–207.

Peters, N.E. and Ratcliffe, E.B., 1998. Tracing Hydrologic Pathways Using Chloride at the Panola Mountain Research Watershed, Georgia, USA. Water, Air, & Soil Pollution, 105(1-2): 263-275.

Philippe, E. et al., 2010. Improvement of a conceptual unsaturated zone scheme: a case study of the Seine river basin. Hydrological Processes, in press.

Pinder, F.G. and Jones, J.F., 1969. Determination of the groundwater component of peak discharge from the chemistry of total runoff. Water Resources Research, 5(2): 438-445.

Pinder, G.F. and Sauer, S.P., 1971. Numerical simulation of flood wave modification due to bank storage effects. Water Resources Research, 7(1): 63-70.

Pionke, H.B., Gburek, W.J. and Folmar, G.J., 1993. Quantifying stormflow components in a Pennsylvania watershed when 18O input and storm conditions vary. Journal of Hydrology, 148(1-4): 169.

Plummer, L.N., Bexfield, L.M., Anderholm, S.K., Sanford, W.E. and Busenberg, E., 2004. Hydrochemical tracers in the Middle Rio Grande Basin, USA: 1. Conceptualization of groundwater flow. Hydrogeology Journal, 12(4): 359-388.

Ponce, V.M. and Chaganti, P.V., 1994. Variable-parameter Muskingum-Cunge revisited. Journal of Hydrology, 162(3-4): 433–439.

Ponce, V.M., Pandey, R.P. and Kumar, S., 1999. Groundwater recharge by channel infiltration in El Barbon Basin, Baja California, Mexico. Journal of Hydrology, 214(1-4): 1-7.

Ponce, V.M. and Simons, D.B., 1977. Shallow wave propagation in open channel flow. Journal of the Hydraulics Division. ASCE 103 HY12: 1461–1476.

Ponce, V.M. and Yevjevich, V., 1978. Muskingum-Cunge method with variable parameters. Journal of the Hydraulics Division. ASCE, 104(12): 1663–1667.

Prosser, I.P., Rustomji, P., Young, W., Moran, C.J. and Hughes, A.O., 2001a. Constructing river basin sediment budgets for the national land and water resources audit. CSIRO Land and Water Tech. Report no 15/01. CSIRO Land and Water, Canberra.

Prudic, D.E., Konikow, L.F. and Banta, E.R., 2004. A new streamflow-routing (SFR1) package to simulate stream–aquifer interaction with Modflow 2000. United States Geological Survey, Open File Report 2004-1042.

Qu, Y. and Duffy, C.J., 2007. A semidiscrete finite volume formulation for multiprocess watershed simulation. Water Resources Research, 43(8, W08419.1-W08419).

Querner, E.P., 1997. Description and application of the combined surface and groundwater flow model MOGROW. Journal of Hydrology, 192(1-4): 158–188.

Quintana-Seguí, P. et al., 2008. The SAFRAN atmospheric analysis. Description and Validation. Journal of Applied Meteorology and Climatology, 47: 92-107.

Rabeni, C.F. and Jacobson, R.B., 1993. The importance of fluvial hydraulics for fish-habitat restoration in low-gradient alluvial streams. Freshwater Biolagy, 29: 211-220.

Ran, Q., Heppner, C.H., VanderKwaak, J.E. and Loague, K., 2007. Further testing of the Integrated Hydrology Model (InHM): Multiple-species sediment transport. Hydrological Processes, 21: 1522–1531.

Rassam, D.W., Pagendam, D.E. and Hunter, H.M., 2008. Conceptualisation and application of models for groundwater-surface water interactions and nitrate attenuation potential in riparian zones. Environmental Modelling & Software, 23(7): 859-875.

Refsgaard, J.C., 2001. Discussion of model validation in relation to the regional and global scale. In: Model Validation: Perspectives in Hydrological Science. eds. Anderson M.G. and Bates, P.D., John Wiley and Sons. 461-483.

Refsgaard, J.C. et al., 1998. An integrated model for the Danubian Lowland - methodology and applications. Water Resources Management, 12: 433-465.

Refsgaard, J.C. and Storm, B., 1995. MIKE SHE, in Computer Models of Watershed Hydrology, edited by V. P. Singh, pp. 809-846, Water Resources Publications, Highlands Ranch, CO, USA. 809-846.

Refsgaard, J.C., Thorsen, M., Jensen, J.B., Kleeschulte, S. and HANSEN, S., 1999. Large scale modelling of groundwater contamination from nitrate leaching. Journal of hydrology, 221(3-4): 117-140.

Reilly, T. and Goodman, D., 1985. Quantitative analysis of salt water-freshwater relationships in groundwater systems– a historical perspective. Journal of Hydrology, 80: 125–160.

Reynolds, R.J., 1987. Diffusivity of a glacial-outwash aquifer by the floodwave-response-technique. Ground Water, 25(3): 290–298.

Rhoads, B.L., 1992. Statistical models of fluvial systems. Journal of Geomorphology, 5: 433-455.

Richard, L.C., 1976. Finite Element Solution of Saint-Venant Equations. Journal of the Hydraulics Division, ASCE, 102(6): 759-775.

Rodell, M., Houser, P.R., Berg, A.A. and Famiglietti, J.S., 2005. Evaluation of 10 Methods for Initializing a Land Surface Model. Journal of Hydrometeorology, 6(2): 146-155.

Ross, B.B., N., C.D. and O., S.V., 1979. A finite element model of overland and channel flow for assessing the hydrological impact of land-use change. Journal of Hydrology, 41: 10–30.

Rushton, K., 2007. Representation in regional models of saturated river–aquifer interaction for gaining/losing rivers. Journal of Hydrology, 334(1-2): 262– 281.

Ryan, R., Packman, A. and Welty, C., 2004. Estimation of solute transport and storage parameters in a stream with anthropogenically produced unsteady flow and industrial bromide input. Water Resources Research, 40(1).

Saleh, F.S. et al., 2010. Contribution of 1D river flow modeling to the quantification of stream-aquifer interactions in a regional hydrological model, proceedings of XVIII International Conference on Water Resources, Barcelona.

Sanford, W., 2002. Recharge and groundwater models: an overview. Hydrogeology Journal, 10(1): 110.
Sanford, W.E., Plummer, L.N., McAda, D.P., Bexfield, L.M. and Anderholm, S.K., 2004. Hydrochemical tracers in the Middle Rio Grande Basin, USA: 2. Calibration of a groundwater-flow model. 12(4): 389-407.
Schornburgk, S. and Pointet, T., 2003. Pré-étude des inter-relations Nappes - cours d'eau de l'Oise entre Compiègne et Pontoise. Rapport final. Étude réalisée dans le cadre des opérations de Service public du BRGM 2003- 02PIR327.
Schoups, G. et al., 2005. Sustainability of irrigated agriculture in the San Joaquin Valley, California., Proceedings of the National Academy of Sciences, USA, pp. 15352–15356.
Schumm, S.A., 1960. The shape of alluvial channels in relation to sediment type. U.S. Geological Survey Prof. Paper 352-B: 17-30.
Selker, J.S. et al., 2006. Distributed fiber-optic temperature sensing for hydrologic systems. Water Resources Research, 42, W12202.
Semmens, D.J. et al., 2008. KINEROS2 and the AGWA modeling framework. Hydrological modelling in arid and semi-arid areas, Cambridge University Press, Cambridge: 41–48.
Sherman, L.K., 1932. Stream-flow from rainfall by the unit-graph method. Eng. News-Rec., 108: 501-505.
Singh, K.P. and McConkey, S., 1989. Hydraulic geometry of streams and stream habitat assessment. Journal of Water Resources Planning and Management, 115(5): 583–597.
Smerdon, B.D., Medoza, C.A. and Devito, K.J., 2007. Simulations of fully coupled lake groundwater exchange in a subhumid climate with an integrated hydrologic model. Water Resources Research, 43: W01416.
Smith, A.J. and Townley, L.R., 2002. Influence of regional setting on the interaction between shallow lakes and aquifers. Water Resources Research, 38 (9): 1170.
Smith, A.J. and Turner, J.V., 2001. Density-dependent surface water-groundwater interaction and nutrient discharge in the Swan-Canning Estuary. Hydrological Processes, 15(13): 2595-2616.
Smith, R.E., Goodrich, D.C., Woolhiser, D.A. and Unkrich, C.L., 1995. KINEROS - a kinematic runoff and erosion model. Computer Models of Watershed Hydrology. Water Resources Publications, Highlands Ranch, Colorado: 697–732.
Smith, R.E. and Hebbert, R.H.B., 1983. Mathematical simulation of interdependent surface and subsurface hydrologic response. Water Resources Research, 19: 987–1001.
Smith, R.E. and Woolhiser, D.A., 1971. Overland flow on an infiltrating surface. Water Resources Research, 7(4): 899-913.
Smith, R.H., 1978. Development of a Flood Routing Model for Small Meandering Rivers, University of Missouri at Rolla, MO.
Snell, J.D. and Sivapalan, M., 1995. On the application of the meta-channel concept: Construction of the meta-channel hydraulic geometry for a natural catchment. Hydrological Processes, 9(5-6): 485-505.
Sokrut, N., 2001. A distributed coupled model of surface and subsurface dynamics as a tool for catchment management. Licentiate Thesis, Royal Institute of
Technology, Department of Land and Water Resources Engineering, Stockholm, Sweden.
Sophocleous, M., 2002. Interactions between groundwater and surface water: the state of the science. Hydrogeology Journal, 10: 52-67.
Sophocleous, M.A., 1991. Stream-floodwave propagation through the Great Bend alluvial aquifer, Kansas: Field measurements and numerical simulations. Journal of Hydrology, 124(3-4): 207-228.

Sorman, A.U., Abdulrazzak, M.J. and Morel-Seytoux, H.J., 1997. Groundwater recharge estimation from ephemeral streams. Case study: Wadi Tabalah, Saudi Arabia. Hydrological Processes, 11(12): 1607-1619.

Spanoudaki, K., Stamou, A.I. and Nanou-Giannarou, A., 2009. Development and verification of a 3-D integrated surface water-groundwater model. Journal of Hydrology, 375(3-4): 410.

Sparks, T., 2004. Integrated modelling of 2-D surface water and groundwater flow with contaminant transport, Proceedings of XXXI IAHR Congress, Seoul, Korea.

Squillace, P.J., 1996. Observed and simulated movement of bank-storage water. Ground Water, 34(1): 121-134.

Stephens, D.B., 1988. Field study of ephemeral stream infiltration and recharge. National Technical Information Service, Springfield VA. 22161.

Stewardson, M., 2005. Hydraulic geometry of stream reaches. Journal of Hydrology, 306: 97–111.

Stoker, J.J., 1957a. Water Waves, The Mathematical Theory with Applications. Interscience Publishers, New York.

Stoker, J.J., 1957b. Water waves: The mathematical theory with applications. Pure and Appl. Math., vol. 4, Interscience, New York.

Strelkoff, T., 1970. Numerical solution of Saint-Venant equations. Journal of hydraulic Division. ASCE, 96.

Sudicky, E.A., Jones, J.P., Park, Y.-J., Brookfield, A.E. and Colautti, D., 2008. Simulating complex flow and transport dynamics in an integrated surfacesubsurface modeling framework. Geosciences Journal, 12: 107–122.

Sudicky, E.A. et al., 2005. On the challenge of integrated surface-subsurface flow and transport modelling at multiple catchment scales, Salt Lake City Annual Meeting, Salt Lake City, pp. 28.

Sun, P., Li, H., Boufadel, M.C., Geng, X. and Chen, S., 2008. An analytical solution and case study of groundwater head response to dual tide in an island leaky confined aquifer. Water Resources Research, 44(12).

Swain, E.D. and Wexler, E.J., 1996. A Coupled Surface-Water and Ground-Water flow Model (MODBRANCH) for Simulation of Stream-Aquifer Interaction: U.S. Geological Survey Techniques of Water-Resources Investigations, book 6, chap. A6.

Swamee, P.K. and Singh, S.K., 2003. Estimation of aquifer diffusivity from stream stage variation. Journal of Hydrologic Engineering, 8(1): 20–24.

Tamura, N. and Kojiri, T., 2002. Water quantity and turbidity simulation with distributed runoff model in the Yellow River basin. Flood Defence. Science press, New York, 2: 1699-1705.

Tang, X., Knight, D.W. and Samuels, P.G., 1999. Volume conservation in Variable Parameter Muskingum-Cunge Method. Journal of Hydraulic Engineering-ASCE, 125(6): 610–620.

Tao, T. and Kouwen, N., 1989. Remote Sensing and Fully Distributed Modeling for Flood Forecasting. Journal of Water Resources Planning and Management, ASCE, 115(6): 809-823.

Thierion, C. et al., 2010. Modelling the coupled surface water and ground water system of the upper Rhine graben, proceedings of XVIII International Conference on Water Resources, Barcelona.

Thompson, J.R., Sørenson, H.R., Gavin, H. and Refsgaard, A., 2004. Application of the coupled MIKE SHE/MIKE 11 modelling system to a lowland wet grassland in southeast England. Journal of Hydrology, 293(1-4): 151.

Todini, E., 2007. A mass conservative and water storage consistent variable parameter Muskingum-Cunge approach. Hydrol. Earth Syst. Sci. Discuss., 4: 1549–1592.

Todini, E. and Bossi, A., 1986. PAB (Parabolic and Backwater) an unconditionally stable flood routing 15 scheme particularly suitedfor real timeforecasting and control. Journal of Hydraulic Research, 24(5): 405-424.

Tokai, A., Kojiri, T. and Yoshikawa, H., 2002. Case study of basin wide environmental quality assessment based on the distributed runoff model., 6th Water Resources Symposium, Japan, pp. 229-234.

Tsai, C.W., 2003. Applicability of Kinematic, Noninertia, and Quasi-Steady Dynamic Wave Models to Unsteady Flow Routing. Journal of Hydraulic Engineering, 129(8): 613-627.

Uhlenbrook, S., Seibert, J., Rodhe, A. and Leibundgut, C., 1999. Prediction uncertainty of conceptual rainfall-runoff models caused by problems to identify model parameters and structure. Journal of Hydrological Science, 44(5): 279–299.

VanderKwaak, J.E., 1999. Numerical Simulation of Flow and Chemical Transport in Integrated Surface-Subsurface Hydrologic Systems, University of Waterloo, Ontario, Canada.

VanderKwaak, J.E. and Loague, K., 2001. Hydrologic-response simulations for the R-5 catchment with a comprehensive physics-based model. Water Resources Research, 37(4): 999-1013.

VanderKwaak, J.E. and Sudicky, E.A., 2000. Application of a physically-based numerical model of surface and subsurface water flow and solute transport., Calibration and Reliability in Groundwater Modelling, IAHS Publication No. 265, ModelCARE 99. IAHS, Zurich, pp. 515–523.

Vogt, T., Schneider, P., Hahn-Woernle, L. and Cirpka, O.A., 2010. Estimation of seepage rates in a losing stream by means of fiber-optic high-resolution vertical temperature profiling. Journal of Hydrology, 380.: 154-164.

Von Gunten, H.R., Waber, U.E. and Krähenbühl, U., 1988. The reactor accident at chernobyl: A possibility to test colloid-controlled transport of radionuclides in a shallow aquifer. Journal of Contaminant Hydrology, 2(3): 237.

Waber, U.E., Lienert, C. and Von G, H.R., 1990. Colloid-related infiltration of trace metals from a river to shallow groundwater. Journal of Contaminant Hydrology, 6(3): 251.

Waichler, S.R. and Wigmosta, M.S., 2004. Application of hydrograph shape and channel infiltration models to an arid watershed. Journal of Hydrological Engineering, 9(5): 433-439.

Walker, J.F., Hunt, R.J., Markstrom, S.L., Hay, L.E. and Doherty, J., 2008. Using a Coupled Groundwater/Surface-Water Model to Predict Climate-Change Impacts to Lakes in the Trout Lake Watershed, Northern Wisconsin, The third Interagency Conference on Research in the Watersheds, Estes Park, CO.

Wallingford, H.R., 1997. SIS user reference manual, HR Wallingford, Wallingford, OXON.

Wang, X., Stone, P.H. and Marotzke, J., 1999. Global thermohaline circulation. Part I – Sensitivity to atmospheric moisture transport. Journal of Climatology, 12: 71-82.

Weng, P.h., Giraud, F., Fleury, P. and Chevallier, C., 2003. Characterising and modeling groundwater discharge in an agricultural wetland on the French Atlantic coast. Hydrology and Earth System Sciences, 7: 33–42.

Werner, A.D., Gallagher, M.R. and Weeks, S.W., 2006. Regional-scale, fully coupled modelling of stream-aquifer interaction in a tropical catchment. Journal of Hydrology, 328(3-4): 497.

Westbrook, S. et al., 2005. Interaction between shallow groundwater, saline surface water and contaminant discharge at a seasonally and tidally forced estuarine boundary. Journal of Hydrology, 302: 255-269.
Western, A.W., Finlayson, B.L., Mcmahon, T.A. and Oneill, I.C., 1997. A method for characterising longitudinal irregularity in river channels. Journal of Geomorphology, 21: 39–51.
Western, A.W., O'Neill, I.C. and McMahon, T.A., 1994. Sophisticated Stream Modelling: Some Practical Limitations, Water Down Under 94: Groundwater/Surface Hydrology Common Interest Papers; Preprints of Papers. Barton, ACT: Institution of Engineers, Australia, pp. 513-518.
Wheater, H.S., Butler, A.P., Stewart, E.J. and Hamilton, G.S., 1991. A multivariate spatial - temporal model of rainfall in south west Saudi Arabia. I. Spacial rainfall characteristics and model formulations. Journal of Hydrology, 125: 175–199.
Whitaker, M.P.L., 2000. Estimating bank storage and evapotranspiration using soil physical and hydrological techniques in a gaining reach of the San Pedro River, Arizona., University of Arizona.
Wigmosta, M.S. and Burges, S.J., 1997. An adaptive modeling and monitoring approach to describe the hydrologic behavior of small catchments. Journal of Hydrology, 202: 48–77.
Wigmosta, M.S., Vail, L.W. and Lettenmaier, D.P., 1994. A distributed hydrology–vegetation model for complex terrain. Water Resources Research, 30: 1665–1679.
Wijffels, S.E., Scimtt, R.W., Bryden, H.L. and Stigebrandt, A., 1992. On the transport of freshwater by the oceans. J. Phys. Oceanogr., 22: 155-162.
Wilkinson, P.L., Anderson, M.G. and Lloyd, D.M., 2002. An integrated hydrological model for rain-induced landslide prediction. Earth Surface Processes and Landforms, 27(1285–1297).
Williams, G.P., 1978. Bank-full discharge of rivers. Water Resource Research, 14(6): 1141-1154.
Wilson, E.M., 1990. Engineering Hydrology, pp. 110, 196, and 301, Macmillan, Indianapolis, Indiana.
Winter, T.C., 1995. Recent advances in understanding the interaction of groundwater and surface water. Reviews of Geophysics, 33(S1): 985–994.
Winter, T.C., 1998. Relation of streams, lakes, and wetlands to Research groundwater flow systems. Hydrogeology Journal, 7(1): 28-45.
Winter, T.C., 2002. Subaqueous capping and natural recovery: Understanding the hydro-geologic setting at contaminated sites: Dredging Operations and Environmental Research (DOER) Technical Notes Collection (TN DOER-C26, U.S. Army Engineer Research and Development Center, Vicksburg, MS.: 1-16.
Wooding, R.A., 1965. A hydraulic model for the catchment-stream problem: I. Kinematic-wave theory. Journal of Hydrology, 3(3-4): 254-267.
Woolhiser, D.A. and Liggett, J.A., 1967. Unsteady, one-dimensional flow over a plane-The rising hydrograph. Water Resources Research, 3(3): 753-771.
Woolhiser, D.A., Smith, R.E. and Goodrich, D.C., 1990a. KINEROS, A Kinematic Runoff and Erosion Model: Documentation and User Manual. US Department of Agriculture, Agricultural Research Service, ARS-77: 130.
Woolhiser, D.A., Smith, R.E. and Goodrich, D.C., 1990b. KINEROS, a kinematic runoff and erosion model: documentation and user manual. US Department of Agriculture, Agricultural Research Service, ARS-77.

Yatheendradas, S. et al., 2008. Understanding uncertainty in distributed flash flood forecasting for semi arid regions. Water Resources Research, in press, doi:10.1029/2007WR005940.

Yeh, G.T. and Huang, G.B., 2003. A Numerical Model to Simulate Water Flow in Watershed Systems of 1-D Stream-River Network, 2-D Overland Regime, and 3-D Subsurface Media (WASH123D: Version 1.5), Technical Report. Dept. of Civil and Environmental Engineering, University of Central Florida, Orlando, Florida.

Yim, C. and Mohsen, M., 1992. Simulation of tidal effects on contaminant transport in porous media. Ground Water, 30(1): 78–86.